



LEHIGH
UNIVERSITY

Library &
Technology
Services

The Preserve: Lehigh Library Digital Collections

Preparation and Characterization of Nanostructured Multilayered Films.

Citation

Keiser, William Edwin. *Preparation and Characterization of Nanostructured Multilayered Films*. 1997, <https://preserve.lehigh.edu/lehigh-scholarship/graduate-publications-theses-dissertations/theses-dissertations/preparation-25>.

Find more at <https://preserve.lehigh.edu/>

This document is brought to you for free and open access by Lehigh Preserve. It has been accepted for inclusion by an authorized administrator of Lehigh Preserve. For more information, please contact preserve@lehigh.edu.

**Preparation and Characterization
of Nanostructured Multilayered Films**

by

Elaine Robbins Kleinfeld

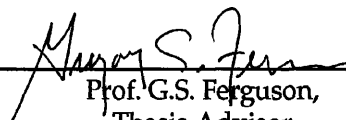
Presented to the Graduate and Research Committee
of Lehigh University
in Candidacy for the Degree of

Doctor of Philosophy
in
Chemistry

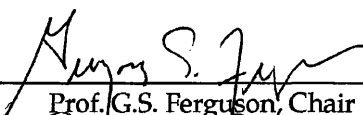
Lehigh University
May 9, 1997

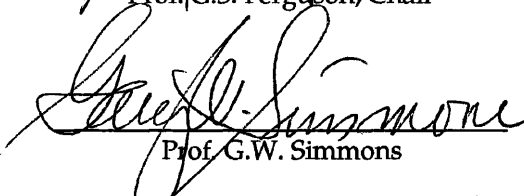
Approved and recommended for acceptance as a dissertation in partial fulfillment of the requirements for the degree of Doctor of Philosophy in Chemistry.

5/8/97
Date


Prof. G.S. Ferguson,
Thesis Advisor

Special Committee directing the work of Elaine Robbins Kleinfeld:


Prof. G.S. Ferguson, Chair


Prof. G.W. Simmons


Prof. S.L. Regen


Prof. M.S. Malcuit

© Copyright 1997 Elaine Robbins Kleinfeld
All Rights Reserved

Acknowledgements

My deep gratitude is extended first of all toward my advisor, Greg Ferguson, who provided insight and inspiration throughout this work. Second only to his extraordinary guidance, no force was more significant in shaping my graduate education than the AT&T Bell Laboratories Ph.D. Scholarship. In this vein, sincere thanks are extended not only toward the AT&T Foundation and its officers for making the award possible, but also toward scientists Mark Cardillo, Alex Harris, and Chris Chidsey, both for inspiring my interest in materials chemistry and for mentoring my early years in this field. I am also grateful to those at Bell Laboratories who provided valuable technical support for my research, including Theo Siegrist, Lisa Dhar, Steve Buratto, and Tom Putvinski.

We sincerely appreciate the financial support provided for our research by Southern Clay, Inc. We are especially grateful to C.E. Bert Powell and J. Scott Leigh for their significant technical assistance and ongoing interest in our work, and to Randy Chapman, Gordon Paterson, and Carl Bauer for additional technical support. We further acknowledge Lehigh University for additional direct and indirect financial support. A generous gift from P.E.O. is gratefully acknowledged.

Technical assistance for our research was provided by many members of the Lehigh community, including Al Miller, Olga Shaffer, Prof. Dale Simpson, George Yasko, Prof. Michael Freund, Prof. Jim Roberts, Bill Anderson, and D.J. Wang. Furthermore, I am grateful to the members of my special committee, Professors Gary Simmons, Steven Regen, and Michelle Malcuit, for their guidance throughout this work and for careful reading of the dissertation.

Of course, I would be remiss if I failed to acknowledge the direct contributions to the work in this dissertation by Lehigh undergraduates Holly L. Deak and Barbara A. MacNeill, as well as the valued technical assistance of Ferguson group members past and present, including Deborah H. Carey, Paul D. Mumbauer, Joann S. Monko, Patricia L. Kennedy Twaddle, Manju Agrawal, Jason H. Rouse, Mong-Tung Lee, and Maki Uragami.

Dedication

This dissertation is dedicated to my husband, Jeff, to my daughter, Linda, and to my parents, without whose love and support I couldn't have persevered.

Table of Contents

Abstract	1
Chapter 1: A Brief Overview of Techniques for Forming Multilayered Films, and an Overview of Our Early Work in This Field	3
Part One: Background	3
1.1 Introduction	3
1.2 Methods of Film Formation	6
Part Two: Our Preliminary Studies on Multilayered Films	13
1.3 Thin Films of Titanium Dioxide	13
1.4 Toward Composite Films from Sheet Silicates and Monomeric Cations	25
1.5 Toward Multilayered Films from Silicates and Crosslinked Cationic Networks	28
1.6 Formation of Films from Cationic Polyelectrolytes and Sheet Silicates ..	34
1.7 Materials and Methods	38
1.8 References and Notes	44
Chapter 2: Initial Studies and Groundwork in the PDDA/Laponite System	50
2.1 Abstract	50
2.2 Introduction	51
2.3 Results and Discussion	51
2.4 Conclusions	70
2.5 Experimental Methods	72
2.6 References and Notes	75
Chapter 3: Stepwise Adsorption of Ordered Organic/Inorganic Multilayers onto Solid Surfaces	79
3.1 Abstract	79
3.2 Introduction	80
3.3 Results and Discussion	84
3.4 Conclusions	125
3.5 Experimental Methods	127
3.6 References and Notes	133
Chapter 4: Healing of Defects in the Stepwise Formation of Multilayered Films	139
4.1 Abstract	139
4.2 Introduction	139
4.3 Results and Discussion	142
4.4 Conclusions	149

Chapter 4, continued	
4.5 Experimental Methods	150
4.6 References and Notes	152
Chapter 5: Rapid, Reversible Sorption of Water from the Vapor by a Multilayered Composite Film: A Nanostructured Humidity Sensor	156
5.1 Abstract	156
5.2 Introduction	156
5.3 Results and Discussion	157
5.4 Conclusions	172
5.5 Addendum	172
5.6 Experimental Methods	173
5.7 References and Notes	175
Chapter 6: Interference Effects and Photochromism in Dye-Containing Polyelectrolyte-Clay Multilayered Films	178
6.1 Abstract	178
6.2 Introduction	178
6.3 Results	182
6.4 Conclusions	214
6.5 Experimental Methods	214
6.6 References and Notes	223
Chapter 7: Studies of the Structure, Composition, and Kinetics of Adsorption of Poly(diallyldimethylammonium)/Montmorillonite Composite Films	226
7.1 Abstract	226
7.2 Introduction	227
7.3 Description of Film Components	231
7.4 Results and Discussion	233
7.5 Conclusions	264
7.6 Experimental Methods	265
7.7 References and Notes	270
Chapter 8: Formation of Films From Sheet Silicates and Oxy-Aluminum Species	275
8.1 Abstract	275
8.2 Introduction	275
8.3 Results and Discussion	277
8.4 Experimental Methods	288
8.5 References and Notes	292

Chapter 9: Conclusions	294
9.1 Concluding Remarks	294
9.2 References and Notes	295
Biography of Elaine Robbins Kleinfeld	296

Table of Figures

Chapter 1: A Brief Overview of Techniques for Forming Multilayered Films, and an Overview of Our Early Work in This Field

1.1	Highly schematic illustration of the formation of a two-component multilayered film	4
1.2	Formation of a film by the Langmuir–Blodgett Technique	8
1.3	Formation of a multilayered film by alternate adsorption and activation of self-assembled monolayers	10
1.4	Formation of a multilayered film by alternate adsorption of anionic and cationic polyelectrolytes onto a pretreated surface	12
1.5	Schematic illustration of the adsorption cycle that was repeated to form an ultrathin film of TiO_2	15
1.6	Ellipsometric thickness of a TiO_2 overlayer as a function of the number of adsorption cycles.	17
1.7	X-ray photoelectron survey spectrum of a three-layer film of TiO_2 on a silicon wafer	19
1.8	Intensity of Ti 2p photoemission as a function of the number of adsorption cycles	20
1.9	Natural logarithm of the intensity of Si 2p photoemission	22
1.10	Normalized intensity of the Ti 2p photoemission as a function of the angle between the surface normal and the detector	23
1.11	Schematic illustrations of the exfoliation and flocculation of a sodium smectite and a surface analog to this behavior	26
1.12	Schematic illustration of the proposed surface chelate effect	30
1.13	Schematic representation of the first steps in the formation of a multilayered film by successive treatments with TTA and an anionic sheet silicate	32
1.14	Schematic representation of the preparation of a multilayered film by alternate adsorption of a cationic polyelectrolyte and individual sheets of an anionic sheet silicate	35
1.15	Schematic diagram of the procedure used to mount samples for analysis by x-ray diffractometry	43

Chapter 2: Initial Studies and Groundwork in the PDDA/Laponite System

2.1	Schematic diagram of the preparation of a multilayered film by alternate adsorption of PDDA and Laponite	53
2.2	Ellipsometric thickness of a multilayered structure on a single-crystal silicon substrate as a function of the number of adsorption cycles	56
2.3	Photograph of a bare silicon wafer and multilayered films of various thicknesses on silicon substrates	59
2.4	Schematic diagram of the use of TTA to promote adsorption of Laponite to a silicon wafer	60
2.5	The x-ray diffraction pattern of a 60-cycle multilayered film of PDDA and Laponite on a silicon substrate	62

2.6	AFM image and AFM trace of a sample that had been prepared by performing one adsorption cycle on a bare silicon wafer	64
2.7	Structure of poly(D-lysine hydrobromide) and growth in thickness of a polylysine/Laponite composite film	67
2.8	Structure of poly(<i>N</i> -methyl-4-vinylpyridinium bromide) and growth in thickness of a PMVP/Laponite composite film	68
2.9	X-ray diffraction pattern of a PMVP/Laponite composite film	69
2.10	Ellipsometric growth of a film formed by sequential adsorptions of components in the order PDDA/Laponite/PMVP/Laponite	71

Chapter 3: Stepwise Adsorption of Ordered Organic/Inorganic Multilayers onto Solid Surfaces

3.1	Schematic diagram of the preparation of a composite film from PDDA or PMVP and Laponite	81
3.2	Structures of the cationic polyelectrolytes used in the formation of multilayered films	86
3.3	Ellipsometric thickness of PDDA/Laponite films as a function of the number of adsorption cycles on gold, silver, and copper substrates	87
3.4	Growth of a PMVP/Laponite multilayer on a fused quartz slide	91
3.5	X-ray photoelectron survey spectrum of a sample prepared by the adsorption of PDDA, then Laponite, then PDDA onto a gold-coated silicon wafer	95
3.6	X-ray diffraction pattern of a 50-cycle film formed by adsorption of PDDA from a 5% solution and Laponite from a 0.2% suspension onto gold	98
3.7	X-ray diffraction pattern of a 50-cycle film formed by adsorption of PMVP from a 1% solution and Laponite from a 0.2% suspension onto a fused quartz slide	101
3.8	X-ray diffraction pattern of Laponite RD	104
3.9	Ellipsometric thickness as a function of the number of adsorption cycles when different concentrations of PDDA were used in the formation of composite films	108
3.10	Dependence of film growth on the concentration of the polymer solution used to form the film	110
3.11	Dependence of film growth on the duration of the adsorption treatments	112
3.12	Schematic diagram of the use of thiocholine chloride to promote adhesion of Laponite sheets to gold	114
3.13	Cyclic voltammograms taken using gold electrodes that were bare or treated with 5, 10, or 15 cycles	117
3.14	Results of test of resistance to corrosion	122
3.15	Dark-field optical micrographs of copper substrates	124

Chapter 4: Healing of Defects in the Stepwise Formation of Multilayered Films

4.1	Schematic illustrations of the limitations to structural order in multilayered films prepared by various techniques	141
-----	---	-----

Chapter 4, continued	
4.2	Ellipsometric growth of multilayers as a function of the number of adsorption cycles on bare silicon and various SAMs 143
4.3	Schematic illustration of the adsorption of a composite film onto a SAM 146
4.4	AFM images of films adsorbed onto a SAM on silver and onto bare silver 148
Chapter 5: Rapid, Reversible Sorption of Water from the Vapor by a Multilayered Composite Film: A Nanostructured Humidity Sensor	
5.1	Schematic diagram of the structure of a PDDA/Laponite multilayered film 158
5.2	Ellipsometric study of film thickness and refractive index as a function of relative humidity 160
5.3	Schematic diagram of the composition of samples 1 – 5 164
5.4	Quartz-crystal-microbalance study of relative mass uptake as a function of relative humidity 168
5.5	Change in resonant frequency of a quartz crystal coated with a 10-cycle film as a function of time of exposure to a jet of dry or wet nitrogen 170
Chapter 6: Interference Effects and Photochromism in Dye-Containing Polyelectrolyte/Clay Multilayered Films	
6.1	Photochromism of the spiropyran/merocyanine pair 180
6.2	Reaction scheme that was used for the synthesis of PVP-SP 184
6.3	Ellipsometric thickness of multilayered films of PVP-SP and Laponite or montmorillonite on silicon 187
6.4	Ultraviolet-visible spectrophotometry of PVP-SP/Laponite films 189
6.5	Absorbance at 250 nm as a function of the number of adsorption cycles for a film formed from PVP-SP and montmorillonite on fused quartz 192
6.6	Difference between recorded spectra and hypothetical spectra that was attributed to interference effects 195
6.7	Kinetics of thermal isomerization of a photochromic spiropyran dye in a 60-cycle film of Laponite and PVP-SP 199
6.8	Kinetics of thermal isomerization of a photochromic spiropyran dye in a 30-cycle film of montmorillonite and PVP-SP 200
6.9	Kinetics of thermal isomerization of a photochromic spiropyran dye in a dip-cast film of PVP-SP 201
6.10	Kinetics of thermal isomerization of a photochromic spiropyran dye in various films (normalized data) 206
6.11	Isomers of the merocyanine form of the dye 208
6.12	X-ray diffraction pattern of a 40-cycle film made from PVP-SP and Laponite 210
6.13	X-ray diffraction pattern of a 20-cycle film made from PVP-SP and montmorillonite 212

Chapter 7: Studies of the Structure, Composition, and Kinetics of Adsorption of Poly(diallyldimethylammonium)/Montmorillonite Composite Films

7.1	Schematic diagram of the formation of a composite film from a solution of PDDA and a suspension of montmorillonite	229
7.2	Precursors to multilayered composite films	232
7.3	Ellipsometric growth per adsorption step as a function of polymer concentration	234
7.4	X-ray diffraction patterns of samples 1 – 3 and Mont	238
7.5	Low-angle XRD patterns of samples 1 – 3 and Mont highlighting the (001) reflections	239
7.6	Schematic diagram of the experimental setup used to obtain data for omega scans	244
7.7	Omega scan of the (003) reflection of sample 2	247
7.8	Omega scan of the (003) reflection of sample 3	250
7.9	Three possibilities for the nature of the disordered material within the films	252
7.10	Schematic diagram of the adsorption of montmorillonite onto a surface bearing “excess” polymer	256
7.11	Adsorption kinetics of the PDDA/montmorillonite system (individual components)	259
7.12	Adsorption kinetics of the PDDA/montmorillonite system (overall growth in a complete cycle)	262

Chapter 8: Formation of Films from Sheet Silicates and Oxy-Aluminum Species

8.1	Schematic diagram of the structure of the $[Al_{13}O_4(OH)_{24}(H_2O)_{12}]^{7+}$ polyoxycation	276
8.2	Ellipsometric growth of multilayered films formed from partially neutralized Laponite suspensions and Al_{13} solutions	279
8.3	Ellipsometric growth of multilayered films from dialyzed montmorillonite suspensions and Al_{13} solutions	281
8.4	The x-ray diffraction pattern of a film prepared by 30 cycles of treatments with an Al_{13} solution and a dialyzed montmorillonite suspension	283
8.5	Schematic illustration of the proposed “surface chelate effect”	286
8.6	The ^{27}Al NMR spectrum of an Al_{13} polyoxycation solution	290

Abstract

Our interest in the field of multilayered films was inspired by their potential usefulness in optical and sensing applications, and by a fundamental interest in the manipulation of matter at the nanometer scale. The work presented in this dissertation represents a new method for the formation of multilayered films exhibiting an unprecedented degree of structural order among films adsorbed from solution onto flat substrates. This method involves the alternate adsorption of a cationic polyelectrolyte and single sheets of an anionic silicate mineral via Coulombic interactions. Elucidating the characteristics of the growth and structure of these films was a central focus of our research. Ellipsometry and ultraviolet–visible spectrophotometry demonstrated that the films exhibited regular growth, and the films’ lateral uniformity allowed them to serve as antireflective coatings. X-ray diffractometry indicated that the ordered material in the films comprised an ABAB arrangement of the polymer and silicate.

In previous methods for the preparation of multilayered films by self-assembly of monomeric precursors, defects occurring during any preparative step can propagate as the film grows in thickness, resulting in a decrease in structural order. In contrast, our films displayed a high degree of structural order despite the fact that defects (i.e., sheet edges) occur in every layer. We demonstrated that the “two-dimensional” nature of the silicate allowed sheets adsorbing in any given cycle to patch over defects that had formed during preceding cycles. This characteristic allowed substrates that were resistant to the adsorption of either component individually to be covered by a film over the course of several adsorption cycles.

Thin films such as ours offer promise for use in sensors due to their large area/mass ratio and the ease with which they can be incorporated into microelectronic devices. Our composite multilayered films responded in a dramatic

and reversible way to changes in relative humidity, and we used ellipsometry and micro-gravimetry to characterize this response. The kinetics of water sorption were remarkably fast: the majority of the water sorbed upon turnover between environments of low and high humidity was gained or lost within three seconds.

A Brief Overview of Techniques for Forming Multilayered Films, and an Overview of Our Early Work in This Field

PART ONE: BACKGROUND

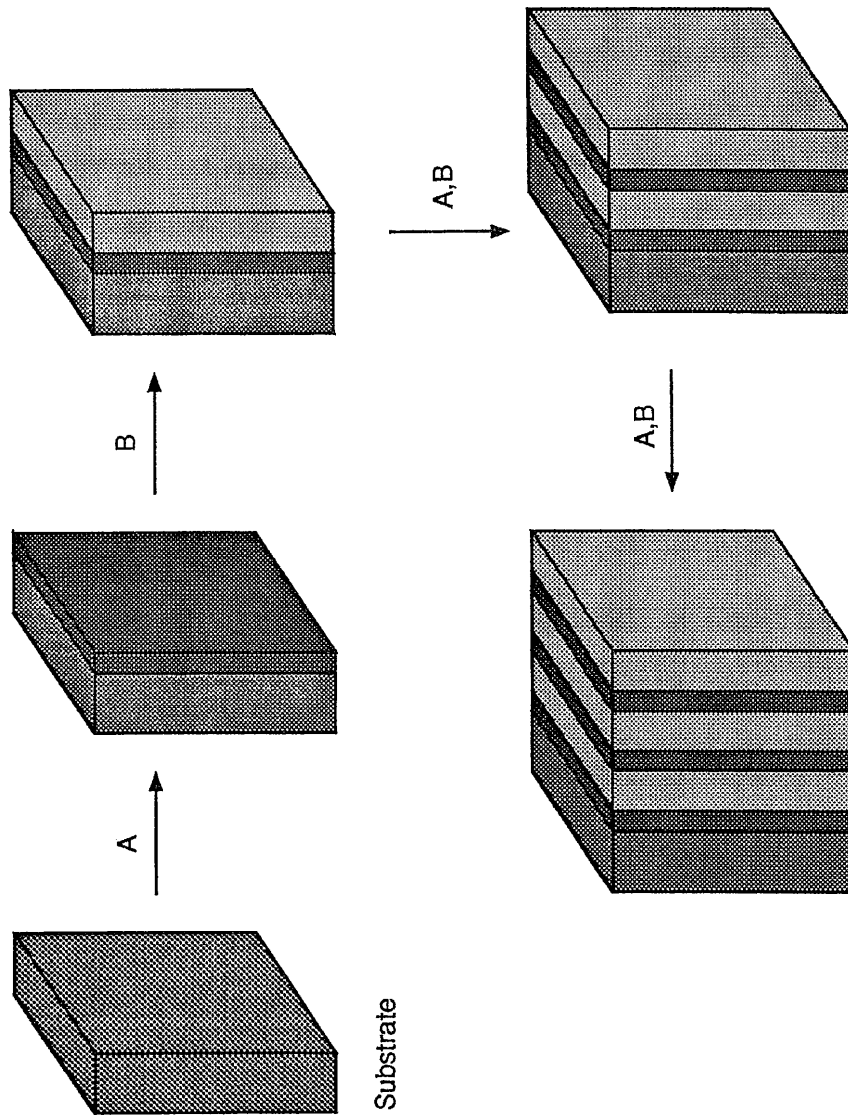
1.1 Introduction—Why Multilayered Films?

Multilayered films are typically prepared “from the substrate up,” in a stepwise fashion, by exposing a substrate in turn to two or more different materials to form discrete layers (Figure 1.1). The field of multilayered thin and ultrathin films is extremely broad, reflecting the fact that film properties can be optimized for a great variety of applications by varying the nature and periodicity of the layered materials. The properties of multilayered films can be enhanced relative to those of bulk materials as a result of effects due to film periodicity, the presence of features having confined or limited dimensions, or enhanced surface area.

Layering dissimilar components in a periodic (i.e., a nonrandom) fashion can give rise to properties not exhibited by either material alone. For example, the periodic layering of elements having high and low atomic number can result in films with high x-ray reflectivity,¹ just as periodic layering of materials having low and high refractive index can result in films with enhanced or reduced optical reflectivity.² Films made of alternating layers of an electron-rich material and an electron-deficient material can be active for photoinduced electron transfer.³

Materials spatially limited to atomic or nanometer-scale dimensions frequently exhibit properties vastly different from those of bulk materials.^{4,5} For example, small particles of conducting or semiconducting materials can exhibit anomalous electrical, optical, or magnetic behavior.^{4,5} Multilayered films constitute an ideal matrix in which such guests may be formed or included, and also possess the advantage of

Figure 1.1. Highly schematic illustration of the formation of a two-component multilayered film. The substrate is exposed alternately to species A and B, resulting in formation of distinct layers on the substrate surface. Each layer, which extends much farther in a plane parallel to the substrate surface than in the direction normal to the surface, has a composition which may differ significantly from that of A or B.



having precisely controllable thickness, which can allow optimization of these properties.

Layering a porous material can provide advantages related to enhanced surface area. For example, nanoscale pores or void spaces within a multilayered structure can impart sensing capabilities.⁶ The greatly enhanced surface area of such structures can result in enhanced sensitivity by multiplying the number of sites available for interacting with an analyte.

In addition to these practical applications, we were deeply intrigued by several fundamental issues. For example, new methods for manipulating matter at the nanometer scale, and for forming complex, ordered structures from simple precursors have the potential to advance the synthesis of solid-state materials significantly.⁴ The approach of building nanostructured materials in a stepwise fashion has greater potential for the formation of atomic-scale structures than micromachining of bulk materials.⁴

1.2 Methods of Film Formation

The method used to form a particular film often depends upon its desired composition or properties, though more than one route may be available for the incorporation of any particular material. The different methods for film formation fall into three broad categories: physical deposition, chemical deposition, and molecular self-assembly.

1.2.1. Physical Deposition. Physical depositions involve the transfer of a substance from one place to another, with little or no change in its chemical identity. Evaporation, for example, involves heating a substance of interest to the point at which it vaporizes, and allowing it to condense onto a substrate. Although valuable for the formation of films of many elements, alloys, and inorganic compounds, this

technique has limited applicability toward the formation of films from species that would decompose below the temperatures necessary for vaporization, including many complex organic molecules and metastable inorganic phases.⁷ A “gentler” physical technique for preparation of multilayered films is the Langmuir–Blodgett method,⁸ in which pre-formed monolayers of amphiphilic molecules are transferred from a water/air interface onto a flat substrate (Figure 1.2). Because of the milder conditions used, this technique can be used to form highly ordered multilayers from complex organic molecules. Unfortunately, because such films are held together primarily by van der Waals interactions, they are unstable with respect to molecular reorientation unless crosslinked in a separate step.⁸ In a related technique, researchers have recently formed films of inorganic colloids (e.g., lead zirconium titanate) by transfer of the film components from the water/air interface onto flat surfaces.⁹

1.2.2. Chemical Deposition. Chemical deposition involves the transfer of reagents in the vapor or solution phase to a substrate, where they react to form a film with a composition that differs significantly from that of the precursor(s). Examples of such techniques include chemical vapor deposition¹⁰ and atomic layer epitaxy.¹¹ Thus, for example, a substrate may be coated with a film of titanium dioxide by alternate treatments with vapor-phase titanium tetrachloride and water,¹² or by alternate treatments with solution-phase titanium (IV) tetra-*n*-butoxide and water.¹³ These techniques are useful for the preparation of a great variety of inorganic solids, and are especially useful for providing uniform coverage of substrates having irregular topography (e.g., microelectronic components).¹⁴ Moreover, because chemical deposition occurs initially via reaction at the substrate surface, a substrate can be selectively coated if it features both reactive and unreactive areas on its surface.^{10,11,15}

*1.2.3. Molecular Self-Assembly.*¹⁶ This technique has features in common with both

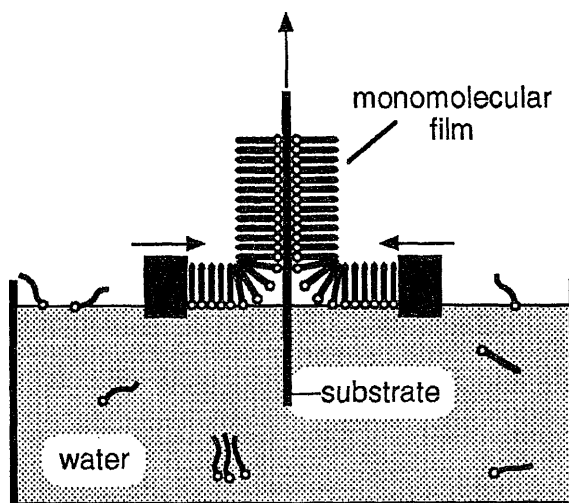


Figure 1.2. Formation of a film by the Langmuir-Blodgett technique. Amphiphilic molecules ($\text{C}_{18}\text{H}_{37}\text{O}_2$) at the water-air interface are compressed to form an ordered monolayer and are then transferred to a substrate. This process can be repeated to form a multilayered film. The molecules are greatly exaggerated in size in this figure.

physical and chemical deposition. In molecular self-assembly, films are adsorbed by chemical reactions that occur between the substrate and molecules in the solution⁸ or vapor¹⁷ phase, yet much of the original composition of the precursors is maintained in the final film. Molecules used in the formation of this type of film typically consist of a long alkyl (or functional) chain having a head group that is capable of a strong interaction with the target substrate. The combination of the head group/substrate interaction with the significant van der Waals interactions between the alkyl chains themselves often results in a significant degree of in-plane order in complete monolayers. For example, octadecyltrichlorosilane ($C_{18}H_{35}SiCl_3$) reacts with the hydrated surface of silicon dioxide to form a self-assembled monolayer (SAM) bound to the substrate through siloxane linkages and hydrogen-bonding interactions. In this type of SAM, the alkyl chains, having an all-trans conformation, are close-packed and oriented nearly perpendicularly outward.^{8,18} The mild conditions and minimal decomposition involved in forming films by molecular assembly allow surfaces to be functionalized with complex organic molecules having designed properties. Such films have proven useful for fundamental studies of intermolecular interactions.^{19,20} Furthermore, adsorption of molecules with reactive tail groups allows for multilayer formation.²¹⁻²³ Such schemes typically involve two steps: adsorption of a self-assembled monolayer, followed by activation of the resulting surface so that the next SAM can adsorb. For example, siloxane multilayers can be formed by alternate adsorption of an ω -functionalized silane and treatment of the resulting surface to provide hydroxyl groups.²¹ Metal phosphonate multilayers can be formed by alternately treating a surface with organic bisphosphonates and metal compounds.²² Such approaches, depicted schematically in Figure 1.3, can produce films displaying photochromic behavior,²⁴ high dielectric strength,²⁵ or nonlinear optical activity,^{26,27} depending on the organic spacer between the phosphonate groups. By related

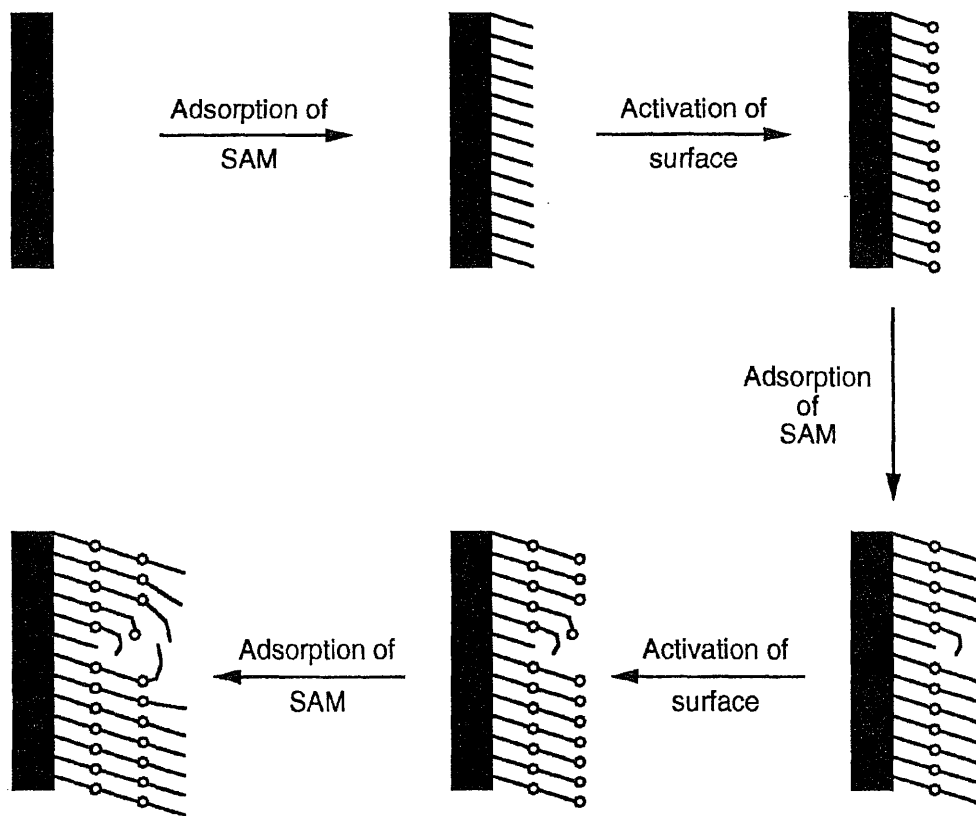


Figure 1.3. Formation of a multilayered film by alternate adsorption and activation of self-assembled monolayers. One way in which a defect may form and propagate in a film is shown.

techniques, films have recently been prepared by the formation of metal–ligand bonds.^{28,29} Another related approach, which has received widespread attention recently, is the formation of films by Coulombic interactions (i.e., successive adsorption of oppositely charged polyelectrolytes by ion exchange).^{30–35} This technique was pioneered by Iler in a paper published in 1966,³⁰ which focused on the formation of films by alternate treatments with anionic colloidal silica spheres and cationic colloidal fibrils of alumina. This paper foreshadowed some later work by others in suggesting several classes of materials that could be used as film components, including cationic and anionic polyelectrolytes. Films formed by the adsorption of organic and/or inorganic polyelectrolytes have more recently been investigated for modifying electrode surfaces,³² for molecular sensing,³⁵ and offer promise for use as antistatic coatings.³⁴

Attempts to form well-ordered films by self-assembly have met with inherent difficulties, however. For example, films produced by the adsorption of individual monomers, though commonly exhibiting regular ellipsometric growth, become increasingly disordered as additional layers are added unless each reaction cycle results either in quantitative reaction or in the filling of gaps associated with sites that failed to react in previous cycles (Figure 1.3).³⁶ We believe that it is at least partially due to this limitation that XRD patterns of films formed on flat substrates tend not to exhibit distinct Bragg peaks.^{27,36} One approach that obviates the problem of loss of sites involves the successive adsorption of oppositely charged polyelectrolytes.^{30–32,34} Interpenetration of the components in such systems,³⁷ however, decreases the attainable degree of structural order in the direction normal to the substrate surface (Figure 1.4).

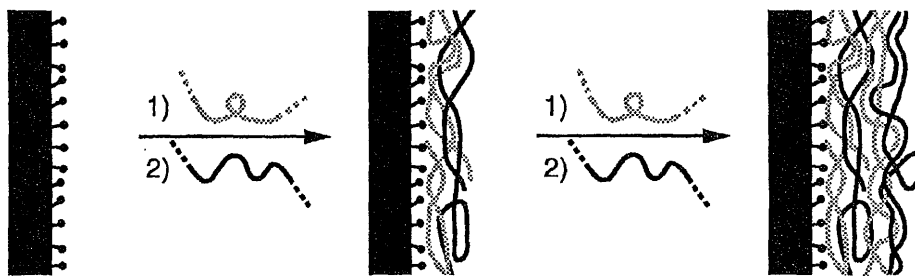


Figure 1.4. Formation of a multilayered film by alternate adsorption of anionic and cationic polyelectrolytes onto a pretreated surface. Significant interpenetration of the components limits the degree of structural order attainable in such systems.

PART TWO: OUR PRELIMINARY STUDIES ON MULTILAYERED FILMS

Before beginning the project that constituted the majority of my doctoral research, we pursued various new synthetic approaches to the formation of multilayered films. These approaches are reviewed briefly in the sections that follow.

1.3 Thin Films of Titanium Dioxide

(This section is reprinted in part from Kleinfeld, E.R.; Ferguson, G.S. In *Molecularly Designed Ultrafine/Nanostructured Materials*; Gonsalves, K.E.; Chow, G.M.; Xiao, T.D.; Cammarata, R.C., Eds.; Mater. Res. Soc. Symp. Proc. 351; Materials Research Society: Pittsburgh, PA, 1994; p 419. Copyright 1994 Materials Research Society.)

1.3.1. Background. Several groups have reported that a single atomic layer of titanium dioxide could be formed by the reaction of a titanium (IV) alkoxide from the vapor phase³⁸ or from solution³⁹ at the surface of hydrated silica gel, via a reaction similar to that used for the production of relatively thick films by the sol-gel method.^{40,41} Use of this high-surface-area substrate allowed some uncertainty to remain, however, as to whether the titanium dioxide had adsorbed as a dense and complete monolayer, or as thick islands of material having the same mass as *expected* from a monolayer. We investigated the adsorption of ultrathin layers of TiO₂ by forming them on well-defined substrates, polished silicon wafers. The native oxide on a silicon wafer, while not possessing the high surface area of silica gel, does undergo similar surface chemistry. Flat substrates allow characterization of overlayers by various techniques such as optical ellipsometry, angle-resolved x-ray photoelectron spectroscopy, and x-ray reflectivity, which do not lend themselves to analysis of high-surface-area materials. Films of oxides formed on silicon wafers can therefore aid in the thorough characterization of surfaces of catalytic interest. In addition, methods developed to form ultrathin films on single-crystal silicon

substrates may be adaptable to allow preparation of multilayers incorporating more than one type of material, which could potentially serve as components for vacuum-ultraviolet/soft-x-ray optics.

1.3.2. Sample Preparation. Titanium dioxide films were prepared as follows. A clean silicon wafer was imported into a glovebox containing a dry nitrogen atmosphere. It was immersed for 30 s in a ~5 mM solution of titanium (IV) tetra-*n*-butoxide in dry toluene (distilled from sodium) and subsequently rinsed with dry toluene. The wafer was then exported from the glovebox and again rinsed with dry toluene. The sample was then rinsed with purified water both to aid in hydrolysis of any unreacted butoxy groups and to remove any adsorbed water-soluble contaminants. Second and subsequent layers were adsorbed by repeating this procedure (Figure 1.5).

1.3.3. Characterization and Discussion. The thickness of the titanium dioxide films was measured by optical ellipsometry (Rudolph Auto-EL III), assuming a refractive index of 1.76 (appropriate for amorphous TiO₂⁴²). If this number was varied to as high a value as 2.1, ellipsometric thicknesses decreased by less than 0.02 nm, so that the exact index used was not critical for these extremely thin films. Initial adsorptions onto clean silicon wafers yielded films with thicknesses of approximately 0.3–0.4 nm. This layer thickness was independent of the amount of time that the substrate spent in the adsorbate solution, over the range that we measured (30 s to 4 days), indicating that the limiting reagent was the hydroxyl groups on the surface of the wafer (silanols and adsorbed water) and not residual water in the solvent. Consistent with the proposed reaction scheme, no adsorption occurred on wafers that had been pre-treated with octadecyltrichlorosilane to provide an unreactive surface of low free energy.

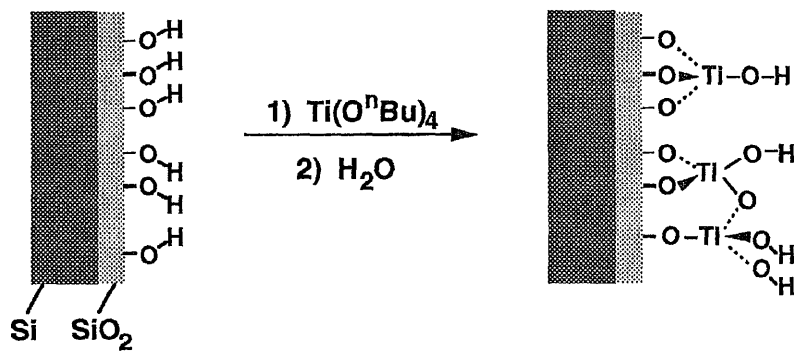


Figure 1.5. Schematic illustration of the adsorption cycle that was repeated to form an ultrathin film of TiO_2 .

As repeated adsorptions were performed on the same wafer, ellipsometric measurements indicated that the thickness of the TiO₂ layer increased linearly. Figure 1.6 shows that the thickness of the first layer and the slope of thickness *vs.* number of adsorptions were not perfectly consistent from day to day, though they were highly consistent for different wafers prepared on a particular day. This variability might have been associated with variations in temperature or in the level of residual water in the glovebox. The intercepts of the linear least-squares fits to the data were always non-zero (~0.2–0.3 nm), implying that a greater amount of TiO₂ was adsorbed in the first cycle than in subsequent cycles (slopes ~0.1 nm/cycle). Alternatively, the non-zero intercepts could be due to a layer of adventitious contamination adsorbed at the outer surface of the TiO₂ due to its high surface free energy. Control wafers that were treated with the same rinsing procedure as the experimental wafers—but not immersed in a titanium butoxide solution—did not adsorb sufficient contamination to account for the non-zero intercepts. The expected thickness of an amorphous TiO₂ monolayer, calculated assuming tetrahedral coordination of each titanium to four oxygen atoms, and using tabulated covalent radii⁴³ is 0.335 nm. These results thus indicate that, whereas a dense and complete monolayer may have adsorbed in the first cycle, less than this amount of material adsorbed in subsequent cycles.

We expected the TiO₂ layers to have an amorphous network structure, because they were formed at low temperatures via surface alcoholysis, involving nearly thermoneutral exchange of one oxygen ligand for another. Two experimental results were consistent with this expectation. First, the layers dissolved in isopropanol, indicating that the titanium atoms were accessible to nucleophiles. Second, no peaks associated with known phases of crystalline TiO₂ were present in x-ray diffractograms of these samples. This latter result should be interpreted with

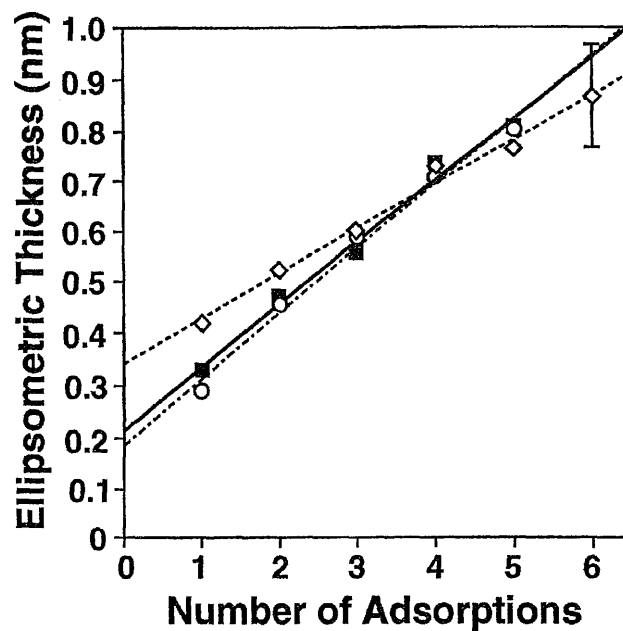


Figure 1.6. Ellipsometric thickness of a TiO_2 overlayer as a function of the number of adsorption cycles. Each symbol represents the average of layer thicknesses measured on three samples treated side-by-side. Different shapes (and the corresponding linear least-squares fits) represent experiments performed on different days. The error bar represents the largest range in data observed among any three samples prepared on a single day; a typical range was 50–75% of the one shown.

caution, however: while the absence of peaks does provide evidence against the formation of large, isolated crystallites of anatase or rutile, uniform films as thin as the ones studied, even if crystalline, might give rise to peaks broadened to the point of being undetectable. Amorphous films of TiO₂ prepared by atomic layer epitaxy⁴⁴ have been reported to undergo transitions to the crystalline phases anatase and rutile upon heating to 350 and 550 °C, respectively; we expect that similar densification and crystallization of the amorphous networks formed by our method would have occurred upon annealing, an avenue of inquiry that was not explored.

The elemental composition of the adsorbed films was determined by XPS (Scienta ESCA-300). The spectra of wafers with 1–5 TiO₂ layers contained peaks due to titanium as well as silicon, oxygen, and carbon; some of the wafers also showed trace amounts of contamination by fluorine (most likely from the fluoropolymer tweezers and reaction vessels used) and nitrogen. A representative survey spectrum from a sample with 3 TiO₂ layers is shown in Figure 1.7. The expected intensity of the Ti photoemission from an overlayer is given by equation (1):⁴⁵

$$I(\text{Ti}) = I_{\infty}(\text{Ti}) [1 - \exp(-d/\lambda \cos\theta)] \quad (1)$$

where $I(\text{Ti})$ is the observed intensity; $I_{\infty}(\text{Ti})$ is the intensity that would be observed for an infinitely thick sample of TiO₂; d is the thickness of the TiO₂ overlayer, λ is the inelastic electron mean free path (assumed to be 2.5 nm⁴⁶); and θ is the detector angle, with 0° defined as the surface normal. Similarly, the substrate photoemission, that from elemental and oxidized silicon, should be attenuated exponentially by the TiO₂ overlayer as shown in equation (2):

$$I(\text{Si}) = I_o(\text{Si}) \exp(-d/\lambda \cos\theta) \quad (2)$$

where $I_o(\text{Si})$ is the intensity that would be observed in the absence of the overlayer. Either signal may in addition be attenuated exponentially by an overlayer of contamination. Figure 1.8 shows the intensity of the Ti 2p signal, measured at 0° (i.e.,

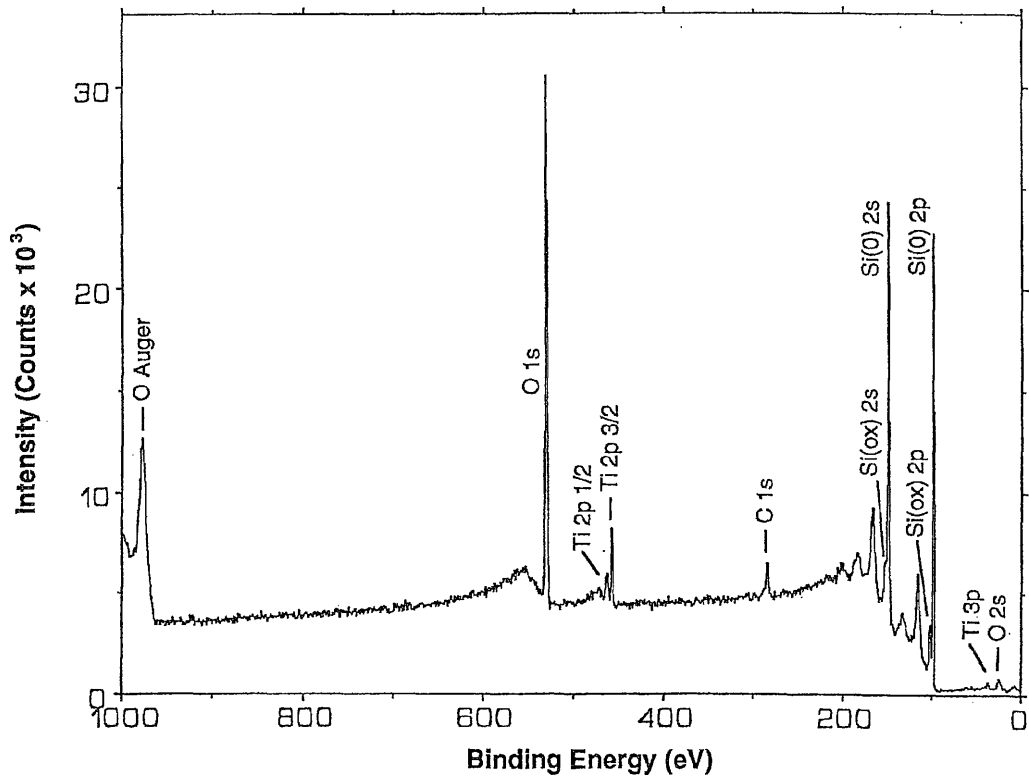


Figure 1.7. X-ray photoelectron survey spectrum of a 3-layer film of TiO_2 on a silicon wafer. The spectrum was obtained at a take-off angle of 90° (i.e., normal emission).

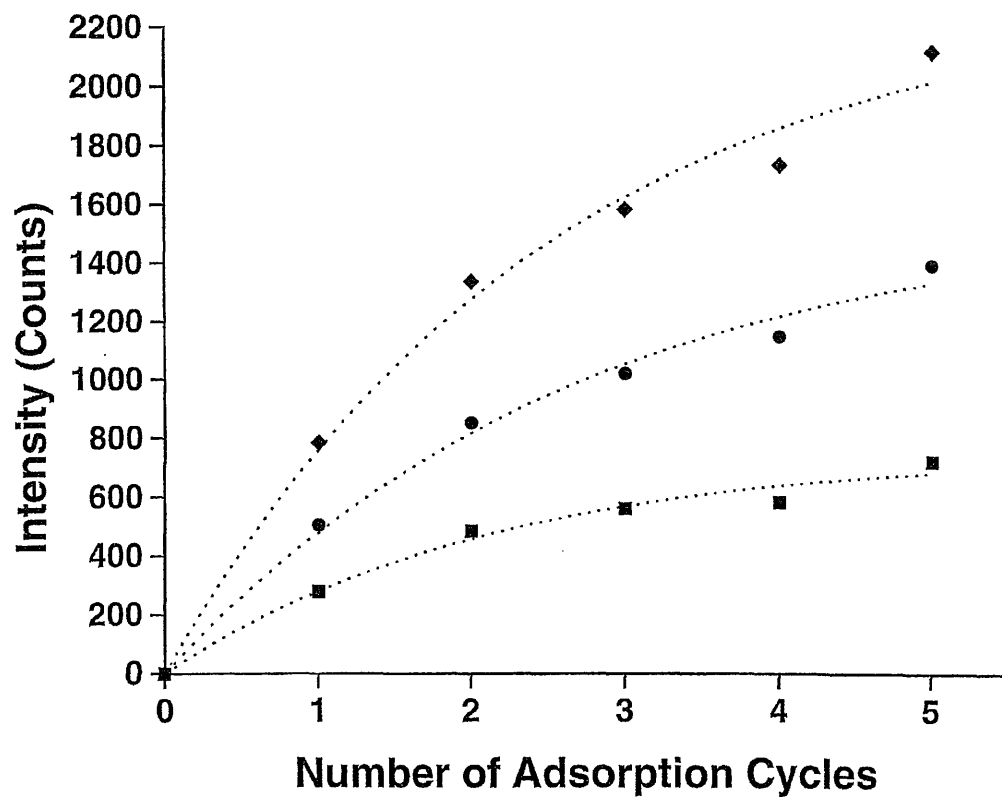


Figure 1.8. Intensity of Ti 2p photoemission as a function of the number of adsorption cycles: squares—Ti 2p_{1/2}; circles—Ti 2p_{3/2}; diamonds—Ti 2p_{total}. The data were fit using equation (1), yielding optimized values of growth per cycle of 1.2, 0.9, or 1.0 nm, respectively. A value of 2.5 nm for the inelastic electron mean free path was assumed.

normal emission), as a function of the number of adsorption cycles. Assuming $\lambda = 2.5$ nm, the variables in equation (1) were optimized to fit the data for photoemission from the Ti 2p_{1/2} region, the Ti 2p_{3/2} region, or the entire Ti 2p region. The results for these regions indicated that the film growth was 1.2, 0.9, or 1.0 nm per cycle, respectively. Figure 1.9 shows the attenuation of the oxidized and non-oxidized silicon peaks with the number of TiO₂ overlayers. The observed attenuation indicates that the TiO₂ layers were approximately 0.1 nm in thickness on average, which is consistent with the ellipsometric results given earlier, but does not indicate that the initial adsorption was thicker than any subsequent adsorption. The order-of-magnitude difference between the results obtained from the Ti photoemission and the Si photoemission is troubling, and has not been resolved satisfactorily.

Angle-resolved XPS measurements were obtained to investigate whether the TiO₂ formed islands or gave smooth coverage of the substrate after one cycle. The normalized intensity of photoemission from an overlayer of a given adsorbate as a function of angle is given by equation (3):

$$\frac{I}{I_n} = \frac{\beta [1 - \exp(-d/\beta\lambda\cos\theta)] \exp(-d'/\lambda\cos\theta)}{\beta [1 - \exp(-d/\beta\lambda)] \exp(-d'/\lambda)} \quad (3)$$

where I is the intensity of photoemission at a given angle, I_n is the intensity at 0° (i.e., normal emission), β is the fraction of the surface covered by the adsorbate, d is the average thickness of the adsorbed layer, and d' is the thickness of a uniform overlayer of contamination.^{45,47} The optimal least-squares fit to equation (3) was obtained with the following values: λ , 2.5 nm (for such a thin layer, varying this parameter within the range of 1.25 to 5.0 nm made almost no difference); d , 0.2 nm; β , 1.0; d' , 0.2 nm. Despite simultaneous optimization of all these parameters, however, the data were not satisfactorily fit for detector angles between 50° and 65° from the surface normal. Furthermore, the theoretical lines shown in Figure 1.10 for

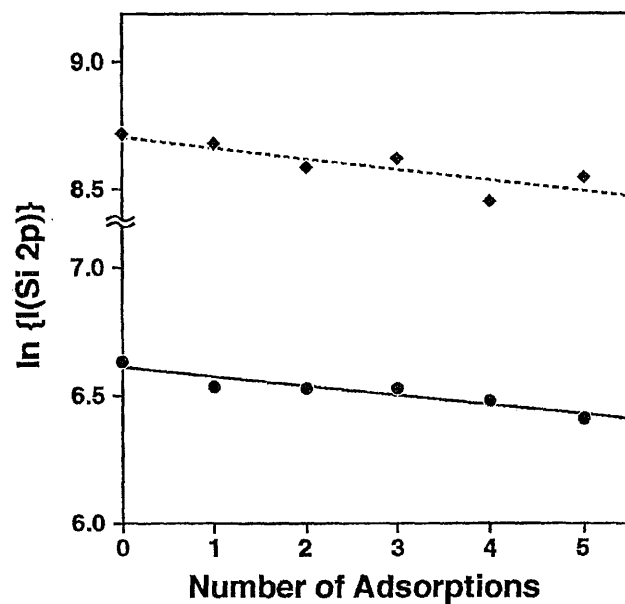


Figure 1.9. Natural logarithm of the intensity of Si 2p photoemission (circles—oxidized silicon; diamonds—elemental silicon). The linear least-squares fit to the data indicated growth per cycle of 0.1 nm. A value of 2.5 nm for the inelastic electron mean free path was assumed.

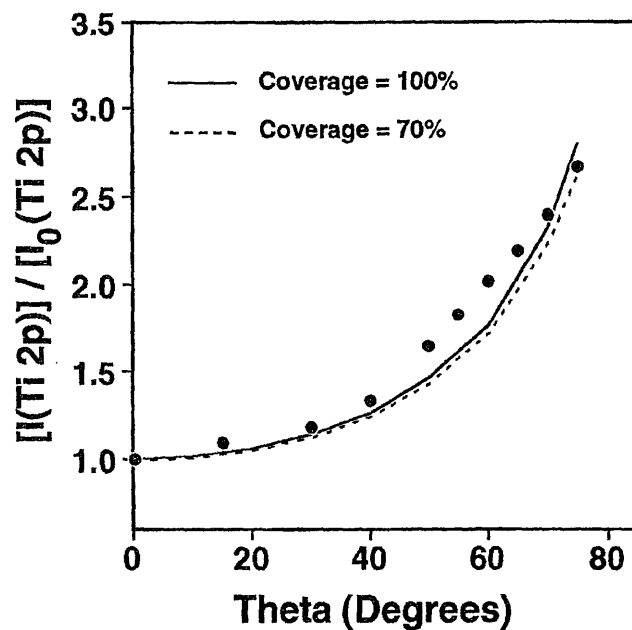


Figure 1.10. Normalized intensity of the Ti 2p photoemission as a function of the angle between the surface normal and the detector. Lines shown are optimized fits to the data, assuming the inelastic electron mean free path (λ) to be 2.5 nm. Results indicate that the TiO₂ overlayer thickness was 0.2 nm, and that it was covered with a layer of contamination that was 0.2 nm in thickness. Lines for 100% and 70% coverage are shown to illustrate the insensitivity of this analysis to the surface coverage for such a thin overlayer.

100% and 70% coverage, with other parameters assuming the ideal values given above, demonstrate that for films as thin as this one, variations in coverage have little effect on the fit to the data. Consequently, although the best fit to the data was obtained for 100% coverage, we cannot conclude that full coverage was in fact obtained.

1.3.4. Summary. This work demonstrated that films of titanium dioxide could be grown layer-by-layer on silicon wafers via chemical methods that should form strong bonds between the TiO₂ overlayer and the substrate. The ellipsometric results indicated that the limited number of reactive sites (surface hydroxyls) restricted growth to one monolayer or less per adsorption cycle. Ellipsometry further indicated that the first adsorbed layer was thicker than subsequent layers, but that the film thickness increased linearly as more layers were adsorbed. X-ray photoelectron spectroscopy gave internally inconsistent results regarding the formation of the overlayers. Whereas Ti photoemission indicated that each adsorbed layer was approximately 1 nm in thickness, Si photoemission was more consistent with the ellipsometric results in indicating that each adsorbed layer was of the order of 0.1 nm in thickness. Neither of the photoemission results indicated that the first TiO₂ layer was thicker than subsequent layers; this result indicates that the ellipsometric results were influenced by a layer of contamination that adsorbed along with the first titanium layer.

While repeated treatments with titanium butoxide and water did provide films that grew regularly, the process was very time-consuming: forming a 5-cycle film (less than 1 nm in thickness) on a set of samples was a full day's work. As such, we sought a method that would allow more facile formation of films of practical thickness.

1.4 Toward Composite Films from Sheet Silicates and Monomeric Cations

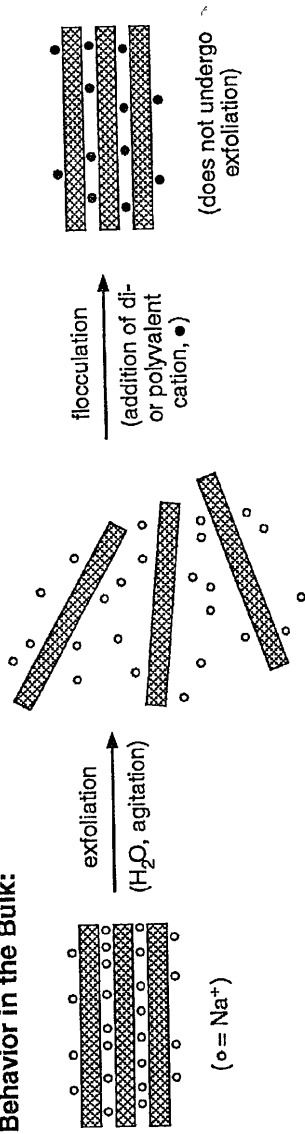
As mentioned earlier, achieving structural order in multilayered films formed by adsorption of components from solution is difficult. Alternate adsorption and activation of SAMs can lead to the propagation of defects (Figure 1.3), while alternate adsorption of oppositely charged polyelectrolytes can lead to interpenetration of adjacent layers (Figure 1.4). One strategy for avoiding both of these difficulties would be to incorporate a sheet-like component into each repeat unit of the monolayer. To this end, we attempted the stepwise assembly of films by treating surfaces alternately with an anionic aqueous suspension of a sheet silicate and an aqueous solution of a cationic species. We hoped that the adsorption of intact crystalline sheets by ion exchange would provide a stepwise approach to the formation of designer intercalation compounds at surfaces, while also proving to be more versatile than techniques relying upon the formation of covalent bonds. Furthermore, we hoped to observe a high degree of structural order in the resulting films, due to the tendency of silicate sheets to orient parallel.⁴⁸

The ability of some sheet silicates to exfoliate in aqueous suspension into single anionic sheets with a very high aspect ratio has been thoroughly studied.⁴⁹ Laponite RD, in particular, is a synthetic form of hectorite designed to disperse rapidly under a small applied shear. Given that the presence of di- or polyvalent cations in even trace concentrations causes flocculation of silicate suspensions,⁵⁰ our first approach was to form composite films by treating a surface alternately with a silicate suspension and a solution of a divalent cation (Ca^{++}) to cause repeated “flocculation” of single layers of silicate sheets onto a surface (Figure 1.11).

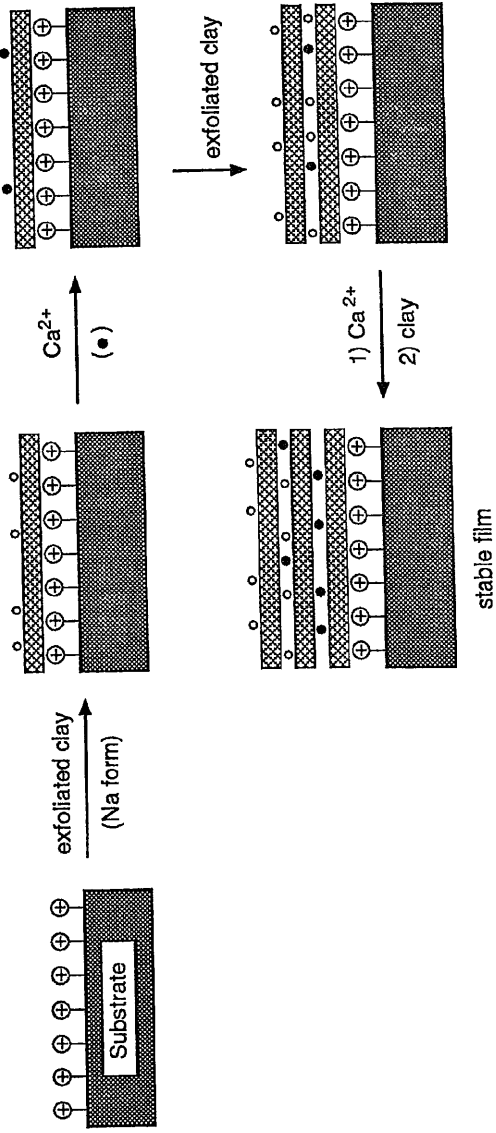
The strong affinity of sheet silicates for ammonium compounds has been well documented.⁵¹ To promote the adsorption of the first silicate layer, a silicon wafer was therefore treated with *N*-trimethoxysilylpropyl-*N,N,N*-trimethylammonium

Figure 1.11. Schematic illustrations of: a) exfoliation and flocculation of a sodium smectite (e.g., Laponite); and b) a surface analog to this behavior that was proposed for the formation of a stable multilayered film.

a) Behavior in the Bulk:



b) Proposed Surface Analog:

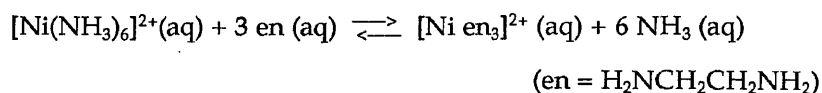


chloride, TTA [(MeO)₃Si(CH₂)₃N(CH₃)₃⁺ Cl⁻], to provide a surface bearing ammonium groups. Although subsequent treatment with a freshly prepared, partially neutralized Laponite suspension did result in a small increase in thickness (0.3–0.4 nm),⁵² additional treatments with Ca⁺⁺ and silicate resulted in either an insignificant increase in thickness or a small decrease in thickness. We inferred that this scheme was failing due to two inherent problems: first, there was no obvious driving force for the adsorption of calcium ions in excess of the amount needed to neutralize the surface charge of the silicate; and second, rinsing the surface with water following a Ca⁺⁺ treatment could allow this ion to be exchanged for protons. This preparative scheme was not pursued at length, and the results of these experiments should be viewed as preliminary, having been obtained before we understood how best to prepare fully exfoliated Laponite suspensions. In subsequent experiments under optimized conditions, however, alternate treatments with Al³⁺ and Laponite also resulted in poor growth which nearly ceased altogether within a few cycles, suggesting that the experiments with Ca⁺⁺ and Laponite had reached a valid conclusion,³⁰ even if the experimental conditions had not been optimized.

1.5 Toward Multilayered Films from Silicates and Crosslinked Cationic Networks

Having encountered some difficulty in forming films from sheet silicates and monomeric cations, we considered the possibility of adsorbing monomers that could later be crosslinked to form a cationic bilayer, such as TTA. We hypothesized that the strong affinity of ammonium compounds for sheet silicates⁵¹ would allow a monolayer of this compound to adsorb, and that the terminal silane functionality would allow not only crosslinking within the adsorbed layer but also subsequent adsorption of a second layer in an orientation opposite to that of the first. This

crosslinking was expected to stabilize the adsorbed layer, both during and after its formation, by a mechanism related to the “chelate effect” of coordination chemistry. This entropic effect is responsible, for example, for causing the equilibrium in the following chemical equation to lie much farther to the right than would be expected solely from enthalpic considerations:⁵³



The process of coordinating three ethylenediamine molecules liberates six ammonia molecules, providing a significant entropic driving force for the forward reaction. An alternative, more intuitive explanation of the reason for this phenomenon is that once one end of an ethylenediamine molecule is coordinated to the nickel center, the second amine group on the same molecule is held in the vicinity of the metal center as well, making its coordination more likely than if it were part of a free molecule in solution. One related practical implication of this effect is that once both amine groups on a single ethylenediamine molecule are coordinated to the nickel center, loss of that ligand can only occur if both groups are simultaneously displaced from the metal center. By extension to our system, treatment of a silicate-terminated sample with a solution of monomeric cations may result in their adsorption onto the anionic silicate surface. Upon rinsing this surface or treating it with a silicate suspension, however, the cations may be displaced by protons from the contacting water. A cross-linked cationic layer, in contrast, should be more difficult to displace from the surface due to a “surface-chelate” effect: in order for such a species to be displaced, the multiple points of attachment would have to be broken simultaneously. This hypothesis is depicted schematically in Figure 1.12. Thus we proposed a three-step adsorption cycle in which a substrate would be alternately treated once with clay and twice with the silane (Figure 1.13, treatments 3 – 6).

Figure 1.12. Schematic illustration of the proposed "surface chelate effect." In (a), each adsorbed monomeric cation is, due to its limited size, most likely associated with only one or two negative sites on the silicate sheet. These ions are therefore readily lost to a silicate suspension to which the sample is exposed in a subsequent step. For entropic reasons, few of the ions that leave the surface are likely to re-adsorb. In contrast, the species depicted in (b) is bound to the silicate sheet through multiple points of attachment. Although the conformation of this adsorbed species may change, with individual sites adsorbing or desorbing from the silicate sheet, the large number of sites that would have to desorb simultaneously in order for the entire molecule to be lost makes such an event unlikely.

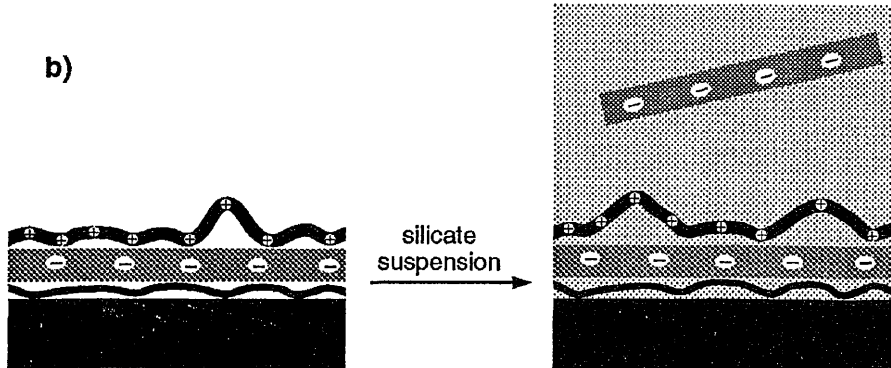
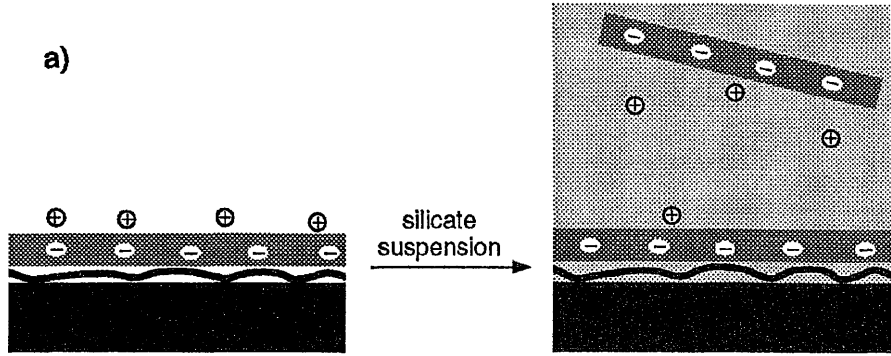
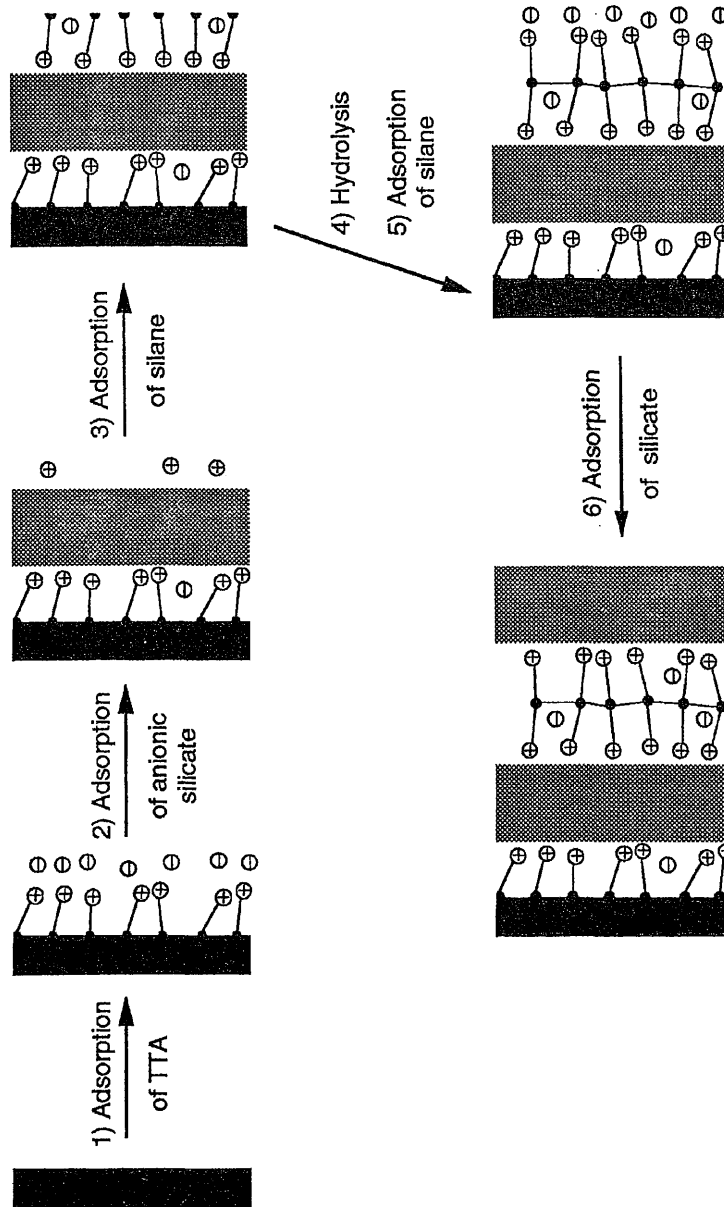


Figure 1.13. Schematic representation of the first steps in the formation of a multilayered film by successive treatments with N-trimethoxysilylpropyl-N,N,N-trimethylammonium chloride (TTA) and an anionic sheet silicate.



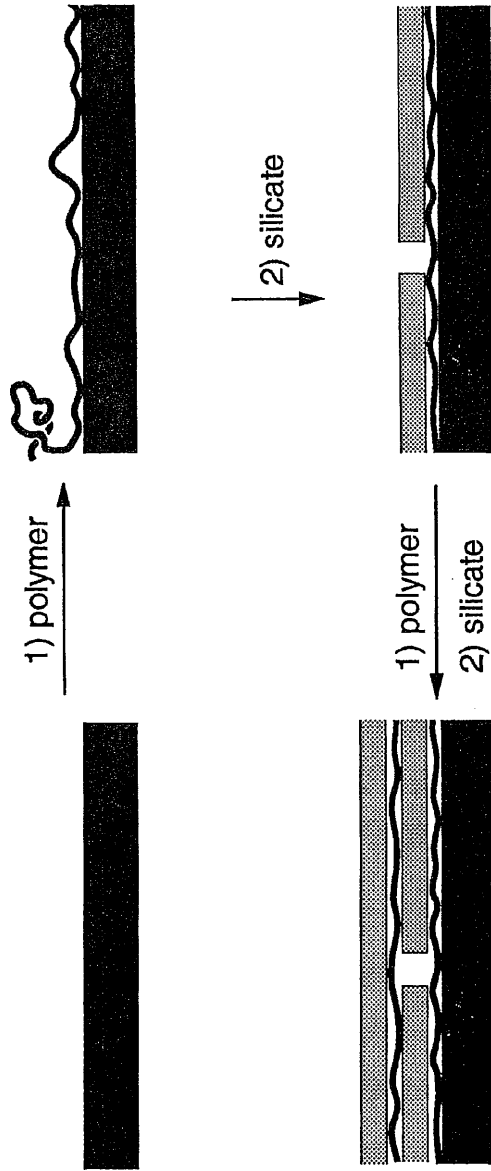
To promote adhesion between the substrate and the first silicate sheet, we treated silicon wafers with TTA in chloroform to provide a positively charged surface, and then treated the surface with Laponite (0.2% w/w, brief dip), which led to adsorption of a layer of the silicate 0.7 – 0.9 nm in thickness. The ellipsometric growth observed in steps 3 – 6 was about half of that expected for each adsorbed layer. The principal difficulty with this approach appeared to be the instability of the crosslinked silane bilayer with respect to dissolution or desorption upon treatment with the basic Laponite suspension. In addition, the long reaction times necessary for silane adsorption (~15 min) and hydrolysis (hours) were inconvenient for the preparation of many-layered samples.

1.6 Formation of Films from Cationic Polyelectrolytes and Sheet Silicates

The difficulties in forming multilayered films from monomeric silanes and sheet silicates prompted us to try a cationic polyelectrolyte in place of the silane. Presumably, as had been expected from the silane, a cationic polyelectrolyte would adsorb to an anionic clay sheet due to Coulombic interactions, and be stable with respect to desorption from the surface due to a chelate effect. If the amount that adsorbed was sufficient to invert the surface charge to positive, this new surface should allow adsorption of an additional clay sheet in a subsequent step (Figure 1.14).³³ This scheme succeeded nearly from the first attempt, and provided a very rich system for further study, as described in detail in the several chapters that follow. A brief overview of these studies is presented below.

Films were formed by alternate treatments with an aqueous solution of a cationic polyelectrolyte and an aqueous suspension of an exfoliated silicate. This method was distinguished from other methods for the formation of multilayered films that were based upon self-assembly or electrostatic assembly by the speed and ease of

Figure 1.14. Schematic representation of the preparation of a multilayered film by alternate adsorption of a cationic polyelectrolyte and individual sheets of an anionic sheet silicate.



film formation: typical reaction steps used in literature methods take between 15 minutes and several hours; we observed regular and reproducible growth when treatments lasting only 5 s were used. X-ray diffractograms of our multilayered films indicated that they were much more highly ordered than any previously reported films prepared by adsorption from solution onto flat substrates and exhibited a lattice spacing of ~1.45 nm in the direction normal to the substrate surface.

This method offered further advantages in the areas of versatility in choice of film components and ease and simplicity of film preparation. Adjacent layers in films that have been formed by the self-assembly of small molecules²¹⁻²³ are typically held together by covalent bonds; such methods are therefore limited to certain combinations of precursors. The mechanism of formation of our films (ion exchange) allowed films to be formed from a variety of polycationic and polyanionic precursors, as demonstrated by us^{33,54} and others.⁵⁵

The films offer an interesting system for both fundamental study and technological applications. As noted earlier, we were intrigued by the challenge of building complex, ordered structures from simple precursors. Toward this end, much of my effort has been directed toward investigating the effects on film growth characteristics and film structure caused by modifying various relevant parameters, including polymer concentration, adsorption time, and identity of cationic polyelectrolyte, silicate mineral, and substrate. These topics are covered in detail in Chapters 2, 3, 7, and 8.

Several early but key observations about the films' characteristics or properties inspired many of the studies we undertook. For example, having noted that the films responded to changes in ambient relative humidity, we characterized this response using both ellipsometry and micro-gravimetry. We found not only that a film's thickness increased by 22% upon a change in its environment from low to high

humidity, but also that this remarkable transformation was largely complete within seconds after the humid environment was introduced. This study is detailed in Chapter 5.³⁵

A second study was based upon our inference that the “two-dimensional” nature of the silicate sheets allowed defects that had occurred in any given cycle to be patched over, or “healed,” in subsequent cycles. We tested the limits of this behavior by forming PDDA/Laponite films on surfaces resistant to adsorption of either component individually: methyl-terminated SAMs on silicon dioxide and silver. This study, detailed in Chapter 4, revealed that islands could initially form at isolated imperfections in the SAMs and then grow vertically and laterally as repeated cycles were performed, eventually coalescing to cover the surface of the SAM.⁵⁶

The films’ transparency and uniformity suggested their potential usefulness in optical applications. We were especially interested in their use as anti-reflective coatings and as a medium for holographic data storage. With these goals in mind, we synthesized and grafted a photochromic dye onto poly(vinylpyridine) to create a cationic polyelectrolyte, and used this polymer in the stepwise formation of composite multilayered films. These films not only exhibited photochromic behavior, but also eliminated roughly half of the reflection losses exhibited by the air/fused quartz interface. This study is detailed in Chapter 7.

1.7 Materials and Methods

A few materials and instruments were central to the completion of my doctoral research. Specific details regarding the preparation and handling of these materials and the operating parameters for these instruments are presented here; modifications to these procedures are noted where applicable.

1.7.1. Preparation of Silicon Substrates. The overwhelming majority of the

composite films were prepared on silicon wafers. These wafers (Wacker Siltronic, supplied by WaferNet, Inc., San Jose, CA) were (100)-oriented, p-doped (boron), and 0.50–0.55 mm in thickness. The nature and level of doping were not expected to influence film formation or structure. Before use, wafers were typically broken into 1-cm x 2.5-cm pieces. Because the wafers were single crystals, they could simply be nicked at the edge with a diamond scribe and snapped into rectangular pieces with gloved hands. The scribe was then used to label each sample with a serial number on the unpolished side. The silicon dust generated by the scribing process was removed by swabbing the backs of the pieces with a cotton swab (plastic stem) saturated with ethanol, and the samples were then stored in individual glass vials until use. The use of ethanol in the swabbing step is important, as some other common solvents (e.g., isopropanol) leach an unidentified substance from the swabs that transfers to the silicon wafers and can be difficult to remove.

Shortly before they were to be used, wafers were swabbed on the polished side with ethanol, rinsed with purified water (Millipore Milli-Q, $\geq 15 \text{ M}\Omega\text{-cm}$), and placed into a glass or Teflon container. A 2:1 solution of concentrated sulfuric acid and 30% hydrogen peroxide (Caution: significant heat is evolved upon mixing these two chemicals, and the resulting “piranha solution” can react violently with organic substances!) was poured over the wafers, which were then allowed to soak for at least 30 min. The piranha solution was then poured into a large water bath and neutralized, and the wafers were rinsed several times with purified water. As the final cleaning step, wafers were removed from the rinse water with teflon (or teflon-coated) tweezers, rinsed with purified water from a wash bottle, and blown dry with a jet of nitrogen. Following cleaning, wafers were stored in teflon vials until use. If a wafer that had been cleaned within approximately the preceding four days was completely wettable by water (i.e., if rinse water did not bead up from any part of

the wafer) it was typically used without further cleaning. Wafers older than this, and non-wettable wafers of any age, were re-cleaned, beginning with a treatment with piranha solution.

1.7.2. *Silicate Suspensions.* Laponite RD. Laponite RD was provided as a white, free-flowing powder by Southern Clay, Inc., Gonzales, TX, and was used as received. To approximately 50 mL of water in a base-bath-cleaned, 100-mL volumetric flask was added 0.5 g Laponite RD powder with rapid stirring. To prevent clumping of the powder, it was added to the water in very small increments (a “dusting”). The turbid suspension was then diluted to 100 mL with additional purified water and allowed to stir for several hours or until clear. Suspensions prepared on a given day were not used until the following day, in order to allow full separation of the individual platelets. This 0.5% stock suspension could be used for several months, and was typically diluted to 0.2% w/w with purified water before use. Individually prepared portions of 0.2% suspensions were used within one week of preparation: since they were in active use, they were believed to be at greater risk of contamination.

Montmorillonite. Sodium-ion-exchanged sodium montmorillonite was provided as an aqueous suspension by Southern Clay, Inc., and was centrifuged and diluted before use. A Sorvall RC-5B Refrigerated Superspeed Centrifuge, equipped with a GSA rotor, was used at ~20°C to obtain a slightly turbid suspension containing the <0.046 μm-diameter fraction. The centrifuging conditions were calculated using equation (4):⁵⁷

$$D^2 = C \frac{\eta \log_{10}(R/S)}{t (N^2) (\Delta s)} \quad (4)$$

in which D is the maximum particle diameter left in suspension, in μm; C is a

constant having the value 6.30×10^{10} (this number is unitless other than conversion factors among various SI units and allows numbers with convenient units to be used directly); η is the viscosity of the medium, in Pa s (for water at 20°C, $\eta = 0.001005$ Pa s [equivalent units: $\text{kg m}^{-1} \text{s}^{-1}$]); R is the distance to the sediment from the center of the rotor; S is the distance to the meniscus of the suspension from the center of the rotor; t is the centrifugation time in minutes; N is the centrifuge speed in revolutions per minute; and Δs is the difference in density between the particles and the medium (1.502 g/mL for montmorillonite in water at 20°C). The suspension was centrifuged at 3050 rpm for 30 min and 8800 rpm for 38 min, with $S = 11.8$ cm and $R = 16.5$ cm (using an estimated sediment thickness of 0.3 cm). Following centrifugation, the composition of the suspension was determined by drying three separate aliquots of the suspension, ~10 g each, in 20 mL glass scintillation vials for 24 h at 150°C. The vials were removed from the oven, immediately capped, cooled to room temperature, opened briefly to release the partial vacuum inside, and their mass determined. The suspension composition determined by this analysis [0.33% (w/w)] should be interpreted with caution, as it is strongly dependent upon the temperature used to dry the samples (clays lose mass incrementally up to temperatures in the hundreds of degrees Celsius⁵⁸) and to the subsequent treatment of the samples (after 5 h exposure to ambient temperature and humidity, the mass of the clay solids increased 15–18%, a change attributable to the sorption of atmospheric water⁵⁹). The montmorillonite suspension was typically diluted from 0.33% to 0.20% (w/w) with Milli-Q water before use. Individual diluted portions were used within one week.

1.7.3. Ellipsometry. The growth of the multilayered films was monitored under ambient conditions using optical ellipsometry (Rudolph Auto-EL III nulling ellipsometer). Measurements were made with HeNe laser light ($\lambda = 632.8$ nm) at an angle of incidence (ϕ) of 70°, employing the manufacturer's program 211000. This

program operates under the assumption that the substrate is elemental silicon with an index of refraction (n) of $3.858 - 0.018i$. The thickness of the native oxide on the elemental silicon substrates was measured using an assumed index of 1.50 prior to adsorption of the film of interest. Calculations of film thickness typically assumed a refractive index of 1.50, and were made with the further assumption that the multilayered film and the native oxide (SiO_2) comprised a single smooth film on the elemental silicon substrate.

1.7.4. X-Ray Diffractometry. X-ray diffractometry was performed in the Department of Earth and Environmental Sciences, Williams Hall. Samples had to be broken before use to approximately 1.5 cm x 1 cm to fit into the well in the sample mount. As depicted in Figure 1.15, one or two small beads of modeling clay (~3 mm in diameter) were placed into the well, and the sample was placed on top of them. It was found to be advantageous to rotate the sample slightly away from “square” in the plane of the mount to eliminate from the resulting diffraction pattern a peak at $33^\circ 2\theta$, which was attributed to the forbidden (200) reflection of silicon. Two base-bath-cleaned glass microscope slides were used, edge on, to press the sample down into the well until its face was flush with the mount. Alignment of the sample was confirmed in two ways: first, by viewing the sample at a grazing angle; and second, by pressing down on the sample with the glass slides again while viewing it from this perspective. Any motion during pressing indicated that the sample was not well aligned. For analysis, the Philips APD 3720 powder diffractometer was operated in $\theta/2\theta$ mode using monochromatized $\text{CuK}\alpha$ radiation ($\lambda = 0.154$ nm) and operating at 45 kV and 30 mA. Data were obtained using a 0.05° step and 3 s/step collection time.

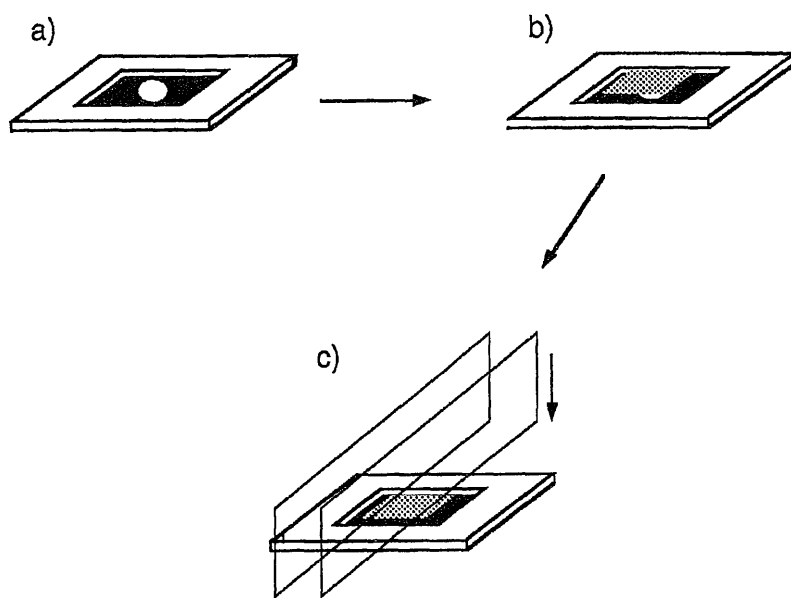


Figure 1.15. Steps in mounting a sample for analysis by x-ray diffractometry: (a) one or two balls of clay ~ 3 mm in diameter are placed in the well of a mount; (b) a sample is placed on the ball(s) of clay; (c) two glass slides are used edge-on (and at the edges of the sample) to press the sample down until it is flush with the surface of the mount.

1.8 References and Notes

1. Slaughter, J.M.; Falco, C.M. *Nucl. Instr. Meth. Phys. Res.* **1992**, A319, 163.
Underwood, J.H.; Barbee, T.W., Jr. *Appl. Optics* **1981**, 20, 3027.
2. Vašíček, A. *Optics of Thin Films*; Interscience: New York, 1960; Chapters 3 and 4.
3. Ungashe, S.B.; Wilson, W.L.; Katz, H.E.; Scheller, G.R.; Putvinski, T.M. *J. Am. Chem. Soc.* **1992**, 114, 8717. Keller, S.W.; Johnson, S.A.; Brigham, E.S.; Yonemoto, E.H.; Mallouk, T.E. *J. Am. Chem. Soc.* **1995**, 117, 12879.
4. Ozin, G.A. *Adv. Mater.* **1992**, 4, 612.
5. Stucky, G.D. *Progress in Inorganic Chemistry*; Wiley: New York, 1992; Vol. 40, p 99. Stucky, G.D.; MacDougall, J.E. *Science* **1990**, 247, 669.
6. Yan, Y.; Bein, T. In *Synthesis/Characterization and Novel Applications of Molecular Sieve Materials*; Bedard, R.L.; Bein, T.; Davis, M.E.; Garces, J.; Maroni, V.A.; Stucky, G.D., Eds.; Mater. Res. Soc. Symp. Proc. 233; Materials Research Society: Pittsburgh, PA, 1991, p 175. Cao, G.; Mallouk, T.E. *Inorg. Chem.* **1991**, 30, 1434.
7. For a discussion of the importance of “soft-chemical” approaches for the formation of films and bulk structures of metastable compounds, see: Stein, A.; Keller, S.W.; Mallouk, T.E. *Science* **1993**, 259, 1558.
8. Ulman, A. *An Introduction to Ultrathin Organic Films: From Langmuir–Blodgett to Self-Assembly*; Academic: Boston, 1991.
9. Fendler, J.H.; Kotov, N.A.; Zavala, G. *J. Phys. Chem.* **1995**, 99, 12375.
10. *Chemical Vapor Deposition: Principles and Applications*; Hitchman, M.L.; Jensen, K.F., Eds.; Academic: New York, 1993.
11. Herman, M.A.; Sitter, H. *Molecular Beam Epitaxy*; Springer Series in Materials Science Vol. 7; Springer–Verlag: New York, 1989, pp 23–25, 247–251.
12. Lakomaa, E.-L.; Haukka, S.; Suntola, T. *Appl. Surf. Sci.* **1992**, 60/61, 742.

13. Kleinfeld, E.R.; Ferguson, G.S. In *Molecularly Designed Ultrafine/Nanostructured Materials*; Gonsalves, K.E.; Chow, G.M.; Xiao, T.D.; Cammarata, R.C., Eds.; Mater. Res. Soc. Symp. Proc. 351; Materials Research Society: Pittsburgh, PA, 1994; p 419. See also section 1.3.
14. George, J. *Preparation of Thin Films*; Marcel Dekker: New York, 1992; p 225.
15. See, for example: Tsubouchi, K.; Masu, K. *Thin Solid Films* **1993**, *228*, 312.
16. Bigelow, W.C.; Pickett, D.L.; Zisman, W.A. *J. Colloid Interface Sci.* **1946**, *1*, 513.
Zisman, W.A. *Adv. Chem. Ser.* **1964**, *43*, 1.
17. Haller, I. *J. Am. Chem. Soc.* **1978**, *100*, 8050. Jönsson, U.; Olofsson, G.; Malmqvist, M.; Rönnberg, I.; *Thin Solid Films* **1985**, *124*, 117. Nuzzo, R.G.; Zegarski, B.R.; Dubois, L.H. *J. Am. Chem. Soc.* **1987**, *109*, 733. Thomas, R.C.; Sun, L.; Crooks, R.M.; Ricco, A.J. *Langmuir* **1991**, *7*, 620. Ferguson, G.S.; Chaudhury, M.K.; Biebuyck, H.A.; Whitesides, G.M. *Macromolecules* **1993**, *26*, 5870.
18. Sagiv, J. *J. Am. Chem. Soc.* **1980**, *102*, 92.
19. Ong, T.H.; Davies, P.B.; Bain, C.D. *Langmuir* **1993**, *9*, 1836. Frisbie, C.D.; Rozsnyai, L.F.; Noy, A.; Wrighton, M.S.; Lieber, C.M. *Science* **1994**, *265*, 2071.
Vezenov, D.V.; Noy, A.; Rozsnyai, L.F.; Lieber, C.M. *J. Am. Chem. Soc.* **1997**, *119*, 2006.
20. Dubois, L.H.; Nuzzo, R.G. *Ann. Rev. Phys. Chem.* **1992**, *43*, 437. Yang, H.C.; Dermody, D.L.; Xu, C.; Ricco, A.J.; Crooks, M. *Langmuir* **1996**, *12*, 726, and references therein. Thomas, R.C.; Houston, J.E.; Crooks, R.M.; Kim, T.; Michalske, T.A. *J. Am. Chem. Soc.* **1995**, *117*, 3830. Newby, B.-M. Z.; Chaudhury, M.K.; Brown, H.R. *Science* **1995**, *269*, 1407. Chaudhury, M.K.; Whitesides, G.M. *Science* **1992**, *256*, 1539.
21. Netzer, L.; Iscovici, R.; Sagiv, J. *Thin Solid Films* **1983**, *99*, 235. Tillman, N.;

- Ulman, A.; Penner, T.L. *Langmuir* **1989**, *5*, 101.
22. Cao, G.; Hong, H.-G.; Mallouk, T.E. *Acc. Chem. Res.* **1992**, *25*, 420. Yang, H.C.; Aoki, K.; Hong, H.-G.; Sackett, D.D.; Arendt, M.F.; Yau, S.-L.; Bell, C.M.; Mallouk, T.E. *J. Am. Chem. Soc.* **1993**, *115*, 11855. Bent, S.F.; Schilling, M.L.; Wilson, W.L.; Katz, H.E.; Harris, A.L. *Chem. Mater.* **1994**, *6*, 122.
23. Evans, S.D.; Ulman, A.; Goppert-Berarducci, K.E.; Gerenser, L.J.; *J. Am. Chem. Soc.* **1991**, *113*, 5866.
24. Poojary, D.M.; Vermeulen, L.A.; Vicenzi, E.; Clearfield, A.; Thompson, M.E. *Chem. Mater.* **1994**, *6*, 1845.
25. Katz, H.E.; Schilling, M.L. *Chem. Mater.* **1993**, *5*, 1162.
26. Katz, H.E.; Scheller, G.; Putvinski, T.M.; Schilling, M.L.; Wilson, W.L.; Chidsey, C.E.D. *Science* **1991**, *254*, 1485.
27. Yitzchaik, S.; Marks, T.J. *Acc. Chem. Res.* **1996**, *29*, 197.
28. Watanabe, S.; Regen, S.L. *J. Am. Chem. Soc.* **1994**, *116*, 8855. Ansell, M.A.; Zeppenfeld, A.C.; Ham, W.K.; Page, C.J. In *Molecularly Designed Ultrafine/Nanostructured Materials*; Gonsalves, K.E.; Chow, G.M.; Xiao, T.D.; Cammarata, R.C., Eds.; Mater. Res. Soc. Symp. Proc. 351; Materials Research Society: Pittsburgh, PA, 1994; p 171. Ansell, M.A.; Zeppenfeld, A.C.; Yoshimoto, K.; Cogan, E.B.; Page, C.J. *Chem. Mater.* **1996**, *8*, 591.
29. Bell, C.M.; Arendt, M.F.; Gomez, L.; Schmehl, R.H.; Mallouk, T.E. *J. Am. Chem. Soc.* **1994**, *116*, 8374.
30. Iler, R.K. *J. Colloid Interface Sci.* **1966**, *21*, 569.
31. Decher, G.; Eßler, F.; Hong, J.-D.; Lowack, K.; Schmitt, J.; Lvov, Y. *Polym. Prepr.* **1993**, *34(1)*, 745. Lvov, Y.; Haas, H.; Decher, G.; Möhwald, H.; Kalachev, A. *J. Phys. Chem.* **1993**, *97*, 12835.
32. Ingersoll, D.; Kulesza, P.J.; Faulkner, L.R. *J. Electrochem. Soc.* **1994**, *141*, 140.

33. Kleinfeld, E.R.; Ferguson, G.S. *Science* **1994**, *265*, 370.
34. Cheung, J.H.; Fou, A.F.; Rubner, M.F. *Thin Solid Films* **1994**, *244*, 985.
35. Kleinfeld, E.R.; Ferguson, G.S. *Chem. Mater.* **1995**, *7*, 2327.
36. Byrd, H.; Whipps, S.; Pike, J.K.; Ma, J.; Nagler, S.E.; Talham, D.R. *J. Am. Chem. Soc.* **1994**, *116*, 295.
37. Schmitt, J.; Grünewald, T.; Decher, G.; Pershan, P.S.; Kjaer, K.; Lösche, M. *Macromolecules* **1993**, *26*, 7058.
38. Asakura, K.; Inukai, J.; Iwasawa, Y. *J. Phys. Chem.* **1992**, *96*, 829.
39. Srinivasan, S.; Datye, A.K.; Hampden-Smith, M.; Wachs, I.E.; Deo, G.; Jehng, J.M.; Turek, A.M.; Peden, C.H.F. *J. Catal.* **1991**, *131*, 260.
40. Jurek, K.; Guglielmi, M.; Kuncová, G.; Renner, O.; Lukes, F.; Navrátil, M.; Krousky, E.; Vorlíček, V.; Kokesova, K.; *J. Mat. Sci.* **1992**, *27*, 2549.
41. Selvaraj, U.; Prasadarao, A.V.; Komarneni, S.; Roy, R. *J. Am. Ceram. Soc.* **1992**, *75*, 1167.
42. Exarhos, G.J.; Hess, N.J. In *Crystallization and Related Phenomena in Amorphous Materials*, Libera, M.; Haynes, T.E.; Cebe, P.; Dickinson, J.E., Jr., Eds.; Mater. Res. Soc. Symp. Proc. 321; Materials Research Society: Pittsburgh, PA, 1994; p 393.
43. Rodgers, G.E. *Introduction to Coordination, Solid State, and Descriptive Inorganic Chemistry*; McGraw-Hill: New York, 1994; p 164.
44. Haukka, S.; Lakomaa, E.-L.; Jylhä, O.; Vilhunen, J.; Hornytzkyj, S. *Langmuir* **1993**, *9*, 3497.
45. Fadley, C.S. *J. Electron Spect. Rel. Phenom.* **1974**, *5*, 725.
46. Seah, M.P.; Dench, W.A. *Surface Interface Anal.* **1979**, *1*, 2.
47. Brunner, J.; Zogg, H. *J. Electron Spect. Rel. Phenom.* **1974**, *5*, 911.
48. *X-Ray Diffraction by Polycrystalline Materials*; Peiser, H.S.; Rooksby, H.P.; Wilson, A.J.C., Eds.; Wright: Bristol, UK, 1955, p 466.

49. van Olphen, H. *An Introduction to Clay Colloid Chemistry*, 2nd ed.; Wiley-Interscience: New York, 1977.
50. Reference 49, p 24.
51. Grim, R.E. *Clay Mineralogy*, 2nd ed. McGraw-Hill: New York, 1968; pp 353 – 368.
52. Subsequent optimization of the conditions used to prepare Laponite suspensions led to an increase in the amount of the silicate that adsorbed onto wafers that had been treated with TTA, as described in more detail in Chapter 2.
53. Cotton, F.A.; Wilkinson, G. *Advanced Inorganic Chemistry*, 4th ed.; Wiley-Interscience: New York, 1980; pp 71 – 73.
54. Kleinfeld, E.R.; Ferguson, G.S. In *Solid-State Ionics*; Nazri, G.-A.; Tarascon, J.-M.; Schreiber, M., Eds; Mat. Res. Soc. Symp. Proc. 369; Materials Research Society: Pittsburgh, PA, 1995; p 697; see also Chapter 2 of this dissertation.
55. Keller, S.W.; Kim, H.-N.; Mallouk, T.E. *J. Am. Chem. Soc.* **1994**, *116*, 8817. Lvov, Y.; Haas, H.; Decher, G.; Möhwald, H.; Mikhailov, A.; Mtchedlishvily, B.; Morgunova, E.; Vainshtein, B. *Langmuir* **1994**, *10*, 4232. Fendler, J.H. *Chem. Mater.* **1996**, *8*, 1616, and references therein.
56. Kleinfeld, E.R.; Ferguson, G.S. *Chem. Mater.* **1996**, *8*, 1575.
57. Jackson, M.L. *Soil Chemical Analysis—Advanced Course*; Published by the Author, Department of Soil Science, University of Wisconsin, Madison, WI 53706, Ed. 2, pp 127, 129, 144, 146. Note that in the discussion of the angle-head centrifuge on p 144 and in Figure 3-8, p 146, R and S are interchanged relative to their definitions on pp 127, 129. The author presents on p 144 a discussion of turbidity currents in angle-head centrifuges. If the calculations are modified to include turbidity currents (in this case, $R = 12.1$ cm, $S = 11.8$ cm), the clay fraction left in suspension after centrifugation is calculated as <0.0125 μm . This

number seems less credible, if the slight turbidity of the centrifuged suspension is any indication of the particle size.

58. Reference 51, p 283.

59. Mooney, R.W.; Keenan, A.G.; Wood, L.A. *J. Am. Chem. Soc.* **1952**, *74*, 1367, 1371.

Initial Studies and Groundwork In the PDDA/Laponite System

This chapter includes material that has been modified with permission from: Kleinfeld, E.R.; Ferguson, G.S. *Science* **1994**, *265*, 370. Copyright 1994 American Association for the Advancement of Science; and from: Kleinfeld, E.R.; Ferguson, G.S. In *Solid State Ionics IV*; Nazri, G.-A.; Tarascon, J.-M.; Schreiber, M., Eds.; Mater. Res. Soc. Symp. Proc. 369; Materials Research Society: Pittsburgh, PA, 1995; pp 697–702. Copyright 1995 Materials Research Society.

2.1 Abstract

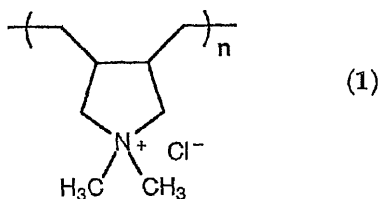
Sequential adsorption of a cationic polyelectrolyte and individual sheets of the silicate mineral Laponite resulted in the controlled, stepwise formation of multilayered films on silicon wafers. Each component adsorbed rapidly by an ion-exchange mechanism, and x-ray diffractometry indicated structural order even in films with thicknesses greater than 0.24 μm . The large lateral extent of the silicate sheets (~ 25 to 35 nanometers) allowed each layer to cover any packing defects in the underlying layer, thus preserving structural order in the growing film. With careful choice of component materials, this method should allow for the preparation of multilayered films with a variety of technologically important properties. To demonstrate the generality of the method in this regard, we used ellipsometry to monitor the growth of films incorporating poly(D-lysine hydrobromide) or poly(N-methyl-4-vinylpyridinium bromide) (PMVP) and Laponite. X-ray diffractometry revealed that PMVP/Laponite films possessed an ordered structure with a lattice spacing of 1.5 nm in the direction normal to the substrate surface.

2.2 Introduction

Ultrathin films and multilayered structures are important for many applications, including x-ray¹ and nonlinear² optics and microelectronics,^{3,4} and are under investigation for use as chemical sensors.⁵ Langmuir–Blodgett (LB) deposition of preformed monolayers from a gas–liquid interface onto a solid planar substrate^{6–8} can provide well-ordered, densely packed mono- and multilayered systems useful for these applications. Unfortunately, LB multilayers are mechanically unstable, held together primarily by van der Waals forces.^{7,8} Spontaneous self-assembly (SA) of molecular adsorbates onto solid substrates⁷ can also provide densely packed monolayers, and has recently been extended to the formation of multilayers in selected systems.^{5,9,10} The presence of covalent bonds or ionic attraction between layers provides additional stability not exhibited by LB systems; however, adsorption of multilayers displaying structural order has proven difficult. In this chapter, we describe a method for the stepwise preparation of nanostructured multilayered films from ultrathin (≤ 1 nm) layers of organic and inorganic macromolecules. Films with thicknesses greater than $0.24 \mu\text{m}$ have been prepared that have sufficient structural order to diffract x-rays.

2.3 Results and Discussion

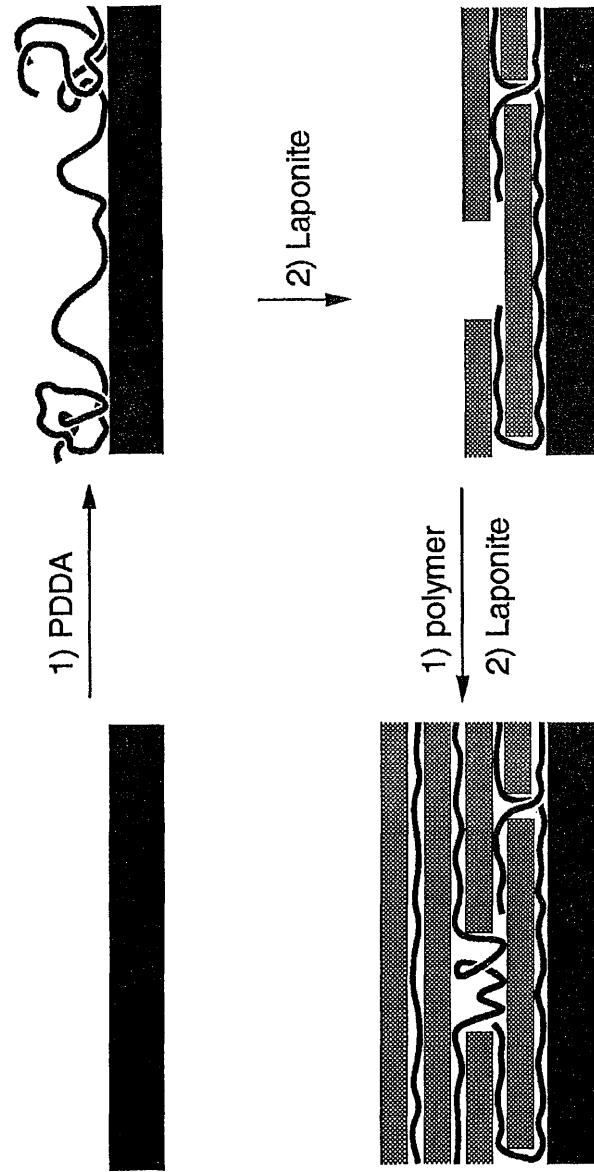
2.3.1. Materials and Methods. Our approach involves alternate adsorption of the polyelectrolyte poly(diallyldimethylammonium chloride), PDDA (1),¹¹ and exfoliated



sheets of synthetic hectorite, a mica-type layered silicate [Laponite RD, Laporte Industries Ltd.]. When stirred in water, this silicate mineral exfoliates into crystalline, quasi-two-dimensional sheets that are ~0.93 nm in thickness and approximately 25 to 35 nm in diameter. The sheets bear a negative charge, which is balanced in the precursor by interlamellar sodium cations that can undergo ion exchange reactions with other cationic materials.¹²⁻¹⁴ Our choice of PDDA for this study was motivated by the strong affinity of hectorite and related minerals for tetraalkylammonium compounds,¹⁵ while Laponite RD was chosen because it readily disperses into stable suspensions upon simply stirring the precursor powder in water. Furthermore, Laponite sheets are sufficiently small that they do not noticeably scatter room light, and the quality of the suspension can thus be assessed visually, clarity indicating full exfoliation, and turbidity indicating flocculation.

To prepare a substrate for a multilayered structure, a (100)-oriented single-crystal silicon wafer bearing a native oxide was cut into small pieces (~1 cm by 2.5 cm), and then cleaned to provide a hydroxylated surface. A 5% (w/w) aqueous solution of PDDA was dripped onto this substrate, and after ~5 s it was rinsed with water and blown dry with nitrogen. Subsequently, a 0.2% (w/w) aqueous dispersion of Laponite was dripped onto the surface, and after ~5 s it was rinsed with water and blown dry with nitrogen. By repetition of this simple two-step adsorption cycle (Figure 2.1), films thicker than 0.2 μm could be prepared in less than 2 hours. An x-ray photoelectron survey spectrum of a silicon substrate that had been treated with PDDA, then Laponite, then PDDA confirmed the presence of those elements in the silicate and the polymer: Si, O, Mg, C, N, and Cl. The absence of sodium, which is present in the precursor mineral as an interlamellar counterion, indicates that it had been exchanged for the cationic polymer. The low expected concentration of lithium on the surface and the low sensitivity factor of the Li 1s orbital explain the absence

Figure 2.1. Schematic diagram of the preparation of a multilayered film by alternate adsorption of PDDA and Laponite. Modified with permission from: Kleinfeld, E.R.; Ferguson, G.S. *Science* **1994**, *265*, 370. Copyright 1994 American Association for the Advancement of Science.

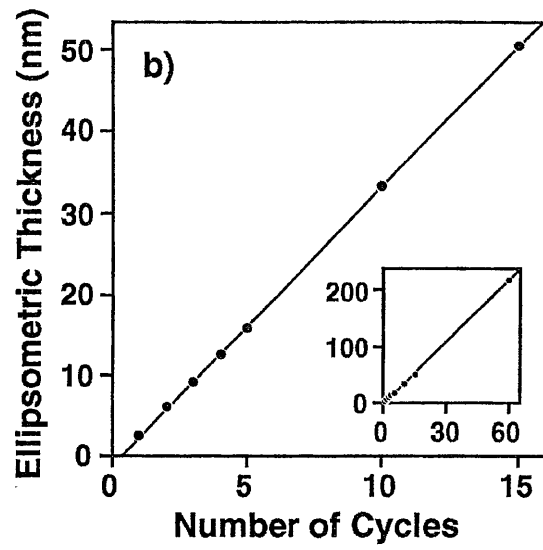
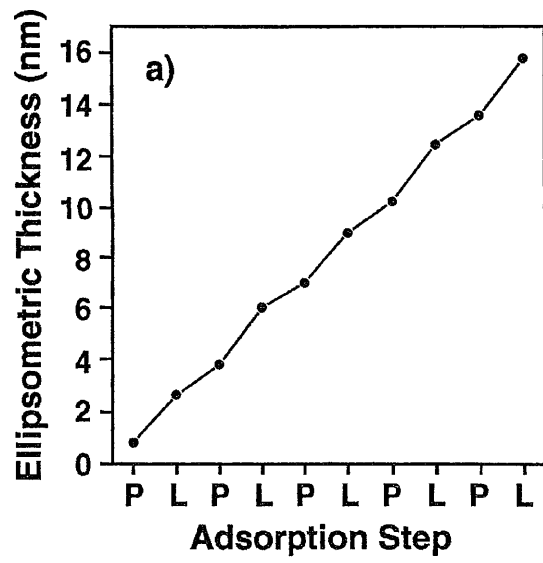


of this peak.¹⁶

2.3.2. Ellipsometric Study of the Characteristics of Film Growth. Optical ellipsometry was used to monitor the growth in thickness of the multilayer structures. In a typical cycle, ~1.1 nm of polymer and ~2.1 nm of silicate were adsorbed (Figure 2.2a). The linear increase in the thickness of the structures with the number of adsorption cycles, as determined ellipsometrically, is shown in Fig. 2.2b. The average thickness added per adsorption cycle increased slightly as the number of cycles increased, from ~3.2 nm after 5 cycles to ~3.6 nm after 60 cycles. The thickness of the multilayered samples was remarkably even: ellipsometric measurements taken on any single Laponite-terminated sample typically agreed to within $\pm 2\%$, and the majority of samples showed less than one-half of that variability. Sample-to-sample reproducibility was also very good. Three samples prepared on different days with 22 cycles had average thicknesses within 2% of one another.

The factors that influence the characteristics of film growth include the duration of adsorption treatments, the concentration of the polymer solution used in preparing the film, and the ambient relative humidity. When the adsorption times were doubled, to 10 s, the average amount of each component that was adsorbed onto the sample surface varied by ~0.1 nm or less, which is within experimental error. When adsorptions were allowed to proceed for extended times (15 min), however, the average thickness added in each of the first 5 cycles increased from ~3.2 to ~3.8 nm. When the concentration of the polymer solution was diluted in increments from 20 to 0.05% (w/w), the amount of polymer adsorbed per cycle decreased monotonically from 2.1 to 0.1 nm. The amount of Laponite adsorbed per cycle from a 0.2% (w/w) suspension correspondingly fell monotonically from 2.7 to 0.6 nm. Films sorb water rapidly and reversibly upon a change in relative humidity, resulting in significant

Figure 2.2. Ellipsometric thickness of a multilayered structure on a single-crystal silicon substrate as a function of the number of adsorption cycles for: (a) individual steps in five cycles (P = PDDA, L = Laponite); and (b) 15 and 60 (inset) complete PDDA/Laponite cycles. Lines shown in (b) are linear least-squares fits to the data. The native oxide on silicon is not included in the reported thicknesses. All data in this figure are averages over three points on each of two samples treated side-by-side, with the exception of the point at 60 cycles, which is an average over five points on one sample. Similar thicknesses were measured on other samples.



changes in their thickness. Further studies on the kinetics of the adsorption of the polymer and silicate and the dependence of film growth on polymer concentration are presented in Chapters 3 and 7, while the response of the films to changes in relative humidity is explored in detail in Chapter 5.

2.3.3. Properties of Polymer/Silicate Composite Films. As an increasing number of layers were adsorbed, samples progressed through a series of well-defined colors due to interference effects, as has also been noted for LB^{6,8} and SA⁹ multilayered systems. No cloudiness was observed in the samples, and, as shown in Figure 2.3, the colors were uniform, with only a small region (less than 1 mm wide) at the sample edges showing non-uniformity.

At the outset of this work, we expected the Laponite to be adsorbed onto the sample surface in a controlled manner by ion exchange of the ammonium groups of the surface-bound polymer for the alkali-metal counterions of the anionic Laponite sheets. Once the surface was covered with a layer of Laponite, further adsorption of the silicate should be inhibited by Coulombic repulsion between the bound and unbound anionic sheets. The adsorption of approximately two Laponite layers (2.0 to 2.2 nm) per adsorption cycle indicates that some of the polymer is associated sufficiently loosely with the surface that it is displaced in the subsequent Laponite adsorption and becomes the “glue” for addition of a second layer of Laponite (Figure 2.1). Consistent with this proposed mechanism, the amount of Laponite adsorbed in a particular cycle could be controlled by varying the amount of polymer adsorbed in that cycle, as noted earlier. Furthermore, only a single layer of Laponite (0.7–1.2 nm in thickness) was adsorbed onto a layer of trimethoxysilylpropyl-*N,N,N*-trimethylammonium chloride, TTA [(CH₃O)₃Si(CH₂)₃N(CH₃)₃Cl], that was 0.5 – 1.1 nm in thickness and covalently bound to the silicon substrate (Figure 2.4). Ion exchange has been used for the adsorption of composite films,¹⁷ but the combination

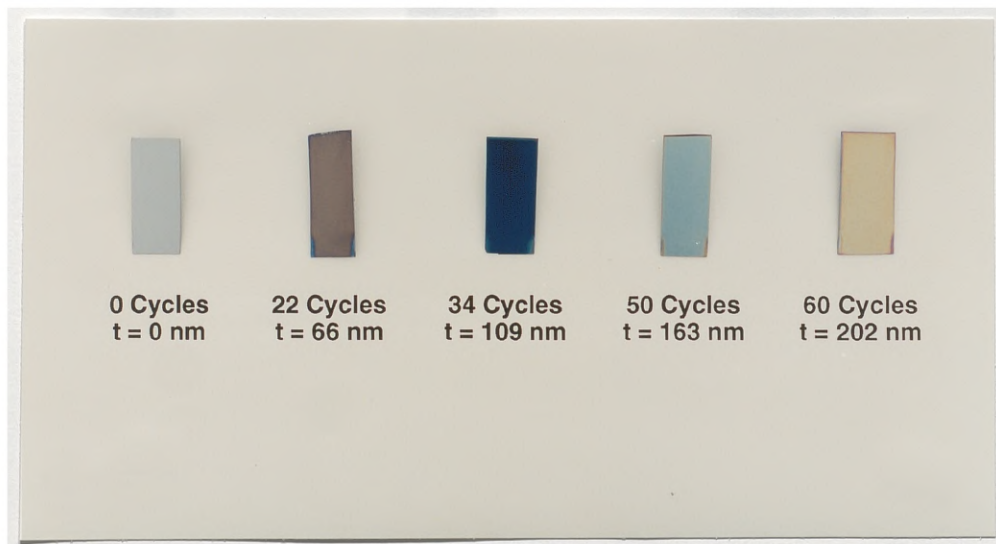


Figure 2.3. Photograph of a bare silicon wafer and multilayered films of various thicknesses on silicon substrates. Interference between the light reflected at the air/film interface and the light reflected at the film/silicon interface produces the observed interference colors. Each sample in the photograph has dimensions of approximately 1 cm x 2.5 cm.

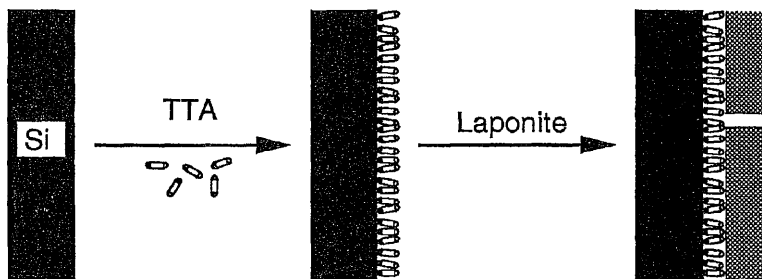


Figure 2.4. Schematic diagram of the use of TTA to promote adsorption of Laponite to a silicon wafer.

of structural order and 1- to 2-nm lattice spacings that characterize PDDA/Laponite multilayers has not been seen previously.

Because the Laponite sheets in a single adsorbed layer will have packing imperfections (that is, open space at their boundaries), the linearity of multilayer growth shown in Fig. 2.2b indicates that this system is self-healing with respect to addition of subsequent layers. We infer that the large lateral extent of the sheets allows coverage of regions where the underlying layer is incomplete. In contrast, other multilayer preparations that rely on formation of each layer through reaction of individual adsorbed molecules with molecules from the contacting solution are less able to recover lost order. In such systems, defects may occur to create unreactive patches that do not participate further in multilayer growth, resulting in a decay in structural order as an increasing number of layers is added.^{9,18} Studies related to the ability of our system to heal defects, and by a related mechanism, to form films on substrates that are resistant to adsorption of either component individually, are described in detail in Chapter 4.

2.3.4. X-Ray Diffractometry. X-ray diffractometry (XRD) provided evidence for the presence of structural order in PDDA/Laponite multilayered films. A grazing-incidence XRD pattern of a multilayer formed by 60 adsorption cycles is shown in Fig. 2.5. The peak at $6.1^\circ 2\theta$, a (001) reflection, corresponds to a layer spacing of 1.45 ± 0.03 nm; (003), (004), and (005) reflections, found at 18.4° , 25.1° , and 30.8° , indicate layer spacings of 1.44 ± 0.02 , 1.42 ± 0.02 , and 1.45 ± 0.03 nm. These spacings are consistent with an ABABAB alternation of the silicate sheets (0.93 nm thick) with polymer layers that are ~ 0.5 nm thick. The Scherrer equation was used to provide an estimate of the size of the ordered domains in the sample.¹⁹ According to this equation, the size of ordered domains (L) in the direction perpendicular to the structural feature giving rise to the peak is given by

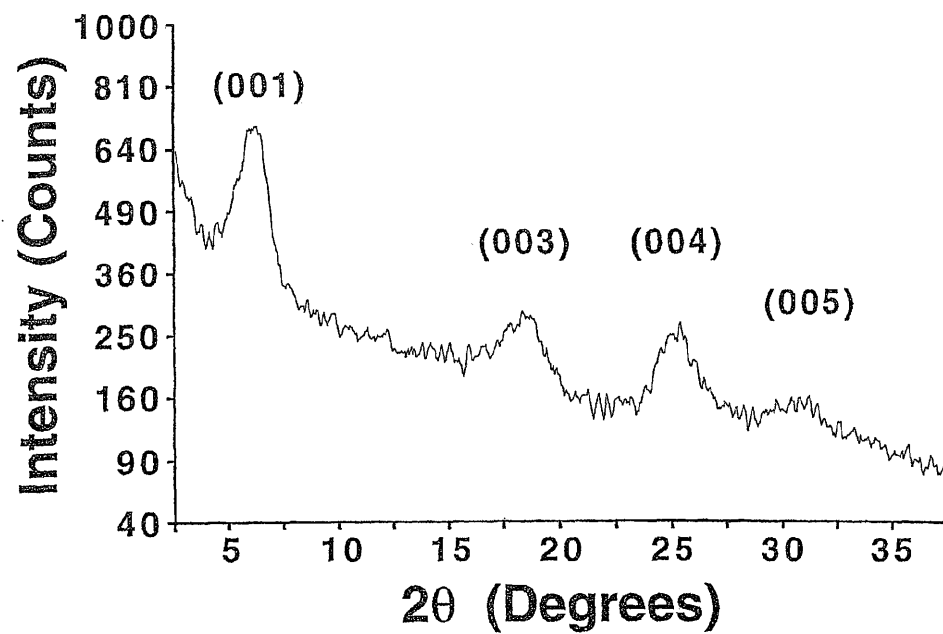


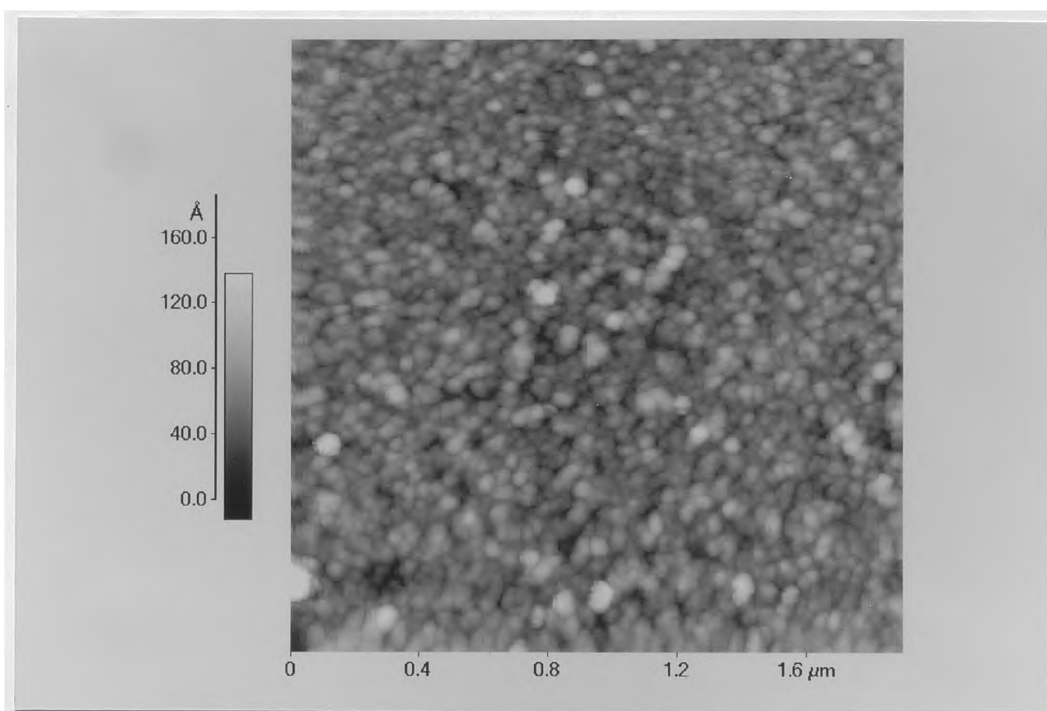
Figure 2.5. The x-ray diffraction pattern of a 60-cycle multilayered film of PDDA and Laponite on a silicon substrate.

$$L = \frac{0.94 \lambda}{B(2\theta) \cos \theta} \quad (1)$$

where λ is the X-ray wavelength, $B(2\theta)$ is the full-width at half-maximum intensity (in radians) of the peak of interest, and θ is the peak position. The values generated by this equation are useful for comparison to similar films, but tend to underestimate actual crystallite sizes revealed by direct methods such as cross-sectional transmission electron microscopy.^{20,21} Application of this equation to the (001) reflection (full width at half height = $1.6^\circ 2\theta$) thus provides a lower limit to the size of the ordered domains in the direction normal to the substrate surface (5.1 nm). Additional peaks occurring at higher angles in the XRD pattern (not shown) could be attributed to the substrate, as they also occurred in diffractograms of bare silicon wafers.²² The absence of reflections corresponding to the Laponite starting material indicates that no intact three-dimensional crystallites of the precursor were incorporated into the structure, and is consistent with the sheets being preferentially oriented parallel or near-parallel to the substrate surface.²³ The tendency of exfoliated silicate sheets to re-stack in a parallel arrangement has been well established.^{14,24} The average growth in thickness per cycle as determined by ellipsometry was not an even multiple of the 1.4-nm periodicity revealed by XRD. This result reflects the fact that ellipsometry gives the average thickness within an illuminated spot ($\sim 1 \text{ mm}^2$ in area). A measured increase in thickness of 3.6 nm indicates that in any one cycle, some regions within the illuminated spot gained two layers, while others gained three.

2.3.5. Atomic Force Microscopy. Atomic force microscopy (AFM) was used to examine the surface topography of the multilayered samples. An AFM image of a 2- μm -by-2- μm area on a sample that had been treated with one PDDA/Laponite adsorption cycle is shown in Figure 2.6a. The image, obtained in attractive

a)



b)

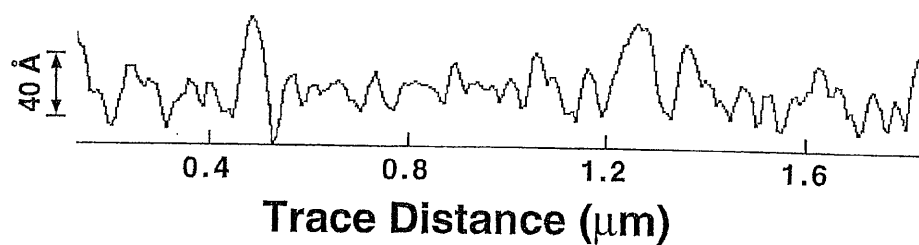


Figure 2.6. (a) AFM image, obtained in attractive mode, of a sample that had been prepared by performing one adsorption cycle on a bare silicon wafer. (b) Trace taken horizontally, approximately one-fourth of the way up from the bottom of the image shown in (a).

("noncontact") mode, reveals the individual Laponite sheets adsorbed at the sample surface. A sample that had been treated with five adsorption cycles gave a similar AFM image, and an image of a bare wafer was nearly flat. A representative trace across the surface that was imaged in Figure 2.6a is shown in Figure 2.6b to give an idea of the lateral dimension of individual platelets and the roughness of the surface. The difference in vertical and lateral scales in both frames of Figure 2.6 exaggerates the roughness of these surfaces; the RMS roughness of the area imaged in Figure 2.6a was only 1.8 nm.

2.3.6. Flexibility of this System Toward the Incorporation of Other Component Materials. The ion-exchange mechanism of adsorption of the components in the multilayered films (i.e., the reliance upon Coulombic interactions rather than upon formation of covalent bonds) suggested that there should be great flexibility with respect to the choice of the polymer and sheet mineral.²⁵ The ability to vary the structure of the polymer systematically in these multilayers would aid greatly in the rational design of films having properties of interest—for example, in chiral sensing^{26,27} or nonlinear optical applications.^{2,28,29} An approach for the preparation of films active for chiral sensing would be incorporation of a polymer with a chiral backbone or chiral substituents into the composite film. Likewise, incorporation of a polymer having a polarizable backbone or substituents would create the possibility of forming composite films with second- or third-order nonlinear optical activity. As model polymers with which to initiate these studies, we chose poly(D-lysine hydrobromide) and poly(*N*-methyl-4-vinylpyridinium bromide) (PMVP).

A multilayered film was formed on a silicon substrate by alternate adsorption (5-s treatments) of poly(D-lysine hydrobromide) [5% (w/w), aqueous] and Laponite RD [0.2% (w/w), aqueous] according to the procedure that was described in detail above for PDDA/Laponite films and as depicted schematically in Figure 2.1. The

growth in film thickness was monitored ellipsometrically and is shown in Figure 2.7. Thicknesses after individual steps in the first five cycles are shown; the film grew approximately 0.4 nm in the lysine-adsorption steps and 1.0 nm in the Laponite-adsorption steps.

Figure 2.8 shows the growth in thickness of multilayers formed from poly(*N*-methyl-4-vinylpyridinium bromide) (PMVP) [10% (w/w), aqueous] and Laponite RD [0.2% (w/w), aqueous] as a function of the number of adsorption cycles. X-ray photoelectron spectroscopy (Scienta ESCA-300) of a sample formed by 25 complete adsorption cycles on Si/SiO₂ revealed the presence of carbon, nitrogen, and bromine from the polymer, and silicon, magnesium, and oxygen from the Laponite. The presence of bromine and the apparent absence of monovalent cations associated with the Laponite (lithium and sodium) suggested that the polymer was present in excess of the cation-exchange capacity of the clay.

The regular growth shown in Figures 2.7 and 2.8 indicated that the adsorption process was predictable and could be continued indefinitely to produce films of precisely controllable thickness; however, these data provided no information concerning the structure of the films. X-ray diffractometry, in contrast, can provide structural information. Figure 2.9 shows the X-ray diffractogram of a sample formed by 46 adsorption cycles of PMVP and Laponite on the native oxide of silicon. The peak at $5.8 \pm 0.2^\circ 2\theta$ is assigned as the (001) reflection of the PMVP/Laponite lattice, indicating a d-spacing of 1.52 ± 0.05 nm. The two peaks centered around 18° and $27^\circ 2\theta$ are too broad and weak to assign with certainty, though they may be higher-order basal reflections from the PMVP/Laponite lattice. The lattice spacing given by the (001) reflection suggests that the Laponite sheets, which are 0.93 nm in thickness, are separated by layers of polymer roughly 0.59 nm in thickness. These values are similar to those for PDDA/Laponite films presented earlier in this

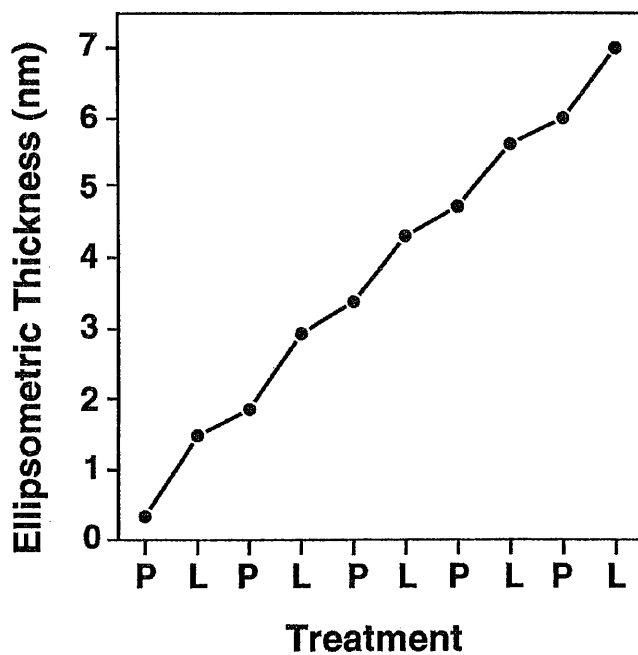
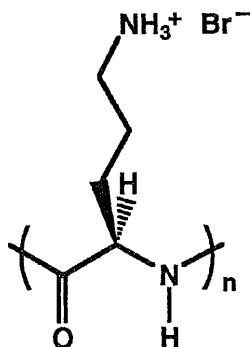


Figure 2.7. Structure of poly(D-lysine hydrobromide) and growth in thickness of a polylysine/Laponite composite film with each treatment in the first five adsorption cycles (P = polylysine; L = Laponite).

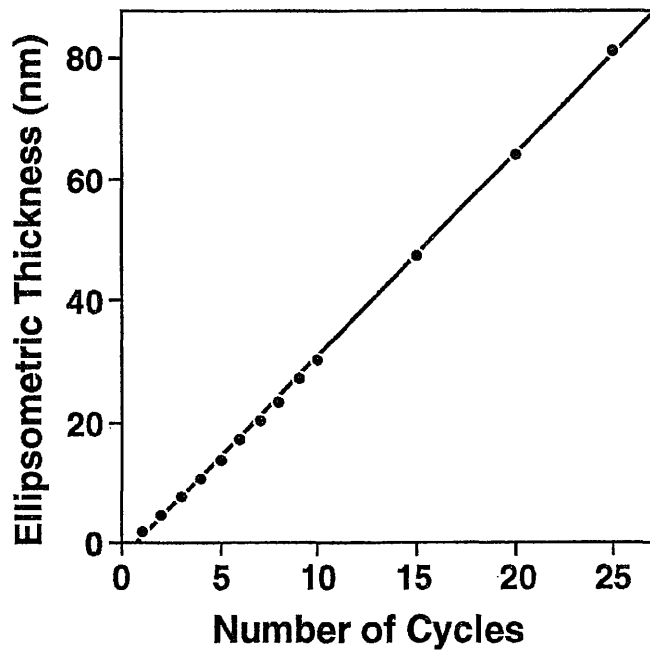
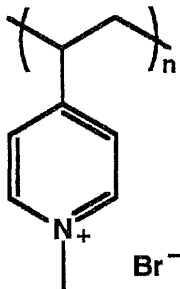


Figure 2.8. Structure of poly(*N*-methyl-4-vinylpyridinium bromide) and growth in thickness of a PMVP/Laponite composite film during 25 complete adsorption cycles.

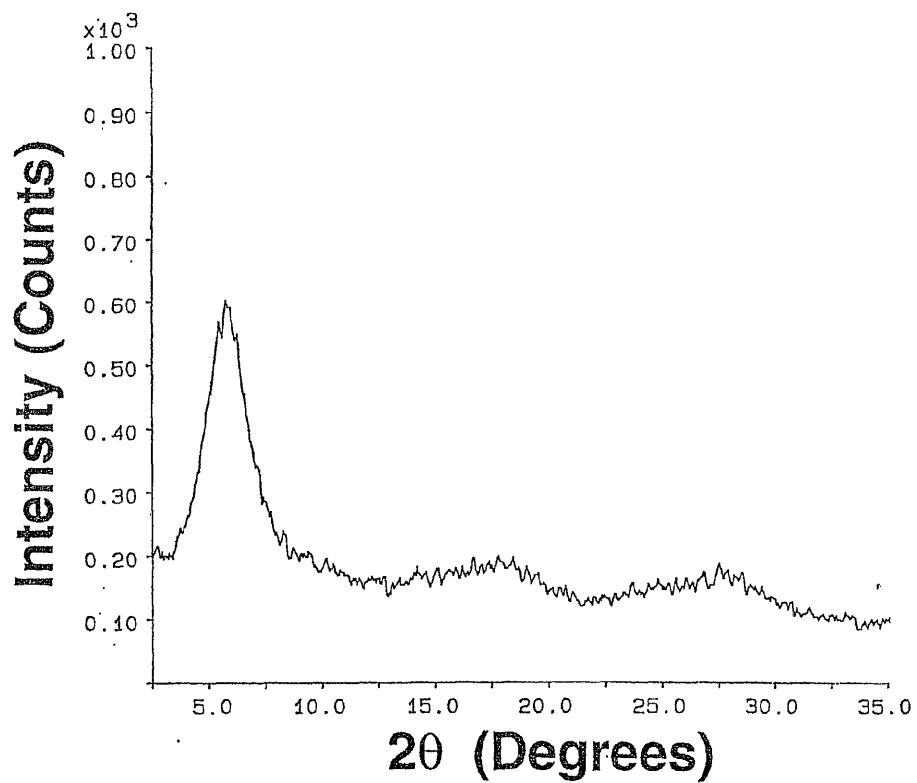


Figure 2.9. X-ray diffraction pattern of a sample prepared by the adsorption of 46 cycles of PMVP and Laponite onto a silicon wafer.

chapter. Optical studies performed on PMVP/Laponite multilayered films are presented in Chapter 3, along with a more detailed discussion of the structure of such a film on fused quartz. We did not attempt to obtain XRD patterns of the other structures discussed in this section.

The ability to form superlattices by the incorporation of more than two components can be important for certain practical applications. For example, films containing alternate layers of electron-rich and electron-deficient materials can exhibit photoinduced charge transfer, of interest in the construction of artificial photosynthetic systems.³⁰ As a step toward such goals, we prepared multilayers incorporating both PDDA [from 5% (w/w) solution] and PMVP [from 10% (w/w) solution]. Figure 2.10 shows the ellipsometric growth of a film formed by adsorbing these components in the order PDDA/Laponite/PMVP/Laponite, along with a schematic diagram of the resulting structure.³¹ Again, the thickness increased in a regular fashion.

2.4 Conclusions

The preparative method described in this chapter offers a potentially powerful new strategy for building ordered organic/inorganic thin films with systematic control over both structure and thickness. It was found to be readily adaptable to other systems that incorporate other substrates, inorganic sheets, and included molecules, as described in greater detail in Chapters 3, 6, 7, and 8. The use of gold substrates, for example, allowed electrodes to be prepared with complex but controllable barrier layers, as described in Chapter 3, and could also allow evaluation of the performance of these multilayered structures as electrical insulators,^{4,32} barriers to diffusion,¹³ or mediators for electron transfer.^{30,34} Deposition of various crystalline materials onto sheet silicates, including oxides³⁴ and metals,³⁵ has been demonstrated, indicating

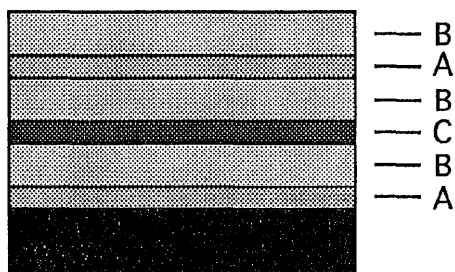
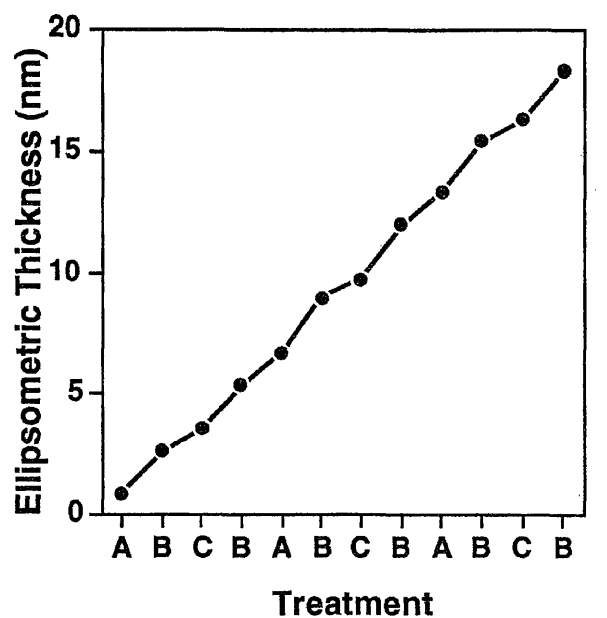


Figure 2.10. Ellipsometric growth of a film formed by sequential adsorptions of components in the order PDDA/Laponite/PMVP/Laponite (A = PDDA; B = Laponite; C = PMVP), along with a schematic illustration of the resulting structure.

that our multilayered films may be of interest as substrates for growth of other materials. Metal-terminated structures, for example, may be of particular interest as metal-insulator-semiconductor (MIS) or metal-insulator-metal (MIM) devices.^{4,36} Preparation of multilayered assemblies with nonlinear optical activity^{2,37} may be possible if polar molecules (monomeric or polymeric) can be oriented non-centrosymmetrically between inorganic sheets. Although we did not pursue this goal, we did evaluate the optical properties of photochromic multilayered films that had been prepared from sheet silicates and a cationic polyelectrolyte bearing a photochromic dye as a pendant group, as detailed in Chapter 6. Finally, adaptation of this method to other layered materials with known intercalation chemistry, including metal dichalcogenides,²³ metal halides,³⁸ and layered metal oxides such as V₂O₅⁽³⁹⁾ and FeOCl,⁴⁰ may allow stepwise preparation of multilayered structures with a range of electronic band gaps.

2.5 Experimental Methods

2.5.1. *Materials.* Poly(diallyldimethylammonium chloride), MW 240,000, and poly(*N*-methyl-4-vinylpyridinium bromide), MW 50,000, were obtained from Polysciences as 20% (w/w) aqueous solutions; poly(D-lysine hydrobromide), MW62,700–67,700, was obtained as a solid from Sigma. Polymer solutions used for multilayered film formation were prepared to the indicated concentrations by the addition of Millipore Milli-Q water (15 – 17 MΩ-cm). Laponite RD (synthetic hectorite) was obtained from Laporte Industries, Limited, in powder form, and has been reported to have an elemental composition consistent with the approximate molecular formula Si₈[Mg_{5.5}Li_{0.4}H_{4.0}O_{24.0}]^{0.7-}Na_{0.7}^{0.7+}.⁽⁴¹⁾ It was added to Milli-Q water with stirring to form a 0.5% (w/w) dispersion; stirring was continued until the dispersion appeared clear (typically for several hours). The dispersion was then

allowed to stand overnight without stirring to allow complete separation of the silicate sheets, and was diluted to 0.2% (w/w) before use. Silicon wafers [p-doped, (100)-oriented] were manufactured by Wacker Siltronic and had a native oxide approximately 1.5 nm in thickness.

2.5.2. Sample Preparation. Silicon substrates were cleaned shortly before use by immersion for at least 30 min in a 1:2 (v/v) solution of 30% H₂O₂ and concentrated H₂SO₄ (CAUTION: *This "piranha" solution reacts violently with organic materials!*) and were rinsed thoroughly with Milli-Q water and dried with a jet of nitrogen.

Multilayered films were formed by repeating a two-step cycle under the following conditions, unless specified otherwise. In the first step, a polymer solution of indicated composition was dripped onto a sample. The sample was then rinsed after 5 s with purified water and dried with a jet of nitrogen. In the second step, a 0.2% (w/w) suspension of Laponite RD was dripped onto a sample. The sample was then rinsed after 5 s and dried as above. The extent of rinsing was found to affect the observed growth per cycle: whereas many of our initial results (including the data shown in Figure 2.2) were obtained with a minimal rinse, more extensive rinsing during the preparation led to adsorption of slightly less material per cycle (by ~0.2 nm). Typically, no pre-treatment was used to promote adhesion between the substrate and the multilayered film. In one set of experiments, however, a covalently bound, positively charged layer was formed by treatment of a silicon wafer with a 1–2 mmol solution of (CH₃O)₃Si(CH₂)₃N(CH₃)₃Cl (Huls America) in chloroform for 15 min, followed by rinsing with chloroform and drying with nitrogen, affording a monolayer with an ellipsometric thickness of ~0.6 nm. In a separate case, to provide a surface as favorable as possible for the adsorption of polylysine, a silicon wafer was treated with two adsorption cycles using a 5% (w/w) solution of PDDA and a 0.2% w/w suspension of Laponite.

2.5.3. *Ellipsometry.* The growth of multilayered films on silicon was monitored by optical ellipsometry, using a Rudolph Auto-EL III nulling ellipsometer with HeNe laser light ($\lambda = 632.8$ nm). Measurements were performed under ambient conditions with the angle of incidence (ϕ) set at 70° . The thickness of the native oxide of silicon (~ 1.5 nm) was measured assuming a refractive index of 1.5, and assuming a standard refractive index for the silicon substrate ($n = 3.858$, $k = 0.018$). This thickness was later subtracted from the overall film thickness determined using an assumed refractive index of 1.5, a value which was representative of those measured experimentally for thicker films (1.48–1.59). The measured refractive index increased with increasing multilayer thickness.

2.5.4. *X-ray Photoelectron Spectroscopy (XPS).* The elemental composition of films on silicon was determined using a Scienta ESCA-300 X-ray photoelectron spectrometer with monochromatized Al K_α radiation from a rotating anode source. For the film made by adsorbing PDDA, then Laponite, then PDDA onto a silicon wafer, a take-off angle of 45° , pass energy of 150 eV, energy step of 1 eV, and slit width of 0.8 mm were used. For the 25-cycle film made from PMVP and Laponite on a silicon wafer, pass energy of 150 eV, energy step of 0.25 eV, and slit width of 1.1 mm were used. The take-off angle was not recorded, but was most likely 45° . No charging effects were observed, because the substrates were conductive and the overlayers were thin.

2.5.5. *X-ray Diffraction.* X-ray diffractometry was performed in $\theta/2\theta$ mode using a Philips APD 3720 powder diffractometer with monochromatized CuK_α radiation ($\lambda = 0.154$ nm) operating at 45 kV and 30 mA. Data were obtained using a 0.05° step and 3 s/step collection time. Samples were broken into ~ 1 cm \times $\sim (1-1.5$ cm) pieces before analysis to allow them to fit into the sample holders.

2.5.6. *Atomic Force Microscopy.* The AFM image was acquired under ambient

conditions, in attractive (“noncontact”) mode, using a Parks Scientific Instruments Autoprobe cp with an Ultralever (silicon) probe tip. The scan rate was 1 Hz, and the image was corrected for tilt and curvature.

Acknowledgements. We gratefully acknowledge O. Shaffer for assistance in obtaining AFM images, D. Simpson for helpful discussions regarding the interpretation of x-ray diffractograms (obtained with the assistance of G. Yasko), A. Miller and D. Carey for technical assistance with the x-ray photoemission spectroscopic analysis, and Lehigh University for supporting the Scienta ESCA-300 Laboratory. Silicon wafers used as substrates were donated by WaferNet, Inc.

2.6 References

1. Barbee, T.W., Jr. *SPIE* **1985**, 563, 2; Spiller, E. In *Physics, Fabrication, and Application of Multilayered Structures*; Dhez, P.; Weisbuch, C., Eds.; Plenum: New York, 1988; pp 271–309.
2. Katz, H.E.; Scheller, G.; Putvinski, T.M.; Schilling, M.L.; Wilson, W.L.; Chidsey, C.E.D. *Science* **1991**, 254, 1485. Yitzchaik, S.; Marks, T.J. *Acc. Chem. Res.* **1996**, 29, 197.
3. Katz, H.E.; Schilling, M.L. *Chem. Mater.* **1993**, 5, 1162.
4. Kepley, L.J.; Sackett, D.D.; Bell, C.M.; Mallouk, T.E. *Thin Solid Films* **1992**, 208, 132.
5. Cao, G.; Hong, H.-G.; Mallouk, T.E. *Acc. Chem. Res.* **1992**, 25, 420.
6. Blodgett, K.B. *J. Am. Chem. Soc.* **1935**, 57, 1007.
7. Ulman, A. *An Introduction to Ultrathin Organic Films: From Langmuir–Blodgett to Self-Assembly*; Boston: Academic Press, 1991.
8. Gaines, G.L., Jr. *Insoluble Monolayers at Liquid–Gas Interfaces*; Interscience: New

- York, 1966.
9. Tillman, N.; Ulman, A.; Penner, T.L. *Langmuir* **1989**, *5*, 101.
 10. Lee, H.; Kepley, L.J.; Hong, H.-G.; Mallouk, T.E. *J. Am. Chem. Soc.* **1988**, *110*, 618. Evans, S. D.; Ulman, A.; Goppert-Berarducci, K.E.; Gerenser, L.J. *J. Am. Chem. Soc.* **1991**, *113*, 5866.
 11. For elucidation of the structure of PDDA, see: Masterman, C.; Dando, N.R.; Weaver, D.G.; Seyferth, D. *J. Polymer Sci. B: Polymer Phys.* **1994**, *32*, 2263, and references therein.
 12. *Intercalation in Layered Materials*; Dresselhaus, M.S., Ed.; Plenum: New York, 1986.
 13. Yano, K.; Usuki, A.; Okada, A.; Kurauchi, T.; Kamigaito, O. *J. Polym. Sci. A: Polym. Chem.* **1993**, *31*, 2493.
 14. Jordan, J.W. *J. Phys. Colloid Chem.* **1949**, *53*, 294.
 15. Brahimi, B.; Labbe, P.; Reverdy, G. *Langmuir* **1992**, *8*, 1908.
 16. In addition to the elements named, this spectrum revealed a trace amount of oxidized sulfur on the sample (S 2s, 232.0 eV), most likely due to the cleaning procedure used. See Kern, W. *J. Electrochem. Soc.* **1990**, *137*, 1887.
 17. Decher, G.; Eßler, F.; Hong, J.-D.; Lowack, K.; Schmitt, J.; Lvov, Y. *Polym. Prepr.* **1993**, *34* (1), 745. Lvov, Y.; Haas, H.; Decher, G.; Möhwald, H.; Kalachev, A. *J. Phys. Chem.* **1993**, *97*, 12835. Iler, R.K. *J. Colloid Interface Sci.* **1966**, *21*, 569.
 18. Byrd, H.; Whipps, S.; Pike, J.K.; Ma, J.; Nagler, S.E.; Talham, D.R. *J. Am. Chem. Soc.* **1994**, *116*, 295.
 19. Warren, B.E. *X-Ray Diffraction*; Addison-Wesley: Reading, MA, 1969; pp 251–254.
 20. Drits, V.A.; Tchoubar, C. *X-Ray Diffraction by Disordered Lamellar Structures*, Springer-Verlag: New York, 1990, pp 21–22.

21. Vaia, R.A.; Jandt, K.D.; Kramer, E.J.; Giannelis, E.P. *Chem. Mater.* **1996**, *8*, 2628.
22. In the XRD pattern of the first 60-cycle film we prepared, one additional feature was present: a broad peak of very low intensity at $\sim 13.3^\circ$ ($d = 0.66$ nm). This peak was not identified, and it was never observed in any future pattern, possibly because subsequent samples had been rinsed more extensively both during multilayer formation and shortly before XRD analysis.
23. Divigalpitiya, W.M.R.; Frindt, R.F.; Morrison, S.R. *Science* **1989**, *246*, 369.
24. Peiser, H.S.; Rooksby, H.P.; Wilson, A.J.C., Eds., *X-Ray Diffraction by Polycrystalline Materials*; Wright: Bristol, UK, 1955; p 466.
25. Evidence for regular growth of thin films by alternate adsorption of polyanions such as α -Zr(HPO₄)₂ and Ti₂NbO₇⁻ and polycations such as polyallylamine and cytochrome *c* has recently been reported; see: Keller, S.W.; Kim, H.-N.; Mallouk, T.E. *J. Am. Chem. Soc.* **1994**, *116*, 8817.
26. Brousseau, L.C.; Aoki, K.; Garcia, M.E.; Cao, G.; Mallouk, T.E. In *Multifunctional Mesoporous Inorganic Solids*; Sequeira, C.A.C.; Hudson, M.J., Eds.; Kluwer Academic: Boston, 1993; pp 225–236.
27. Nakamura, Y.; Yamagishi, A.; Matumoto, S.; Tohkubo, K.; Ohtu, Y.; Yamaguchi, M. *J. Chromatography* **1989**, *482*, 165.
28. Li, D.; Ratner, M.A.; Marks, T.J.; Zhang, C.H.; Yang, J.; Wong, G.K. *J. Am. Chem. Soc.* **1990**, *112*, 7389.
29. Lacroix, P.G.; Clément, R.; Nakatani, K.; Zyss, J.; Ledoux, I. *Science* **1994**, *263*, 658.
30. Ungashe, S.B.; Wilson, W.L.; Katz, H.E.; Scheller, G.R.; Putvinski, T.M. *J. Am. Chem. Soc.* **1992**, *114*, 8717. Keller, S.W.; Johnson, S.A.; Brigham, E.S.; Yonemoto, E.H.; Mallouk, T.E. *J. Am. Chem. Soc.* **1995**, *117*, 12879.
31. Decher, G.; Lvov, Y.; Schmitt, J. *Thin Solid Films* **1994**, *244*, 772.

32. Porter, M.D.; Bright, T.B.; Allara, D.L.; Chidsey, C.E.D. *J. Am. Chem. Soc.* **1987**, *109*, 3559.
33. Lee, H.; Kepley, L.J.; Hong, H.-G.; Akhter, S.; Mallouk, T.E. *J. Phys. Chem.* **1988**, *92*, 2597.
34. Steinberg, S.; Ducker, W.; Vigil, G.; Hyukjin, C.; Frank, C.; Tseng, M.Z.; Clarke, D.R.; Israelachvili, J.N. *Science* **1993**, *260*, 656.
35. Liu, H.-Y.; Fan, F.-R.F.; Bard, A.J. *J. Electrochem. Soc.* **1985**, *132*, 2666.
Stiddard, M.H.B. *Thin Solid Films* **1982**, *94*, 1. Waser, R.; Weil, K.G. *J. Electroanal. Chem.* **1983**, *150*, 89. Putnam, A.; Blackford, B.L.; Jericho, M.H.; Watanabe, M.O. *Surf. Sci.* **1989**, *217*, 276.
36. Feldheim, D.L.; Grabar, K.C.; Natan, M.J.; Mallouk, T.E. *J. Am. Chem. Soc.* **1996**, *118*, 7640.
37. Li, D.; Ratner, M.A.; Marks, T.J.; Zhang, C.; Yang, J.; Wong, G.K. *J. Am. Chem. Soc.* **1990**, *112*, 7389.
38. Day, P.; Ledsham, R.D. *Mol. Cryst. Liq. Cryst.* **1982**, *86*, 163.
39. Wu, C.-G.; Kanatzidis, M.G.; Marcy, H.O.; DeGroot, D.C.; Kannewurf, C.R. In *Lower-Dimensional Systems and Molecular Electronics*; Metzger, R.M.; Day, P.G.; Papavassiliou, C., Eds.; Plenum: New York, 1991; pp 427–433.
40. Bringley, J.F.; Averill, B.A. *Chem. Mater.* **1990**, *2*, 180.
41. Ramsay, J.D.F. *J. Colloid Interface Sci.* **1986**, *109*, 441.

Stepwise Adsorption of Ordered Organic/ Inorganic Multilayers onto Solid Surfaces

3.1 Abstract

Multilayered films were formed on gold, silver, copper, and silicon dioxide surfaces by alternate adsorption of a cationic polyelectrolyte and the anionic sheets of an exfoliated clay. Ellipsometric measurements showed that these films grew linearly in thickness as a function of the number of adsorption cycles. Ultraviolet spectrophotometry of a film on fused quartz showed a linear increase in absorbance with the number of adsorption cycles, demonstrating that films can readily be formed on substrates of interest for optical applications. The growth of the films during each adsorption cycle could be precisely controlled by varying the concentration of the polymer solution: when adsorption treatments were 5 s in duration, use of a 10% (w/w) solution of poly(diallyldimethylammonium chloride), PDDA, led to growth in the first few cycles on silicon of 3.7 nm/cycle, whereas use of a 0.25% PDDA solution led to growth of 1.1 nm/cycle. Intermediate PDDA concentrations led to intermediate growth per cycle. A study of adsorption kinetics (using 5% PDDA solutions) showed that the two components adsorb extremely rapidly; within 5 s the film growth per cycle had reached 76% of the growth attained in 15 min. The films possessed sufficient order in the direction normal to the substrate surface to diffract X-rays, and their expected elemental composition was confirmed using X-ray photoelectron spectroscopy. These results establish the generality of the method for formation of composite films on a variety of substrates. Probes of film structure using cyclic voltammetry revealed that the films are permeable, allowing rapid diffusion of $\text{Fe}(\text{CN})_6^{3-/4-}$ ions to and from a gold electrode surface. Heating films to 700 °C caused the silicate sheets to melt, forming thinner, glassy films that were

sufficiently nonporous to inhibit corrosion of stainless steel by a solution of FeCl_3 . The tendency of copper substrates to discolor upon adsorption of multilayered films was explored. A series of experiments revealed that the PDDA solution catalyzed the oxidation of $\text{Cu}(0)$ to $\text{Cu}(I)$ by air, whereupon the availability of chloride ions (counterion to the cationic polymer) resulted in immediate precipitation of CuCl .

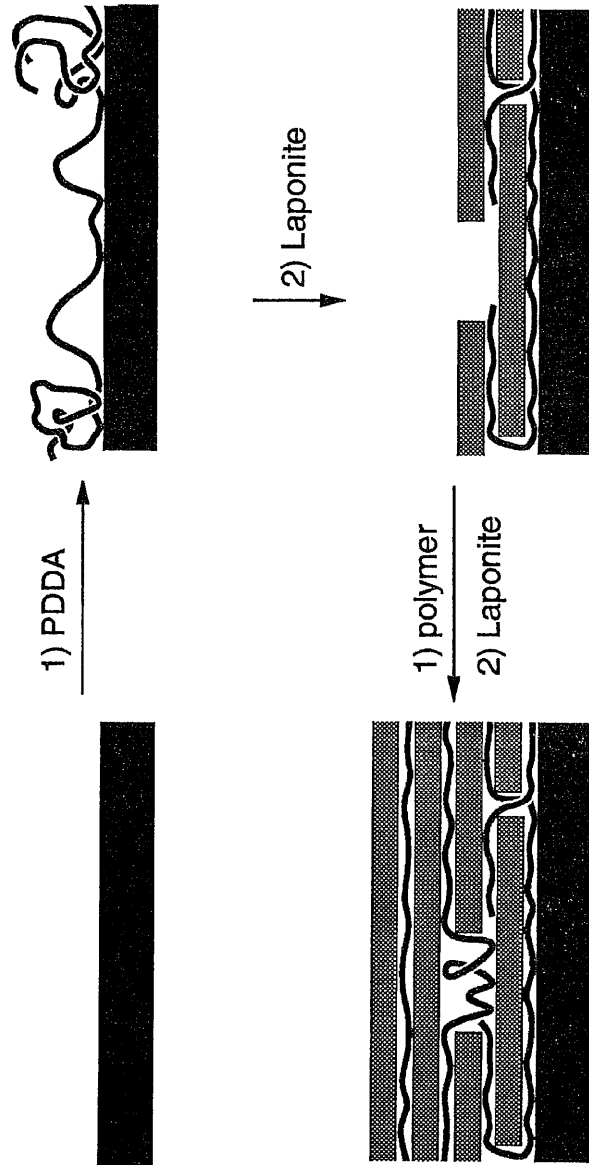
3.2 Introduction

Multilayered films are attractive systems for fundamental study and practical applications because their thickness and structure can, in principle, be precisely controlled. In particular, films formed by stepwise addition of molecularly thin single layers offer promise for use as sensors and selective barriers,¹ as nonlinear optical elements,² and in microelectronics applications.³ Synthetic approaches to this type of multilayered film have included the Langmuir–Blodgett technique,³ repeated adsorption and activation of self-assembled monolayers,^{2,5} and the alternate adsorption of positively and negatively charged polyelectrolytes.^{6–8}

We recently developed a rapid and convenient method for the preparation of multilayered films that possess structural order in the direction normal to the substrate surface—the alternate adsorption of a cationic polyelectrolyte and the anionic sheets of a synthetic clay (Figure 3.1).^{7,9} We found not only that there was no need for pretreatment to promote adhesion of these films to silicon wafers,^{9,10} but also that this method and particular combination of precursors were advantageous because they imparted the ability to “heal” defects—even macroscopically large defects as described in Chapter 4¹¹—during the adsorption of a film. Furthermore, the crystalline silicate layers prevent significant interpenetration of the components in the film, undoubtedly enhancing the degree of structural order that is attainable.

Our initial work raised several questions, including whether the system was

Figure 3.1. Schematic diagram of the preparation of a composite film from a cationic polyelectrolyte—poly(diallyldimethylammonium chloride), PDDA, or poly(N-methyl-4-vinylpyridinium bromide), PMVP—and Laponite.



sufficiently general that films having similar properties could be formed on other substrates. Gold was of particular interest, due to its widespread use both in electrochemical (e.g., sensor) and microelectronics applications. Silver and copper are of interest for microelectronics applications as well. In addition, the uniformity of the films over macroscopic distances suggested that they could be useful in optical applications. To explore this possibility, transparent fused quartz was also used as a substrate for the evaluation of film growth, uniformity, and structure.

Our early studies, detailed in Chapter 2, had employed a 5% (w/w) solution of poly(diallyldimethylammonium chloride), PDDA, a concentration that afforded regular and reproducible film growth. Based upon literature studies of polymer adsorption at surfaces as a function of solution concentration,¹² we anticipated that changes in this parameter would give rise to changes in the amount of material adsorbed per cycle. This chapter presents results demonstrating that the concentration of the polymer solution is indeed a parameter that can be varied to fine-tune the amount of material that adsorbs per cycle, allowing additional flexibility in film preparation. Most of our initial studies also used a very brief adsorption period (~5 s), in contrast to the longer times typically used by others in similar systems.^{8c,10,13} The observation of regular and reproducible growth in the PDDA/Laponite system without the need to exert precise control over the duration of adsorption treatments suggested that beyond the initial 5-s period, adsorption most likely proceeded rather slowly. The kinetics of the adsorption processes were therefore interesting: If other desirable properties of a system can be maintained, shorter adsorption treatments are preferable from the standpoint that they allow thick films to be prepared within practical amounts of time.

The tendency of the films to sorb water rapidly and reversibly, as discussed in chapter 5,¹⁴ indicated that they were porous and capable of a significant degree of

swelling. To investigate the permeability of the films toward larger species, and thus to probe the character of the internal spaces of the swollen multilayers, we formed films of various thicknesses on gold electrodes and performed a preliminary study evaluating their influence on the redox behavior of the ferri-/ferrocyanide redox couple in aqueous solution. The ability to form composite films to precise and uniform thicknesses created the possibility of transforming them into derivative films maintaining these characteristics while imparting additional properties of interest. In this vein, we explored whether treatment at elevated temperatures would result in densification of the structure, creating uniform and nonporous films. Films were heated to 700 °C in flowing argon, and the refractive index, thickness, hardness, and porosity of the resulting films were evaluated. The ability to use fused films as decorative and functional coatings for stainless steel was also tested. Finally, the tendency of copper substrates to discolor upon adsorption of composite films was investigated.

3.3 Results and Discussion

3.3.1. Materials and Methods. Films were adsorbed on reflective substrates—gold, silver, copper, and silicon—by dripping a 5% (w/w) solution of poly(diallyldimethylammonium chloride), PDDA, onto the substrate (unless the concentration is noted otherwise), extensively rinsing the surface with water after ~5 s (unless the time is noted otherwise), blowing it dry with a jet of nitrogen, dripping on a 0.2% (w/w) suspension of Laponite, and rinsing after ~5 s and drying as above. In some studies, fused quartz microscope slides were used as substrates and growth was monitored using ultraviolet (UV) spectrophotometry. In these studies, poly(*N*-methyl-4-vinylpyridinium bromide), PMVP, was used rather than PDDA due to its absorbance in the uv region. To coat both sides of the slides evenly, these substrates

were alternately dipped for ~5 s each into a 1% (w/w) solution of PMVP and a 0.2% (w/w) suspension of Laponite, and extensively rinsed with water and blown dry with a jet of nitrogen after each step as described above.

The structures of the two linear cationic polyelectrolytes used in film formation are shown in Figure 3.2.¹⁵ The molecular weight of the PDDA was 200,000–350,000, and that of the PMVP was 50,000. Laponite, a synthetic form of hectorite, is a sheet silicate mineral similar in structure to talc. In talc, individual lamellae are made up of a central layer of edge-sharing MgO_6 octahedra and two outer layers of corner-sharing SiO_4 tetrahedra and are charge-neutral. In hectorite, partial substitution of lithium for magnesium in the octahedral sheet results in a deficiency of positive charge that is compensated by interlayer sodium ions. Water can be intercalated reversibly into the interlayer spaces, and under appropriate conditions the lamellae may be fully exfoliated to form a suspension of individual sheets. Fully dehydrated hectorite has a d-spacing (along the direction normal to the sheets) of 0.96 nm; however, this thickness includes the interlamellar cations. The d-spacing of talc, 0.93 nm, may provide a better estimate of the true thickness of the isolated sheets.¹⁶

3.3.2. Film Growth on Metals. On metallic substrates, the thickness of the multilayered films was monitored ellipsometrically, assuming a single smooth film with a refractive index of 1.5. This index was representative of values measured ellipsometrically for films 40–200 nm in thickness (*vide infra*). Figure 3.3 shows the growth in thickness of multilayers on gold, silver, and copper as a function of the number of adsorption cycles when 5-s treatments with 5% PDDA and 0.2% Laponite were used. In the first ten adsorption cycles on gold (Figure 3.3a, inset), the multilayer structures grew approximately 3.3 nm per cycle, roughly 1.2 nm during the polymer-adsorption step and 2.1 nm during the silicate-adsorption step. This pattern of growth also characterized adsorptions onto silicon wafers, as reported

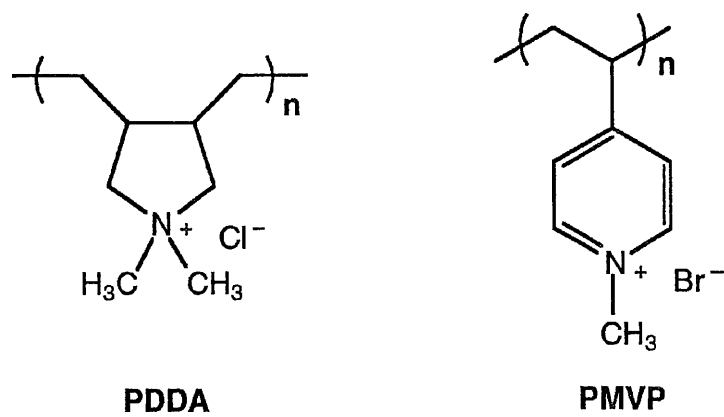
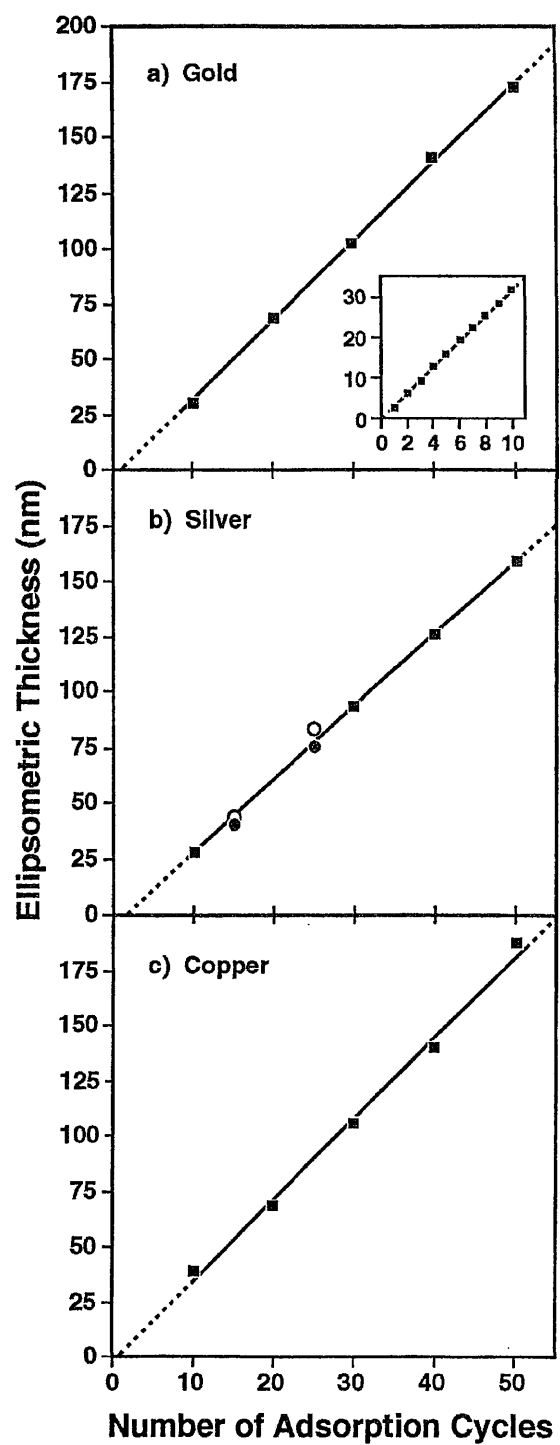


Figure 3.2. Structures of the cationic polyelectrolytes used in the formation of multilayered films.

Figure 3.3. Ellipsometric thickness of PDDA/Laponite films as a function of the number of adsorption cycles on (a) gold, (b) silver, and (c) copper substrates, assuming a refractive index of 1.5. The slope of the linear least-squares fit in the inset is 3.2 nm/cycle, while for 10–50 cycles on gold, silver, and copper, the slopes are 3.6, 3.3, and 3.7 nm/cycle, respectively.¹⁷ The squares represent average thicknesses measured on single samples of each substrate. The least-squares fit for silver does not include the filled and open circles, which represent measurements on two additional, independent samples and indicate the level of sample-to-sample variability observed in this system. The point for 20 cycles on silver was omitted, because the values for Δ and Ψ used to calculate thickness were in a region where slight changes in Ψ ($\pm 0.01^\circ$, which is within experimental error) resulted in large changes in calculated thickness (>15 nm), and were therefore judged unreliable.

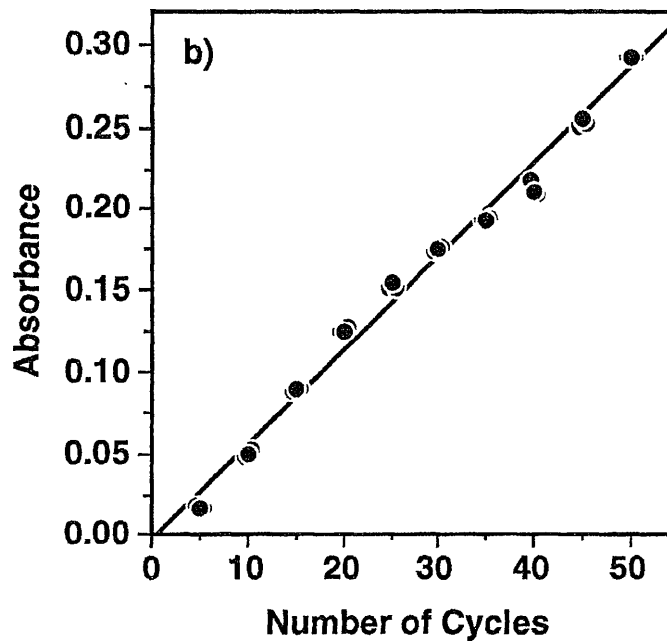
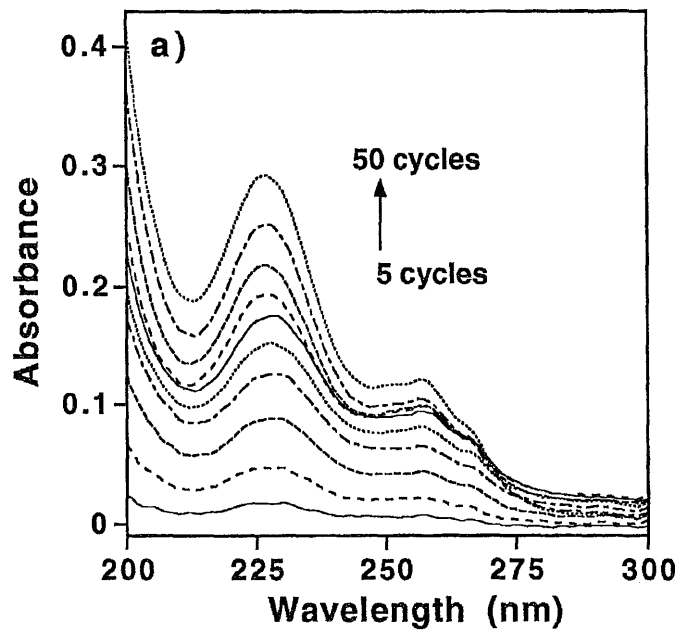


earlier.⁹ The slopes of the linear least-squares fits in Figure 3.3 for 10 – 50 cycles are 3.6 nm/cycle on gold, 3.3 nm/cycle on silver, and 3.7 nm/cycle on copper.¹⁷ The differences in these slopes may be attributable, at least in part, to differences in relative humidity on the days that the films were prepared, as water vapor readily swells these structures (Chapter 5).¹⁴ Comparison of the data for film growth on gold presented in Figure 3.3a and in its inset indicates that the average thickness added per cycle on gold increased slightly as the number of cycles increased. This behavior may be due to a change in refractive index as the film grew in thickness. Unfortunately, refractive indices determined ellipsometrically for films as thin as those shown in the inset are not as reliable as those determined for thicker films;¹⁸ we were therefore unable to confirm or rule out this possibility. The small apparent drift in growth per cycle on a particular substrate may, alternatively, be characteristic of PDDA/Laponite films: a similar variation was observed for films on silicon, where a slope of 3.2 nm/cycle was observed for the first five cycles and a slope of 3.6 nm/cycle was observed for the first 60.⁹ The linear increase in film thickness with the number of cycles indicates that the adsorption process is regular, with the large lateral extent of the Laponite sheets in any given layer (~25–35 nm) providing coverage of packing defects (i.e., spaces at platelet edges) in the immediately underlying layer.^{9,11}

3.3.3. Film Growth on Quartz. For monitoring the growth of multilayered films on transparent fused quartz substrates, we used ultraviolet (uv) spectrophotometry. The use of poly(*N*-methyl-4-vinylpyridinium bromide), PMVP, rather than PDDA in this study was therefore motivated by the need for a cationic polyelectrolyte with absorptions in the near-uv region. We had previously demonstrated ellipsometrically that films formed from PMVP (10% w/w) and Laponite (0.2% w/w) displayed regular growth on Si/SiO₂ substrates (Chapter 2).¹⁹ The present study employed

PMVP at a concentration of 1% (w/w) and Laponite at a concentration of 0.2% (w/w). The duration of the adsorption treatments was, as usual, 5 s, but to ensure that both sides of the quartz slides were coated evenly, these substrates were coated by dipping into the component solutions, rather than by dripping. Spectra of PMVP/Laponite films were obtained between 200 and 300 nm, and absorbance was quantified at a λ_{max} of 227 nm. This peak occurred at 226 nm in an aqueous solution of 0.004% (w/w) PMVP; neither a 0.2% (w/w) Laponite suspension nor a film produced by evaporation of water from a Laponite suspension contained this feature. Representative spectra taken periodically during formation of a multilayered film are shown in Figure 3.4a, and a plot of absorbance as a function of the number of adsorption cycles is shown in Figure 3.4b. Individual data points in Figure 3.4b represent absorbance values taken using a single sample. To estimate the uncertainty in these values attributable to sample positioning, three spectra were taken from this sample every five cycles, removing and replacing the sample in the spectrophotometer between spectra. The slope of the linear least-squares fit in Figure 3.4b is 0.0058 absorbance units per cycle; the linearity of this plot indicates that the growth of the film was uniform, provided that the Beer–Lambert law holds in these films. Similar results were obtained from other samples. Thus the ellipsometric¹⁹ and spectrophotometric data were consistent with one another in indicating that PMVP/Laponite films display regular growth. The molar absorptivity of the polymer was measured by a serial dilution experiment to be $6970 \text{ cm}^{-1}\text{M}^{-1}$.²⁰ Use of this value, along with the observed slope in the linear least-squares fit to the data of absorbance as a function of the number of adsorption cycles, indicated that the density of monomer units adsorbing per cycle was $5.01 \times 10^{14} \text{ molecules/cm}^2$. This density, in turn, corresponds to an area of $20.0 \text{ \AA}^2/\text{molecule}$, which is somewhat smaller than the minimum area occupied by an individual monomer unit of the

Figure 3.4. Growth of a PMVP/Laponite multilayer on a fused quartz slide, monitored using uv spectrophotometry: a) Representative spectra obtained after increments of 5 cycles; b) Absorbance at a λ_{max} of 227 nm as a function of the number of adsorption cycles. The slope of the linear least-squares fit indicates an increase of 0.0058 absorbance units per cycle. Measurements were performed in triplicate after each five cycles to provide an estimate of the uncertainty associated with sample positioning, as explained in more detail in the text. Some of the points in (b) have been offset slightly in the x-direction for clarity of presentation.



polymer, ca. 24 \AA^2 , estimated using a CPK model. All values generated from this analysis should be viewed with caution, as they indicate that the chromophores were apparently very concentrated in the film, whereas the Beer–Lambert law applies to dilute solutions. In addition, the chromophores within the films may exhibit a preferred orientation, giving rise to an effective absorptivity different from that measured in solution. The data may suggest, however, that the polymer layer adsorbed in each cycle was not limited to a single dense monolayer, but was rather a thicker layer, containing loops and tails that extended away from the substrate surface, as depicted in Figure 3.1.

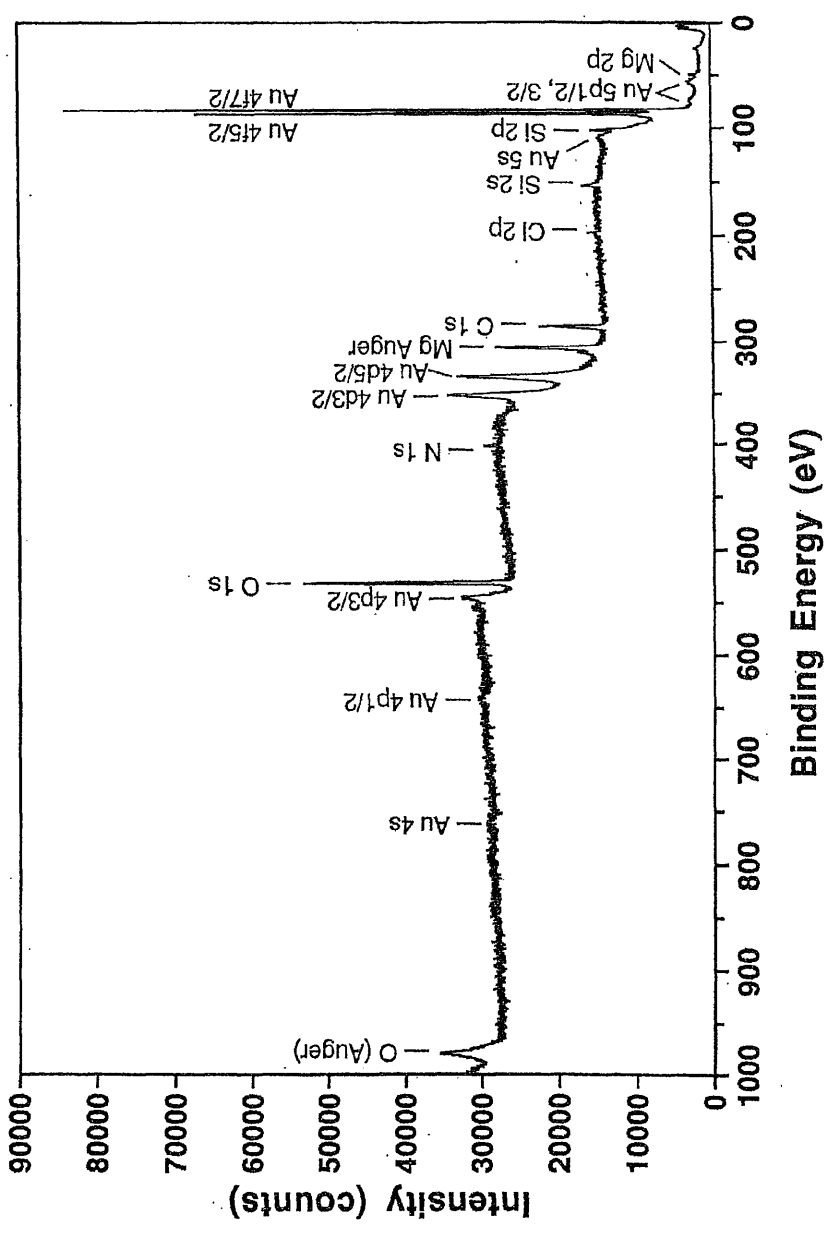
3.3.4. Interference Effects Displayed by Multilayered Films. As films grew in thickness on silicon wafers, a series of vivid, uniform colors was observed due to interference between the light reflected from the air/film interface and the light reflected from the film/substrate interface.⁹ In contrast, only subtle colors were observed on gold, copper, and quartz, and none were seen on silver. We attribute these differences to the fact that interference effects are maximized when the intensity of the light reflected from the air/film interface is similar to the intensity of the light reflected from the film/substrate interface. The vivid colors of films on silicon wafers indicate that the reflected intensities from the air/film and film/substrate interfaces are similar, whereas the subdued (or absent) interference colors from the films on fused quartz and the metals result from the reflected intensity at the film/substrate interface having been significantly reduced (quartz) or enhanced (metals).^{8a,21} The slight undulation present in the graph of uv absorbance versus layer number for the film on fused quartz (Figure 3.4b) suggests that interference effects are influencing these results as well. Adding support to this hypothesis is the fact that graphs of uv absorbance versus layer number taken at 200 and 300 nm show similar undulations, but occurring at a lower and higher number of

adsorption cycles, respectively. A more subtle undulation was present in data obtained by others for a system involving the alternate adsorption of oppositely charged organic polyelectrolytes.¹³ Its opposite sign suggests that in their system the refractive index of the film was higher than that of the substrate, rather than lower as was the case in our system.

3.3.5. Elemental Composition of a Composite Film. X-ray photoelectron spectroscopy (XPS) of a sample formed by the adsorption of PDDA, then Laponite, then PDDA onto a gold substrate confirmed the presence of the elements that were expected, based upon the composition of the component materials and substrate:²² gold, carbon, nitrogen, chlorine, silicon, oxygen, and magnesium (Figure 3.5). Lithium was not detected in the survey spectrum; its absence reflects its low concentration in Laponite as well as the low sensitivity factor of the Li $1s_{1/2}$ orbital. This peak might also be especially difficult to detect in a film on this substrate due to a possible overlap with the Au $5p_{3/2}$ peak. Sodium, which is present in Laponite as an interlamellar cation, also did not appear in the spectrum, presumably because it had been exchanged for the cationic polymer. These results are consistent with those for a similar film on a silicon substrate, in which silicon, oxygen, magnesium, carbon, nitrogen, and chlorine were detected (Chapter 2).⁹

3.3.6. X-Ray Diffractometry. Although ellipsometric measurements and uv spectrophotometry were useful for demonstrating regularity in the growth of multilayers, they provided little or no information about the internal structure of the films. We have shown previously that this synthetic method can be used to prepare multilayers on silicon wafers that are sufficiently ordered in the growth direction to diffract x-rays.⁹ To investigate the generality of the method in this regard, we used x-ray diffractometry (XRD) to examine one of the samples prepared on a gold substrate. The diffraction pattern of a sample prepared by 50 adsorption cycles of

Figure 3.5. X-ray photoelectron survey spectrum of a sample prepared by the adsorption of PDDA, then Laponite, then PDDA onto a gold-coated silicon wafer. The concentration of the PDDA solution was 5% (w/w) and that of the Laponite RD suspension was 0.2% (w/w). Adsorption treatments were 5 s in duration.

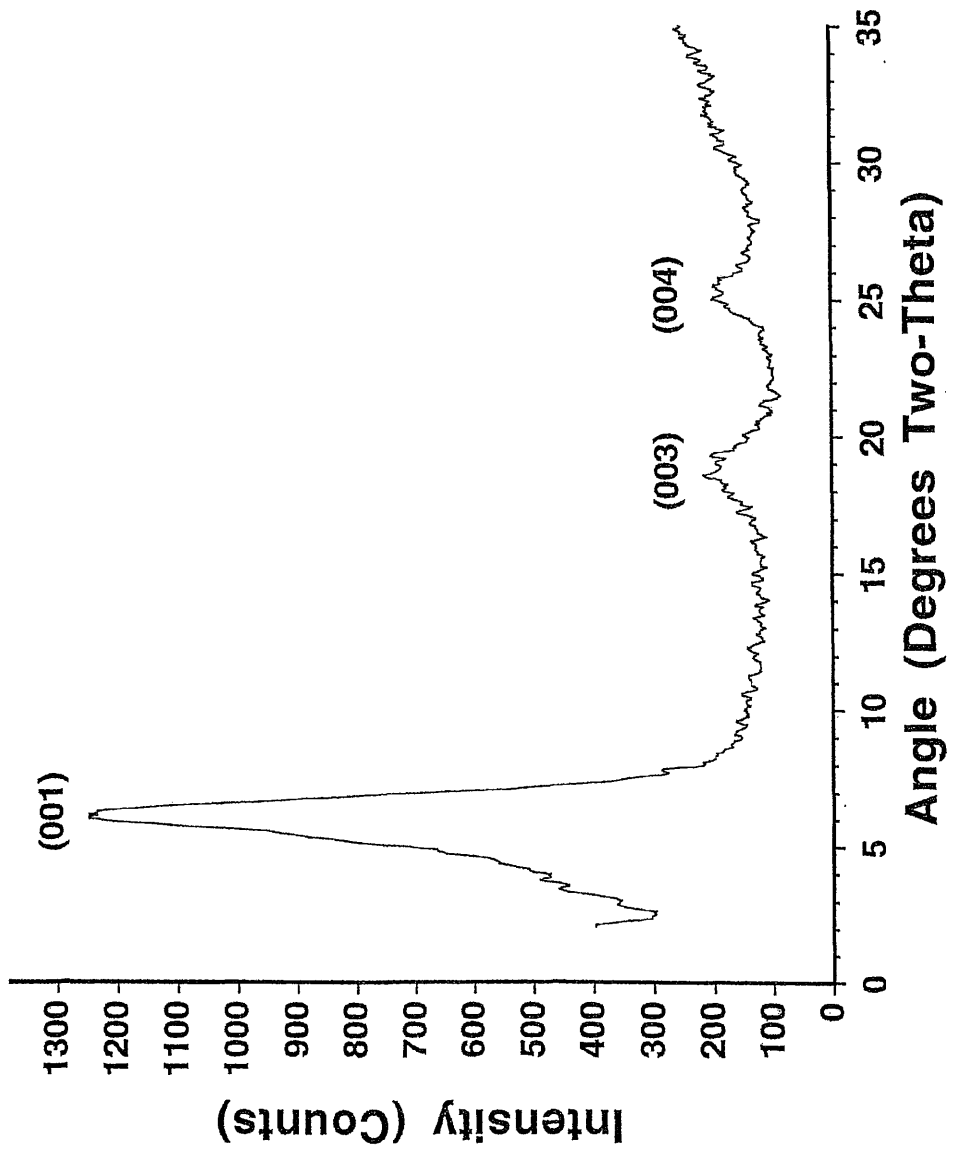


5% PDDA and 0.2% Laponite on gold is shown in Figure 3.6. The (001) reflection at $6.0^\circ 2\theta$ indicates a lattice spacing of 1.47 ± 0.02 nm; the (003) and (004) reflections at 18.7° and 25.1° indicate lattice spacings of 1.43 and 1.42 ± 0.02 nm.²³ The absence of the (002) reflection is attributable to destructive interference between x-rays reflected from different scattering planes within the unit cell. Patterns very similar in appearance to the one in Figure 3.6 were obtained from 50-cycle samples prepared on silver and copper substrates.

To a first-order approximation, application of the Bragg equation to the peaks in an XRD pattern allows calculation of the dimensions of crystalline unit cells. In the data presented above, however, the basal reflections occurred in positions indicating slightly different lattice spacings. This phenomenon can occur whenever the peaks in an XRD pattern are significantly broadened, and has been termed “apparent irrationality”²⁴ to distinguish it from the “true” irrationality that results when a lattice contains cells of differing dimensions (e.g., randomly interstratified sheet minerals). Apparent irrationality results from the tendency of broadened XRD peaks to shift in the direction of increasing values of the square of the structure factor.²⁴ Although all the (00*l*) peaks are affected, the (001) peak is affected most strongly, so the true d-spacing is closer to those indicated by the higher-order reflections (~1.43 nm). This lattice spacing is consistent with a structure in which Laponite layers, ~0.93 nm in thickness, alternate with PDDA layers ~0.5 nm in thickness to form a composite structure with an ABAB arrangement. Further discussion of apparent irrationality in the XRD patterns of composite films is presented in Chapter 7.

The Scherrer equation was used to provide an estimate of the size of the ordered domains in the sample.²⁵ According to this equation, the size of ordered domains (*L*) in the direction perpendicular to the diffracting planes is given by

Figure 3.6. X-ray diffraction pattern of a 50-cycle film formed by adsorption of PDDA from a 5% (w/w) solution and Laponite from a 0.2% (w/w) suspension onto gold. The labeled peaks indicate a lattice spacing of ~ 1.43 nm.



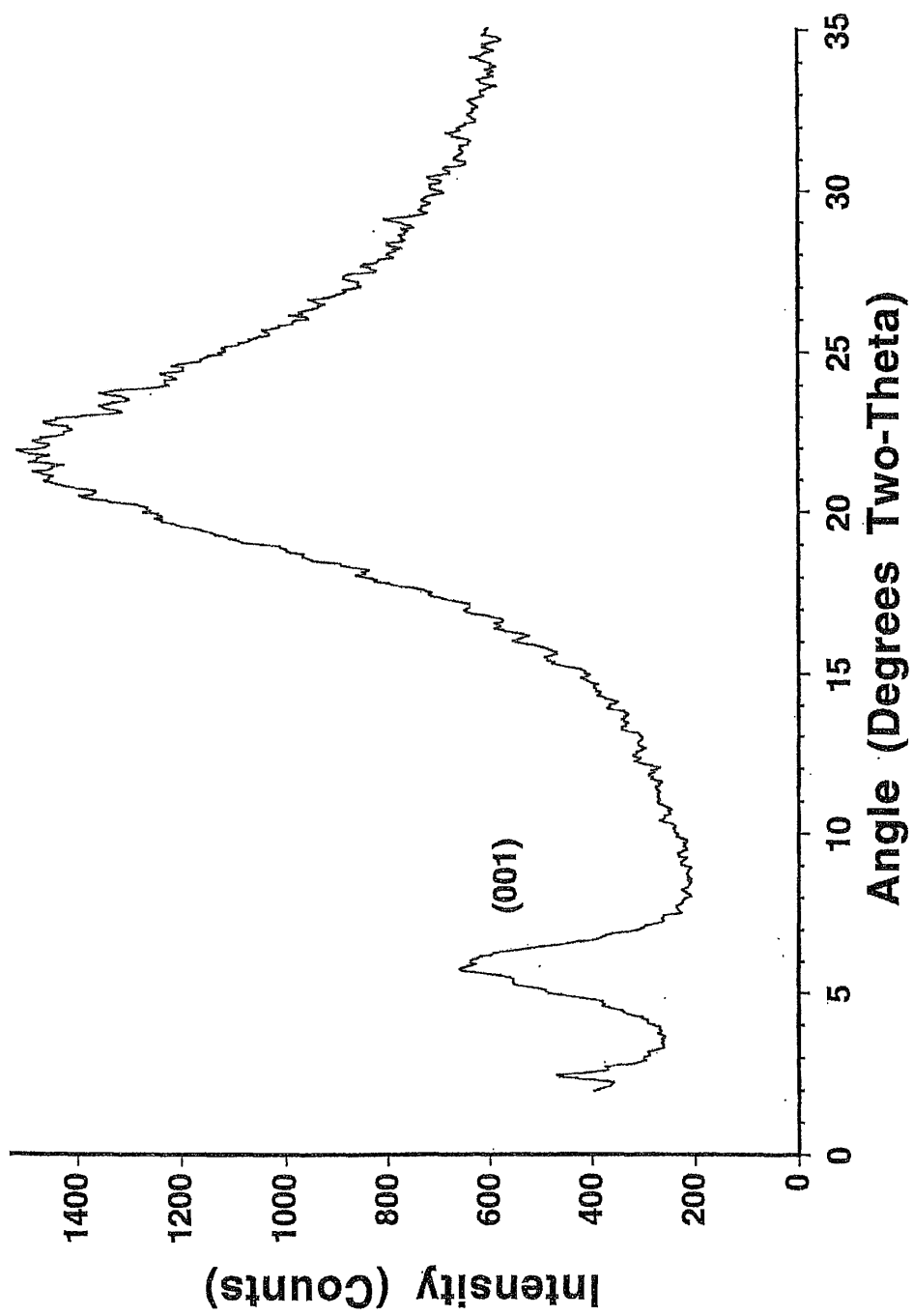
$$L = 0.94 \lambda / \{B(2\theta) \cos \theta\}$$

where λ is the X-ray wavelength, $B(2\theta)$ is the full-width at half-maximum intensity (in radians) of the peak of interest, and θ is the peak position. The values generated by this equation are useful for comparison to similar films, but tend to underestimate actual crystallite sizes revealed by direct methods such as cross-sectional transmission electron microscopy.²⁶ For the (001) peak in the pattern shown in Figure 3.6, $\lambda = 0.154$ nm, $B(2\theta) = 1.9^\circ = 0.033$ rad, and $\theta = 3.0^\circ$, giving an estimated domain size of 4.3 nm in the direction normal to the silicate sheets. Alternatively, the peaks may be broadened due to variability in the interlayer spacings, as discussed in Chapter 7.

In our original paper, noting that the ellipsometric growth per cycle was more than twice the d-spacing of the composite lattice when a 5% PDDA solution was used, we proposed that polymer chains that are loosely associated with the sample surface may be displaced away from the surface during a subsequent treatment with the Laponite suspension, and may bind a second layer of the silicate, as shown in Figure 3.1.⁹ The Scherrer analysis of the XRD patterns in the present paper adds weight to this model, by indicating that the ordered crystallites in the films are at least three unit cells in thickness. To our knowledge, no plausible mechanism has been proposed for the formation of ordered crystallites this large in the absence of polymer displacement. Of course, under conditions in which growth per cycle did not exceed the unit-cell spacing,²⁷ this mechanism would be expected to occur with less frequency, and might even be undetectable by indirect methods.

An XRD pattern of a sample prepared by 50 adsorption cycles of 1% PMVP and 0.2% Laponite on a quartz slide is shown in Figure 3.7. The peak at $5.7^\circ 2\theta$, with a FWHM of 1.7° , is assigned to the (001) reflection of the PMVP/Laponite lattice, and gives a calculated d-spacing of 1.55 ± 0.02 nm. Higher order (00*l*) peaks, if present,

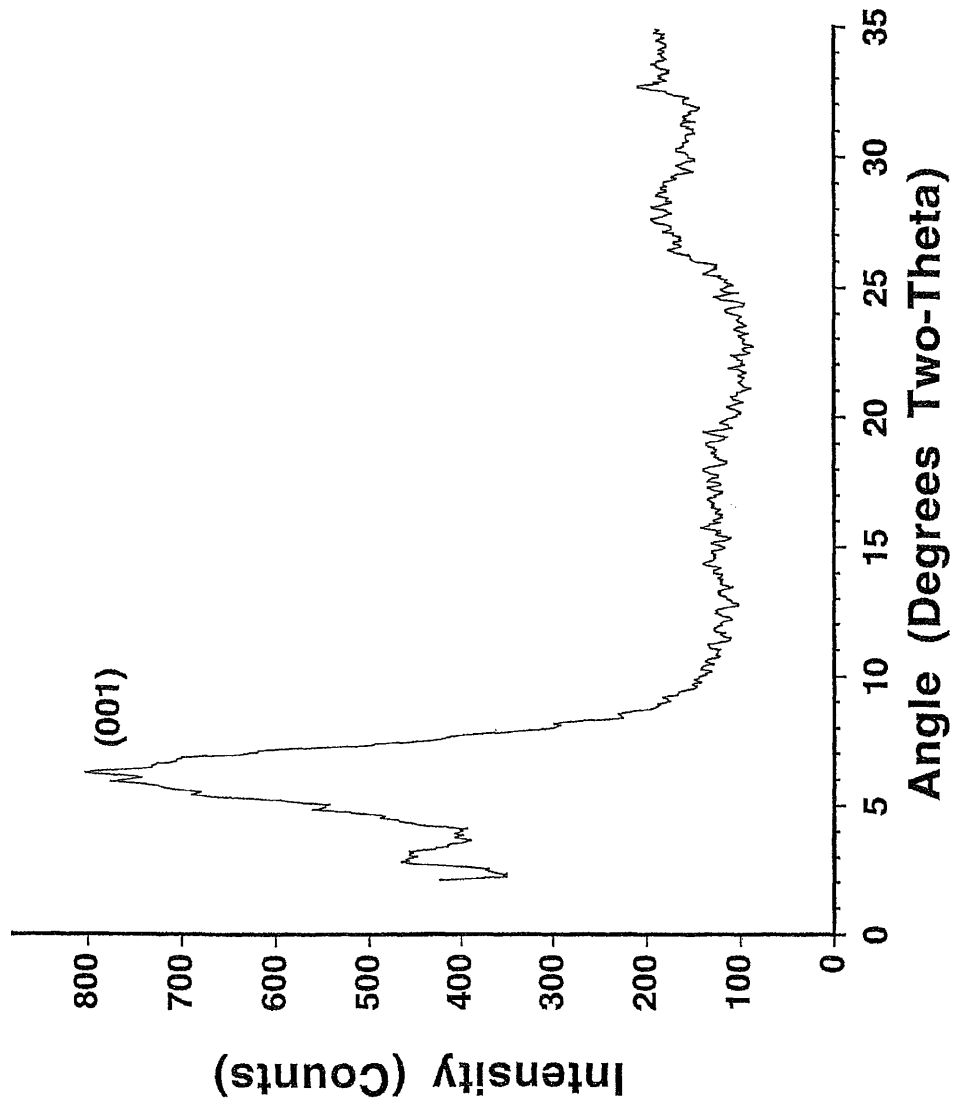
Figure 3.7. X-ray diffraction pattern of a 50-cycle film formed by adsorption of PMVP from a 1% (w/w) solution and Laponite from a 0.2% (w/w) suspension onto a fused quartz slide. The labeled peak indicates a lattice spacing of ~ 1.55 nm. The intense feature at $21^\circ 2\theta$ is attributable to the fused quartz substrate, while the low-intensity peak near $2.5^\circ 2\theta$ is believed to be an instrumental artifact.



are obscured by the broad feature near $21^\circ 2\theta$, which is attributable to the fused quartz substrate. The estimated size of the ordered domains in this film is 5.0 nm, from which we infer that the d-spacing calculated from the position of the (001) peak may be exaggerated due to small-crystallite effects as explained above for the PDDA/Laponite film. The absence of distinct higher-order reflections in this pattern prevents more accurate determination of the true film structure. We believe that the small peak at $2.5^\circ 2\theta$ is an instrumental artifact, as peaks similar or identical in position appear irreproducibly in many patterns obtained using this instrument, and do not appear in patterns of samples prepared identically but analyzed on other diffractometers.

As a control experiment, we obtained diffraction patterns of films of the individual polymeric precursors, PDDA and PMVP, which were prepared by the evaporation of solutions onto silicon substrates. These patterns bear no resemblance to the patterns shown in Figures 3.6 and 3.7, indicating that the peaks observed in patterns of the composite films are not due to crystallites of these components. The XRD pattern of as-supplied, powdered Laponite contains no distinct (00 l) reflections, indicating that this material is poorly ordered in the c-axis direction and thus ruling out the possibility that order in our films is due to "unexfoliated crystallites" of this starting material. The XRD pattern of a film prepared by evaporation of a 0.1% suspension of Laponite alone onto silicon is shown in Figure 3.8. This film was uneven in thickness, but averaged approximately 150 nm. The (001) peak occurs at $6.3^\circ 2\theta$, indicating a d-spacing of 1.40 ± 0.02 nm; other films of evaporated Laponite on silicon have had (001) peaks in positions indicating d-spacings between 1.4 and 1.5 nm. The FWHM of the (001) reflection (2.9°) is consistent with an estimated domain size of 2.9 nm. Other features in this pattern are too weak and broad to be assigned with certainty. D-spacings near 1.24 nm are

Figure 3.8. X-ray diffraction pattern of Laponite RD. The sample was prepared by dripping a 0.1% suspension of Laponite onto a silicon wafer and allowing the water to evaporate under ambient conditions. The labeled peak indicates a lattice spacing of ~ 1.40 nm.



found for sodium smectites containing one interlamellar layer of water;²⁸ the discrepancy between that value and ours most likely results from small-crystallite effects and exemplifies the difficulties in determining d-spacings from a single reflection (as was also true for the PMVP/Laponite results given above). Strikingly, the narrower (00l) peaks in the patterns of our composite films indicate that the layer-by-layer adsorption process induced a higher degree of structural order than was obtained by simple evaporation of the Laponite suspension.

3.3.7. Dependence of Film Growth on Polymer Solution Concentration. In typical preparations of PDDA/Laponite films, we have used a polymer solution concentration of 5% (w/w) and have observed linear growth in thickness of roughly 3.5 nm per cycle. X-ray diffractometry, however, showed that the unit-cell spacing is ~1.43 nm,⁹ indicating that under these conditions more than one layer of unit cells was adsorbed in each cycle. Our model for adsorption, depicted in Figure 3.1, involves uniform coverage of the substrate in each cycle (a result confirmed by AFM, as shown in chapter 2⁹) and addition of more than one unit cell due to excess adsorption of polymer under these conditions. This model implies that achieving growth consistent with the adsorption of one monolayer of each component should be possible by modifying the polymer adsorption conditions. Typical polymer adsorption isotherms demonstrate that the limiting amount of a polymer adsorbed onto a particular substrate increases with increasing concentration of the polymer in solution.²⁹ Furthermore, kinetics studies indicate that even after very short periods of time, more material adsorbs from solutions of high concentration than from solutions of low concentration.^{12,30} Although, in general, such studies have been performed with polymer solutions far lower in concentration than those used in the present study, we expected to observe similar trends.

To determine the effect of polymer concentration on multilayer growth, films

were adsorbed onto silicon substrates using solutions of PDDA having concentrations of 0.25%, 1%, 5%, and 10% (w/w), with all other conditions being held constant. As shown in Figure 3.9, linear growth was observed for each concentration studied, with the amount adsorbed per cycle increasing with increasing polymer concentration. The slopes of the linear least-squares fits were 1.1, 2.0, 2.9, and 3.7 nm/cycle for films prepared using the 0.25%, 1%, 5%, and 10% PDDA solutions, respectively. The data for each concentration of PDDA were obtained on individual silicon samples, and each data point corresponds to a single measurement at a particular site on a sample. Significantly, the XRD pattern of a film made from 0.25% PDDA and 0.2% Laponite had peak positions very similar to those in the pattern of the film formed from 5% PDDA and 0.2% Laponite discussed earlier. The calculated domain size in this case was 6.5 nm, compared to a domain size of 4.3 nm for a film made from 5% PDDA. This result indicated that the ordered material in the two films was similar in structure, an ordered ABAB arrangement of the polymer and silicate having a d-spacing of ~1.43 nm. The growth in thickness per cycle using the 0.25% solution, 1.1 nm, was *less than* this d-spacing, indicating that in any particular cycle, the film growth was incomplete, with addition of one unit cell in some areas and none in others. This result indicated that regular growth could occur in the PDDA/Laponite system even when less than a full monolayer was adsorbed in each cycle.

Under the conditions used in this experiment, a four- to ten-fold increase in the polymer concentration was required in order to double the overall growth in thickness per cycle when 5-s adsorption treatments were used. To determine the portions of this growth that were attributable to individual treatments with each of the two components, we measured the ellipsometric growth resulting from each adsorption treatment (PDDA or Laponite) for two cycles, using a variety of polymer

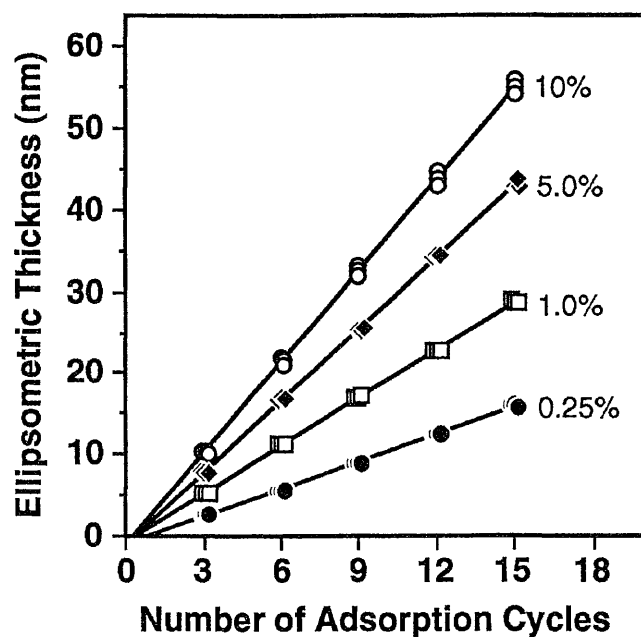


Figure 3.9. Ellipsometric thickness as a function of the number of adsorption cycles when different concentrations of PDDA were used in the formation of composite films. The concentration of the Laponite suspension was the same in all cases (0.2% w/w). Linear least-squares fits to the data gave slopes of 1.1, 2.0, 2.9, and 3.7 nm per cycle for the films made from 0.25%, 1%, 5%, and 10% PDDA solutions, respectively. Some points have been offset in the x-direction for clarity of presentation.

concentrations (Figure 3.10). In all cases, the same Laponite suspension was used (0.2% w/w). To minimize substrate effects in these experiments, two cycles of 5% PDDA and 0.2% Laponite were adsorbed onto the silicon substrates prior to the adsorptions of interest. Individual data points in Figure 3.10 represent average growth on a particular sample in one treatment or cycle. The ellipsometric thickness of the adsorbed polymer layer increased monotonically with increasing polymer concentration (lowest trace). These results were obtained after allowing the polymer solutions to remain on the silicon surfaces for only 5 s, and do not represent limiting values. In turn, the ellipsometric thickness of the silicate adsorbed onto each of these samples also increased monotonically (middle trace). We attribute the ability to adsorb more than a monolayer thickness of Laponite for certain polymer concentrations to the ability of some loosely adsorbed polymer to be displaced from the surface and to attract a second layer of Laponite.⁹ The apparent negative curvature to these data suggests that there is a limit to the amount of Laponite that can be adsorbed in this way. The results from these studies demonstrate that polymer concentration is one easily controllable variable that can be used to “fine-tune” the amount of material adsorbed per cycle. As a result, conditions could be chosen so that the average amount of material adsorbing per cycle corresponded to the thickness of one unit cell.⁷ Such a correspondence between adsorbed amount and unit cell thickness alone would not necessarily imply that the material adsorbed as a single, complete layer during each treatment, however, as it would fail to rule out the possibility that excess growth occurred in some areas while it was incomplete in others.

3.3.8. Adsorption Kinetics of the PDDA/Laponite System. In typical preparations of PDDA/Laponite films, we have used adsorption treatments lasting roughly 5 s. As noted above, the adsorbed layers were not expected to reach limiting thicknesses

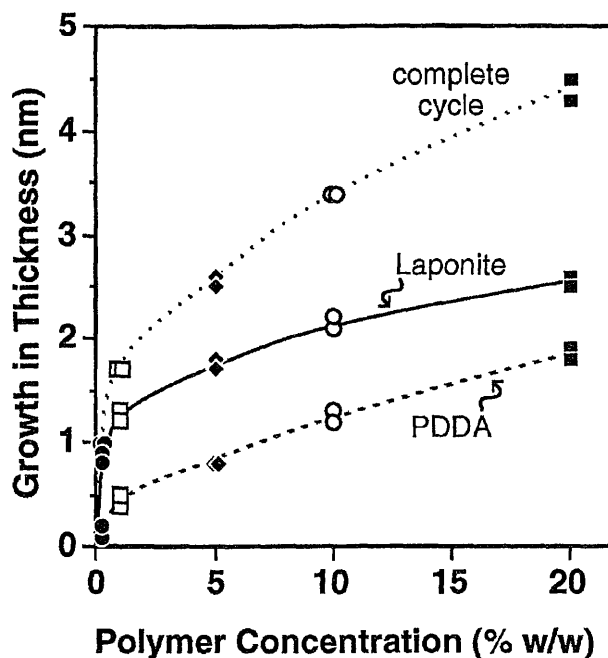


Figure 3.10. Dependence of film growth on the concentration of the polymer solution used to form the film. Lower trace: increase in thickness when PDDA solutions of different concentration were dripped onto substrates and rinsed and blown dry after ~5 s. Middle trace: increase in thickness when a 0.2% (w/w) suspension of Laponite was dripped onto each of these samples and rinsed and blown dry after ~5 s. Upper trace: Total growth in thickness (sum of PDDA and Laponite traces) for each of these samples. The substrates were silicon wafers that had been treated with two cycles of 5% PDDA and 0.2% Laponite. Each data point represents the average of three measurements taken on a single sample during one adsorption cycle. Some points have been offset slightly in the x-direction for clarity of presentation. The lines are guides for the eye.

within this time period; nonetheless, we have consistently observed reproducible and regular growth when these conditions were used. We therefore inferred that, even after this brief period of time, the rate of adsorption had slowed to the point that small variations in adsorption time would not significantly affect the results. To test this inference quantitatively, we determined the dependence of ellipsometric growth per cycle on the duration of the adsorption treatments. Films were adsorbed from 5% (w/w) PDDA and 0.2% (w/w) Laponite onto bare silicon substrates, allowing each component to remain on the surface for 5 s, 15 s, 1 min, or 15 min. All other conditions were held constant, with the exception that for the 15-min adsorption treatments, the wafer was immersed into the component solutions rather than having the solutions dripped onto the surface. As shown in Figure 3.11a, regular growth was observed for each sample, with the amount adsorbed per cycle increasing with increasing adsorption time. Each data point in Figure 3.11a corresponds to the average of three measurements taken on a particular sample, and a separate sample was used for each adsorption time studied. The height of the open diamonds corresponds to the largest scatter (full range) observed on any sample. Figure 3.11b shows the average increase in thickness per adsorption step or cycle, derived from the data plotted in Figure 3.11a. From these data it is clear that even though the amount adsorbed did not reach a limiting value within 5 s, further adsorption was relatively slow after this time. The general shape of the polymer adsorption curve (lowest trace) is similar to that observed by others for adsorption of polyelectrolytes,³⁰ although the polymer concentration used here was far higher than is typical for such studies.

3.3.9. *Effect of Relative Humidity on Apparent Growth per Cycle.* Films made from PDDA and Laponite sorb water from the air, causing changes in both their thickness and refractive index, as detailed in chapter 5.^{14,31} For example, the ellipsometric

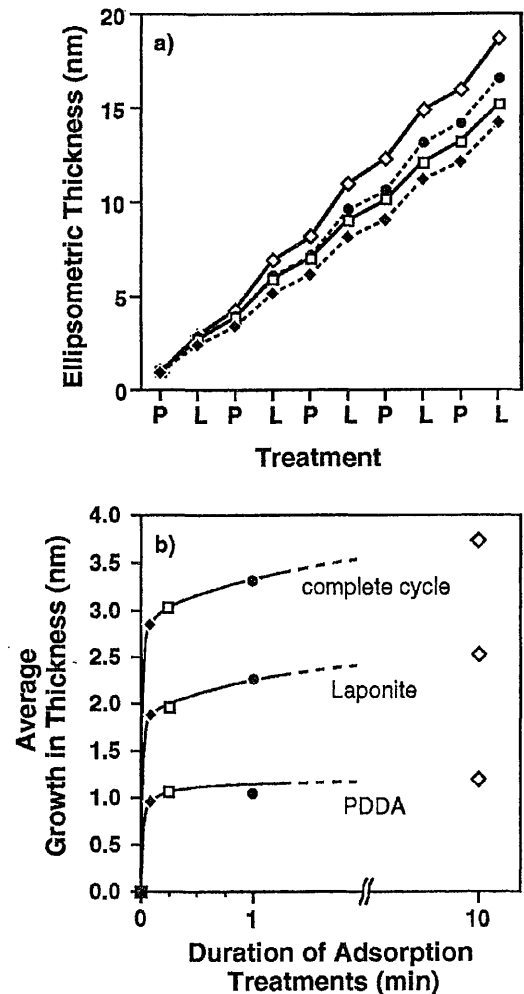


Figure 3.11. Dependence of film growth on the duration of the adsorption treatments. a) Ellipsometric thickness of films formed by alternate treatments with 5% PDDA (P) and 0.2% Laponite (L) for various adsorption times (filled diamonds—5 s; squares—15 s; circles—1 min; open diamonds—10 min). b) Average growth in thickness observed for each step or cycle for the data shown in (a): lower trace—growth during polymer adsorption step; middle trace—growth during Laponite adsorption step; upper trace—total growth in thickness (sum of PDDA and Laponite traces).

thickness of a 25-cycle film increased by 22% when the relative humidity (RH) of its environment was changed from ~0% to ~87%. Use of a quartz crystal microbalance to monitor the kinetics of mass uptake or release showed that the sorption of water was reversible and very rapid, being largely complete within seconds after a change in environment between ~0% and ~95% RH. As a result, the ambient relative humidity has an effect on ellipsometric growth per cycle. We infer that differences in RH account for much or all of the variability in growth per cycle that we observe from day to day.

3.3.10. Use of a Pretreatment to Promote Adhesion of the First Silicate Layer. Many methods for forming multilayered films by sequential adsorption of polyelectrolytes begin with pretreatment of the substrate to promote adhesion of the first component of the film.^{6,8c} As demonstrated in our original paper for silicon substrates⁹ and above for metals and quartz, *no* pretreatment is necessary for forming films of PDDA or PMVP and Laponite.^{8a,8d,10} In fact, we have shown that these films will grow on substrates that have little or no propensity to adsorb either component individually, as discussed in chapter 4.¹¹ Since a primer layer may be desired for specific applications, however (for example, to strengthen adhesion between the substrate and the film), we sought to demonstrate that such a layer could be used in the formation of PDDA/Laponite films on gold. A clean gold surface was treated with an aqueous solution of thiocholine chloride [$\text{HS}(\text{CH}_2)_2\text{NMe}_3\text{Cl}$] to form a covalently bound, positively charged monolayer, and then with an aqueous suspension of Laponite (Figure 3.12). Ellipsometric measurements indicated that addition of the thiocholine monolayer resulted in an increase in thickness of 0.4 nm, and analysis by X-ray photoelectron spectroscopy (XPS) confirmed the presence of sulfur, nitrogen, and chlorine on the treated Au surface. As expected, only a single layer of Laponite (~0.9 nm in thickness) adsorbed onto this treated surface.³² This limited adsorption

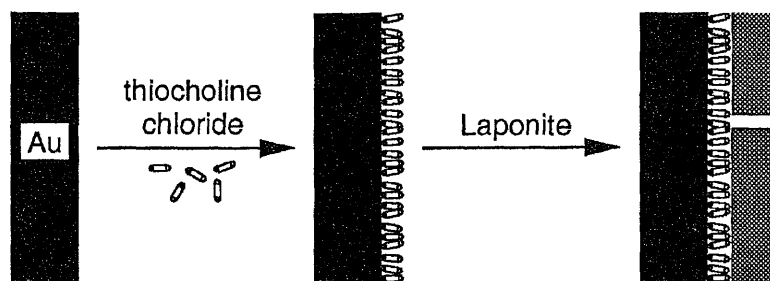


Figure 3.12. Schematic diagram of the use of thiocholine chloride to promote adhesion of Laponite sheets to gold.

was consistent with the idea advanced earlier, when polymer solutions of high concentration had been used, that adsorption of Laponite in excess of a monolayer could be attributed to the presence of excess, loosely-bound polymer at the sample surfaces: in the present case, when the positively charged species was limited to a covalently bound monolayer, the adsorption of the silicate was limited to a single layer as well. After the adsorption of Laponite, XPS showed that silicon, magnesium, and oxygen were present,³³ in addition to sulfur and nitrogen, consistent with the scheme depicted in Figure 3.12. Neither sodium nor chlorine was detected, presumably either because of good correspondence between the positive (thiocholine) sites and negative (Laponite) sites, or because any charge imbalance was compensated by other ions present in this system (i.e., proton or hydroxide). A control experiment was performed in which ethanethiol was used instead of thiocholine chloride. Surprisingly, treatment of the ethanethiol-treated-gold surface with Laponite also resulted in an increase in thickness (~0.6 nm). Laponite did not, however, adsorb onto bare gold.

3.3.11. Permeability of PDDA/Laponite films to aqueous ions. As discussed in chapter 5,¹⁴ PDDA/Laponite films are highly permeable to water from the vapor phase, which raises the question of pore size within the films, and the permeability of the films to larger species. We explored these issues by studying the redox behavior of aqueous ions at film-covered electrodes. Others have found that coating electrodes with clays or polymers has a dramatic effect on the redox behavior of various species.³⁴ The ability to form PDDA/Laponite films that are uniform and exceedingly thin enables detailed studies of the effects of film structure and composition on electrochemical properties that are not possible with many other methods of film formation. As a preliminary study in this regard, we prepared films of various thicknesses on gold electrodes and used cyclic voltammetry to evaluate the

permeability of the films to the aqueous $\text{Fe}(\text{CN})_6^{3-/4-}$ (ferri-/ferrocyanide) redox couple. The gold electrodes, used bare or treated with 5, 10, or 15 adsorption cycles, were immersed for 5 min in a deoxygenated 1.0 M NaCl solution and then transferred to a deoxygenated solution of 10 mM $\text{K}_3\text{Fe}(\text{CN})_6$ in 1.0 M NaCl, whereupon a scan of potential was begun within 20 s.³⁵ The films were permeable to this electroactive ion, and several trends were evident in the voltammograms obtained under these conditions (Figure 3.13). First, the separation between the cathodic and anodic peaks increased from 72 mV on bare electrodes to 170 mV on 15-cycle electrodes.³⁶ As the peak separation increased, the anodic peak remained at a nearly constant potential (~ 300 mV), indicating a negative shift in the formal potential. In addition, the anodic peak current decreased in a roughly linear fashion with increasing film thickness.

The increase in peak separation indicates that $\text{Fe}(\text{CN})_6^{3-/4-}$ ions reached the electrode surface more slowly due to the longer diffusion path they had to take around the silicate sheets, a path made even more tortuous by the presence of the polymer. The decrease in anodic current indicates that the ferrocyanide ions formed at the electrode were rapidly exchanged out of the film in preference for ferricyanide or chloride ions.³⁷ The shift in the formal potential is also consistent with the ferrocyanide ion having a low partition coefficient for incorporation into the film from the electrolyte solution, relative to the ferricyanide ion.³⁷ The relative magnitudes and absolute (but not relative) positions of the *cathodic* peaks varied for apparently identical electrodes, which may be due to variation in the exact length of time each electrode was immersed in the ferricyanide solution before a scan was begun.³⁸ Voltammograms taken under analogous conditions using solutions of ferrocyanide instead of ferricyanide also showed a negative shift in the formal potential with increasing film thickness, as well as an increase in peak separation and a decrease in

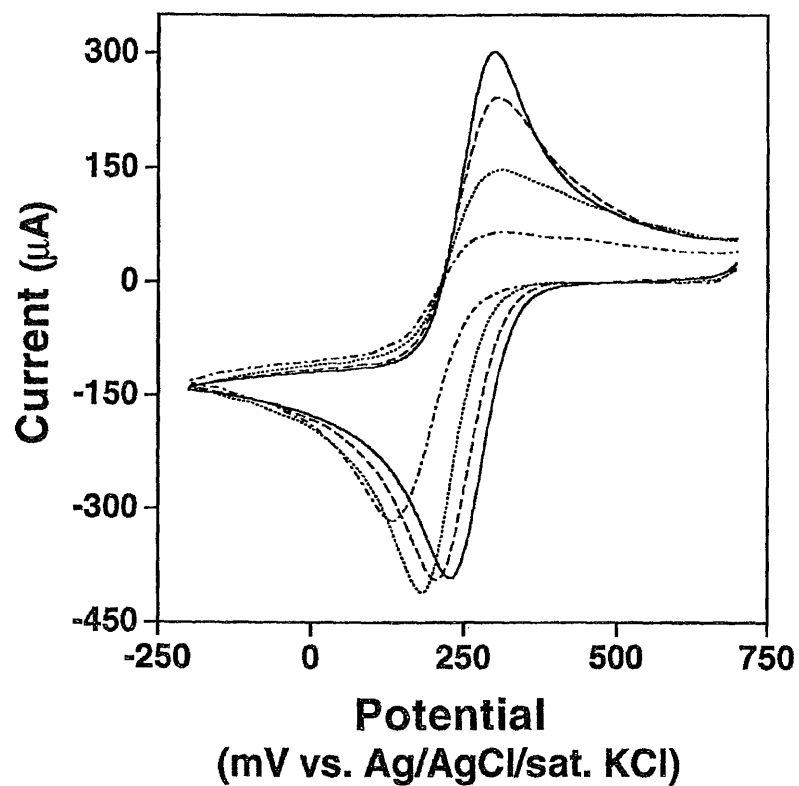


Figure 3.13. Cyclic voltammograms taken in a deoxygenated aqueous solution of 10 mM $K_3Fe(CN)_6$ /1M NaCl on gold electrodes used bare or after having been treated with various numbers of adsorption cycles: (—) bare gold; (----) 5 cycles; (.....) 10 cycles; (-·-·-·) 15 cycles.

anodic peak current. Even in these scans, the cathodic peak currents were greater than the anodic peak currents for the film-covered electrodes, confirming the tendency of ferricyanide to be preferentially incorporated into the films.

3.3.12 Melting of Multilayered Films. Because composite multilayered films could be formed to very precise and uniform thicknesses, we were interested in using them as precursors to other types of films. One straightforward way of modifying the films was by melting (fusing) the clay sheets into a continuous, glassy matrix. Such films were expected to be more robust than their precursor films, and were also expected to become nonporous, properties that would be advantageous for various purposes, including optical applications and protective or decorative coatings. Films were formed on silicon substrates using 5-s treatments with 5% PDDA or 10% PMVP, and 0.2% Laponite RD, and were fused by heating at 700 °C for 3 hours under flowing argon. The properties of two films treated in this way are summarized in Table 3.1.

The heat treatment caused the thickness of sample 1 to decrease by 41% and that of sample 2 to decrease by 44%, and caused their refractive indices to decrease by 4% and 1%, respectively. Before heat treatment, polycation/silicate films are easily deformable (for example, being partially or completely removed from substrates by rubbing with a gloved finger); however, following heat treatment, the films were not deformed under such conditions. In fact, the Mohs hardness of sample 2 following heat-treatment was 5.5, which is approximately that of fused silica (i.e., glass). Comparison of the x-ray diffraction patterns of pre- and post-heated films revealed only traces in the latter of peaks assigned to the multilayer structure, confirming that the films had, in their transformation into a glassy matrix, become nearly amorphous. Consistent with a decrease in their porosity, the films' response to changes in relative humidity (described briefly in Section 3.3.9 and in

Table 3.1. Pre- and Post-Fusion Properties of Composite Films

<u>Sample Number</u>	<u>Film Composition</u>	<u>Number of Cycles</u>	<u>Pre-Fusion n.t</u>	<u>Post-Fusion n.t</u>
1	PDDA/ Laponite	67	1.57, 198 nm	1.51, 116 nm
2	PMVP/ Laponite	46	1.56, 139 nm	1.54, 78 nm

detail in Chapter 5) was greatly attenuated as well. One simple and qualitative way to monitor the response of the films has been to observe (visually) the changes in interference color that occur when multilayered films are exposed alternately to humid and dry environments. After heat treatment, any response by sample 1 to humid air was undiscernible with the naked eye, while sample 2 gave a barely detectable response that may have been attributable to condensation of water on the sample surface.

The changes observed upon heat treatment of the films can be explained based upon results reported by others for related systems. Heating natural hectorite from room temperature to 700 °C has been reported to result in a loss of water totalling 6% of the mass of the original clay sample.³⁹ Although this number may not correspond quantitatively to the changes in our films, we nonetheless expect that significant loss of water occurred. Heating polymers such as poly(furfuryl alcohol) and poly(acrylonitrile) in silicate matrices under the conditions we used has been reported to result in their conversion into graphite, and some decomposition or transformation of the PDDA or PMVP in the composite films probably occurred as well.⁴⁰ The loss of material associated with decomposition or depolymerization of the polymer, in addition to the loss of water mentioned earlier, helps to explain how the films could lose such a significant percentage of their original thickness without an increase in their refractive index. The loss of structural order in the films was not unexpected, since many smectites melt below 700 °C, yet do not crystallize into other phases (e.g, quartz or cristobalite) unless much higher temperatures are reached.⁴¹ The failure of the heat-treated films to respond to changes in relative humidity suggested that their porosity had been greatly reduced or eliminated. In summary, all of our observations were consistent with melting of the Laponite sheets to form a continuous glassy matrix, possibly accompanied by decomposition or transformation of the

interlamellar polymer into another form.

The apparently nonporous nature of the fused films suggested their potential usefulness as protective or decorative coatings. Two classes of stainless-steel substrates, described by the manufacturer as having silicon-rich and iron-rich surfaces, were used either bare or after having been coated with 20 cycles (5% PDDA and 0.2% Laponite, 5-s treatments). All were heated at 700 °C for 3 h under flowing argon. Assuming that the film-adsorption characteristics that were exhibited by other substrates held for stainless steel, these films were an estimated 60 nm in thickness before heat treatment and 35 nm afterwards. Following heat treatment, the coated substrates appeared yellow-gold in color, while the uncoated samples appeared light to royal blue. The corrosion resistance of the substrates was then tested according to a modification of ASTM method G48-76A. Briefly, the substrates were immersed nearly vertical (with the film-coated or smooth side of the samples pointed slightly down), in separate 90-mL aliquots of 0.4 M aqueous solutions of FeCl_3 in covered beakers for 45 h. After the first 24 h, each sample was removed from the corrosive solution, rinsed, inspected, and replaced. After 45 h, the samples were removed, rinsed, and blown dry with nitrogen.

As shown in Figure 3.14, the coated samples sustained far less damage during this test than the uncoated samples, as judged by the total percentage of their surfaces that appeared corroded (light areas). The two classes of substrates behaved differently, however. On the silicon-rich substrates, the major difference was in the number of defects (the coated sample having fewer), whereas on the iron-rich substrates, the major difference was in their size (those on the coated sample being smaller). In the non-corroded areas, the color of the coated samples was similar or the same as that observed before the test, and these areas appeared mirror-smooth. In contrast, the color of the uncoated samples had become mottled and their surfaces

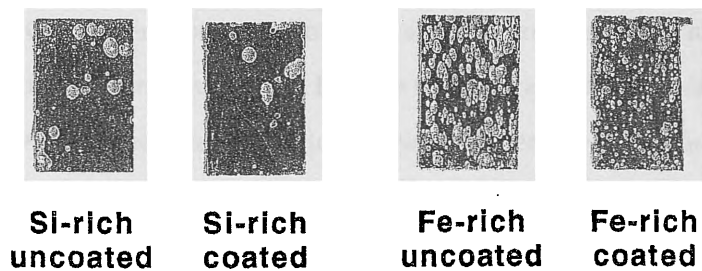


Figure 3.14. Results of test of resistance to corrosion. Stainless steel samples, either coated with a 20-cycle film of PDDA and Laponite or left bare, had been heat-treated at 700°C for 3 h under flowing argon, then immersed for 45 h in a 0.4 M solution of FeCl₃. In this photocopy, samples are shown at their actual size.

appeared roughened.

3.3.13. *Corrosion of Copper Substrates.* In most cases, the formation of a multilayered film proceeds smoothly, with films displaying the uniformity and clarity that would be needed for optical applications. Indeed, in the present work, films on silicon, quartz, gold, and silver substrates appeared uniform across the samples as they grew in thickness, with no cloudiness or other sign of disorder within the multilayers. On copper substrates, however, slightly darkened spots and streaks appeared within the first few cycles. Because these darkened areas scattered the light from the ellipsometer laser ($\sim 30 \mu\text{W}$ HeNe) to a greater extent than the lighter areas, we suspected that they were rougher. We used dark-field optical microscopy, a technique especially useful for the evaluation of rough surfaces, to examine a copper sample that had been treated with four adsorption cycles.⁴² As shown in Figure 3.15a, minute irregularities were present on the surface of this sample. A higher density of these features occurred in the areas that looked dark to the unaided eye (lower left). In contrast, very few features of this size were present on bare copper (Figure 3.15b). Dark-field microscopy can exaggerate the size of features,⁴³ so to rule out the possibility that the irregularities in the image in Figure 3.15a were associated with platelets of Laponite, we obtained dark-field images of a silicon wafer that had been treated with four adsorption cycles as well as a bare silicon wafer for comparison. Both of these images were similar in appearance to Figure 3.15b, but had an even lower concentration of irregularities than shown there. From these results we concluded that the features were due to a change in the substrate and not simply to the adsorption of the film.

To determine whether either the Laponite or the PDDA was facilitating corrosion of the copper substrates, pieces of copper foil ($\sim 100 \text{ nm} \times 1 \text{ cm} \times 2 \text{ cm}$) were stirred overnight either in an aqueous suspension of Laponite (0.2%) in the presence of air

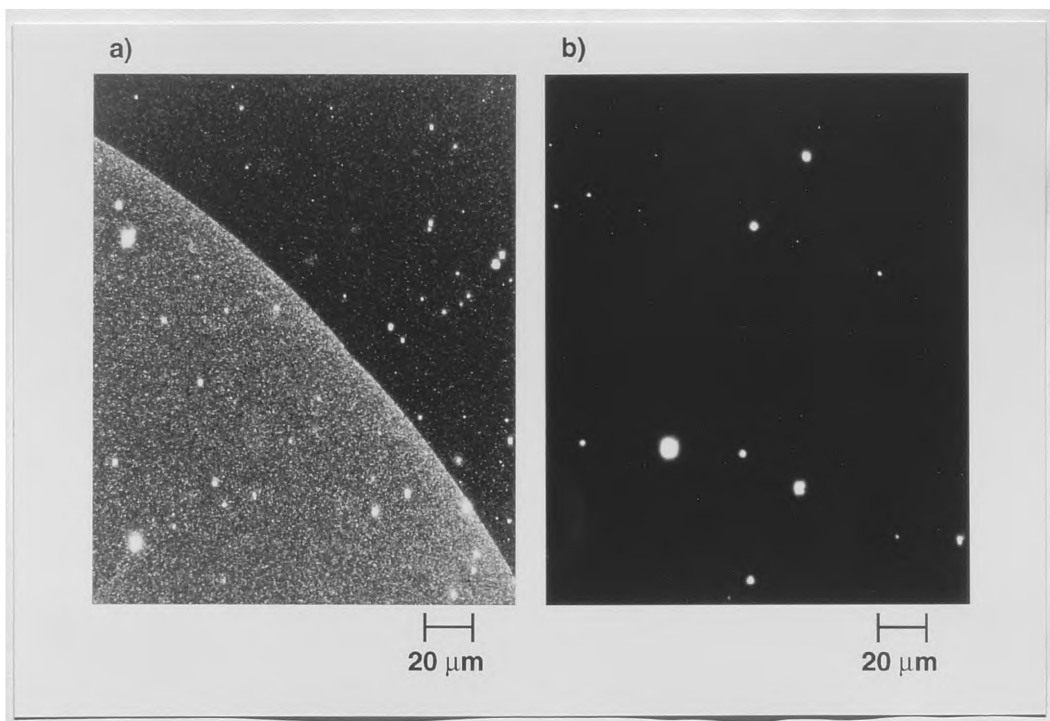


Figure 3.15. Dark-field optical micrographs of: a) a copper substrate that had been treated with four cycles of 5% PDDA and 0.2% Laponite; b) a bare copper substrate. The brighter half of image (a), on the lower left, corresponds to an area that appeared slightly darkened to the unaided eye. The photographs shown in the copy above were obtained at a magnification of 500x.

(a); or in an aqueous solution of PDDA (5% w/w), either under nitrogen (b) or in the presence of air (c). No change was observed in cases (a) or (b). The foil stirred in PDDA in the presence of air (c), however, dissolved completely, yielding a faint blue precipitate that we presumed to be mainly CuCl, chloride ions having been present as the counterion to the polymer. To test this hypothesis, we performed qualitative analysis on the precipitate that was formed by stirring a copper slug in aqueous PDDA for several hours. The insoluble precipitate was collected by centrifugation and washed several times with purified water. Upon treatment of this precipitate with concentrated HNO₃, a blue color characteristic of the presence of Cu(II) ions was noted. Addition of AgNO₃ (aq) to this solution, in turn, produced a white precipitate, consistent with the presence of chloride as the counterion. These observations are consistent with CuCl as the identity of the original precipitate, and indicate that the polymer catalyzed the oxidation of Cu(0) to Cu(I) by oxygen,⁴⁴ whereupon immediate precipitation with chloride presumably inhibited further oxidation to Cu(II). We therefore attribute the uneven appearance of multilayered films grown on copper to the dissolution of copper and, possibly, the precipitation of granules of CuCl onto the samples.

3.4 Conclusions

We recently introduced a new method for the layer-by-layer formation of ordered multilayered films by the alternate adsorption of a cationic polyelectrolyte and an anionic sheet silicate from aqueous solution or suspension.⁹ The present work investigated the generality of this method for the formation of films having similar properties under a variety of conditions.

Films formed by alternating 5-s treatments with 5% PDDA and 0.2% Laponite RD on gold, silver, and copper substrates displayed the regular growth and structural

order that had characterized films grown on silicon substrates. As anticipated, the amount of material that adsorbed per cycle varied directly with the concentration of the polymer solution used to form the films when 5-s treatments were used. X-ray diffraction patterns of films made using 5% and 0.25% PDDA revealed that they were ordered, having d-spacings of 1.43 nm. Significantly, the ellipsometric growth in thickness per cycle failed in either case to bear any apparent relation to the lattice d-spacing. This discrepancy is understandable, given that ellipsometry determines an average thickness within a macroscopic illuminated spot ($\sim 1 \text{ mm}^2$). In the case of the film made from 5% PDDA, therefore, the ellipsometric growth of 3.6 nm/cycle indicates that in any particular cycle, two layers adsorbed in some areas, while three layers adsorbed in others. Similarly, for the film made from 0.25% PDDA, the ellipsometric growth of 1.1 nm/cycle indicates that in any particular cycle, a full unit cell adsorbed in some areas, while little or no material adsorbed in others. The presence of structural order in films made under these very different conditions lends weight to the idea that the silicate sheets in any given layer are capable of patching over defects in underlying layers, thus allowing regular growth to continue (and structural order to be preserved) even though every layer necessarily contains defects.

The regularity and reproducibility of film growth on a variety of substrates when 5-s adsorption treatments were used suggested that adsorption was not occurring extremely rapidly near the 5-s mark. Although investigation of shorter adsorption periods was impractical, investigation of longer adsorption periods supported this idea: within 5 s, the overall growth per cycle had attained over 93% of the level attained within the first 10 s, and over 75% of that attained within the first 10 min.

The uniformity of the films had suggested their potential usefulness in optical applications. The present work demonstrated that film growth on fused quartz proceeded in a regular manner and could be monitored using uv spectrophotometry.

The observation that the uv data were affected by interference phenomena indicated that films formed on this substrate were uniform in thickness, and XRD confirmed the presence of structural order within the films.

The ability to form uniform, ordered, and exceedingly thin films on gold substrates allowed investigation of the character of their internal structure using cyclic voltammetry. The films were found to be permeable to the ferri-/ferrocyanide redox couple, and the increased path length to the electrode surface that these ions had to traverse in the presence of the films resulted in an increased peak separation. In addition, the films were found to expel ferrocyanide ions in preference for ferricyanide and/or chloride ions. Fusion of the films into a glassy matrix greatly reduced or eliminated this porosity, and the glassy films inhibited corrosion of stainless steel by iron (III) chloride.

3.5 Experimental Methods

3.5.1. Materials. Poly(diallyldimethylammonium chloride), PDDA (Polysciences, MW 240,000, or Aldrich, MW 200,000–350,000), and poly(*N*-methyl-4-vinylpyridinium bromide), PMVP (Polysciences, MW 50,000), were obtained as 20% (w/w) aqueous solutions, and were diluted with Millipore Milli-Q water (~16 M Ω -cm) to the stated concentrations. The molecular weights of these polymers were supplied by the manufacturers. Laponite RD (synthetic hectorite) was obtained from Laporte Industries, Limited, in powder form. It was added to Milli-Q water with rapid stirring to form a 0.5% (w/w) dispersion; stirring was continued until the dispersion appeared clear, typically for several hours. The dispersion was then allowed to stand overnight without stirring to allow complete separation of the silicate sheets, and was diluted to 0.2% (w/w) before use. Individual Laponite sheets are less than 1 nm in thickness and approximately 25–35 nm in diameter; the

elemental composition of Laponite RD [66.2% SiO₂, 30.2% MgO, 2.9% Na₂O, 0.7% LiO₂ (w/w)] and its properties have been described elsewhere.¹⁶ Thiocholine chloride was prepared from acetylthiocholine chloride (Sigma) according to a literature method.⁴⁵ Ethanethiol (Aldrich, 97%), FeCl₃•6H₂O (Fisher, Certified ACS grade), potassium ferricyanide [K₃Fe(CN)₆] (Aldrich, 99+%), potassium ferrocyanide trihydrate [K₄Fe(CN)₆•3H₂O] (Baker, ACS Reagent), and sodium chloride (Fisher, 99+%) were used as received.

3.5.2. *Substrate Preparation.* Silicon substrates [Wacker Siltronic, (100)-oriented, p-doped] were broken into ~1 x 2.5-cm pieces, swabbed with ethanol to remove silicon dust, and cleaned with a ~1:2 (v/v) solution of 30% H₂O₂ and concentrated H₂SO₄ for a minimum of 30 minutes (Caution: this “piranha solution” reacts violently with organic materials!), and were rinsed thoroughly with Milli-Q water and dried with a jet of nitrogen. Fused quartz microscope slides, 1 mm in thickness (Chemglass), were cut into 1.3 x 3.8-cm pieces, and cleaned in the same manner as silicon. Gold substrates were prepared by thermal evaporation of at least 100 nm of gold (99.99%, Aldrich) onto silicon wafers that had been treated with 3-mercaptopropyltrimethoxysilane according to a literature method,⁴⁶ and were then broken into ~1 x 2.5-cm pieces. Silver and copper substrates were prepared by the thermal evaporation of a minimum of 100 nm of either metal (Ag: 99.99+%; Cu: 99.999%, Aldrich) onto silicon wafers that had been treated with dilute, aqueous hydrofluoric acid to remove the native oxide. Adhesion of copper to this hydride-terminated silicon was excellent, and adhesion of silver, while not as strong, was adequate for our purposes. Silver and copper substrates were then broken into ~1 x 2.5-cm pieces and rinsed with water before use. No substrates were pre-treated to promote adhesion of the multilayered films, with the exception of one set of experiments, in which a covalently bonded, positively charged monolayer was

formed by immersion of evaporated gold substrates in a ~5 mM aqueous solution of thiocholine chloride for 20 minutes, followed by extensive rinsing with water. Copper foil was prepared by the evaporation of ~100 nm of Cu onto a cleaned silicon wafer bearing a native oxide. The poor interfacial adhesion allowed removal of the copper foil by a jet of purified water. Samples of stainless steel, "Buffed 434," having an iron-rich surface, and "Brite 434," having a silicon-rich surface, were supplied by Armco, Inc., Middletown, OH, and were cleaned with an alkaline cleaning solution, rinsed with water, and blown dry with nitrogen.

3.5.3. Multilayer Preparation. Multilayered films were formed on gold, silver, copper, and silicon substrates by repeating a two-step adsorption cycle using the following conditions, unless stated otherwise. In the first step, the substrate was treated with several drops of a 5% (w/w) aqueous solution of PDDA, rinsed after approximately 5 s with Milli-Q water, and blown dry with N₂. In the second step, it was treated with several drops of a 0.2% (w/w) aqueous dispersion of Laponite, rinsed after approximately 5 s, and blown dry. Multilayers were prepared on quartz by a similar method. To allow study by ultraviolet spectrophotometry, however, PMVP [a 1% (w/w) solution] was used in place of PDDA, and substrates were dipped into the solutions to coat both sides evenly.

3.5.4. Ellipsometry. The growth of multilayered films on gold, silver, copper, and silicon was monitored by optical ellipsometry, using a Rudolph Auto-EL III nulling ellipsometer with HeNe laser light ($\lambda = 632.8$ nm). Measurements were performed under ambient conditions with the angle of incidence set at 70°. For gold, silver, and copper, the real and complex parts of the index of refraction, n and k , were determined for three spots on each bare substrate, and the average constants used in determinations of film thickness for that sample. For determination of multilayer thickness, a single smooth film was assumed, and a refractive index of 1.5 was used

except where otherwise noted. For silicon substrates, the thickness of the native oxide (~1.5 nm) was measured assuming a refractive index of 1.5, and assuming a standard refractive index for the silicon substrate ($n = 3.858$, $k = 0.018$). This thickness was later subtracted from the overall film thickness determined using an assumed refractive index of 1.5. The ellipsometer was also used to determine simultaneously both the thickness of the transparent films and the real component of their refractive index. Refractive indices were calculated only for films that were 40 – 200 nm in thickness; ellipsometry gives more reliable refractive indices for films in this thickness regime than for thinner films.^{18,47}

3.5.5. Ultraviolet (UV) Spectrophotometry. The growth of multilayered films on quartz was monitored by UV spectrophotometry. A Shimadzu UV-2101PC spectrophotometer with a PMT detector was used in absorbance mode to obtain spectra between 200 and 300 nm, using a spectral bandwidth of 1.0 nm and sampling interval of 1.0 nm. A fused quartz slide bearing a multilayered film on both sides was placed diagonally in a cuvette such that the angle of incidence of the sample beam on the slide was 45°. An identical but uncoated slide was similarly oriented in a cuvette in the reference beam. Three spectra were taken after every five cycles, removing and replacing the sample in the instrument between spectra, to obtain an estimate of the uncertainty in the absorbance values associated with sample positioning. According to the manufacturer of the spectrophotometer, the beam area is 4 mm x 11 mm.

3.5.6. X-ray Photoelectron Spectroscopy (XPS). The elemental composition of the films on gold was determined using a Scienta ESCA-300 X-ray photoelectron spectrometer with monochromatized Al K_{α} radiation from a rotating anode source. A take-off angle of 45°, pass energy of 150 eV, energy step of 0.25 eV, and slit width of 0.8 mm were used for all spectra. The spectra were referenced to the Au $4f_{7/2}$ line

at 84.00 eV. No charging effects were observed, because the substrates were conductive and the overlayers were thin.

3.5.7. X-ray Diffraction. X-ray diffractometry was performed in $\theta/2\theta$ mode using a Philips APD 3720 powder diffractometer with monochromatized $\text{CuK}\alpha$ radiation ($\lambda = 1.54 \text{ \AA}$) operating at 45 kV and 30 mA. Data were obtained using a 0.05° step and 3 s/step collection time. Substrates bearing multilayered films were broken into $\sim 1 \text{ cm} \times \sim (1-1.5 \text{ cm})$ pieces before analysis to allow them to fit into the sample holders.

3.5.8. Cyclic Voltammetry. Gold electrodes were prepared by thermal evaporation of approximately 100 nm of gold (99.99%, Aldrich) onto glass that had been treated with 3-mercaptopropyltrimethoxysilane according to a literature method.⁴⁶ The exposed area of the electrodes was 0.4 cm^2 ; other areas were coated with Torr-Seal (Varian Associates). These electrodes were used bare, or after having been treated with 5, 10, or 15 adsorption cycles. Cyclic voltammograms were obtained using a Bioanalytical Systems BAS 100B/W potentiostat, with a scan range of +700 mV to -200 mV and a scan rate of 20 mV/s. A platinum wire auxiliary electrode and Ag/AgCl/saturated KCl reference electrode were used. Each multilayer-coated electrode was immersed for 5 min in a deoxygenated aqueous solution of NaCl (1.00 M), then transferred to a deoxygenated aqueous solution of $\text{K}_3\text{Fe}(\text{CN})_6$ or $\text{K}_4\text{Fe}(\text{CN})_6$ (10.0 mM) in 1.00 M NaCl, whereupon a cyclic voltammogram was begun within 20 s.³⁵ The measured internal resistance for the thickest films studied was less than 50Ω . The voltammograms were Fourier filtered as necessary to remove a low-magnitude, high-frequency (2.5 Hz) signal.

3.5.9. Fusion of Multilayered Films. Multilayered films were formed on silicon and stainless steel substrates by alternate 5-s treatments with 5% PDDA and 0.2% Laponite. These composite films, as well as bare steel samples, were placed in a

fused quartz tube in a tube furnace (Electro-Applications, Inc., Canonsburg, PA) and heated to 700 °C for 3 h under flowing argon, then cooled to room temperature. Rates of heating and cooling were not carefully controlled. Mohs hardness testing was performed by gently attempting to scratch the surface of the film with minerals of known hardness. The films were found to have a hardness in between fluorapatite (5) and feldspar (6).⁴⁸

3.5.10 Corrosion Testing of Fused Films on Stainless Steel. The corrosion resistance of the steel samples, either coated or uncoated, was tested using a modification of ASTM method G48-76A. Samples were immersed in a 90 mL of a 0.4 M solution of FeCl₃ in separate, covered beakers for a total of 45 h. The samples were oriented at a slight tilt (nearly vertical), with the smooth or film-coated side down. After the first 24 h, the samples were removed, rinsed, and replaced. After 45 h, the samples were removed, rinsed, and blown dry with a jet of nitrogen. The results of this test were evaluated visually.

3.5.11. Optical Microscopy. A Reichert-Jung MeF3 microscope with a quartz halogen light source was used in dark-field mode to obtain images of a copper sample that had been treated with four adsorption cycles, a silicon wafer that had been treated with four adsorption cycles, a bare copper surface, and a bare silicon wafer. Photographs were obtained at a magnification of 500x.

Acknowledgments. Holly L. Deak performed the uv study of film growth on quartz and provided the sample for XRD analysis; her support was provided (1995) by the NSF Undergraduate Research Traineeship Program, "Chemistry of Materials Synthesis and Processing," #DMR-9218093. We thank Prof. M.S. Freund for helpful discussions of the electrochemistry and for allowing us use of a potentiostat. We further acknowledge the technical assistance of A.C. Miller with the XPS work, G.

Yasko with the XRD work, and A. Benschoter with the dark-field optical microscopy. E.R.K. gratefully acknowledges the support provided by an AT&T Bell Laboratories Ph.D. Scholarship. We acknowledge Southern Clay Products for support of this work and Lehigh University for support of this work and the Scienta ESCA-300 facility.

3.6 References and Notes

1. Brousseau, L.C.; Aoki, K.; Garcia, M.E.; Cao, G.; Mallouk, T.E. in *Multifunctional Mesoporous Inorganic Solids*; Sequeira, C.A.C.; Hudson, M.J., Eds.; Boston: Kluwer, 1993; pp 225–236. Rubenstein, I.; Steinberg, S.; Tor, Y.; Shanzer, A.; Sagiv, J. *Nature* **1988**, *332*, 426.
2. Katz, H.E.; Scheller, G.; Putvinski, T.M.; Schilling, M.L.; Wilson, W.L.; Chidsey, C.E.D. *Science* **1991**, *254*, 1485. Li, D.; Ratner, M.A.; Marks, T.J.; Zhang, C.; Yang, J.; Wong, G.K. *J. Am. Chem. Soc.* **1990**, *112*, 7389.
3. Kan, K.K.; Petty, M.C.; Roberts, G.G. in *The Physics of MOS Insulators*; Lucovsky, G.; Pantelides, S.; Galeener, F., Eds.; Proc. International Topical Conf.; Pergamon: New York, 1980, pp. 344–348. Kepley, L.J.; Sackett, D.D.; Bell, C.M.; Mallouk, T.E. *Thin Solid Films* **1992**, *208*, 132. Katz, H.E.; Narvaez, P.; Harley, E.R. *Thin Solid Films* **1994**, *252*, 4.
4. Ulman, A. *An Introduction to Ultrathin Organic Films: From Langmuir–Blodgett to Self-Assembly*; Academic: Boston, 1991.
5. a) Netzer, L.; Iscovici, R.; Sagiv, J. *Thin Solid Films* **1983**, *99*, 235. b) Cao, G.; Hong, H.-G.; Mallouk, T.E. *Acc. Chem. Res.* **1992**, *25*, 420. c) Tillman, N.; Ulman, A.; Penner, T.L. *Langmuir* **1989**, *5*, 101. d) Evans, S.D.; Ulman, A.; Goppert-Berarducci, K.E.; Gerenser, L.J. *J. Am. Chem. Soc.* **1991**, *113*, 5866.
6. Decher, G.; Eßler, F.; Hong, J.-D.; Lowack, K.; Schmitt, J.; Lvov, Y. *Polym. Prepr.*

- 1993, 34 (1), 745. Lvov, Y.; Haas, H.; Decher, G.; Möhwald, H.; Kalachev, A. *J. Phys. Chem.* **1993**, 97, 12835.
7. A similar procedure for formation of organic/inorganic and all-inorganic composite films has been reported recently: Keller, S.W.; Kim, H.-N.; Mallouk, T.E. *J. Am. Chem. Soc.* **1994**, 116, 8817. See also: Kaschak, D.M.; Mallouk, T.E. *J. Am. Chem. Soc.* **1996**, 118, 4222.
 8. a) Iler, R.K. *J. Colloid Interface Sci.* **1966**, 21, 569.
b) Gaines, G.L. *Thin Solid Films* **1983**, 99, 243.
c) Cheung, J.H.; Fou, A.F.; Rubner, M.F. *Thin Solid Films* **1994**, 244, 985.
d) Ingersoll, D.; Kulesza, P.J.; Faulkner, L.R. *J. Electrochem. Soc.* **1994**, 141, 140.
 9. Kleinfeld, E.R.; Ferguson, G.S. *Science* **1994**, 265, 370. Ferguson, G.S., Kleinfeld, E.R. *Advanced Materials* **1995**, 7, 414.
 10. Kotov, N.A.; Dékány, I.; Fendler, J.H. *J. Phys. Chem.* **1995**, 99, 13065.
 11. Kleinfeld, E.R.; Ferguson, G.S. *Chem. Mater.* **1996**, 8, 1575.
 12. Parsons, D.; Harrop, R.; Mahers, E.G. *Colloids Surfaces* **1992**, 64, 151.
 13. Decher, G.; Hong, J.D.; Schmitt, J. *Thin Solid Films* **1992**, 210/211, 831.
 14. Kleinfeld, E.R.; Ferguson, G.S. *Chem. Mater.* **1995**, 7, 2327.
 15. For elucidation of the structure of PDDA, see: Masterman, T.C.; Dando, N.R.; Weaver, D.G.; Seyferth, D. *J. Polym. Sci. B.: Polym. Phys.* **1994**, 32, 2263 and references therein.
 16. For a more detailed discussion of the structure of this mineral, see (a) reference 22; b) Grim, R.E. *Clay Mineralogy*; McGraw-Hill: New York, 1968, pp 77–92; c) Liu, X.; Thomas, J.K.; *Langmuir* **1991**, 7, 2808.
 17. The calculated ellipsometric thicknesses depended on the assumed refractive index. When the thicknesses were recalculated using the average refractive indices measured ellipsometrically for multilayers on each of the different metals,

the slopes were 3.3 nm/cycle on gold ($n_{\text{avg}} = 1.55$; range = 1.50–1.65), 3.3 nm/cycle on silver ($n_{\text{avg}} = 1.50$; range = 1.42–1.58), and 3.1 nm/cycle on copper ($n_{\text{avg}} = 1.64$; range = 1.44–1.85). The higher index of refraction of films on copper may reflect the incorporation of crystallites of CuCl into the films (*vide infra*).

18. Tompkins, H. G. *A User's Guide to Ellipsometry*; Academic: Boston, 1993; pp 40–43.
19. Kleinfeld, E.R.; Ferguson, G.S. in *Solid-State Ionics*; Nazri, G.A.; Tarascon, J.-M.; Schreiber, M., Eds; Mat. Res. Soc. Symp. Proc. 369; Materials Research Society: Pittsburgh, 1995, p. 697.
20. MacNeill, B.A.; Kleinfeld, E.R.; Ferguson, G.S., unpublished results.
21. At normal incidence, the reflectivities of the bare substrates are as follows: fused quartz, 3.4%; silicon, 35%; copper, 63%; gold, 75%; and silver, 93%. Reflectivities for quartz and silicon were calculated based upon their refractive indices (Vasicek, A. *Optics of Thin Films*; Interscience: New York, 1960; pp 31, 302) and those for gold, silver, and copper were obtained from *CRC Handbook*, 70th ed.; Weast, R.C.; Lide, D.R., Eds.; CRC Press: Boca Raton, FL, 1990; p E-405.
22. Ramsay, J. D. F.; Swanton, S.W.; Bunce, J. J. *Chem. Soc. Faraday Trans.* **1990**, *86*, 3919.
23. A sharp, intense peak due to the (111) reflection of gold was present at $38.2^\circ 2\theta$. Furthermore, a very sharp peak at $33.0^\circ 2\theta$ was sometimes seen, and its presence was sensitively dependent on sample orientation. This peak is attributed to the forbidden (200) reflection of silicon, which may be allowed on substrates with extended surfaces, due to surface reconstruction. Alternatively, this peak may be associated with the (400) reflection of the first harmonic of the Cu K_α

- radiation, which has a wavelength of $\lambda/2$, or 0.077 nm. (T. Siegrist, Lucent Technologies, Inc., personal communication.)
24. Reynolds, R.C. *Acta Cryst. A* **1968**, *24*, 319. Ross, M. *Z. Kristallogr.* **1968**, *126*, 80.
 25. Warren, B.E. *X-Ray Diffraction*; Addison-Wesley: Reading, MA, 1969; pp 251–254.
 26. Drits, V.A.; Tchoubar, C. *X-Ray Diffraction by Disordered Lamellar Structures*, Springer-Verlag: New York, 1990, pp 21–22. Vaia, R.A.; Jandt, K.D.; Kramer, E.J.; Giannelis, E.P. *Chem. Mater.* **1996**, *8*, 2628.
 27. Kaschak, D.M.; Mallouk, T.E. *J. Am. Chem. Soc.* **1996**, *118*, 4222.
 28. Ref. 16b, p. 261.
 29. Hasegawa, M.; Kitano, H. *Langmuir* **1992**, *8*, 1582.
 30. Marra, J.; van der Schee, H.A.; Fleer, G.J.; Lyklema, J. In *Adsorption from Solution*; Ottewill, R.H.; Rochester, C.H.; Smith, A.L., Eds.; Academic: New York, 1983; p. 245.
 31. Sukhorukov, G.B.; Schmitt, J.; Decher, G. *Ber. Bunsenges. Phys. Chem.* **1996**, *100*, 948.
 32. A Laponite layer of similar thickness (0.9–1.1 nm) was adsorbed onto a silicon/silicon dioxide surface that had been treated with trimethoxysilylpropyl-*N,N,N*-trimethylammonium chloride, as discussed in Chapter 2.⁹
 33. Survey spectra obtained at a takeoff angle of 45° indicated that a small amount of oxygen was present on the thiocholine-treated gold samples (9 atom%), but the amount of oxygen increased significantly upon adsorption of Laponite (to 25 atom%).
 34. Bard, A.J. and Mallouk, T.E. in *Molecular Design of Electrode Surfaces*; Murray, R.W., Ed.; Techniques of Chemistry Series Vol. 22; Wiley: New York, 1992; pp

- 271–312, and references therein. Murray, R.W. In *Ann. Rev. Mater. Sci.*; Huggins, R.A.; Giordmaine, J.A.; Wachtman, J.B., Jr., Eds.; Annual Reviews: Palo Alto, 1984; Vol.14, pp 145–169, and references therein.
35. Similar experimental conditions have been reported: Lee, S.A.; Fitch, A. *J. Phys. Chem.* **1990**, *94*, 4998.
36. Only a small fraction of the observed increase in peak separation is attributable to changes in the internal resistance of the cell.
37. Similar effects have been observed for electrodes coated with a cationic polyelectrolyte. See: Niwa, K.; Doblhofer, K. *Electrochim. Acta* **1986**, *31*, 549.
38. Fitch, A. *J. Electroanal. Chem.* **1990**, *284*, 237.
39. Ross, C.S.; Hendricks, S.B. *Minerals of the Montmorillonite Group*, Profess. Paper 205B; U.S. Geol. Surv.: 1945; pp 23–80.
40. Kyotani, T.; Suzuki, K.-Y.; Sonobe, N.; Tomita, A.; Chida, Y.; Hara, R. *Carbon* **1993**, *31*, 149. Bandosz, T.J.; Putyera, K.; Jagiello, J.; Schwarz, J.A. *Carbon* **1994**, *32*, 659.
41. Grim, R.E.; Kulbicki, G. *Bull. Soc. Franc. Ceram.* **1957**, *36*, 21.
42. In dark-field optical microscopy, only light that has been scattered by irregular surface features passes through the objective, and therefore this technique is especially useful for evaluation of rough surfaces. See: Williams, D.B.; Pelton, A.R.; Gronsky, R. *Images of Materials*, Oxford University: New York, 1991, p. 8.
43. Van Olphen, H. *An Introduction to Clay Colloid Chemistry*, Wiley: New York, 1977, p. 2. In this book, the technique is referred to as ultramicroscopy.
44. Cotton, F.A.; Wilkinson, G. *Advanced Inorganic Chemistry*, 4th ed.; Wiley–Interscience: New York, 1980; p 800.
45. Guo, W.-X. A.; Ziegler, D.M. *Anal. Biochem.* **1991**, *198*, 143.
46. Goss, C.A.; Charych, D.H.; Majda, M. *Anal. Chem.* **1991**, *63*, 85.

47. This thickness range is appropriate when the index of a film is near 1.5; for films of significantly higher or lower index, a different range would be appropriate.
48. *CRC Handbook of Chemistry and Physics*, 70th ed.; Lide, D.R., Ed.; CRC Press: Boca Raton, FL, 1992; p 12-149.

Healing of Defects in the Stepwise Formation of Multilayered Films

Reprinted with permission from Kleinfeld, E.R.; Ferguson, G.S. *Chem. Mater.* 1996, 8, 1575. Copyright 1996, American Chemical Society.

4.1 Abstract

When multilayered films are prepared by the alternate self-assembly and activation of molecular adsorbates, defects occurring in any layer can be propagated into subsequent layers. In contrast, sequential adsorption of a polyelectrolyte and sheet silicate allows healing of defects formed in any given layer. In a dramatic demonstration of this property, multilayered films were formed on model low-energy surfaces (self-assembled monolayers [SAMs]) that have little or no propensity to adsorb either component individually. The growth of multilayered structures on these unfavorable surfaces is attributed to the ability of the precursors to adsorb at isolated imperfections in the SAMs, forming islands that grow both vertically and laterally to cover areas of low surface energy during subsequent adsorptions. The ability of these films to form on such unfavorable surfaces indicates that they may be expected to form on most other surfaces without the need for pre-treatment.

4.2 Introduction

Nanostructured solids are of interest in many fields,¹ including optics,² molecular sensing,³ and microelectronics.⁴ In particular, thin films built by the adsorption or deposition of individual layers have great potential due to their precisely controllable thickness and variable molecular structure. In recent years, synthetic strategies have been developed for the formation of multilayered structures⁵⁻⁸ using self-assembled monolayers (SAMs)⁹ as components. Formation of SAMs relies upon chemisorption of individual molecules to a substrate surface, and multilayers may be formed by

alternating the adsorption of a SAM with activation of the new surface to create the next generation of adsorption sites. For this approach to be successful in creating an ordered structure (one with a regular modulation of composition in the direction normal to the substrate surface), a constant, or nearly constant, number of active sites must be maintained at the surface as each layer is added. If sites are lost (e.g, molecules fail to react) in any particular cycle, the resulting defects may be propagated into subsequent layers (Figure 4.1a).¹⁰ The resulting disorder may be evidenced, for example, by the absence of distinct Bragg peaks in the film's x-ray diffraction (XRD) pattern.¹¹ A strategy that overcomes the potential for loss of sites is the alternate adsorption of oppositely charged polyelectrolytes,^{12,13} though interpenetration of the components in adjacent layers¹⁴ (Figure 4.1b) limits the structural order attainable in such systems.

We recently reported a new method for the formation of nanostructural multilayers via alternate adsorption of a cationic polyelectrolyte [poly(diallyldimethylammonium chloride), PDDA] and the anionic sheets of an exfoliated clay (Laponite RD, a synthetic form of hectorite).^{15,16} The regular growth and nanometer-scale order of these composite films indicate that the lateral dimensions of the silicate sheets (~25–35 nm) adsorbed in any cycle are sufficiently large not only to prevent interpenetration by the polymer but also to cover, or “heal,” packing defects formed in the preceding adsorption cycle (Figure 4.1c). Hence, presumably, no such defect is permanent, and a high degree of structural order can be maintained as the films grow in thickness. In this chapter, we provide direct evidence for such “healing” by examining the influence of *macroscopic* defects on the growth of PDDA/Laponite multilayered films. These experiments provide insight into the mechanism of formation of such materials and illustrate the important conceptual advance behind incorporating rigid, “two-dimensional” components into

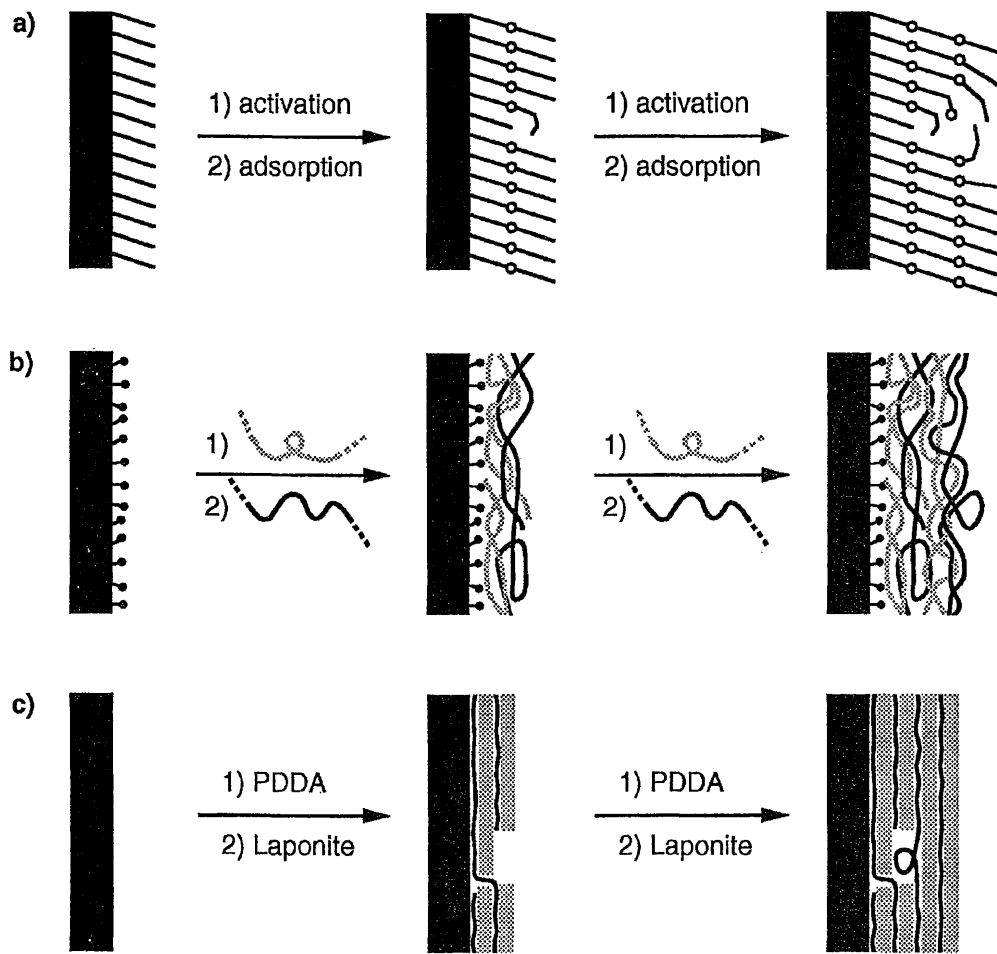


Figure 4.1. Schematic illustrations of: a) the formation and propagation of a defect in a multilayered film prepared by the alternate self-assembly and activation of molecular adsorbates; b) the formation of a film by the alternate adsorption of oppositely charged polyelectrolytes onto a pretreated substrate; and c) the formation and "healing" of a microscopic defect in a film prepared by the alternate adsorption of PDDA and Laponite onto bare Si/SiO₂ (— = PDDA; ■■■ = Laponite).

multilayered films.^{15,16} Our results also have the practical significance of indicating that these films can be grown on a wide variety of substrates, whether or not their surfaces are active with respect to adsorption of either component.

4.3 Results and Discussion

4.3.1. Preparation of Substrates and Multilayered Films. As model “defects” with which to demonstrate healing, we chose substrates with low surface energy and low affinity for the ionic macromolecules used in the adsorptions: ordered, methyl-terminated SAMs formed by adsorption of octadecyltrichlorosilane (OTS) onto Si/SiO₂ and by adsorption of hexadecanethiol (HDT) onto silver.^{9,17} Substrates were treated alternately with a 5% (w/w) aqueous solution of poly(diallyldimethylammonium chloride) (PDDA, Polysciences) for ~5 s, and with a 0.2% (w/w) aqueous suspension of synthetic hectorite (Laponite RD, Laporte Industries, Limited) for ~5 s; samples were thoroughly rinsed with purified water (Millipore Milli-Q, 15 – 17 MΩ-cm) and dried with a jet of nitrogen after each step.¹⁵ In no case were the substrates pre-treated to promote adhesion of these components; the first step in formation of all films was adsorption of PDDA.

4.3.2. Ellipsometric Measurements of Film Growth. The inertness of the SAMs with respect to adsorption of the two macromolecular precursors was confirmed using optical ellipsometry (Rudolph Auto-EL III): a single sequential treatment with PDDA and then with Laponite produced less than 0.2 nm of growth on top of the SAMs on either substrate.¹⁸ Repeated adsorption cycles, however, led eventually to an average growth in thickness of 2.9 nm/cycle on the SAM on Si/SiO₂ and 3.0 nm/cycle on the SAM on Ag, which was nearly identical to the growth seen on bare Si/SiO₂ (3.0 nm/cycle). As shown in Figure 4.2, regular growth began with the fifth cycle on the SAM on Ag and with the seventh cycle on the SAM on Si/SiO₂. To confirm that

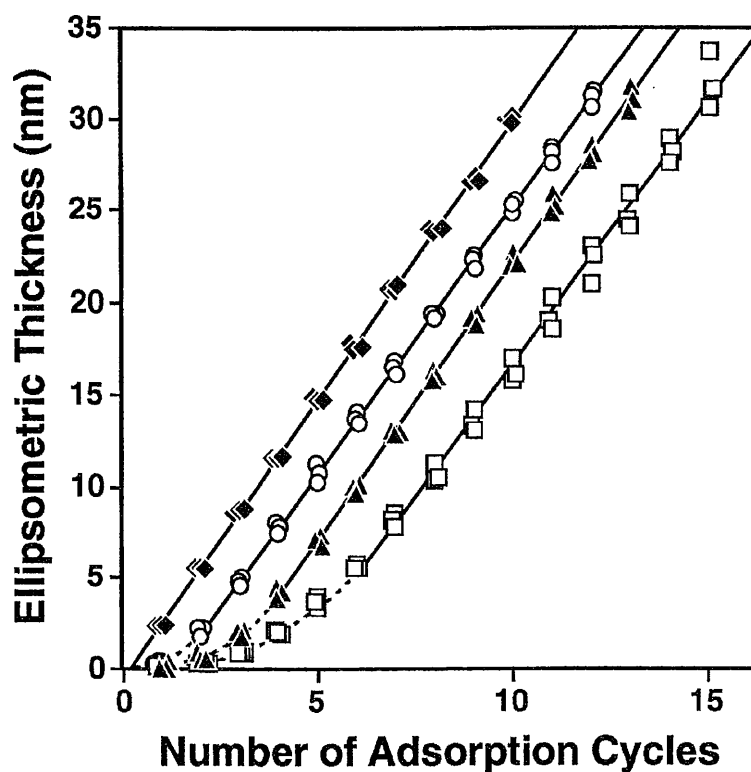


Figure 4.2. Ellipsometric growth of multilayers as a function of the number of adsorption cycles on: bare Si/SiO₂ (◆); SAMs formed by adsorption of HDT onto Ag (▲) and OTS onto Si/SiO₂ (□); and an incomplete SAM formed by adsorption of OTS onto Si/SiO₂ (○). Dashed curves are guides for the eye through data *not* included in the least-squares (solid) lines. The data shown in this figure are from individual samples; similar results were seen on other samples.

multiple adsorption cycles were necessary—that the entire surface could not be covered in a single cycle using longer adsorption times—we allowed SAMs on Si/SiO₂ to soak in the PDDA solution and then in the Laponite suspension for 16 h each. The samples emerged dry from the component solutions and rinse water, with the exception of a few tiny droplets pinned at isolated sites. The total growth in thickness on these samples was less than 0.6 nm, compared to ~5 nm of growth on bare Si/SiO₂ substrates that were treated in the same way.

The changes in ellipsometric thickness displayed in Figure 4.2 were accompanied by qualitative changes in the wettability of the substrate surfaces. The SAMs were initially hydrophobic, and the reagent solutions and rinse water rolled around easily on their surfaces. Within only two cycles for the SAMs on Ag, however, small spots (<1 mm across) remained wet after application of the reagent solutions and the rinse water, and within six adsorption cycles the entire surface remained wet. The SAMs on Si/SiO₂ were more resistant to growth, requiring four cycles before small spots remained wet and seven before the entire surface of the sample remained wet. For comparison, the bare Si/SiO₂ surface was hydrophilic and remained so throughout formation of the multilayer.

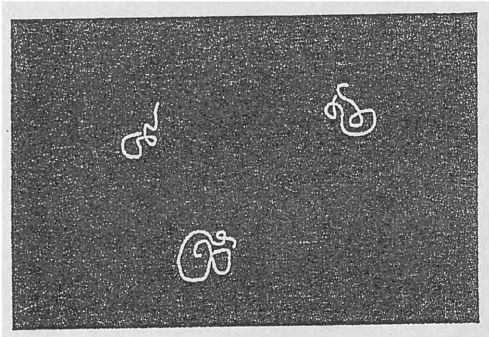
To confirm that the multilayers were formed on top of the methyl-terminated monolayers, and did not displace them from the surface, we performed 17 adsorption cycles on a SAM on Si/SiO₂, monitoring the growth ellipsometrically, and then gently swabbed and rinsed the sample with ethanol and water to remove the multilayer structure. Advancing and receding contact angles of water (109–111° and 95–99°) and hexadecane (42–43° and 41–42°) on this surface were similar to those measured prior to adsorption of the multilayer. Furthermore, the ellipsometric thickness of the SAM was 2.5 nm, the same as was measured before adsorption of the multilayer. These results provide strong evidence that the alkylsiloxane

monolayer remained intact throughout adsorption of the multilayer.¹⁹

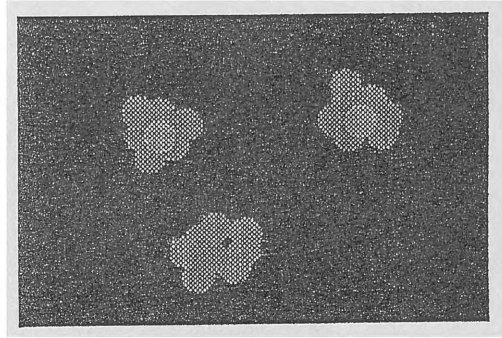
4.3.3. Model for Multilayer Growth. Since PDDA and Laponite each have little or no affinity for the surfaces of the SAMs on either substrate, we infer that multilayer growth begins by adsorption of the polymer at imperfections²⁰ in the SAM. In any place where the polymer adsorbs, Laponite may then adsorb, forming an island that is ideal for adsorption of more polymer, and then more Laponite, in subsequent steps. As growth of the film progresses, these islands coalesce to cover the low-energy surface of the SAM. By this mechanism of island growth and coalescence, depicted schematically in Figure 4.3, the entire surface can eventually be rendered active for adsorption. This creation of active sites starkly contrasts with the loss of sites that can occur during growth of multilayered films by the alternate self-assembly and activation of molecular adsorbates. It is remarkable, in fact, that a film supported by such tenuous contacts to a surface can survive the extensive rinsing that follows each adsorption step. The similarity in eventual ellipsometric growth per cycle for films formed on SAMs and films formed on the bare substrates (i.e., the similarity in the slopes of the least-squares lines in Figure 4.2) suggests that after nucleation of the films on the SAMs, the growth mechanism is similar to that on the bare substrates. Ellipsometry measures an average thickness over a macroscopic area, however, and thus these results alone cannot conclusively rule out other modes of film growth, such as the formation of isolated particles of material on the sample surface.

4.3.4. Determination of Film Topography by Atomic Force Microscopy. To investigate these issues, we determined the topography of films formed on a SAM on Ag and on bare Ag (Figure 4.4) using atomic force microscopy (AFM, Park Scientific Instruments SFM-BD2-210).²¹ One would expect the process depicted in Figure 4.3 to produce tall, broad topological features that would not be present in a film formed

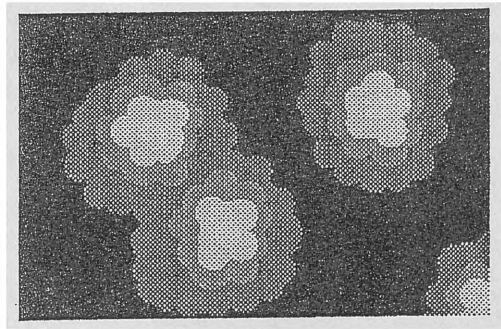
Figure 4.3. Schematic illustration of the adsorption of a composite film onto a SAM (a "macroscopic defect"). Polymer chains adsorbed at imperfections in the SAM during an initial treatment attract Laponite sheets during a subsequent treatment. As more cycles are performed, islands grow and then coalesce to form a film that covers the substrate, providing a surface upon which regular growth can occur.



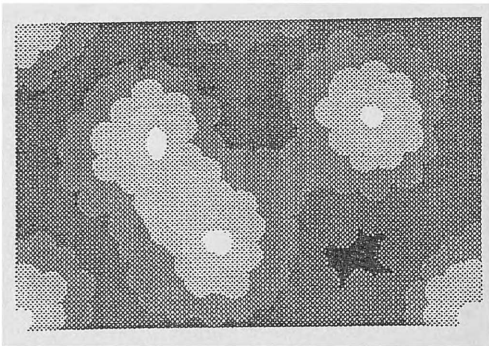
Laponite
→



↓
A few
cycles



←
Additional
cycles



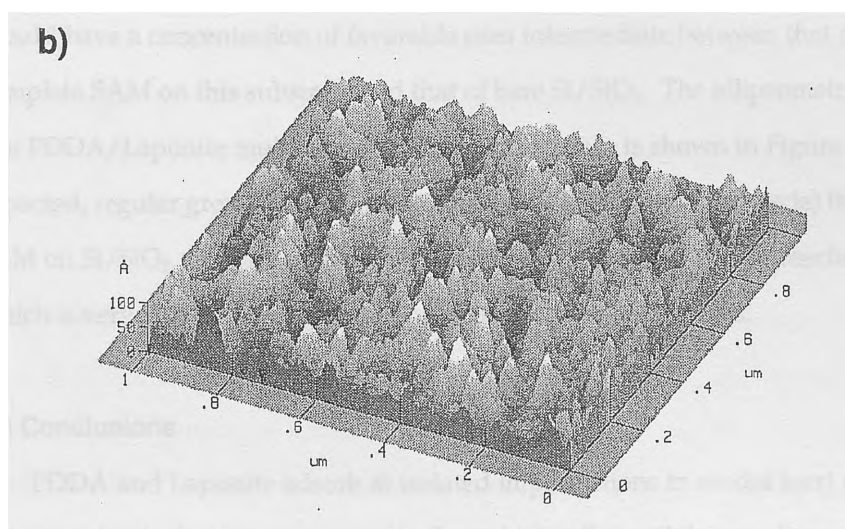
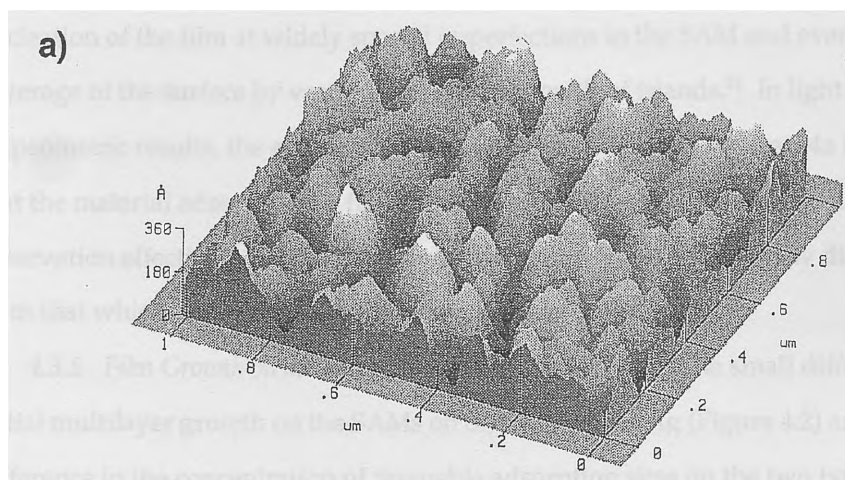


Figure 4.4. AFM images, obtained in attractive mode, of: a) a 10-cycle film adsorbed onto a SAM on Ag; b) an 8-cycle film adsorbed onto bare Ag. The roughness of these surfaces is exaggerated by the difference between the vertical and lateral scales of length.

on bare Ag. The larger features evident in Figure 4.4a are indeed consistent with the nucleation of the film at widely spaced imperfections in the SAM and eventual coverage of the surface by vertical and lateral growth of islands.²² In light of the ellipsometric results, the absence of large, isolated particles in Figure 4.4a indicates that the material adsorbed as a film covering all, or nearly all, of the substrate. This observation effectively rules out any modes of growth that are radically different from that which occurs on the more favorable substrates.

4.3.5. Film Growth on an Incomplete SAM. We infer that the small differences in initial multilayer growth on the SAMs on Si/SiO₂ and on Ag (Figure 4.2) are due to a difference in the concentration of favorable adsorption sites on the two types of surfaces.²³ The greater the concentration of these sites, the more readily a film should adsorb. To test this hypothesis, we prepared an incomplete SAM on Si/SiO₂, which should have a concentration of favorable sites intermediate between that of a complete SAM on this substrate and that of bare Si/SiO₂. The ellipsometric growth of a PDDA/Laponite multilayered film on this surface is shown in Figure 4.2. As expected, regular growth began earlier on this surface (in the third cycle) than on the SAM on Si/SiO₂. The average thickness added per cycle eventually reached 2.9 nm, which is very similar to the growth observed on the other samples.

4.4 Conclusions

PDDA and Laponite adsorb at isolated imperfections in model inert surfaces, forming islands that later grow vertically and laterally until they coalesce. These results conclusively demonstrate that PDDA/Laponite films are able to heal any microscopic defects that occur in their formation. The fact that they can form on model inert surfaces indicates that they should be expected to form on a great variety of other surfaces without the need for pre-treatment. The ability to adsorb films on

surfaces of low free energy also highlights the difficulties inherent in the creation of protective coatings, for example in applications involving the prevention of protein adsorption or biofouling;²⁴ even small imperfections in such coatings may result in their ultimate failure if the adsorption can be mediated by these sites.

4.5 Experimental Methods

4.5.1. Preparation of Substrates. Silicon wafers were broken into small pieces (~1 cm x ~2 cm) and cleaned by immersion in a 1:2 (v/v) solution of 30% H₂O₂ and concentrated H₂SO₄ (CAUTION: This solution reacts violently with organic materials!). To prepare SAMs, these pieces were treated for 5 min in ~9 mM solutions of octadecyltrichlorosilane (OTS, Aldrich) in 80% hexanes/20%CCl₄ (v/v), followed by rinsing with hexanes and swabbing and rinsing with ethanol. This treatment was repeated, if necessary, to produce films of the expected thickness and with the expected contact angles.⁹ The ellipsometric thickness of the layers thus formed was 2.5 nm, and the advancing contact angles of water and hexadecane were 112–114° and 42–43° respectively. Receding contact angles for the two liquids on this surface were 101–106° and 40–42° respectively. We produced incomplete SAMs on Si/SiO₂ by immersing cleaned silicon wafers in ~7 mM OTS solutions in CHCl₃ for 5–7 min, producing films with an ellipsometric thickness of 1.3 nm. Advancing and receding contact angles of water on this surface, 105–108° and 99–101°, respectively, were lower than would be expected for complete SAMs. The advancing and receding contact angles of hexadecane were surprisingly high: 42–43° and 41–42°. Silver substrates were prepared by the thermal evaporation of at least 90 nm of silver (99.99+%, Aldrich) onto a silicon wafer that had been treated with dilute aqueous hydrofluoric acid to remove the native oxide, and were broken into small pieces before use. To prepare SAMs, these pieces were treated for 1–3 h in ~13 mM

solutions of hexadecanethiol (HDT, Aldrich) in ethanol, followed by rinsing with ethanol. The advancing contact angles of water and hexadecane on this surface were 112–115° and 44–46° respectively, and the receding contact angles of these liquids were 100–103° and 37–40° respectively. These contact angles are similar to those reported by others for ordered monolayers^{17,25}

4.5.2. Ellipsometry. The growth of SAMs and multilayered films on silicon and silver substrates was monitored by optical ellipsometry, using a Rudolph Auto-EL III nulling ellipsometer with HeNe laser light ($\lambda = 632.8$ nm). Measurements were performed under ambient conditions with the angle of incidence set at 70°. The thickness of the native oxide of silicon was measured assuming a refractive index of 1.5, and assuming a standard refractive index for the silicon substrate ($n = 3.858$, $k = 0.018$). When silver substrates were used bare, the real and complex parts of the index of refraction, n and k , were determined for three spots on each substrate, and the average constants used in determinations of film thickness for that sample. When silver substrates were coated with SAMs, n and k were determined following adsorption of the monolayer. For determination of multilayer thickness on all substrates, a single smooth film was assumed, and a refractive index of 1.5 was used.

4.5.3. Preparation of Multilayered Films. Multilayered films were prepared by repetition of the following two-step adsorption cycle, unless noted otherwise. In the first step, the sample was treated for ~5 s with a 5% (w/w) aqueous solution of poly(diallyldimethylammonium chloride) (PDDA, Polysciences), rinsed with purified water (Millipore Milli-Q, 15 – 17 M Ω -cm), and blown dry with a jet of nitrogen. In the second step, the sample was treated for ~5 s with a 0.2% (w/w) dispersion of Laponite RD, rinsed with purified water, and blown dry. In the first few treatments on the SAM surfaces, the adsorption times were somewhat ill-defined, as the drops

of PDDA and Laponite failed to wet the surfaces and were therefore difficult to control.

4.5.4. *Atomic Force Microscopy (AFM)*. Samples were prepared for this study by performing ten adsorption cycles on a SAM on Ag and eight adsorption cycles on a bare Ag surface. Both of these multilayered films had overall ellipsometric thicknesses of 21 nm. The slight apparent difference between the growth per cycle shown for the SAM on Ag in Figure 4.2 and that observed in this case can be attributed to differences in the ambient humidity on the days these samples were prepared.²⁶ AFM images were obtained on a Park Scientific Instruments SFM-BD2-210 under ambient conditions in non-contact (attractive) mode using a Microlever (Si_3N_4) probe tip. The scan rate was 0.5 Hz, and the images were tilt-corrected. Repeated scans over the same area gave similar images, indicating that no damage to the samples was occurring.

Acknowledgements. We are indebted to Lisa Dhar and Mark Cardillo of AT&T Bell Laboratories for the AFM images. E.R.K. gratefully acknowledges an AT&T Bell Laboratories Ph.D. Scholarship. We further acknowledge financial support from Lehigh University.

4.6 References and Notes

1. Ozin, G.A. *Adv. Mater.* **1992**, *4*, 612.
2. Katz, H.E.; Scheller, G.; Putvinski, T.M.; Schilling, M.L.; Wilson, W.L.; Chidsey, C.E.D. *Science* **1991**, *254*, 1485. Li, D.; Ratner, M.A.; Marks, T.J.; Zhang, C.; Yang, J.; Wong, G.K. *J. Am. Chem. Soc.* **1990**, *112*, 7389.
3. Brousseau, L.C.; Aoki, K.; Garcia, M.E.; Cao, G.; Mallouk, T.E. in *Multifunctional Mesoporous Inorganic Solids*, Sequeira, C.A.C.; Hudson, M.J., Eds.; Kluwer:

Netherlands, 1993; pp 225 – 236.

4. Kepley, L.J.; Sackett, D.D.; Bell, C.M.; Mallouk, T.E. *Thin Solid Films* **1992**, *208*, 132. Kaneko, F.; Shibata, M.; Inaba, Y.; Kobayashi, S. *Thin Solid Films* **1989**, *179*, 121.
5. Netzer, L.; Iscovici, R.; Sagiv, J. *Thin Solid Films* **1983**, *99*, 235. Tillman, N.; Ulman, A.; Penner, T.L. *Langmuir* **1989**, *5*, 101. Sagiv, J. U.S. Patent 4 539 061, 1985.
6. Cao, G.; Hong, H.-G.; Mallouk, T.E. *Acc. Chem. Res.* **1992**, *25*, 420.
7. Evans, S.D.; Ulman, A.; Goppert-Berarducci, K.E.; Gerenser, L.J. *J. Am. Chem. Soc.* **1991**, *113*, 5866.
8. Yang, H.C.; Aoki, K.; Hong, H.-G.; Sackett, D.D.; Arendt, M.F.; Yau, S.-L.; Bell, C.M.; Mallouk, T.E. *J. Am. Chem. Soc.* **1993**, *115*, 11855.
9. Ulman, A. *An Introduction to Ultrathin Organic Films: From Langmuir–Blodgett to Self-Assembly*; Academic: New York, 1991.
10. Byrd, H.; Whipps, S.; Pike, J.K.; Ma, J.; Nagler, S.E.; Talham, D.R. *J. Am. Chem. Soc.* **1994**, *116*, 295.
11. Schilling, M.L.; Katz, H.E.; Stein, S.M.; Shane, S.F.; Wilson, W.L.; Buratto, S.; Ungashe, S.B.; Taylor, G.N.; Putvinski, T.M.; Chidsey, C.E.D. *Langmuir* **1993**, *9*, 2156.
12. Lvov, Y.; Haas, H.; Decher, G.; Möhwald, H.; Kalachev, A. *J. Phys. Chem.* **1993**, *97*, 12835.
13. Iler, R.K. *J. Colloid Interface Sci.* **1966**, *21*, 569. Ingersoll, D.; Kulesza, P.J.; Faulkner, L.R. *J. Electrochem. Soc.* **1994**, *141*, 140. Cheung, J.H.; Fou, A.F.; Rubner, M.F. *Thin Solid Films* **1994**, *244*, 985.
14. Schmitt, J.; Grünewald, T.; Decher, G.; Pershan, P.S.; Kjaer, K.; Lösche, M.; *Macromolecules* **1993**, *26*, 7058.

15. Kleinfeld, E.R.; Ferguson, G.S. *Science* **1994**, *265*, 370.
16. For additional examples of systems that use inorganic sheet minerals in an electrostatic assembly scheme, see: Keller, S.W.; Kim, H.-N.; Mallouk, T.E. *J. Am. Chem. Soc.* **1994**, *116*, 8817. Keller, S.W.; Johnson, S.A.; Brigham, E.S.; Yonemoto, E.H.; Mallouk, T.E. *J. Am. Chem. Soc.* **1995**, *117*, 12879. Kotov, N.A.; Dékány, I.; Fendler, J.H. *J. Phys. Chem.* **1995**, *99*, 13065.
17. Walczak, M.M.; Chung, C.; Stole, S.M.; Widrig, C.A.; Porter, M.D. *J. Am. Chem. Soc.* **1991**, *113*, 2370.
18. For comparison, more than 2.2 nm of growth is typically observed during the first adsorption cycle on Si/SiO₂.
19. Iler studied the adsorption of charged colloidal particles onto oxide surfaces that had been rendered hydrophobic by the adsorption of surfactant monolayers.¹³ These particles adsorbed by altering the structure of the physisorbed monolayers, or removing them altogether, in contrast to our findings for adsorption of PDDA and Laponite onto chemisorbed SAMs.
20. To avoid ambiguity, we use the word "imperfections," rather than "defects," to refer to the flaws within the SAMs themselves that allow for the nucleation of the multilayered films.
21. The height scales in these AFM images provide information about the *relative* heights of features in the two samples; a value of zero on those scales does not necessarily imply that the probe tip touched the Ag or SAM surface.
22. Quantitative analysis of the data showed that the film formed on the SAM was more than twice as rough as the film formed on bare Ag (60 Å root-mean-square roughness *vs.* 26 Å). An AFM image of a SAM-coated Ag surface, which should have a topology nearly identical to that of a bare Ag surface, was very similar in appearance to the image in Figure 3.4b and had an rms roughness of 18 Å. The

uncertainty in these values of rms roughness is $\pm 5 \text{ \AA}$.

23. In addition, image-charge interactions between the precursor(s) and the substrates may be important, so that adsorption onto a certain imperfection in a SAM on Ag would be energetically more favorable than adsorption onto a similar imperfection in a SAM on Si/SiO₂.¹⁷ The silicon used in this work (Wacker Siltronic) was p-doped and therefore conducting (resistivity 0.2–70 Ω -cm) but was covered with an oxide approximately 1.5 nm in thickness. The force of attraction between a point charge and an infinite, planar, grounded conductor falls off as the inverse square of the distance between them (see Griffiths, D.J. *Introduction to Electrodynamics*; Prentice Hall: Englewood Cliffs, NJ, Ed. 2, 1989, pp 121–124).
24. Pitt, W.G.; Grasel, T.G.; Cooper, S.L. *Biomaterials* **1988**, *9*, 36.
25. Laibinis, P.E.; Whitesides, G.M.; Allara, D.L.; Tao, Y.-T.; Parikh, A.N.; Nuzzo, R.G. *J. Am. Chem. Soc.* **1991**, *113*, 7152.
26. Kleinfeld, E.R.; Ferguson, G.S. *Chem. Mater.* **1995**, *7*, 2327.

**Rapid, Reversible Sorption of Water from the Vapor
by a Multilayered Composite Film:
A Nanostructured Humidity Sensor**

Reprinted with permission from Kleinfeld, E.R.; Ferguson, G.S. *Chem. Mater.*
1995, 7, 2327. Copyright 1995, American Chemical Society.

5.1 Abstract

Composite films prepared by alternate adsorption of poly(diallyldimethylammonium chloride) and exfoliated sheets of a synthetic sheet-silicate mineral (Laponite RD) respond in a dramatic way to changes in ambient humidity. The structural order in these films and the ability to prepare them to precisely controlled thicknesses provided unique opportunities to study this behavior. Ellipsometric and gravimetric evidence indicate that initially some water fills void spaces in the films, giving rise to a relatively small increase in overall film thickness; further uptake of water then causes greater swelling of the film. This behavior is rapid: water penetrates to depths greater than 139 nm within seconds, and desorbs from the films at a similar rate. The rapid and reversible response of this system makes it interesting from the standpoint of molecular sensing.

5.2 Introduction

Interest in the design and development of sensors has increased dramatically in recent years.¹ Thin films offer unique promise for use in sensors due to their large area/mass ratio and the ease with which they can be incorporated into electronic and microelectronic devices. Advances in this area have included the use of Langmuir-Blodgett multilayered films in various types of sensors,² and layered metal-phosphonates, which have demonstrated shape selectivity.³ The molecular-sieving ability of thin zeolite layers, either attached directly to quartz-crystal

microbalances or deposited in a silica matrix onto surface acoustic wave devices, has also been used for chemically selective sensing.⁴

We have recently described a new method for the formation of ordered ultrathin films by controlled, stepwise adsorption of a cationic polyelectrolyte and single exfoliated sheets of a silicate mineral onto solid surfaces.⁵ Early in this work, we observed that the films underwent dramatic, reversible changes in interference color when exposed to humid air. We have also noticed small variations in the ellipsometric growth per adsorption cycle from day to day that may reflect changes in the ambient humidity.⁶ Based on these observations, we have used ellipsometric and gravimetric measurements to gain additional insight into the sorption of water by the films^{7,8} and to explore the use of the films as sensors. The order, uniformity, and precisely controllable thickness of these films make them attractive for fundamental studies of sensor design and function.

5.3 Results and Discussion

5.3.1. *Qualitative Observations of Response to Changes in Relative Humidity.*

Alternate adsorptions of poly(diallyldimethylammonium chloride) (PDDA) and Laponite form multilayered films (Figure 5.1) with thicknesses that grow linearly with the number of adsorption cycles and that possess order in the direction perpendicular to the substrate surface, as described in chapters 2 and 3.⁵ As these PDDA/Laponite films grow in thickness on silicon substrates, they display a series of vivid colors due to constructive and destructive interference between the light reflected from the surface of the film and that reflected from the silicon substrate.^{5,9,10} The interference color of a coating depends upon both its thickness and its refractive index. The changes in color of particular PDDA/Laponite films in response to differences in relative humidity (RH) thus indicated rapid and reversible swelling of

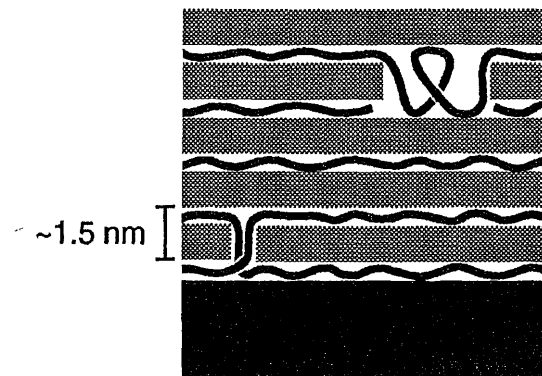




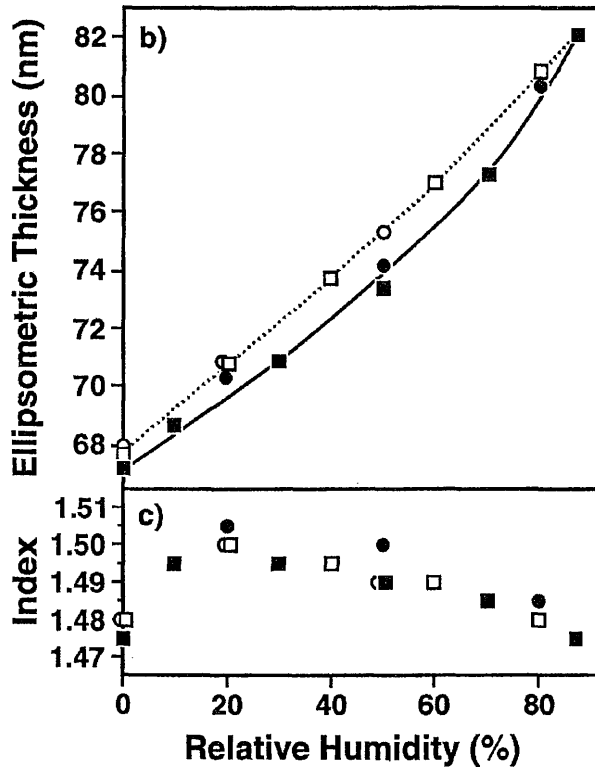
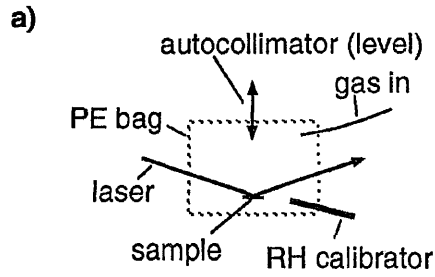
Figure 5.1. Schematic diagram of the structure of a PDDA/Laponite multilayered film ( = PDDA;  = Laponite).

the films. For example, a 67-cycle multilayered film with a thickness of 223 nm (assumed index of refraction, $n = 1.5$), prepared on a wafer bearing a native oxide, appeared deep gold in color. When the sample was held in the vapor above water in a small vial, its interference color rapidly changed to fuchsia, indicating an increase in the film thickness and/or refractive index.⁹ As the sample was removed from the vial, the color began to revert to gold, and this change was complete by the time the entire sample had been removed from the vial. The sample could be cycled into and out of the humid environment many times with no apparent change in its response. Using a video camera operating at 30 frames/s, we examined the time necessary for this same sample to respond to a moving jet of humid air. When the videotape was viewed frame by frame, no trailing of the pink interference color was apparent behind the jet, indicating that the time needed for the sample to undergo this reversible change in color was shorter than the residence time of a single frame (33 ms). The speed of this reversible behavior makes the system quite promising from the standpoint of molecular sensing.¹¹

5.3.2. *Ellipsometric Analysis of Changes in Film Thickness and Refractive Index.*

Ellipsometry was used to quantify the effect of changes in RH on the thickness and refractive index of the multilayered films. A 25-cycle film on silicon was placed into a controlled-atmosphere chamber on an ellipsometer stage, along with a commercial RH calibrator (Figure 5.2a), and the film's thickness and index of refraction were determined as a function of the RH. The thickness increased monotonically with increasing RH, from 67.2 nm at 0.5% RH to 82.1 nm at 87% RH. Measurements taken 5 and 10 min after the calibrator had equilibrated always agreed to within 0.4 nm. The index of refraction also changed systematically as a function of RH. A plot of ellipsometric thickness *vs.* RH is shown in Figure 5.2b, with corresponding refractive indices given in Figure 5.2c. Taken together, the changes in thickness and refractive

Figure 5.2. Ellipsometric study of film thickness and refractive index as a function of relative humidity: a) schematic diagram of the experimental setup; b) ellipsometric thickness of a 25-cycle multilayered film on silicon as a function of relative humidity; c) refractive index of the film, rounded to the nearest 0.005, as a function of RH. The filled symbols (solid line) correspond to thicknesses and indices measured in order of increasing RH; the open symbols (dashed line) correspond to thicknesses and indices measured in order of decreasing RH. The squares represent data obtained during the first cycle; the circles represent data obtained during the second cycle. With the exception of the point at 87% RH, all data were obtained at multiples of 10% RH ($\pm 0.5\%$); some data points have been offset slightly in the horizontal direction for clarity of presentation. The lines are guides for the eye.



index provide insight into the sorption of water into the films. Upon going from 0.5% to 20% RH, for example, the film underwent a sudden increase in refractive index, with a relatively small increase in thickness, indicating that some of the sorbed water entered void spaces in the structure (e.g., spaces between platelet edges and interlamellar spaces). In contrast, upon going from 20 to 87% RH, the film underwent a gradual decrease in refractive index concomitant with a relatively large increase in thickness, suggesting that in this regime, swelling of the film was occurring due to sorption of water into the interlamellar galleries, void spaces in the structure having been filled. We infer that the refractive index drops because the refractive index of water ($n = 1.333$) is lower than that of the film. A small hysteresis was observed (compare solid and dotted lines in Figure 5.2b), which is common for adsorption and desorption of water by smectite minerals.^{7,12} A different 25-cycle sample showed behavior nearly identical to that shown in Figure 5.2. The changes in ellipsometric thickness observed for the 25-cycle samples as a function of RH are sufficient to account for the small variations we have seen in ellipsometric growth per adsorption cycle from day to day. As a control experiment, ellipsometric measurements were made of a bare wafer having a thermal oxide 61 nm in thickness (assumed index of refraction, $n = 1.465$) at 0.5% and 88% RH. The difference in thickness at these two extremes of RH was less than 1 nm, indicating that the changes in thickness of the multilayered samples were due mainly to intercalation of water and not to condensation onto a hydrophilic surface. The measurements in Figure 5.2 reflect reproducible changes in a film under conditions of controlled humidity, and do not appear to depend upon the absolute refractive index, which varies from sample to sample and with the thickness of individual samples.

5.3.3. Visual Evidence of the Sorption of Water into the Films. A more elaborate control experiment allowed us to determine how deeply into the film the water

molecules penetrated, and to conclusively rule out surface condensation as the dominant mechanism for these changes in thickness/refractive index. Five samples were prepared having different thicknesses of adsorbed multilayer and underlying native or thermal oxide (SiO_2), but having approximately the same combined thickness and thus the same interference color. These samples are depicted schematically in Figure 5.3, and details of their composition are given in Table 5.1. The final step in the preparation of all five samples was adsorption of Laponite, which ensured that all their *surfaces* should have the same affinity for H_2O . The response of these samples to water vapor was compared to that of sample 1, whose behavior was described at the beginning of this section. The extent of the change in interference color (i.e., from gold to peach, pink, or fuchsia) was used as a qualitative measure of the increase in thickness and/or refractive index of the film, and thus the amount of water sorbed. Samples 2 – 5 were held over water in a vial and compared to sample 1 in a separate but identical vial. The samples gave a range of responses that corresponded to the thickness of the multilayered films: sample 5, having the thinnest film, acquired only a slight peachy color; sample 2, having the second-thickest film, turned the same deep fuchsia as sample 1. Samples 3 and 4 displayed behavior between these two extremes. These observations indicate that water can be rapidly sorbed into the films to depths greater than 139 nm (sample 3) and confirm that the changes in color cannot be due primarily to condensation of water vapor onto the samples' surfaces.

5.3.4. *Study of Relative Mass Uptake.* Although ellipsometry was useful in measuring the changes in thickness and refractive index of the films that produced visible responses to changes in humidity, this method does not provide a direct measure of the amount of water sorbed. To address this question, we used a quartz-crystal microbalance (QCM). The magnitude of the change in the resonant frequency

Figure 5.3. Schematic diagram of the composition of samples 1 – 5; details are given in the text and in Table 5.1.

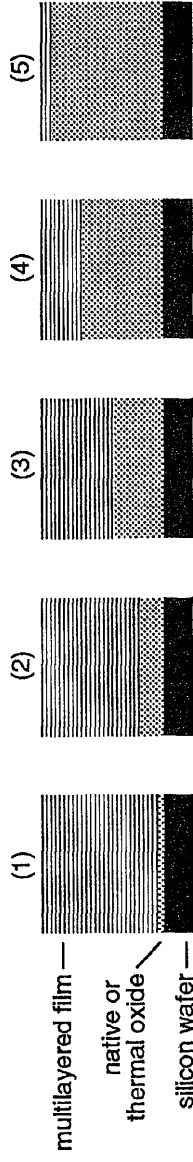


Table 5.1. Thickness of Native or Thermal Oxide on Silicon and of Multilayered Film Adsorbed on Each Substrate.

Sample Number	Oxide Thickness (nm) <u>assumed n = 1.465</u>	Multilayer Thickness (nm) <u>assumed n = 1.5[‡]</u>	Overall Thickness (nm)
1	1.4	223 (67 cycles)	224
2	64	167 (53 cycles)	231
3	88	139 (46 cycles)	227
4	149	80 (27 cycles)	229
5	216	16 (6 cycles)	232

[‡]For any one film, growth has always appeared to be a linear function of the number of adsorption cycles when a constant refractive index is assumed. We have, however, observed variations in refractive index during the growth of individual films and from one film to another. For the films on samples 1 – 5, the measured thicknesses (t) and refractive indices (n) were: 1) t = 206 nm, n = 1.57; 2) t = 168 nm, n = 1.50; 3) t = 144 nm, n = 1.47; 4) t = 70 nm, n = 1.61; 5) t = 16 nm, n = 1.53.

of the crystal is directly proportional to the change in the mass of the film during sorption of water.¹³ A 10-cycle film was adsorbed onto a gold-coated, AT-cut quartz crystal, and its resonant frequency was recorded after it had equilibrated for several minutes in atmospheres of chosen RH (Figure 5.4a). The response of the film to changes in RH (Figure 5.4b) resembles that of bulk montmorillonite, a mineral similar in structure to Laponite.⁷ Others have correlated the inflection point in such curves for montmorillonite with discrete jumps in d-spacing, revealed by x-ray diffraction, and ascribed it to the completion of intercalation of one layer of water in the interlamellar space and the beginning of the uptake of a second layer.⁷ The multilayer-coated crystal responded rapidly to these incremental changes in RH (in fact, more rapidly than the commercial RH calibrator); after the flow rates of wet and dry nitrogen were set to desired values, the QCM often equilibrated to within ± 1 Hz in under 1 min. For the multilayered samples, measurements taken 5 and 10 min after the calibrator had equilibrated always agreed to within 1 Hz. As a control experiment, measurements of resonant frequency were made of a bare quartz crystal at ~0% and 85% RH. The difference in resonant frequency at these two extremes of RH was 6 Hz.

The mass of water intercalated into the multilayered film can be calculated using a form of the Sauerbrey equation (1):¹³

$$M = \frac{-(f - f_0)\rho v A}{2(f_0)^2} \quad (1)$$

where M is the mass of water; f is the frequency of the crystal in an atmosphere at a given RH; f_0 is the frequency of the crystal in an atmosphere at ~0% RH; ρ is the density of quartz, 2.65 g/cm³; v is the shear-wave velocity for an AT-cut quartz crystal, 3.34 x 10⁵ cm/s; and A is the active area of the crystal. Because the active area of the crystal is difficult to define,¹³ the areal density of water (i.e., M/A) was

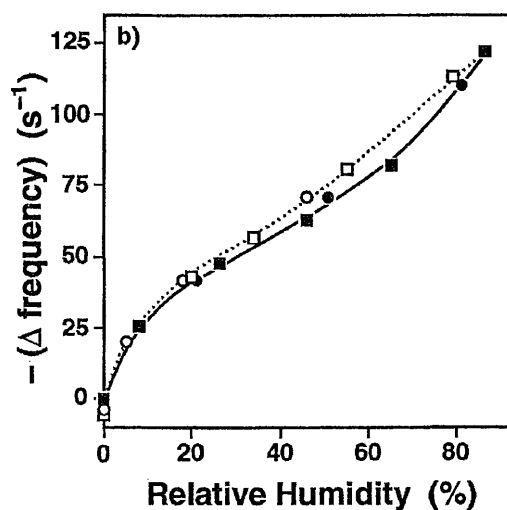
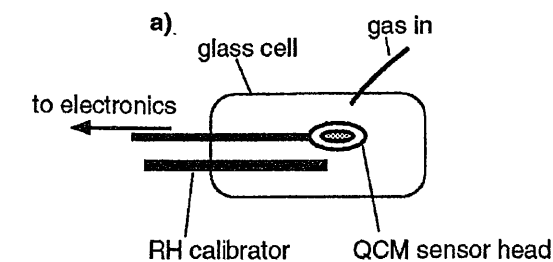


Figure 5.4. Quartz-crystal-microbalance study of relative mass uptake as a function of RH: a) schematic diagram of the experimental setup; b) change in resonant frequency of an oscillating quartz crystal coated with a 10-cycle film of PDDA and Laponite as a function of relative humidity. The filled symbols (solid line) correspond to changes measured in order of increasing RH; the open symbols (dashed line) correspond to changes measured in order of decreasing RH. Data obtained during the first cycle are represented by squares; data obtained during the second cycle are represented by circles. The lines are guides for the eye.

calculated instead. From the data shown in Figure 5.4b, at 86% RH, the film sorbed 1.53×10^{-6} g of water per square centimeter of active area. This value is larger (on a per-cycle basis) than would be estimated from the increase in thickness measured ellipsometrically, for at least two reasons. First, the ellipsometric data indicate that some of the water fills void spaces, not causing swelling (*vide supra*) and therefore not resulting in an increase in ellipsometric thickness. Second, uptake of water by any excess film on the back of the quartz crystal¹⁴ would artificially inflate the results generated by the QCM. This excess film does not affect ellipsometric measurements, which are obtained within a limited area on one side of the substrate.

5.3.5. Kinetics of Water Sorption. Time-resolved QCM experiments allowed measurement of the speed with which water was sorbed by the films. A 10-cycle film, nominally 30 nm in thickness,¹⁵ was adsorbed onto a gold-coated quartz crystal and exposed to a jet of nitrogen that was switched back and forth between ~0% RH and ~95% RH at 120-s intervals. The resonant frequency of the crystal was recorded at 1.5-s intervals (Figure 5.5). The sorption traces show that when the jet was switched to dry nitrogen, the frequency changed by more than 82% of its total range within the first 3 s. Likewise, each time the jet was switched to wet nitrogen, the frequency changed by more than 77% of the total frequency range within the same period. These results explain why the visible changes in interference color appeared complete within seconds when a wafer was cycled into and out of a humid atmosphere (*vide supra*). The path of water molecules diffusing through the film is probably tortuous due to the presence of the Laponite sheets (diameter 25 – 35 nm). Nevertheless, the initial kinetics of sorption are faster than our ability to take measurements, as would be expected based upon the kinetics of sorption of water by similar systems (zeolites¹⁶ and hydrophilic polymers¹⁷). Approximately one minute appeared to be sufficient for the sample to equilibrate to within 1 Hz after the jet had

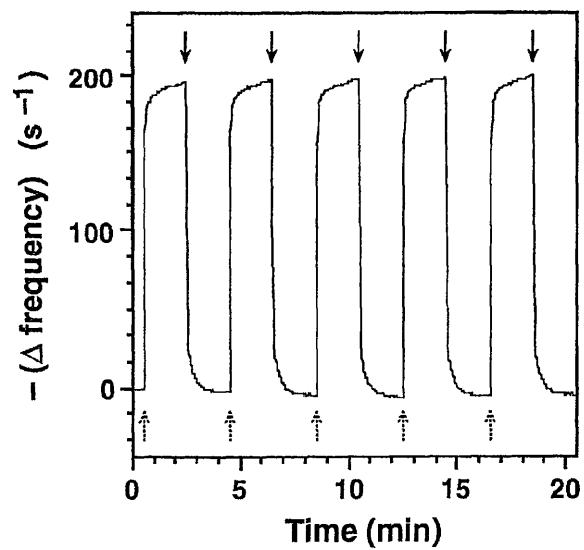


Figure 5.5. Change in resonant frequency of a quartz crystal coated with a 10-cycle multilayered film, as a function of time of exposure to a jet of dry or wet nitrogen. Dashed arrows (pointing up) indicate when the jet was switched to wet nitrogen; solid arrows (pointing down) indicate when the jet was switched to dry nitrogen.

been switched to 0% RH. The kinetics of adsorption mirrored those of desorption; the final phase of equilibration at 95% RH, however, was somewhat slower than at 0% RH.⁷ The tailing in the response curves at longer exposure times to either dry or wet nitrogen is probably due not only to the finite time needed for atmospheric turnover in the glass cell, but also to changes in the heat of desorption of water as a function of the amount of water in the film. The heat of desorption of water from various clay minerals increases as the amount of water in the sample decreases,^{7,18} which makes the sorbed water in a nearly dry film more difficult to remove. By the same argument, the much lower heat of adsorption of water into a nearly saturated film causes further adsorption to proceed more slowly, desorption having become a competitive process. Intercalation of water by clays has been reported to exhibit a slow approach to equilibrium, with desorption being more reproducible than adsorption.⁷

Although the samples prepared for the QCM experiments each behaved in a consistent and reproducible manner, significant differences were observed from sample to sample. For example, whereas one crystal exhibited a difference of 125 Hz between limiting frequencies at ~0 % and ~86% RH, another with the same nominal surface area and composition exhibited a difference of 170 Hz. This variability probably results from differences in sample preparation,¹⁴ which might be minimized by optimization of the adsorption conditions. Given this uncertainty, a more detailed analysis of the absolute mass of water sorbed per structural unit of the multilayered film is not justified. Nonetheless, as was true for the ellipsometric study, the use of these films in practical applications would simply require the calibration of individual samples.

5.4 Conclusions

PDDA/Laponite multilayered films sorb water rapidly and reversibly. Ellipsometric and gravimetric studies indicate that, at first, some water fills void spaces in the structure, swelling the structure to a relatively small extent; further uptake of water into the interlamellar galleries causes greater swelling of the film. Due to the order in these films and corresponding orientation of the constituent silicate sheets (Figure 5.1), we expect that this swelling occurs primarily in the direction normal to the surface. This anisotropy is advantageous because it maximizes changes in thickness measured ellipsometrically and minimizes differential stress at the film/substrate interface as the sample is cycled repeatedly between dry and wet atmospheres. This study has not only provided insight into the sorption of water into these composite films, but has also demonstrated the feasibility of using these unique materials as sensors. The method for preparing these films is flexible with respect to the choice of component materials, as discussed in chapter 2;¹⁹ this versatility may allow design of sensors that are selective for various classes of vapors.

5.5 Addendum

Following the completion of this work, additional studies on the sorption of water by PDDA/Laponite composite films were performed by Barbara A. MacNeill (Lehigh University). These studies demonstrated that infrared (IR) spectroscopy was an additional technique that could be used to quantify water sorption. The use of IR spectroscopy imparts selectivity to the sensing process, as individual chemical species that preconcentrate into the films can potentially be detected by their characteristic absorption frequencies.²⁰

5.6 Experimental Methods

5.6.1. *Materials.* Poly(diallyldimethylammonium chloride) was obtained from Polysciences as a 20% (w/w) aqueous solution, and was diluted with Millipore Milli-Q water (15 – 17 M Ω -cm) to 5% (w/w) before use. Laponite RD (synthetic hectorite) was obtained from Laporte Industries, Limited, in powder form. It was added to Milli-Q water with stirring to form a 0.5% (w/w) dispersion; stirring was continued until the dispersion appeared clear (typically for several hours). The dispersion was then allowed to stand overnight without stirring to allow complete exfoliation of the precursor, and was diluted to 0.2% (w/w) before use. The individual silicate sheets in the suspension are 0.93 nm thick and approximately 25–35 nm in diameter; the composition of Laponite RD [66.2% SiO₂, 30.2% MgO, 2.9% Na₂O, 0.7% LiO₂ (w/w)] and the structure of the exfoliated suspension have been described elsewhere.²¹ Silicon wafers [p-doped, (100)-oriented] were manufactured by Wacker Siltronic and had a native oxide approximately 1.5 nm in thickness, unless stated otherwise.

5.6.2. *Sample Preparation.* Silicon substrates were cleaned shortly before use by immersion for at least 30 min in a 1:2 (v/v) solution of 30% H₂O₂ and concentrated H₂SO₄ (CAUTION: *This “piranha” solution reacts violently with organic materials!*) and were rinsed thoroughly with Milli-Q water and dried with a jet of nitrogen. For one experiment discussed in this paper, wafers were oxidized thermally in an oxygen atmosphere for various periods of time. These wafers were subjected to an additional cleaning step after treatment with piranha solution: immersion in a 50:50 (v/v) solution of 30% H₂O₂ and concentrated NH₄OH for 5 min, followed by rinsing and drying. Multilayered films were formed, as previously described,⁵ by repeating a simple two-step cycle involving alternate adsorptions from a 5% (w/w) solution of

poly(diallyldimethylammonium chloride) and a 0.2% (w/w) suspension of Laponite RD. No pre-treatment of the substrates was used to promote adhesion of the multilayered films.

5.6.3. Ellipsometric Study of Water Sorption. A Rudolph Auto-EL III ellipsometer ($\lambda = 632.8 \text{ nm}$, $\phi = 70^\circ$) was used to measure thicknesses of the multilayered films using an assumed refractive index, or, if desired, to determine simultaneously both thickness and refractive index. The native or thermal oxide on silicon was always measured before adsorption of any multilayer and treated as a separate film. Unless noted otherwise, measurements were performed at ambient humidity and were always performed at room temperature ($\sim 22^\circ \text{C}$). To study the response of the films to changes in RH, samples were placed on the ellipsometer stage which was enclosed in a polyethylene bag having small holes through which an RH calibrator (Vaisala HMC 20)²² and a nitrogen flow of variable humidity were introduced and through which the laser beam was allowed to enter and exit (Figure 5.2a). The approximate volume of this cell was 2 L. The RH was cycled twice between $\sim 0\%$ and $\sim 88\%$. In the first cycle, measurements were taken 5 and 10 min after the RH calibrator had equilibrated at a desired RH. In the second cycle, only one measurement was taken for each RH value, 5 min after the desired RH had been attained. In no case did the calibrator vary more than $\pm 0.5\%$ from this RH during the 10-min measurement period. Nitrogen of various relative humidities (RHs) was prepared by mixing dry nitrogen with nitrogen that had passed through two gas dispersion bubblers filled with Milli-Q water; flow rates were $(5.0 - 20) \times 10^2 \text{ sccm}$.

5.6.4. Gravimetric Studies of Water Sorption. A Sycon STM-100 MF quartz-crystal microbalance (QCM) was used to monitor mass changes resulting from the sorption of water by multilayered films. Gold-coated, AT-cut quartz crystals (6 MHz) were cleaned by rinsing with ethanol and water before use, and multilayered films were

adsorbed according to the same procedure used on the silicon substrates.^{5,15} The QCM sensor head and the RH calibrator were placed in a glass cell (approximate volume 0.45 L) into which a flow of nitrogen could be introduced. Measurements were performed at ambient temperatures (~22°C). Nitrogen of various relative humidities (RHs) was prepared by mixing dry nitrogen with nitrogen that had passed through two gas dispersion bubblers filled with Milli-Q water. For measurement of water sorption as a function of RH, the resonant frequency of the crystal was determined 5 min and 10 min after the RH sensor had equilibrated. The RH was cycled twice, in steps, between ~0% and 88%. Flow rates were $(2.5 - 17) \times 10^2$ sccm. For measurements of water sorption as a function of time, data were taken at 1.5-s intervals as the gas flow was alternated between ~0% RH and ~95% RH (120 s each). Flow rates were $(6.9 - 9.3) \times 10^2$ sccm.

Acknowledgements. E.R.K. gratefully acknowledges an AT&T Bell Laboratories Ph.D. Scholarship. We further acknowledge Lehigh University for financial support of this research, Laporte Industries, Ltd., for a gift of Laponite RD, and WaferNet, Inc., for a donation of silicon wafers.

5.7 References and Notes

1. For reviews, see Janata, J.; Josowicz, M.; DeVaney, D.M. *Anal. Chem.* **1994**, *66*, 207R. Hughes, R.C.; Ricco, A.J.; Butler, M.A.; Martin, S.J. *Science* **1991**, *254*, 74.
2. For a review, see A. Ulman, *An Introduction to Ultrathin Organic Films: From Langmuir–Blodgett to Self-Assembly*. Academic: New York, 1991.
3. Brousseau, L.C.; Aoki, K.; Garcia, M.E.; Cao, G.; Mallouk, T.E. *Multifunctional Mesoporous Inorganic Solids*; C.A.C. Sequeira and M.J. Hudson, Eds.; Kluwer Academic: Netherlands, 1993, 225. Cao, G.; Garcia, M.E.; Alcalá, M.; Burgess,

- L.F.; Mallouk, T.E. *J. Am. Chem. Soc.* **1992**, *114*, 7574.
4. For examples, see Yan, Y.; Bein, T. *J. Phys. Chem.* **1992**, *96*, 9387. Bein, T.; Brown, K.; Frye, G.C.; Brinker, C.J. *J. Am. Chem. Soc.* **1989**, *111*, 7640.
 5. Kleinfeld, E.R.; Ferguson, G.S. *Science* **1994**, *265*, 370.
 6. E.R. Kleinfeld and G.S. Ferguson, unpublished results.
 7. For detailed studies of the sorption of water by montmorillonite, see: Mooney, R.W.; Keenan, A.G.; Wood, L.A. *J. Am. Chem. Soc.* **1952**, *74*, 1367 and 1371.
 8. Swelling of polyelectrolyte films by water has also been noted. See, for example: Decher, G.; Lvov, Y.; Schmitt, J. *Thin Solid Films* **1994**, *244*, 772. Sukhorukov, G.B.; Schmitt, J.; Decher, G. *Ber. Bunsenges. Phys. Chem.* **1996**, *100*, 948.
 9. Pliskin, W.A.; Conrad, E.E. *IBM J. Res. Dev.* **1964**, *8*, 43.
 10. The similarity in refractive index between the multilayered film and the native or thermal oxide of silicon minimizes the reflected intensity at this interface.
 11. The change in interference color in the path of the jet of humid air was not as dramatic as when the sample was allowed to equilibrate in a static humid atmosphere.
 12. Barrer, R.M.; MacLeod, D.M. *Trans. Faraday Soc.* **1954**, *50*, 980.
 13. Lu, C.; Czanderna, A.W., Eds. *Applications of Piezoelectric Quartz-Crystal Microbalances; Methods and Applications 7*. Elsevier: New York, 1984, pp. 26 – 31.
 14. Multilayered films formed from PDDA and Laponite appear to adsorb readily onto a great variety of surfaces (see chapters 3 and 4); it was therefore difficult to limit the growth of the film to the front face of the crystal, and the extent of the growth on the back face may vary from one crystal to another. Application of a removable mask to the back face of the crystal was not considered due to

the risk of contamination of the film during formation of the film or upon removal of the mask.

15. We have determined that, when films are adsorbed onto gold, the ellipsometric growth and film structure are identical or nearly identical to those of films formed on the native oxide of silicon (see chapter 3).
16. Karger, J.; Ruthven, D.M. *Diffusion in Zeolites and Other Microporous Solids*. Wiley: New York, 1992, pp. 203, 400.
17. Vieth, W.R. *Diffusion In and Through Polymers*. Hanser: New York, 1991, pp. 209 – 211.
18. Grim, R.E. *Clay Mineralogy*. McGraw–Hill: New York, 1968, p. 270.
19. Kleinfeld, E.R.; Ferguson, G.S. *Mat. Res. Soc. Symp. Proc.* **1995**, 369, 697. For analogous organic/inorganic composite multilayers from other polyelectrolytes see Keller, S.W.; Kim, H.-N.; Mallouk, T.E. *J. Am. Chem. Soc.* **1994**, 116, 8817.
20. MacNeill, B.A.; Kleinfeld, E.R.; Ferguson, G.S. Manuscript in preparation.
21. Ramsay, J. D. F.; Swanton, S.W.; Bunce, J. J. *Chem. Soc. Faraday Trans.* **1990**, 86, 3919.
22. The action of this calibrator is based on changes in capacitance of a polymer film as a function of RH.

Interference Effects and Photochromism in Dye-Containing Polyelectrolyte/Clay Multilayered Films

6.1 Abstract

A photochromic spiropyran dye was synthesized and grafted onto poly(vinylpyridine). The resulting cationic polyelectrolyte was subsequently used in the formation of multilayered films, in combination with either Laponite RD or montmorillonite. These systems demonstrated regular growth, as determined using both ellipsometry and ultraviolet–visible (uv–vis) spectrophotometry, and the films were optically clear. The uv–vis study of film growth as a function of the number of adsorption cycles served as the first documentation of the ability of polyelectrolyte/silicate multilayered films to serve as antireflective coatings. Reversible changes in the uv–vis spectra of the composite films could be induced by irradiating them with ultraviolet or visible light. These changes were attributable to the isomerization of the dye between the spiropyran and merocyanine forms. The kinetics of colorization or decolorization of the dye in these films were studied when the films were stored in the dark, and were comparable to the kinetics of these processes in a film formed by evaporating a solution of the polyelectrolyte alone onto a quartz slide.

6.2 Introduction

Multilayered films formed in a layer-by-layer fashion by alternate adsorption of a cationic polyelectrolyte and anionic sheet silicate from aqueous solution or suspension exhibit a series of colors as they grow in thickness, as described in chapters 2 and 3. The colors are due to constructive and destructive interference between light reflected at the air/film interface and light reflected at the

film/substrate interface. This characteristic suggested the potential of the films to serve as anti-reflective coatings,¹ which are useful in various optical applications for the minimization of reflection losses as a beam of light passes from component to component in a given device. Current technology for the formation of such coatings typically relies on vacuum evaporation or electron bombardment to volatilize the coating material prior to condensation onto the substrate of interest.² The potential to use our method to form such coatings under ambient conditions, conveniently and inexpensively, therefore attracted our attention.

At the same time, we were also interested in the films' potential usefulness for optical data storage and optical switching applications, and so chose to use a functional polycation for the preparation of these films, poly(vinylpyridine) that had been partially quaternized with a photochromic spiropyran dye, abbreviated PVP-SP. Photochromic molecules undergo reversible isomerization upon irradiation with light of an appropriate wavelength,³ and this isomerization can be reversed thermally, or with light of a different wavelength. The spiropyrans constitute one class of photochromic molecules; the isomerization of a representative spiropyran/merocyanine (SP/MC) pair is shown in Figure 6.1.³ Absorption of a photon of ultraviolet light causes a spiropyran molecule to isomerize to the merocyanine form, and absorption of a photon of visible light causes the reverse. Different equilibrium ratios of the two isomers exist in media of differing polarities, and isomerization occurs thermally toward this ratio. In low-polarity media (e.g., a polymeric film or hydrocarbon solvent), the non-zwitterionic SP isomer typically dominates. In high-polarity media (e.g., a polar solvent or clay suspension), however, the situation may be reversed, and the merocyanine isomer may dominate.⁴ Upon irradiation of a film containing photochromic molecules, the induced shift in the SP:MC ratio causes a change in the refractive index of the film. A hologram,

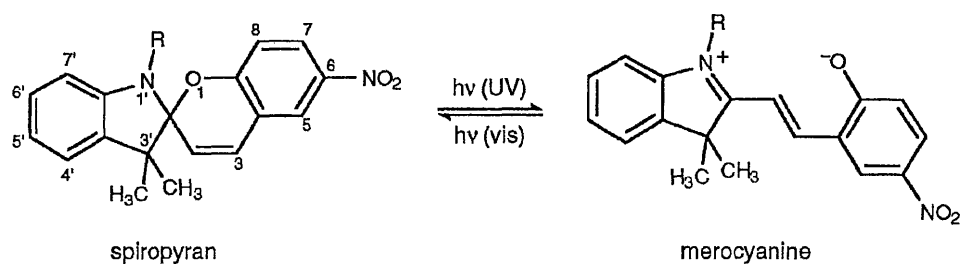


Figure 6.1. Photochromism of the spiropyran/merocyanine pair. Ultraviolet light induces isomerization to the merocyanine form, whereas visible light induces isomerization to the spiropyran form. The thermal equilibrium ratio of the two isomers typically depends on the polarity of their surroundings, and isomerization occurs thermally toward this ratio.

potentially useful for optical data storage or optical switching, can thus be formed by irradiating a film with a spatially varying light field.⁵ Traditional holograms permanently fix an image and are not erasable. For applications including data storage and optical switching, however, the ability to write, erase, and rewrite patterns many times is important. The reversibility of the photo-isomerization of photochromic molecules is therefore of interest for these applications.⁶ One practical limitation to the use of photochromic molecules, however, is their tendency to isomerize thermally toward an equilibrium SP:MC ratio, which would cause undesirable fading of a pattern over time.

Literature reports indicated that cationic spiropyrans intercalated in the interlayer space of clays, either in dispersions^{4,7} or in films formed by the evaporation of dispersions^{7,8} exhibited slower kinetics of thermal isomerization in the dark than similar systems containing no silicate. This effect was attributed, at least in part, to the sheets' ability to restrict the dye sterically, thus inhibiting the conformational changes accompanying isomerization⁷ and to the electrostatic interactions between the dye and the clay sheets,⁴ and would inhibit the thermal fading of a hologram. Forming robust, uniform films from clays by traditional methods is difficult, however, and such films typically scatter light significantly due to internal inhomogeneity and surface roughness.

We recently introduced a method for the formation of multilayered films by the alternate adsorption of a cationic polyelectrolyte and anionic sheet silicate from solution or suspension onto various substrates. These films exhibited linear growth as a function of the number of adsorption cycles and possessed a sufficient degree of structural order to diffract x-rays, as described in chapters 2, 3 and 7.⁹ The generality of the method was established by the successful use of alternative polyelectrolytes and sheet silicates, as discussed in chapters 2 and 7.^{10,11} When films

were formed from poly(diallyldimethylammonium chloride) and montmorillonite, using conditions that limited the ellipsometric growth to approximately one unit cell per adsorption cycle, large ordered domains were present in which the interlayer space was limited to the width of an individual polymer chain.¹⁰ We anticipated that films formed by the alternate adsorption of a sheet silicate and a spiropyran-functionalized cationic polyelectrolyte would therefore possess certain advantages over films prepared by other methods. While maintaining the steric and electrostatic interactions found in other systems involving sheet silicates, our films could also provide the optical clarity, uniformity, and adhesion to substrates typically exhibited by polymer systems and more difficult to attain in films formed by evaporating clay dispersions.⁸

6.3 Results

6.3.1. Materials Used in Film Formation. To form photochromic films, we alternated the adsorption of a spiropyran-containing polymer with the adsorption of single sheets of exfoliated clays. The polymer used in this work was polyvinylpyridine that had been partially quaternized with a spiropyran dye. Two different sheet silicate minerals, Laponite RD and montmorillonite, were used, to investigate whether either gave rise to a superior film. The structures of these two minerals are similar: in each case individual sheets comprise three layers. In montmorillonite, two outer layers containing Si^{4+} ions tetrahedrally coordinated with oxygen surround a central layer in which Al^{3+} ions are octahedrally coordinated with oxygen. Some substitution of Mg^{2+} for Al^{3+} in the central layer gives rise to a deficiency of cationic charge that causes the overall sheet to bear a negative charge. In Laponite, a synthetic form of hectorite, the outer layers are the same as in montmorillonite, but the central layer contains Mg^{2+} octahedrally coordinated with

oxygen. Some substitution of Li^+ for Mg^{2+} gives rise to the deficiency of cationic charge in this mineral. The montmorillonite we used had a higher degree of in-plane crystalline order than the Laponite, and also had larger average sheet diameters (~46 nm *vs.* ~30 nm for the Laponite). Other factors being equal, we expected the montmorillonite films to have a more highly ordered structure. Whether this property would give rise to superior behavior in antireflective or holographic applications was a question we hoped to address.

6.3.2. *Preparation of Poly(vinylpyridine-spiropyran), PVP-SP.* The reaction scheme that was used to synthesize the cationic polyelectrolyte is depicted in Figure 6.2. Briefly, 2,3,3-trimethylindolenine was quaternized with excess 1,5-dibromopentane in refluxing acetone.¹² The desired spiropyran was obtained by reaction of the quaternized indolenine (1) with 2-hydroxy-5-nitrobenzaldehyde (5-nitrosalicylaldehyde) in refluxing butanone, using piperidine as a base.¹³ The spiropyran [1'-(5-bromopentyl)-3',3'-dimethylindoline-6-nitrobenzospiropyran, (2)] was identified by NMR spectrometry¹⁴ and by its photochromic behavior. Furthermore, its molecular ion (M/e 456, 458) and several characteristic fragments were detected using gas chromatography/mass spectrometry. The dye 2 was then used to quaternize poly(vinylpyridine) (MW 20,000) to form the cationic polyelectrolyte poly(vinylpyridine-spiropyran) [PVP-SP, (3)] used in the formation of multilayered films. The extent of functionalization of the polymer was determined by a standard-additions experiment, using ultraviolet-visible (uv-vis) spectrophotometry, to be 7–8 mole % of the vinylpyridine repeat units of the polymer, or 23–25% by mass.

6.3.3. *Formation of Multilayered Films.* Films were formed on silicon wafers or fused-quartz slides by alternate adsorptions of PVP-SP and either Laponite or montmorillonite. In a series of preliminary experiments, various adsorption

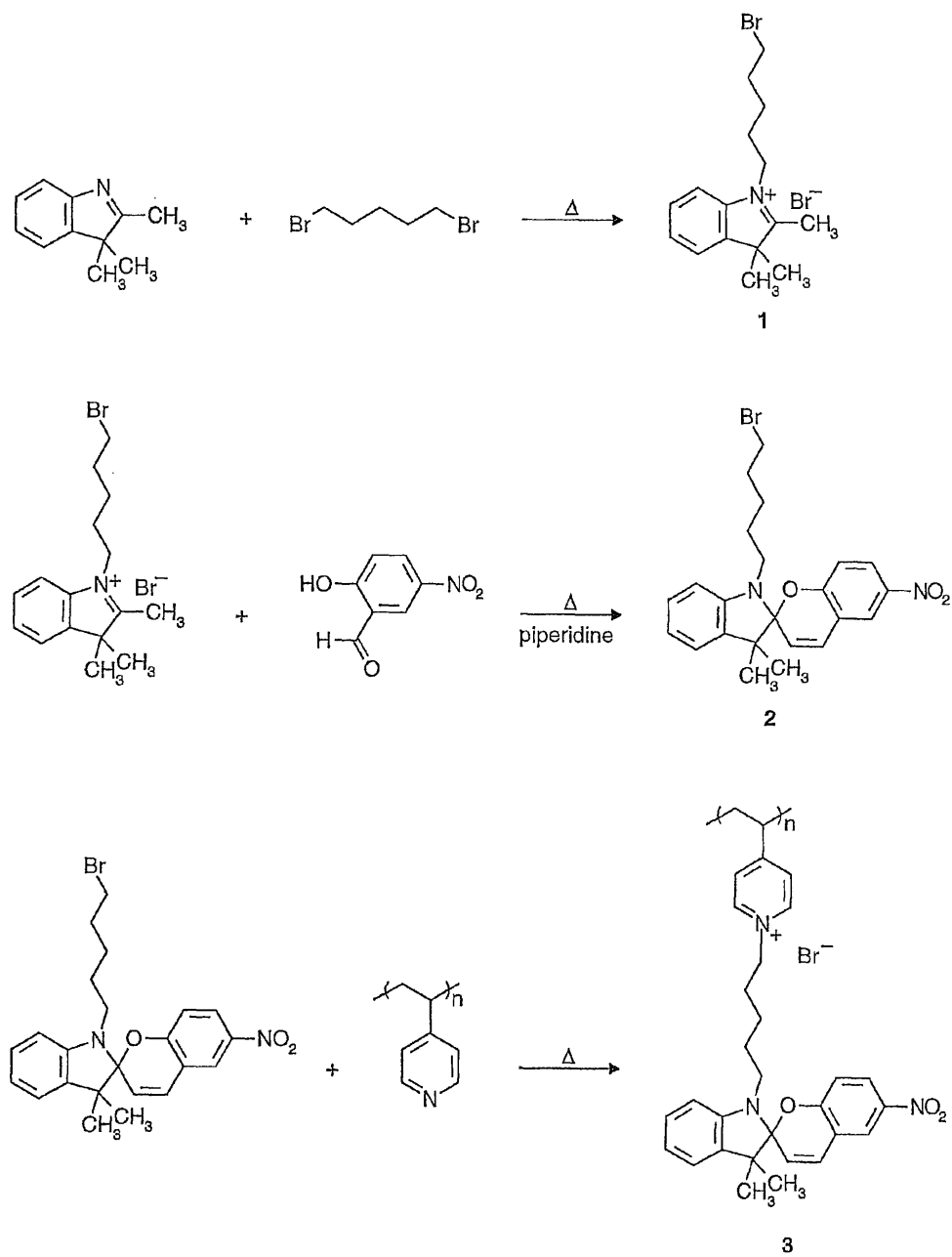


Figure 6.2. Reaction scheme that was used for the synthesis of poly(vinylpyridine-spiropyran), PVP-SP, (3).

conditions were evaluated using silicon substrates on which growth could be monitored ellipsometrically. We expected that growth in the amount of one unit cell per cycle would correlate with an optimal level of structural order in the films,¹⁰ and thus sought conditions that would result in the regular growth of films at this rate, while limiting the adsorption periods to a practical length of time. The experimental parameters examined were extent of neutralization and overall composition of the clay suspensions, adsorption times used for each component, concentration of the polymer solution, and composition of the rinses.

Growth proceeded regularly only when the silicate suspensions were partially neutralized, by dialysis in the case of montmorillonite, and by the addition of acid in the case of Laponite. Apparently, the density of charge inherent in the quaternized centers on the polymer was insufficient to attract a full layer of the anionic silicate, and maintaining some degree of protonation of the polymer backbone was critical to the growth process. Surfaces produced by the adsorption of PVP-SP were not wettable by water, so to facilitate adsorption of the silicate, some methanol was added to the clay suspensions. This addition lowered the surface tension of the suspensions to the point that they wetted PVP-SP-terminated samples.

To provide a more favorable surface than bare SiO₂ for the adsorption of the PVP-SP, the silicon or fused quartz substrates were treated with a 1% (w/w) aqueous solution of poly(diallyldimethylammonium chloride), PDDA, for ~5 s, rinsed with water, and blown dry with nitrogen, and then treated for ~5 s with the silicate suspension that would be used in subsequent cycles, rinsed with the indicated solvent, and blown dry with nitrogen. For films containing Laponite, the following two-step adsorption cycle was repeated: In the first step, the substrate was immersed for 60 s in a 1.9% (w/w) solution of PVP-SP in methanol for ~60 s, rinsed with methanol, and blown dry with nitrogen. In the second step, it was immersed for

60 s in a suspension containing 0.2% Laponite RD (w/w) in H₂O–methanol (56:44 w/w). This suspension had been partially neutralized by the addition of HCl to an ultimate concentration of 0.00040 molal. The slide was then rinsed with a H₂O–methanol solution (50:50 w/w), and blown dry with nitrogen. In films involving montmorillonite, a similar cycle was used, but the compositions of the precursor solution/suspensions were as follows: The polymer solution concentration was 1.0% (w/w) in methanol, and methanol was used to rinse the surface after this treatment. The dialyzed montmorillonite suspension contained the silicate at a nominal concentration of 0.2% (w/w) in H₂O–methanol (65:35 w/w), and a rinse of H₂O–methanol (65:35 w/w) was used after this treatment.

Under these conditions, the growth became regular after the first cycle for both systems. Figure 6.3a shows growth of a film from a 1.9% (w/w) solution of PVP–SP and a 0.2% (w/w) Laponite suspension. Following the first cycle, in which 1.4 nm of PVP–SP and 1.0 nm of Laponite adsorbed, the film grew 0.9–1.0 nm in each polymer adsorption step and 0.7–0.8 nm in each Laponite adsorption step. Figure 6.3b shows growth of a film from a montmorillonite suspension (nominally 0.2% w/w) and a 1.0% (w/w) solution of PVP–SP. Following the first cycle, in which 1.1 nm of PVP–SP and 1.7 nm of Montmorillonite adsorbed, the film grew 0.6–1.1 nm in each polymer adsorption step and 0.8–1.3 nm in each montmorillonite adsorption step.

For the studies of interference effects and photochromism, thicker films were formed on fused-quartz microscope slides, and subtle interference colors appeared and evolved as an increasing number of cycles was performed. Similar effects had been noted on other substrates, as detailed in Chapters 2 and 3.⁹ The growth of these films was monitored by ultraviolet–visible (uv–vis) spectrophotometry, as the transparent substrates were not amenable to ellipsometric measurements. An angle of incidence of 45° was used for all spectra. Figure 6.4a shows a spectrum of a 60-

Figure 6.3. Ellipsometric thickness of multilayered films on silicon as a function of the number of adsorption cycles for: a) 1.9% PVP-SP and 0.2% Laponite RD; and b) 1.0% PVP-SP and 0.2% montmorillonite. Individual data points obtained on single samples are shown. Substrates for this study were silicon wafers that had been treated for 5 s each with 1% PDDA and the silicate suspension (i.e., Laponite or montmorillonite) that was used in subsequent cycles.

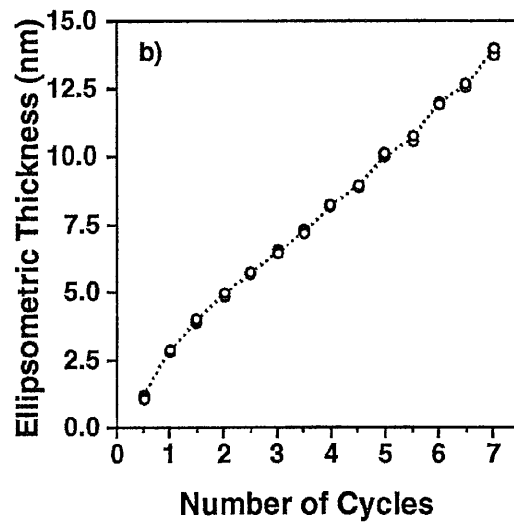
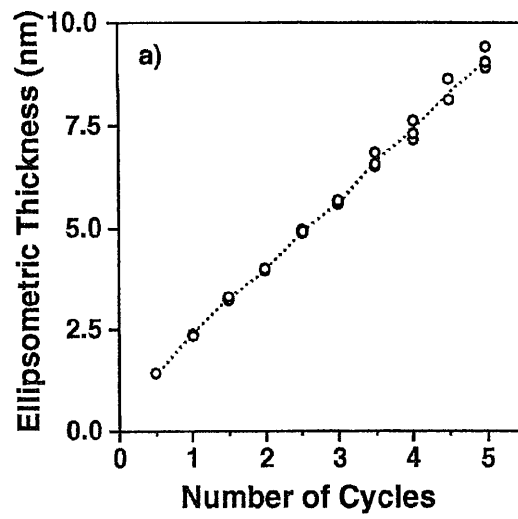
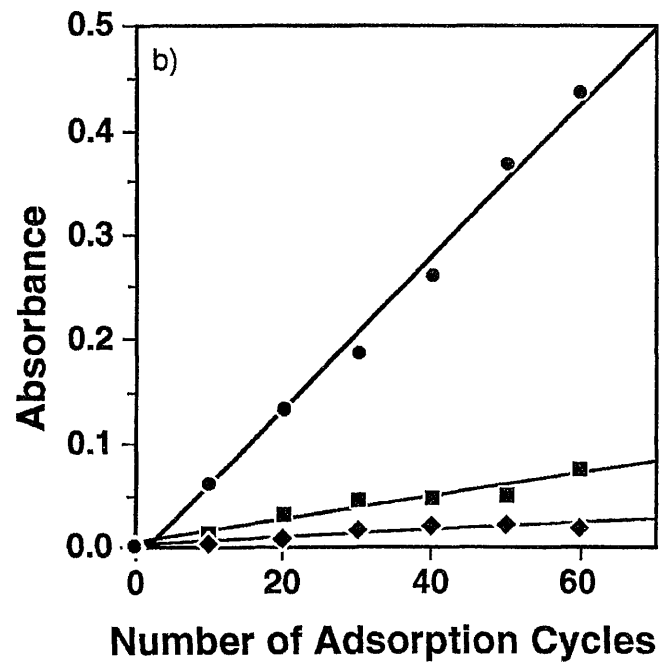
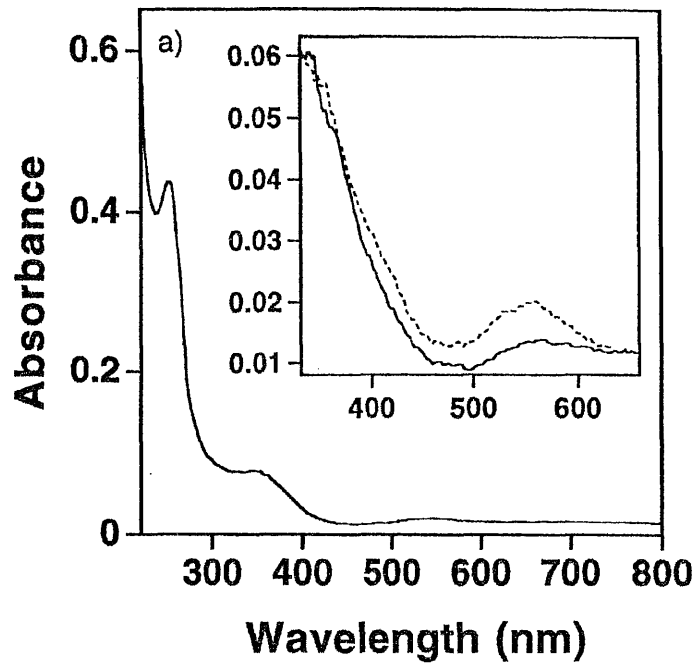


Figure 6.4. Ultraviolet–visible spectrophotometry of PVP-SP/Laponite films: a) Spectrum of a 60-cycle film on fused quartz; inset: 330- to 660-nm region following an extended period of storage in the dark (>900 h), at which point the film was presumably at thermal steady-state (dotted line), and immediately following extended irradiation with visible light, at which point the film had reached an apparent steady state under those conditions (solid line); b) Absorbance at various wavelengths as a function of the number of adsorption cycles for a film formed from PVP-SP and Laponite RD on fused quartz: circles, 252 nm; squares, 350 nm; diamonds, 524 nm.



cycle film of PVP-SP and Laponite, with an inset showing the spectra of the 330- to 660-nm region after an extended period of storage in the dark (>900 h), top, and immediately after visible irradiation, bottom. Figures 6.4b and 6.5 show absorbance at λ_{max} (~250 nm, filled circles) as a function of the number of adsorption cycles for the Laponite- and montmorillonite-based films. This peak is associated principally with the $\pi \rightarrow \pi^*$ transition of the alkylpyridine and alkylpyridinium units of the polymer backbone, though the dye also absorbs in this region. This transition was chosen for quantification of the growth of the film, rather than a feature associated solely with the spiropyran or merocyanine forms of the dye, because it was less susceptible to the influence of thermal isomerization of the dye. For the Laponite/PVP-SP film (Figure 6.4b, $\lambda_{\text{max}} = 252$ nm [filled circles]), the linear least-squares fit to the data had a slope of 0.0073 absorbance units per cycle, whereas for the montmorillonite/PVP-SP film (Figure 6.5, $\lambda_{\text{max}} = 250$ nm), it had a slope of 0.0084 absorbance units per cycle. Provided Beer's law holds in these films, and assuming that the composition and structure of the films were constant as film thickness increased, a linear increase in absorbance with the number of adsorption cycles would indicate linear growth in the thickness of the films.

6.3.4. Interference Effects in Multilayered Films. Closer inspection of the data in Figures 6.4b and 6.5 revealed an undulation of the points about the least-squares lines. We attribute these undulations to interference effects resulting from the presence of the multilayered films. Because the Laponite-based film was prepared to a greater ultimate thickness, the data for that film will be discussed in greater detail. When the optical pathlength of the light reflected at the film/glass interface differed by $\lambda_{\text{max}}/2$ from that of the light reflected at the air/film interface, destructive interference caused a decrease in the intensity of the reflected light and a corresponding increase in the intensity of the transmitted light. This increase in

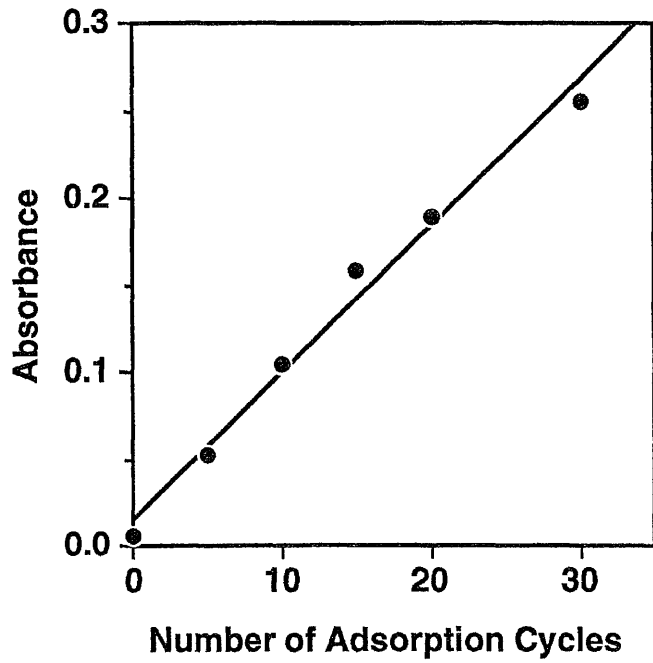


Figure 6.5. Absorbance at 250 nm as a function of the number of adsorption cycles for a film formed from PVP-SP and montmorillonite on fused quartz.

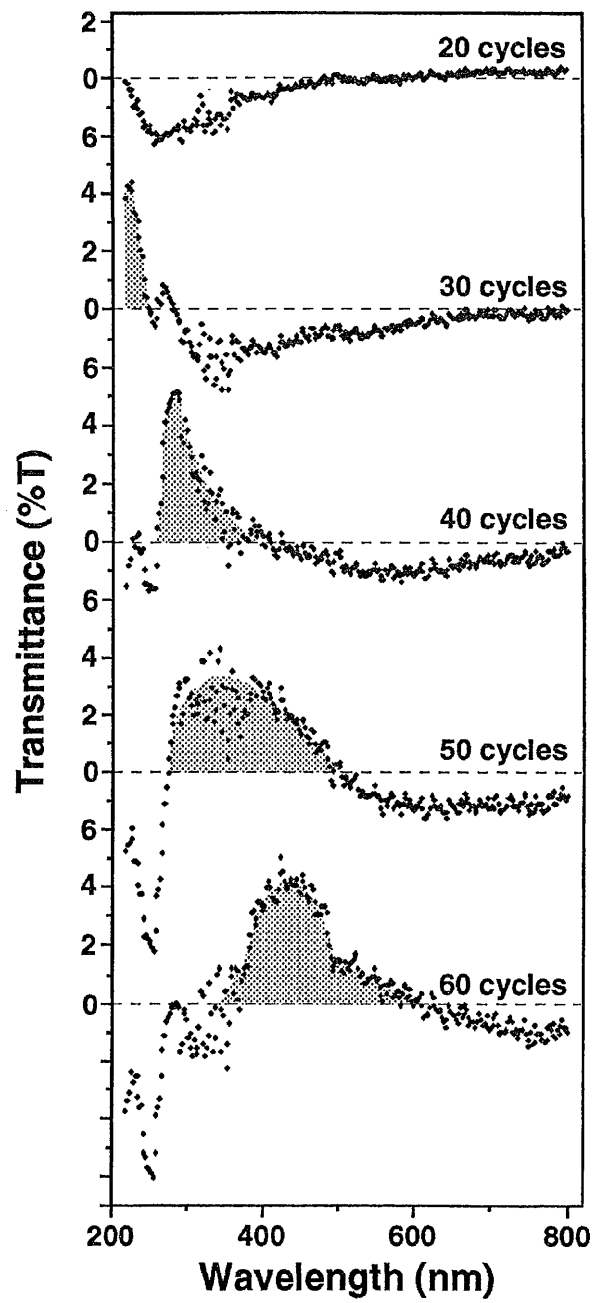
transmittance resulted in lower-than-expected values of absorbance. When the difference in the optical pathlengths approximated λ_{\max} , constructive interference occurred, causing the observed reflectivity to be higher than in cases in which destructive interference had occurred, and to approximate that which would have been exhibited by the bare substrate. This increase in reflectivity caused an apparent increase in absorbance. The conditions for destructive interference depend not only on film thickness and index and on the angle of incidence of the light (45°), but also on wavelength; therefore, as expected, the dip appeared at a higher number of cycles when a longer wavelength was monitored (e.g., 350 nm, Figure 6.4b, squares). When a sufficiently long wavelength was monitored (524 nm, diamonds), the dip only began to manifest itself after 60 cycles had been completed. The data obtained at 350 and 524 nm should be viewed more cautiously than those at 250 nm, however, being more susceptible to artifactual changes associated with isomerization of the dye. Although the raw data in Figure 6.4b show apparently subtle differences, these differences are nonetheless systematic and consistent with theory, and are far more prominent than the variability associated with uncertainty in the data. We note that similar undulations have also been present in data obtained by others studying a similar system, though interference effects were not invoked in those cases (and perhaps not recognized).¹⁵

Difference spectra obtained during formation of the Laponite/PVP-SP film enabled closer scrutiny of these effects. Hypothetical spectra for 20, 30, 40, 50, and 60-cycle films in the *absence* of interference effects were produced by multiplication of the spectrum of the 10-cycle film (in absorbance mode) by factors of 2, 3, 4, 5, or 6. Since the 10-cycle film was too thin to exhibit significant interference effects in the spectral region of interest, the difference between these hypothetical spectra and the actual spectra (both in transmittance) for the 20-, 30-, 40-, 50-, and 60-cycle films

revealed the interference effects clearly (Figure 6.6). In the absence of interference effects and changes in film characteristics (e.g., growth per cycle, roughness), these spectra would be featureless. Instead, a prominent peak (shaded) began to become apparent at 30 cycles, and moved toward increasing wavelength as the number of adsorption cycles increased. This peak corresponds to an increase in the transmitted intensity of the light resulting from interference effects, indicating that the film was serving as an anti-reflective coating and had optimal efficiency for these different wavelengths as its thickness changed. In this spectral region, the refractive index of the fused quartz slide ranges between 1.55 and 1.46 (according to the manufacturer) and the resultant reflection losses for transmission of light through a bare slide at an angle of 45° fall between 8.7% and 11.2%.¹⁶ This range of reflection losses may serve as an estimate of the properties of the film-coated slide at wavelengths far from the moving peak.¹⁶ The peaks themselves therefore indicate the extent to which the reflection losses were diminished: the peak maximum is approximately 4–5%, indicating that roughly one-third to one-half of the total reflection losses were eliminated. The magnitude of the remaining reflection losses (approximately 4–7%) indicate that the difference between the refractive indices of the film and the slide was approximately 0.1 (i.e., if the quartz had an index near 1.5, the film had an index near 1.4).¹⁶ Optimization of the ratio of the refractive indices of the substrate and film would be expected to improve the efficiency of the anti-reflective coating significantly. Further study by our research group in this area is planned.

Other features in the difference spectra in Figure 6.6 are probably not related to interference phenomena. The negative feature near 250 nm, for example, occurs in the same position as the most intense peak of the composite film, and is most prominent in the spectra of the 50- and 60-cycle films. The constant position of this spectral feature argues against its being due to an interference effect. Rather, the

Figure 6.6. Difference (in percent transmittance) between recorded spectra and hypothetical spectra that would have been expected in the absence of interference effects. The shaded regions highlight increases in transmittance associated with the anti-reflective nature of the film. Details of the calculations are provided in the text. All spectra were obtained at an angle of incidence of 45° .



feature may arise from a slight increase in growth per cycle as the film grew in thickness (observed for films formed from PDDA and Laponite on various substrates, as described in chapters 2 and 3⁹). Another possibility is a change in the effective absorptivity of the chromophore, if a change in its average orientation occurred as the film grew in thickness. Additional effects that could cause the appearance of features in these difference spectra include isomerization of the dye in the film over time, as well as increases in surface roughness or internal scattering. Unusually high noise was introduced into the spectra of the thicker films by the subtraction of multiples of the 10-cycle spectrum; this level of noise was not present in the unmodified spectra. The region in which the noise is worst (near 360 nm) occurs where the spectrophotometer changed between a tungsten lamp and a deuterium lamp.

6.3.5. *Photochromism in silicate/PVP-SP films and pure PVP-SP films.* Because all films contained the SP/MC dye, it was possible to induce changes in their uv-vis spectra by irradiation with light. Irradiations with both visible and uv light were performed on all films, and the subsequent *thermal* fade or colorization (due to thermal isomerization toward the equilibrium state) was monitored using uv-vis spectrophotometry. For each film, one type of irradiation caused a far more significant departure from the equilibrium state than the other, and the fade or colorization following this irradiation was studied in greater detail. Interestingly, irradiation both with uv and with visible light caused the dye within the montmorillonite/PVP-SP film to isomerize toward the SP form. Bleaching of spiropyrans under uv irradiation is uncommon, but has precedence, occurring mainly among spiropyrans in which either aromatic ring is functionalized with free carboxy, hydroxy, or amino groups.¹⁷

A 60-cycle film of Laponite and PVP-SP, a 30-cycle film of montmorillonite and

PVP-SP, and a dip-cast film of pure PVP-SP were each separately irradiated with broadband uv light ($\lambda_{\text{max}} = 350 \text{ nm}$) until their uv-vis spectra reached apparent steady-state in the 360- to 640-nm region, the region throughout which the most significant spectral changes occurred. Spectra were obtained within ~1 min of the end of the irradiation, and then the films stored in Al-foil-wrapped glass vials at room temperature. Additional spectra were obtained periodically, and their backgrounds corrected by addition or subtraction of a constant such that the featureless 700- to 800-nm regions in the spectra were coincident. Following the study of the fade from the uv-irradiated state, the films were irradiated with visible light until the spectra again reached apparent steady-state in the 360- to 640-nm region, and spectra were obtained as noted above. For the pure polymer film, the thermal isomerization toward the SP form following uv irradiation was more dramatic than that toward the MC form following visible irradiation, whereas for the two films containing clays, the opposite was true (Figures 6.7, 6.8, and 6.9). The more dramatic isomerizations were studied in greater detail, as these would be the processes responsible for the undesirable fading of holographic images over time.

Absorbance was quantified at a λ_{max} in the 530- to 560-nm region, a spectral region in which the merocyanine form of the dye has a characteristic absorption (Figure 6.4a). To establish that the act of taking uv-vis spectra was not inducing significant changes in the spectra, the Laponite/PVP-SP film was irradiated to steady-state with visible light, and five spectra were then taken in immediate succession (70–90 s intervals). These spectra were nearly identical, and the absorbance at λ_{max} (556 nm) showed no trend.

The position of λ_{max} for the merocyanine isomer reflects the polarity of its environment, occurring at lower wavelengths in higher polarity media.³ In agreement with this well-established finding, λ_{max} for merocyanine in the PVP-SP-only film

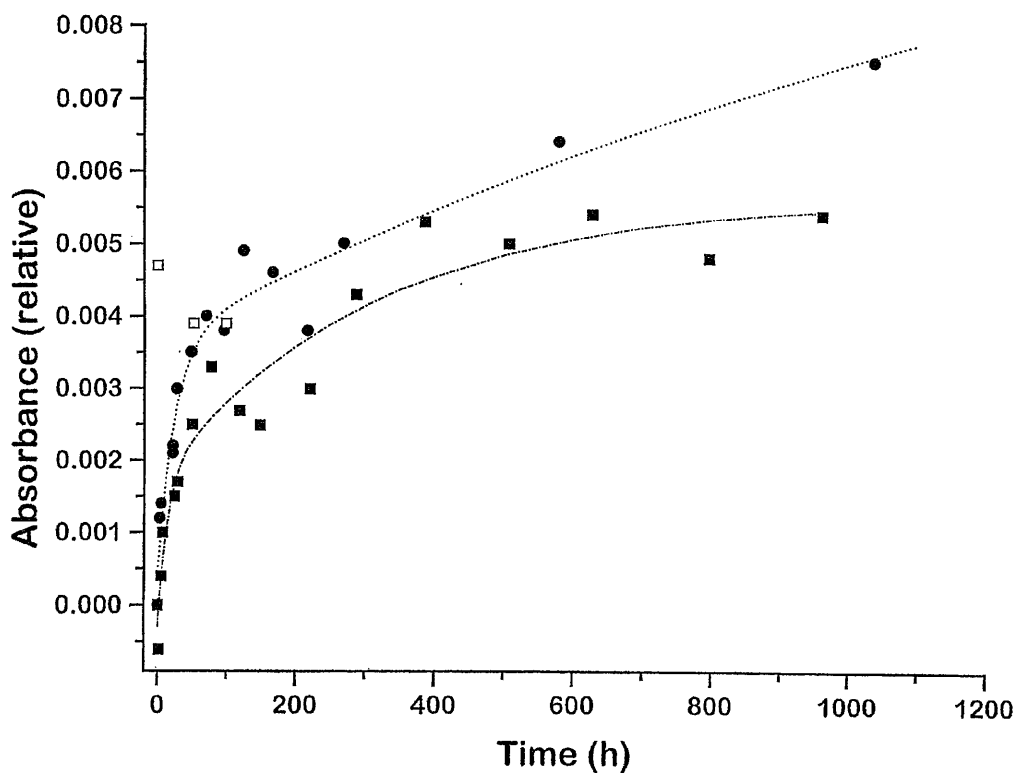


Figure 6.7. Kinetics of thermal isomerization of the photochromic spiropyran dye in a 60-cycle film of Laponite RD and PVP-SP. Absorbance at 556 nm is plotted as a function of time following irradiation with uv light (open squares) or visible light (solid squares). Solid circles show the absorbance at 556 nm as a function of time following irradiation with uv light, when the sample was stored in an atmosphere of flowing dry nitrogen between spectra. The least-squares fits to biexponential decay functions are shown, and the optimized parameters for these fits are given in Table 6.1.

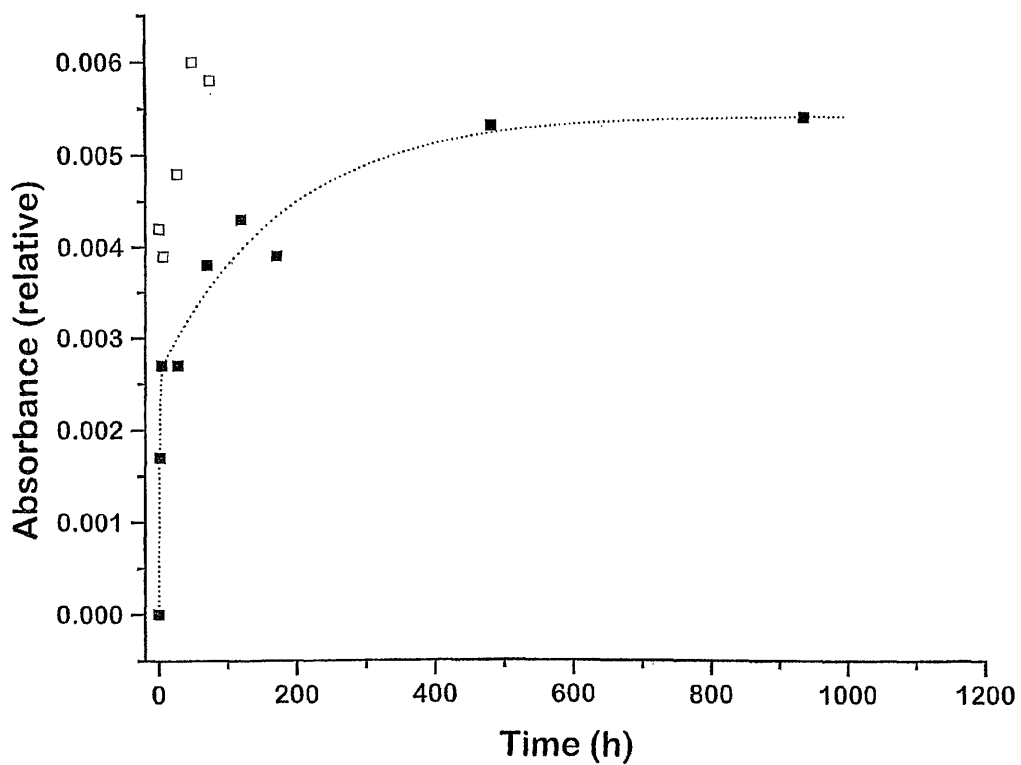


Figure 6.8. Kinetics of thermal isomerization of the photochromic spiropyran dye in a 30-cycle film of montmorillonite and PVP-SP. Absorbance at 532 nm is plotted as a function of time following irradiation with uv light (open squares) or visible light (solid squares). The least-squares fit to the biexponential decay function is shown, and the optimized parameters for the fit are given in Table 6.1.

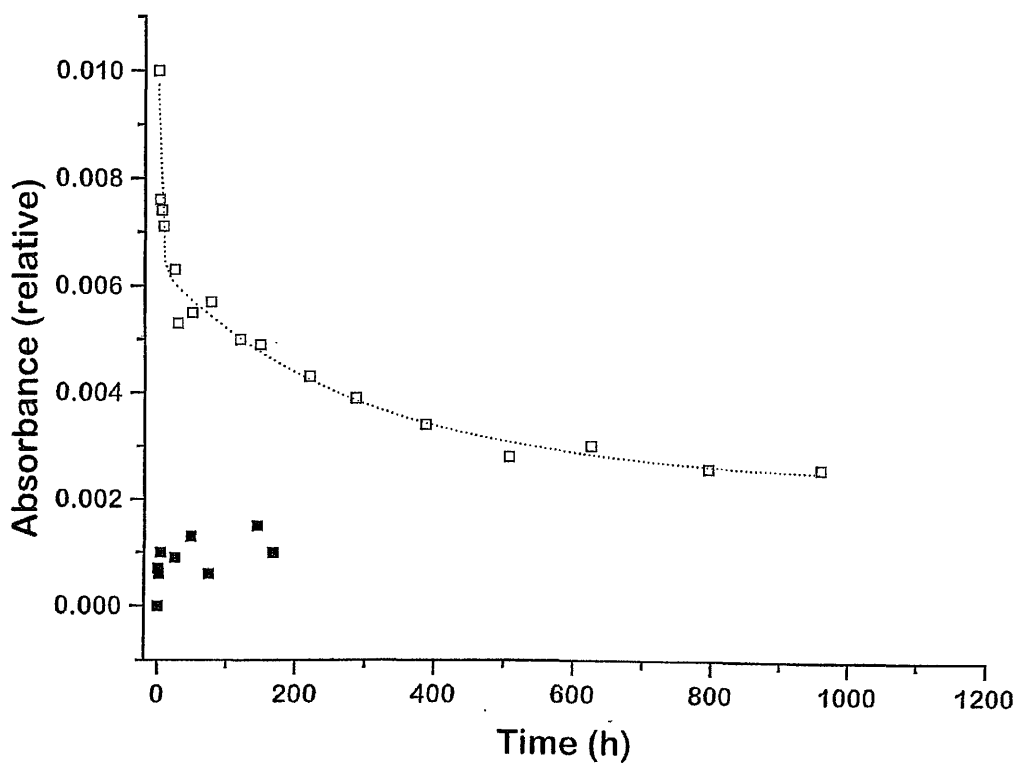


Figure 6.9. Kinetics of thermal isomerization of the photochromic spiropyran dye in a dip-cast film of PVP-SP. Absorbance at 560 nm is plotted as a function of time following irradiation with uv light (open squares) or visible light (solid squares). The least-squares fit to the biexponential decay function is shown, and the optimized parameters are given in Table 6.1.

occurred at 560 nm, whereas that in the montmorillonite/PVP-SP film it occurred at 532 nm, consistent with the polar nature of the clay sheets. The position of this feature in the 60-cycle Laponite/PVP-SP film was significantly influenced by the interference effects described earlier, and therefore occurred at an unexpectedly high value of 556 nm. When this film was thinner (20–40 cycles) and the interference effects had not yet begun to affect this spectral region significantly, λ_{max} occurred at a shorter wavelength (524 nm), as expected.

Thermal isomerizations of spiropyrans are expected to exhibit first-order kinetics,¹⁸ so the fade or colorization data were fit with exponentials. When the data could not be adequately fit with single exponentials, biexponentials were used, i.e., equations having the form:

$$A(t) = A_0 + c_1 \exp(-t/\tau_1) + c_2 \exp(-t/\tau_2)$$

in which $A(t)$ is absorbance at time t ; A_0 is absorbance immediately following the irradiation with ultraviolet or visible light; τ_1 and τ_2 are characteristic time constants for unimolecular decay processes; and c_1 and c_2 are corresponding weighting coefficients. By convention, τ_1 will be assigned to the smaller time constant (corresponding to the faster process), while τ_2 will be assigned to the larger one (slower process). Plots of the absorbance at λ_{max} as a function of the time elapsed after irradiation for each film, including the biexponential fits, are shown in Figures 6.7, 6.8, and 6.9. The optimal values of the adjustable parameters for these fits are summarized in Table 6.1. For practical applications, the important consideration is the kinetics of approach toward equilibrium, and not the direction of that approach. Thus, even though the thermal isomerizations in the polymer-only film and composite films proceeded in opposite directions, the rates of these processes could be directly compared.

The time constant τ_1 for the Laponite/PVP-SP film was somewhat greater than

Table 6.1. Optimized Parameters in Least-Squares Biexponential Fits* to Thermal Isomerizations of SP/MC in Various Films

Film	Conditions	c₁	τ₁ (h)	c₂	τ₂ (h)
PVP-SP/ Laponite RD	ambient	0.0020	13.1	0.0039	301
PVP-SP/ Laponite RD	flowing N ₂	0.0032	25.2	0.0089	1790
PVP-SP/ mont.	ambient	0.0026	1.09	0.0028	181
PVP-SP dip-cast	ambient	0.0034	3.59	0.0040	292

* Data were fit using Origin 3.5 (Microcal Software, Inc.)

that for the pure PVP-SP film (by a factor of 3.65), corresponding to a slower rate of isomerization. In contrast, the time constant τ_2 was similar in magnitude for both. The montmorillonite/PVP-SP film had lower values of both τ_1 and τ_2 than the pure PVP-SP film, by factors of 0.303 and 0.621, respectively, indicating a faster rate of isomerization.

One possible explanation for the lack of larger differences between the composite films and those of the polymer alone is the possibility that water sorbed into the composite films from the laboratory ambient, swelling the films and thus negating the steric restriction that would otherwise be enforced by the clay sheets. As noted in Chapter 5, this behavior had been observed previously, when films formed from Laponite and a different cationic polyelectrolyte [poly(diallyldimethylammonium chloride), PDDA] responded sensitively to changes in atmospheric humidity, swelling significantly as the humidity of their environment was increased. To investigate the possibility that a similar phenomenon was influencing the kinetics of isomerization, the Laponite/PVP-SP film was irradiated with visible light as before, and its colorization monitored as a function of time when it was stored in an atmosphere of flowing dry nitrogen. A biexponential fit to these data is shown in Figure 6.7, alongside the data obtained when the sample was stored in an ambient environment, and the optimized parameters for the fit are given in Table 6.1. These conditions resulted in increases in τ_1 and τ_2 (by factors of 1.92 and 5.96) compared to the film stored under ambient conditions, indicating a slowing in the kinetics of isomerization. The change in τ_2 should be interpreted with caution, however, as a limited number of data points were obtained at the extended times, allowing variability due to noise to affect the calculated τ_2 significantly.

To compare the kinetics of colorization or fade of the different films more closely, the data shown in Figures 6.7–6.9 are shown in a modified form in Figure

6.10. In this figure, the data were normalized such that the first data point occurred at an absorbance value of 0 and the final data point occurred at an arbitrary absorbance value of 0.0054. Because the original data obtained for the polymer-only film had shown decreases in absorbance as a function of time, those data had to be subtracted from a constant prior to scaling. Although the data may appear upon first inspection to overlay one another, closer inspection reveals that the data for the PVP-SP/montmorillonite film (diamonds) do occur above and to the left of those for the polymer-only film (squares), whereas the data for the PVP-SP/Laponite film occur lower and to the right (triangles and circles). It is, however, difficult to discern a significant difference between the kinetics of colorization for the PVP-SP film stored under ambient conditions and those for the same film stored under dry nitrogen, indicating that the apparently high value for τ_2 for the latter film may, as indicated earlier, be an artifact of the large relative uncertainty associated with the absorbance values (± 0.0006 absorbance units) and the infrequency of data collection at long times. An important assumption that must be true in order for these comparisons to be valid is that the films had all reached a thermal steady-state by the time the final data point was obtained.

The fact that biexponential equations were required to obtain reasonable fits to the data is consistent with the interpretation that two independent first-order processes were occurring within the films. The inadequacy of a single-exponential fit (i.e., $c_2 = 0$) has also been reported by others for spiropyrans in clay dispersions and films^{4,7,8} as well as in amorphous media (e.g., homogeneous solutions).¹⁸ Several detailed studies reviewed in reference 18 concluded that, in many systems involving spiropyrans, more than two species were participating in the isomerizations. For the 1'-methyl analog of **2**, the presence of two or more colored isomers (i.e., isomers absorbing in the spectral region associated with merocyanine) was required to

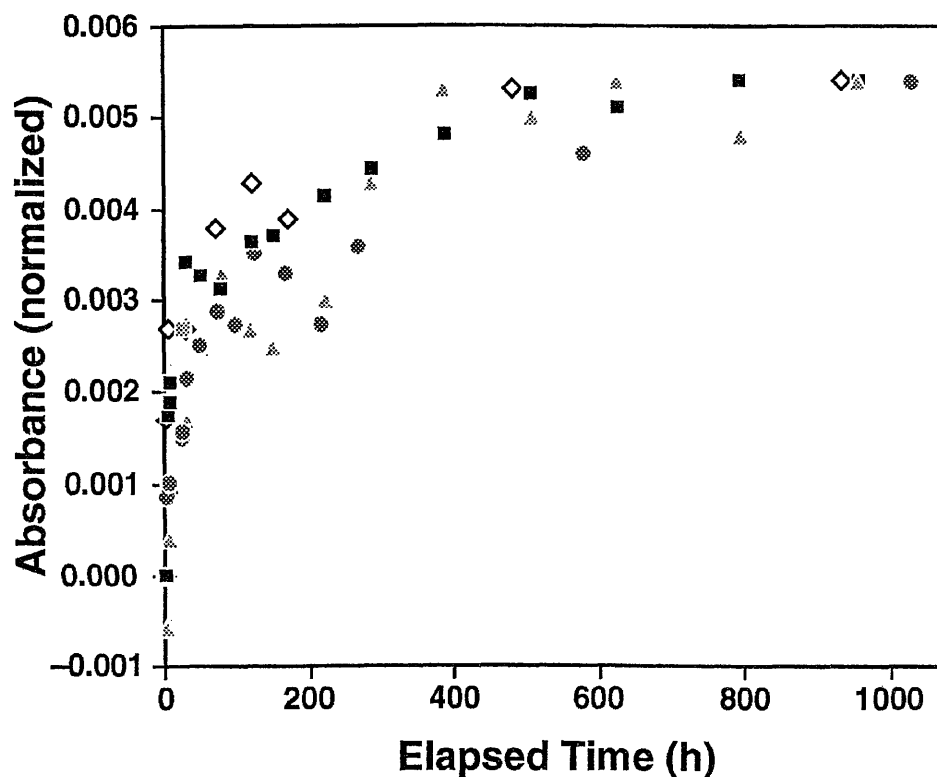


Figure 6.10. Kinetics of thermal isomerization of the photochromic spiropyran dye in various films containing PVP-SP (normalized data). The data from the extended experiments in Figures 6.7, 6.8, and 6.9 were normalized to begin at an absorbance value of zero at the end of the irradiation with visible or uv light, and to end at an arbitrary absorbance value of 0.0054, as described in greater detail in the text: triangles, PVP-SP/Laponite RD film (ambient conditions); circles, PVP-SP/Laponite RD film (flowing dry nitrogen); diamonds, PVP-SP/montmorillonite film; squares, dip-cast PVP-SP film.

account for all the data. Direct spectral evidence (uv-vis) was given for the existence of certain of these species, tentatively proposed to be among the isomers presented in Figure 6.11. Researchers using biexponentials to fit data from clay/spiropyran systems suggested that the spiropyran molecules within the films occupied two different environments,^{4,7,8} although it was not clear that the possibility of multiple colored isomers had been considered.

We had expected the presence of clay sheets to reduce the rate of thermal isomerization of the spiropyran/merocyanine dye within the composite films.^{4,7,8} This effect was not as significant as had been hoped (in the case of the Laponite/PVP-SP film) or was seemingly absent entirely (in the case of the montmorillonite/PVP-SP film). Overlaying the data as shown in Figure 6.10 revealed that despite the differences in the calculated τ values among the different films, their isomerizations proceeded at similar rates and thus that forming a film layer by layer rather than by dip-casting was not worth the extra effort involved.

In the data reported by others, the significant differences observed upon addition of clay to a particular system may actually be due to changes in the polarity of the spiropyran's environment. For example, although in one article a spiropyran in an aqueous clay dispersion exhibited slower kinetics of isomerization than the same spiropyran in chloroform solution (by a factor of 15.8 in τ), the same spiropyran in aqueous solution without clay was reportedly slower by a factor of 56 in τ ! For another spiropyran studied by the same researchers, little difference was observed between an aqueous solution of the dye and an aqueous dispersion of clay intercalated by dye, but the kinetics were significantly faster for the dye in chloroform solution.⁷

6.3.6. *Structural analysis of silicate/PVP-SP composite films.* X-ray diffraction was used to evaluate the structural order of a Laponite/PVP-SP film (40 cycles) and a

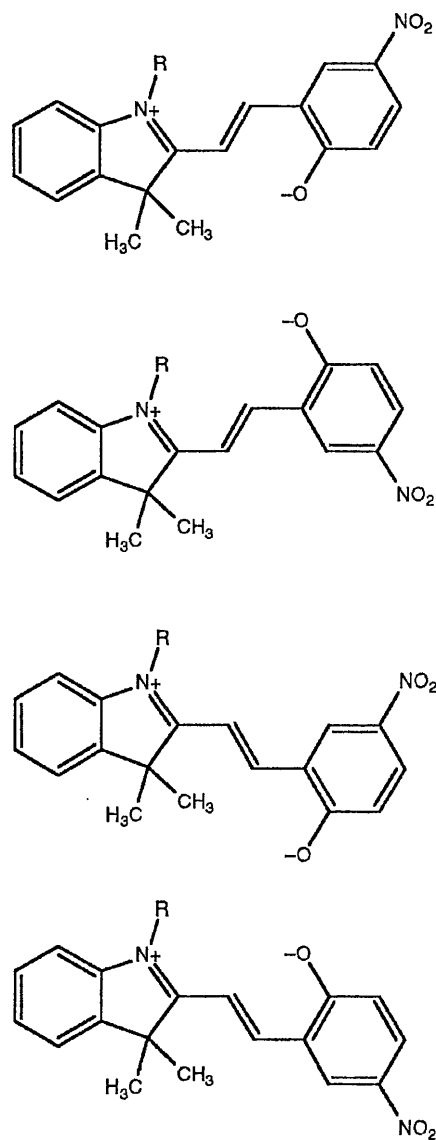


Figure 6.11. Isomers of the merocyanine form of the dye. Studies summarized in reference 18 proposed that differing kinetics for the isomerizations between each of these forms and the spiropyran form may in some systems be responsible for the failure of the thermal isomerizations to follow simple first-order kinetics.

montmorillonite/PVP-SP film (20 cycles) on fused-quartz slides. As shown in Figure 6.12 and 6.13, (001) reflections were observed in the patterns of both samples. For the Laponite-based film (Figure 6.12), the position of the (001) peak was $3.9 \pm 0.1^\circ 2\theta$, giving a calculated d-spacing of 2.26 ± 0.06 nm. The full-width at half-height of the peak was $1.52^\circ 2\theta$, corresponding to a domain size of 5.5 nm, based on the Scherrer equation.¹⁹ For the montmorillonite-based film (Figure 6.13), the position of the (001) peak was $4.46 \pm 0.04^\circ 2\theta$, giving a calculated d-spacing of 1.98 ± 0.02 nm. The full-width at half-height of this peak was $1.37^\circ 2\theta$, corresponding to a domain size of 6.1 nm. Any higher-order reflections on either sample were obscured by the broad reflections from the fused-quartz substrate ($\sim 22^\circ 2\theta$) and an instrumental artifact near $12^\circ 2\theta$. This latter peak was present in all patterns obtained using this diffractometer (used for the studies in this chapter only), and was even present in the pattern of an empty mount.

The observed d-spacings (2.26 nm and 1.98 nm for the Laponite-containing film and montmorillonite-containing film, respectively) were significantly larger than those exhibited by PDDA/silicate films (1.43–1.44 nm). These increases in d-spacings may be attributable to the presence of the bulky dye, although the possibility exists that the d-spacings are inflated; i.e., establishing a true d-spacing from a single reflection is impossible for systems like these, as the positions of the (00*l*) reflections shift significantly for samples in which the crystalline domains are limited in size (see chapter 7).²⁰ Furthermore, the d-spacings of sheet silicates can change in response to changes in relative humidity, as discussed in more detail in Chapter 5. Nonetheless, the presence of these peaks indicates that at least some of the material in the films was ordered. An additional broad feature of low intensity was present at $7.5^\circ 2\theta$ ($d = 1.18$ nm) in the XRD pattern of the montmorillonite/PVP-SP film; the origin of this feature is uncertain, though it may be a (002) reflection whose position has been

Figure 6.12. X-ray diffraction pattern of a 40-cycle film made from 1.9% PVP-SP and 0.2% Laponite RD on a fused quartz slide.

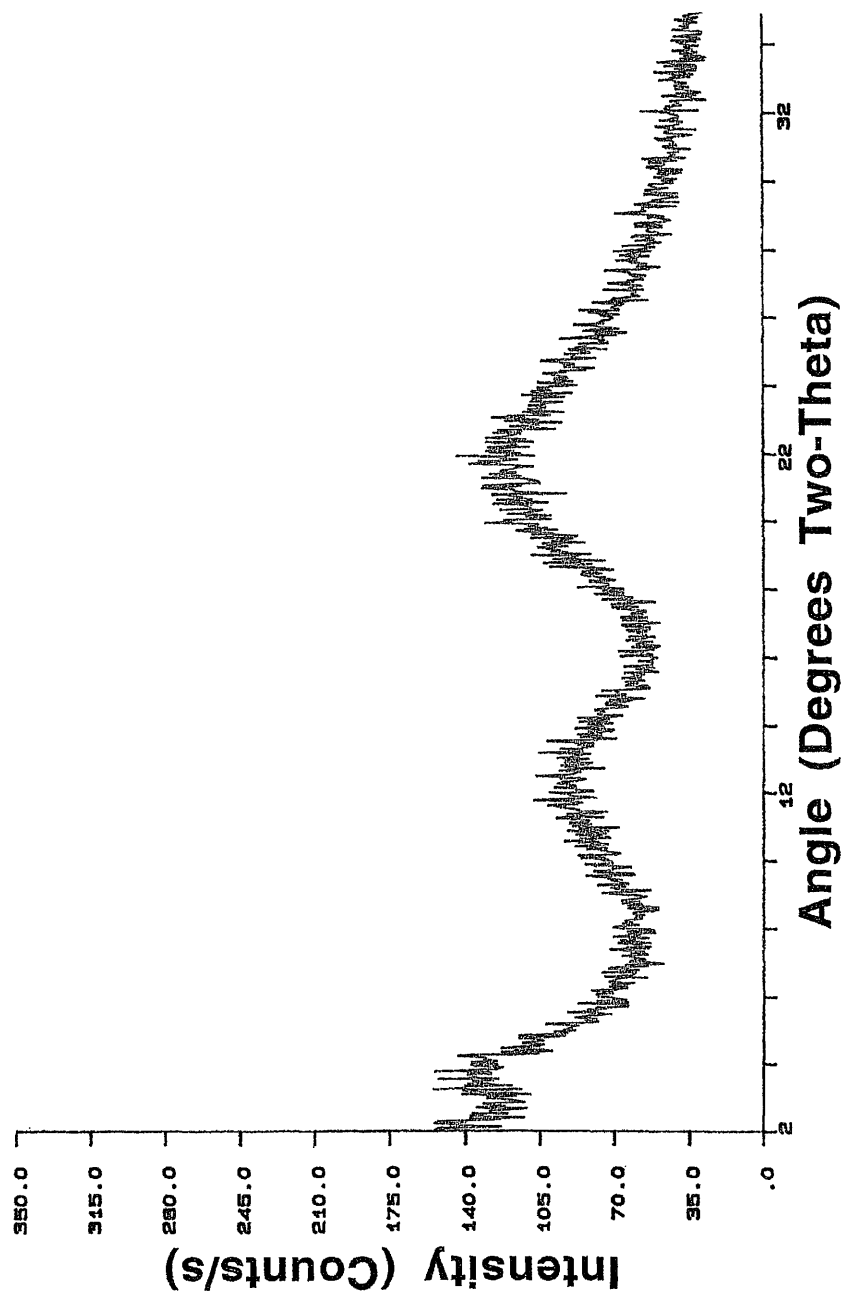
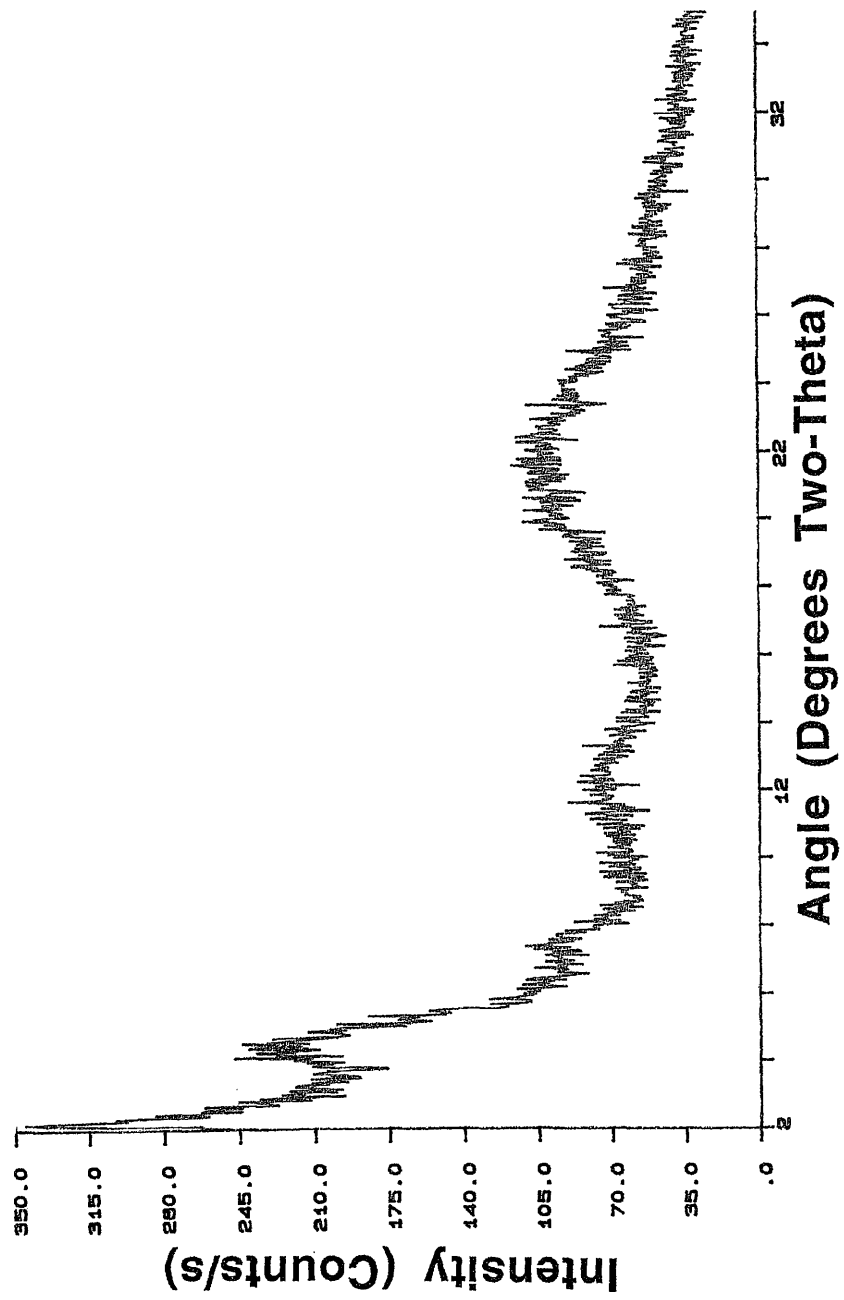


Figure 6.13. X-ray diffraction pattern of a 20-cycle film made from 1.0% PVP-SP and 0.2% montmorillonite on a fused quartz slide.



affected due to a partial overlap with the (001) reflection.

6.4 Conclusions

In conclusion, a photochromic dye was synthesized and grafted onto poly(vinylpyridine). Films were formed from this cationic polyelectrolyte and two anionic silicates, Laponite RD and montmorillonite. The films grew regularly, as demonstrated by both ellipsometry and uv-vis spectrophotometry. Evaluation of the films as antireflective coatings indicated that the presence of the film reduced reflection losses at the air/fused quartz interface by approximately one-third to one-half, a figure which may in the future be increased by decreasing the refractive index of the films. Irradiation of the films with visible and uv light resulted in isomerization of the dye between the spiropyran and merocyanine forms. The kinetics of thermal isomerization of the dye were studied and found to be comparable to the kinetics of a similar process in a dip-cast (polymer-only) film.

6.5 Experimental Methods

6.5.1. Materials Syntheses and Preparations. Several different sets of conditions were used in the preparation and purification of the organic species used in this study. The conditions that proved most successful are summarized in the paragraphs that follow.

Starting Materials. The 1,5-dibromopentane (Lancaster or Aldrich), 2,3,3-trimethylindolenine (Akros or Aldrich), 2-hydroxy-5-nitrobenzaldehyde (Eastman Chemical), and piperidine (Aldrich) were used as received. The poly(vinylpyridine) (PVP, molecular weight: 20,000, Monomer-Polymer & Dajac Labs) was contaminated by a significant concentration of monomer, as revealed by NMR. The PVP was therefore purified by four cycles of dissolution in methanol and

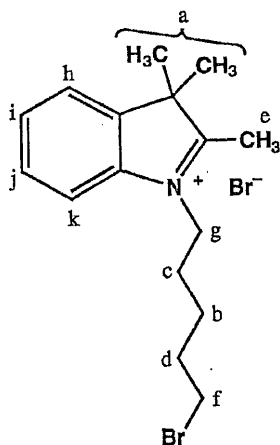
precipitation by pouring this solution into water. The polymer was dried to constant weight at 56°C *in vacuo*. The resulting material appeared clean by TLC and NMR, and no odor of the monomer was present. The recovery was 57% by mass.

Suspensions of Laponite RD and montmorillonite (Southern Clay Products) were prepared as described in chapter 1. These suspensions were then partially neutralized, as described below. Poly(diallyldimethylammonium chloride), MW 200,000-350,000, was obtained from Aldrich as a 20% (w/w) solution, and was diluted to 1% (w/w) with purified water before use.

Synthesis of 1'-5-bromopentyl-2,3,3-trimethylindoleninium bromide (1). 1,5-Dibromopentane (12 mL, 20.26 g, 88 mmol) and 2,3,3-trimethylindolenine (2.95 g, 18.5 mmol) were heated in refluxing acetone (35 mL) for ~19 h. The reaction mixture was allowed to cool to room temperature, at which point the acetone was removed under vacuum. The precipitate that formed over an extended period of time (> 24 h) was separated from the reaction mixture by filtration, then recrystallized from ethanol. These crystals were washed with diethyl ether and dried under reduced pressure. Additional product was obtained from the filtrate following removal of the dibromopentane under reduced pressure with mild heat (warm water bath). These crystals were isolated by filtration and washed with diethyl ether. The overall yield of **1** was 49%. ¹H NMR (360 MHz, CDCl₃): δ 1.6 (m, 8), 1.91 (m, 4), 3.14 (s, 3), 3.37 (t, 2), 4.77 (t, 2), 7.52–7.72 (m, 4). See also Table 6.2.

Synthesis of 1'-(5-bromopentyl)-3',3'-dimethylindoline-6-nitrobenzospiropyran (2). To 2.56 g of **1** (6.6 mmol) in 100 mL refluxing butanone was added 0.7 mL piperidine (7.1 mmol), followed by 1.22 g of 2-hydroxy-5-nitrobenzaldehyde (7.3 mmol) and 30 mL butanone. After refluxing for an additional 3.5 min, the reaction mixture was removed from the heat, and the butanone was removed under vacuum. The resulting solid was extracted with 25 mL of a 50/50 (v/v) solution of toluene

Table 6.2. Quaternized Indolenine (1) ¹H NMR Assignments.



Proton Label	Position (ppm)*	Multiplicity	Expected Integration	Actual Integration
a,b	1.60	m	8	8.21
c,d	1.91	m	4	4.21
e	3.14	s	3	2.98
f	3.37	t	2	2.00
g	4.77	t	2	2.03
h, i, j, k	7.52, 7.72 [‡]	m	4 (total)	3.03, 1.00

* In CDCl₃; residual CHCl₃ corrected to 7.24 ppm.

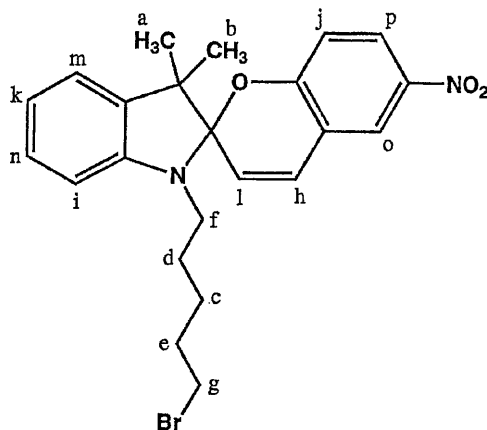
[‡]The positions and fine structure of these peaks differed (~0.1 ppm) from spectrum to spectrum of nominally identical product. (Other peaks showed roughly half this variability). This variability may have been a function of the concentration of the quaternized indolenine in the CDCl₃. A separate experiment showed that addition of alkylammonium chloride or bromide to the NMR tubes containing the product caused shifts in these peaks, suggesting that the presence of these anions may play a role.

and hexanes, and the solution allowed to equilibrate overnight to allow thermal isomerization of the dye to the spiropyran form. To remove a variety of impurities that had been revealed by thin-layer chromatography (TLC), a gentle pressure of nitrogen was used to force the solution through silica gel micro-columns (columns of silica gel 2–3 cm in height in a Pasteur pipet) until the solution was lemon yellow. Excess 2-hydroxy-5-nitrobenzaldehyde was extracted using 100 mL 0.1 M Na₂CO₃ (aq), which turned deep yellow. The solvent was removed from the toluene–hexanes phase (vacuum line, room temperature) and triturated with chloroform. The solid was then heated at 55–60 °C *in vacuo* for 13.5 h to remove the chloroform. The yield of **2** was 81%. ¹H NMR (360 MHz, CDCl₃): δ 1.16 (s, expected integration: 3), 1.26 (s, expected integration: 3) [in our best material, the combined integration of the peaks at 1.16 and 1.26 was 6.80], 1.35–1.90 (m, expected integration: 6; actual integration: 9), 3.14 (m, 2), 3.36 (t, 2), 5.85 (d, 1), 6.54 (d, 1), 6.72, (d, 1), 6.88 (m, 2), 7.07 (d,1), 7.16 (t, 1), 7.99 (m, 2). See also Table 6.3.

Synthesis of poly(vinylpyridine-spiropyran), PVP-SP (**3**). Purified PVP (4.122 g, 39 mmol, monomer basis) and **2** (1.8 g, 3.9 mmol) were dissolved in 250 mL methanol and heated at reflux for ~42 h. The volume of methanol was reduced under reduced pressure (rotary evaporator/water aspirator) to a final volume of about 25 mL, and the polymer was precipitated by addition of 100 mL of 50/50 (v/v) toluene–hexanes. The polymer was further purified by two additional cycles of dissolution in methanol and precipitation by addition of toluene–hexanes, at which point the polymer appeared by TLC to be free of unbound dye. The yield of **3** was 4.65 g (84%, based upon subsequent quantification of the extent of functionalization of the polymer; *vide infra*).

Preparation of a partially neutralized Laponite suspension. To prepare a partially neutralized Laponite suspension for film formation with PVP-SP, the

Table 6.3. Spiropyran (2) ¹H NMR Assignments¹⁴



Proton Label	Position (ppm)*	Multiplicity	Expected Integration	Actual Integration
a,b	1.16, 1.26	s,s	6	6.80
c,d,e	1.35 – 1.90	m	6	8.85
f	3.14	m	2	2.03
g	3.36	t	2	2.08
h	5.85	d	1	0.88
i	6.54	d	1	1.05
j	6.72	d	1	0.96
k,l	6.88	m	2	1.94
m	7.07	d	1	1.07
n	7.16	t	1	1.12
o,p	7.99	m	2	2.00

* In CDCl₃; residual CHCl₃ corrected to 7.24 ppm.

following components were mixed (in order): 4.0 mL of a 0.5% (w/w) Laponite RD suspension, 0.4 mL of purified water, 0.6 mL of 0.0060 M HCl, and 5.0 mL of methanol. Evaluation of such a suspension by scattering of a HeNe laser beam (~30 μ W) demonstrated that this concentration of acid was not sufficient to cause detectable flocculation of the Laponite; higher concentrations of acid did appear to initiate flocculation of the Laponite.

Dialysis of montmorillonite. Cellulose membrane dialysis tubing (16-mm diameter, Sigma product D-9777) was rinsed thoroughly with purified water, then immersed for a total of 7.75 h in purified water, the water having been exchanged after total immersion times of 3 h and 6 h. The tubing was then rinsed again with water and filled with 40 mL of a 0.33% montmorillonite suspension in H₂O (pH 9.7). The filled tubing was immersed without stirring in approximately 200 mL purified water. After total dialysis times of 16.7 h and 21.8 h, the water was changed and the tubing was agitated. After a total of 40.0 h of dialysis, 38 mL of montmorillonite suspension was collected (some lost in transfer); its pH was 7.8. The percent solids of the suspension was not evaluated at this point, but was instead presumed to be insignificantly different from that of the pre-dialyzed suspension. Its slight (or lack of) change in volume, the implausibility of a significant quantity of silicate passing through the dialysis membrane, and the insignificant effect of exchange of protons for sodium ions on the total mass²¹ combine to make this a reasonable assumption. To create a suspension containing 35% by weight methanol, 26 mL of methanol was added to the aqueous suspension. The clarity of the suspension was evaluated by the unaided eye. Flocculation, which would be accompanied by an increase in turbidity, was not observed when these dialysis conditions and dilution were used.

Preparation of substrates. Silicon wafers [p-doped, (100)-oriented, Wacker Siltronic] were cut to dimensions of 10 mm x 25 mm. They were swabbed with

ethanol, rinsed with water, and cleaned by immersion for a minimum of 30 min in piranha solution, a 2:1 (v/v) solution of concentrated H₂SO₄ and 30% H₂O₂ (Caution: this solution reacts violently with organic materials!). Following this treatment, the wafers were rinsed with purified water (Millipore Milli-Q, ≥15 MΩ-cm) and blown dry with a jet of nitrogen. Fused quartz microscope slide (Chemglass) were cut into pieces with dimensions of ~12 mm x 40 mm x 1 mm, and were cleaned in the same manner as the silicon.

6.5.2. Film Preparation. Formation of multilayered films using partially neutralized Laponite and PVP-SP. Silicon and fused quartz substrates were treated for 5 s with 1% PDDA, rinsed with purified water, and blown dry with nitrogen, and then treated for 5 s with the partially neutralized Laponite suspension, rinsed with H₂O-methanol (50/50 w/w), and blown dry. Subsequent to this treatment, a multilayered film was adsorbed by repetition of a two-step cycle. In the first step, the slide was immersed to a depth of 2.5–2.7 cm in a 1.9% w/w solution of PVP-SP in methanol for ~60 s, rinsed with methanol, and blown dry with nitrogen. In the second step, it was immersed to the same depth in the Laponite suspension for ~60 s, rinsed with H₂O-methanol (50/50 w/w), and blown dry with nitrogen.

Formation of multilayered films using dialyzed montmorillonite and PVP-SP. Film preparation was carried out in a manner similar to that described above for Laponite and PVP-SP, with the following exceptions: the rinse following each treatment with montmorillonite was 65% H₂O and 35% methanol (w/w); the polymer concentration was 1% (w/w) in methanol.

Formation of a pure PVP-SP film. A clean quartz slide was suspended from a pair of tweezers on a string. The bottom 2.5–2.7 cm of the slide was immersed in a 1.2% (w/w) solution of PVP-SP in methanol. This setup was surrounded by a paper cylinder to reduce the circulation of air around the slide as it was withdrawn from

the solution at a rate of 0.9 cm/min with a syringe pump (Sage Instruments). This dip-cast PVP-SP film was then allowed to air-dry.

6.5.3. Instrumentation. Nuclear magnetic resonance (NMR) spectrometry.

Proton NMR spectra were obtained using a Bruker AMX 360 spectrometer. On this 360-MHz (8.4-T) instrument, a sweep width of 7.46 KHz was used, and 32768 points were collected per scan. Between 16 and 64 scans were typically averaged, with an acquisition time per scan of 2.19 s and delay of 1.00 s, for a total time between pulses of 3.19 s.

Gas chromatography/mass spectrometry (GC/MS). Mass spectra were obtained using a Hewlett-Packard HP5890A gas chromatograph coupled to a HP5970-series mass selective detector. The background vacuum was $3\text{--}5 \times 10^{-5}$ Torr, the port temperature was 250°C, and the 15-m general purpose, nonpolar column (inner diameter 0.25 mm) was heated from an initial temperature of 50°C to a final temperature of 320°C at a rate of 10°C/min. The flow rate of helium was approximately 1.6 mL/min. Under these conditions, a species eluted at 26.4 min having peaks at M/e 456 and 458, attributed to the molecular ion of the spiropyran dye, and having prominent fragments at 377 (loss of Br), and 158 (2-methylene-3,3-dimethylindolenine).

Determination of the extent of functionalization of the PVP-SP. The extent of functionalization of the PVP-SP was determined by a spectrophotometric standard-additions experiment. Six methanolic solutions were prepared in which the concentration of the polymer was $0.0485 \pm 0.0002\%$ (w/w) and to which 2 was added to a final concentration ranging from 0 to 1.45×10^{-3} molal. The solutions were allowed to equilibrate for a minimum of 22 h to allow thermal isomerization of the dye, and were then transferred to quartz cuvettes (1.0-cm path length). Uv-vis spectra were obtained using the same scan parameters as described below for the

films, with methanol in the reference cuvette. Absorbance was quantified at a λ_{max} of 536 nm, associated with the merocyanine form of the dye. A linear least-squares fit to the data (absorbance vs. concentration of added dye) allowed straightforward calculation of the extent of functionalization of the polymer: 7–8 mole %, based on vinylpyridine monomer units, or 23–25% by mass. Repetition of this experiment with solutions one-fifth as concentrated that had been allowed to equilibrate one week gave nearly identical results.

Ellipsometry. The growth of multilayered films on silicon was monitored by optical ellipsometry, using a Rudolph Auto-EL III nulling ellipsometer with HeNe laser light ($\lambda = 632.8$ nm). Measurements were performed under ambient conditions with the angle of incidence set at 70° . The combined thickness of the native oxide of silicon and the PDDA/silicate primer layer was measured using Program 211000, assuming a refractive index of 1.5, and assuming a standard refractive index for the silicon substrate ($n = 3.858$, $k = 0.018$). For calculations of multilayer thickness, a single smooth film was assumed, and a refractive index of 1.5 was used.

Ultraviolet-visible spectrophotometry. The growth of the multilayered films and their photochromic behavior were evaluated using ultraviolet-visible (uv-vis) spectrophotometry. A Shimadzu UV-2101PC spectrophotometer with a photomultiplier tube (PMT) detector was used in absorbance mode to obtain spectra between 220 and 800 nm, using a spectral bandwidth of 1.0 nm and sampling interval of 2.0 nm. A fused quartz slide bearing a multilayered film on both sides was placed diagonally in a 1.0-cm x 1.0-cm x 4.3-cm fused-quartz cuvette such that the angle of incidence of the sample beam on the slide was 45° . An identical but uncoated slide was similarly oriented in a cuvette in the reference beam. According to the manufacturer of the spectrophotometer, the beam area is 4 mm x 11 mm; only the coated portion of the slide was exposed to the beam.

Photo-irradiation of thin films. To induce isomerization, films were irradiated with either a broadband uv source (Rayonet, $\lambda_{\text{max}} = 350$ nm, Southern New England Ultraviolet Company, Branford, CT) or a broadband visible source (60-watt light bulb, filtered with a longpass filter having a cutoff of 473 nm). Films were irradiated until their uv-vis spectra reached an apparent steady-state, typically ~60 s under uv irradiation and ~60 min under vis irradiation. Data were fit with Origin 3.5 (Microcal Software, Inc., Northampton, MA).

X-Ray Diffractometry. X-ray diffractometry was performed on a Scintag XDS 2000 powder diffractometer with $\text{CuK}_{\alpha 1}$ radiation using a 0.030° step and a 9-s integration time.

Acknowledgements. We gratefully acknowledge Southern Clay, Inc. for support of this work, for donations of Laponite RD and montmorillonite, and for performing x-ray diffractometry. E.R.K. acknowledges fellowships from AT&T Bell Laboratories and Lehigh University.

6.6 References and Notes

1. Vašiček, A. *Optics of Thin Films*; Interscience: New York, 1960; pp 122–139.
2. *Optics Guide 5*; Melles-Griot, Inc.: Irvine, California, 1990; pp 4-18 – 4-19.
3. *Photochromism*; Brown, G.H., Ed.; Techniques of Chemistry, Vol. III; Wiley-Interscience: New York, 1971.
4. Tagaki, K.; Kurematsu, T.; Sawaki, Y. *J. Chem. Soc. Perkin Trans. 2* **1991**, 1517.
5. Cooper, T.M.; Tondiglia, V.; Natarajan, L.V.; Shapiro, M.; Obermeier, K.; Crane, R.L. *Applied Optics* **1993**, *32*, 674.
6. Xue, S.S.; Manivannan, G.; Lessard, R.A. *Thin Solid Films* **1994**, *253*, 228. See also Ref. 3, pp 744–746.

7. Takagi, K.; Kurematsu, T.; Sawaki, Y. *J. Chem. Soc. Perkin Trans. 2* **1995**, 1667.
8. Seki, T.; Ichimura, K. *Macromolecules* **1990**, *23*, 31.
9. Kleinfeld, E.R.; Ferguson, G.S. *Science* **1994**, *265*, 370. Ferguson, G.S.; Kleinfeld, E.R. *Adv. Mater.* **1995**, *7*, 414.
10. Kleinfeld, E.R.; Ferguson, G.S. Manuscript in preparation (see Chapter 7).
11. Kleinfeld, E.R.; Ferguson, G.S. In *Solid State Ionics IV*, Nazri, G.-A.; Tarascon, J.-M.; Schreiber, M., Eds; Mat. Res. Soc. Symp. Proc. 369. Materials Research Society: Pittsburgh, 1995, p 697.
12. Richter, H.J.; Dressler, R.L. *J. Chem. Eng. Data* **1964**, *9*, 406.
13. Vandewyer, P.H.; Smets, G. *J. Polymer Sci. A-1* **1970**, *8*, 2361.
14. Peak positions were compared to those in the spectrum of dibromopentane (Kleinfeld, E.R.; Ferguson, G.S., unpublished results) and in the spectrum of the 1'-methyl analog of **2** (*Handbook of Proton-NMR Spectra and Data*; Asahi Research Center, Eds.; Academic Press: New York, 1986; Vol. 10, p 176.) Because our higher-field instrument allowed greater resolution than that obtained in the *Handbook*, assignments presented here differ in some cases from those published there.
15. Decher, G.; Hong, J.D.; Schmitt, J. *Thin Solid Films* **1992**, *210/211*, 831. Whether these authors recognized the effect of interference phenomena on their data is unclear. The cited article does not, however, mention such phenomena.
16. Reference 1, pp 80–81, 117, 130.
17. Ref. 3, p 99. Shimidzu, I.; Kokado, H.; Inoue, E. *Bull. Chem. Soc. Japan* **1969**, *42*, 1730.
18. Ref. 3, pp 125–164.
19. Warren, B.E. *X-Ray Diffraction*; Dover: New York, 1990; p 253.
20. Drits, V.A.; Tchoubar, C. *X-Ray Diffraction by Disordered Lamellar Structures*;

Springer-Verlag: New York, 1990; pp 40–42. Reynolds, R.C. *Acta Crystallogr.* **1968**, A 24, 319. Trunz, V. *Clays Clay Miner.* **1976**, 24, 84.

21. Less than 2% of the mass of the clay would have been lost if every Na⁺ ion had been replaced by a proton, and the pH of the final suspension indicated that we did not come near this extent of exchange.

Studies of the Structure, Composition, and Kinetics of Adsorption of Poly(diallyldimethylammonium)/Montmorillonite Composite Films

7.1 Abstract

Multilayered films were formed by alternate adsorption of the cationic polyelectrolyte poly(diallyldimethylammonium chloride) (PDDA) and exfoliated, anionic sheets of montmorillonite onto silicon substrates. Various studies were undertaken in order to begin to determine the experimental conditions that would lead to optimization of structural order in the resulting films. The growth, structure, composition, and kinetics of formation depended strongly on the concentration of the polymer solution in the range of 0.05% (w/w) to 5% (w/w), when all other conditions were held constant. Ellipsometric measurements of film thickness showed that films made using 0.05%, 1%, and 5% solutions of PDDA, using 5-s adsorption treatments, grew at average rates of 1.5 nm/cycle, 2.1 nm/cycle, and 2.8 nm/cycle, respectively. Thick films were prepared for evaluation of the effect of polymer solution concentration on the level of structural order in the resulting films. Films for this study were prepared from 0.05%, 1%, and 5% solutions of PDDA, using 5-s adsorption treatments, and all possessed a high degree of structural order as evidenced by x-ray diffractometry. These films all had d-spacings of ~1.44 nm, indicating that the ordered material in the films was an ABAB arrangement of the polymer and silicate; however, the degree of crystallinity of the films decreased as the concentration of the PDDA solutions used to form the films was increased. Omega scans indicated that the crystallites were preferentially oriented with the sheets near-parallel to the substrate surface, but that varying the concentration of the polymer solutions used to form the films made little difference in this characteristic. X-ray

photoelectron spectroscopy revealed that the atomic ratio of N to Al within the films rose as the polymer solution concentration used in forming the films was increased, consistent with the idea that the lower degree of structural order observed in the films made using PDDA solutions of higher concentration was attributable to poorer packing of the excess polymer in the interlayer spaces. Studies of the kinetics of adsorption of the PDDA were performed using 0.05%, 1%, and 5% solutions of PDDA, and using treatments ranging in duration from 5 s to 20 h. These studies revealed that the adsorbed layer of PDDA approached an apparent limiting thickness within approximately two minutes. The montmorillonite adsorption, however, reached an apparent limiting thickness more slowly, with significant amounts of material adsorbing in the 2–10 minute range.

7.2 Introduction

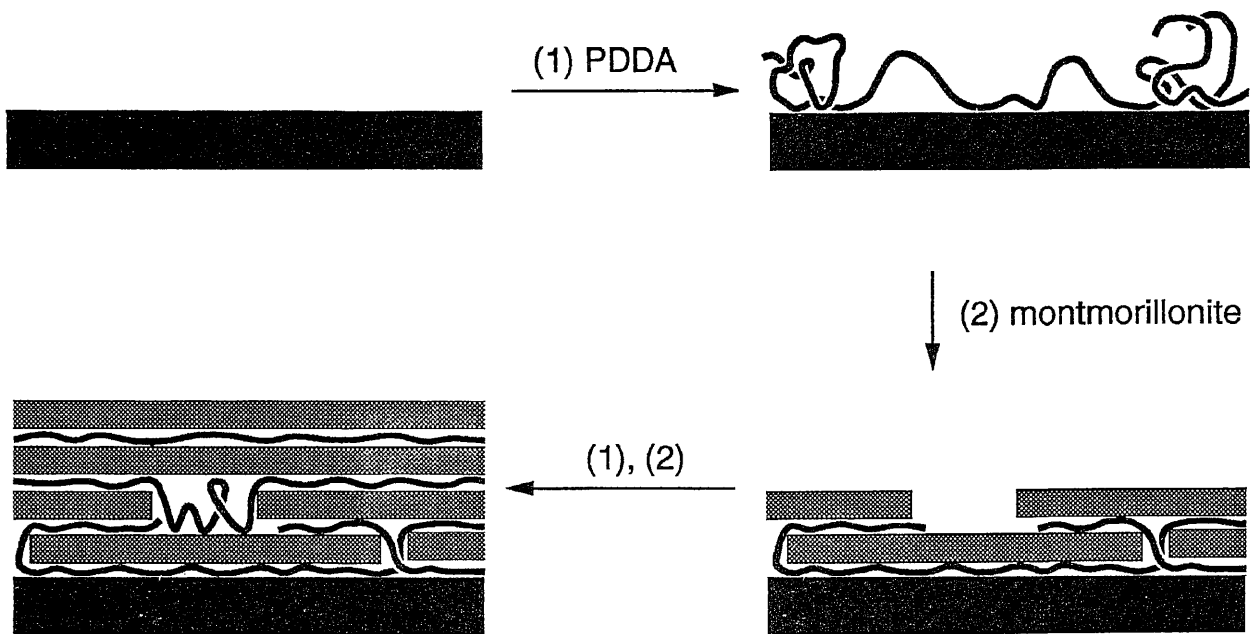
Multilayered films are of interest for a variety of applications, including reflective and nonlinear optical coatings,¹ insulating layers for microelectronics,² and films capable of vectorial electron transfer for artificial photosynthetic systems.³ For all these applications, the formation of well-ordered films is critical, as disorder or defects can significantly reduce film performance. We recently introduced a new method for the formation of ultrathin multilayered films involving the layer-by-layer adsorption of a cationic polyelectrolyte and single platelets of an anionic sheet-silicate mineral onto various surfaces, as described in detail in Chapters 2 and 3.⁴ X-ray diffraction revealed that these films possessed a degree of structural order unprecedented among films adsorbed from solution onto flat substrates.^{5,6} This high level of order was attributed, in part, to the ability of the films to recover from defects that occur during their formation, as described in Chapter 4.⁷ Because films formed by our method have potential for the applications mentioned above, we were

interested in determining the factors that would optimize their degree of structural order.

The films used in previous studies had been formed by a two-step adsorption cycle involving alternate treatments with poly(diallyldimethylammonium chloride) [PDDA, typically from a 5% (w/w) solution] and Laponite RD [synthetic hectorite, from a 0.2% (w/w) suspension of exfoliated platelets]; each component was typically allowed to remain on the surface for approximately 5 s before the surface was rinsed and dried. Under these conditions, the ellipsometric growth of 3.5 nm per cycle was more than twice the 1.4-nm d-spacing (i.e., the unit cell spacing in the direction normal to the silicate sheets) that was revealed by x-ray diffraction. This discrepancy implied that any excess polymer that had adsorbed only loosely during a polymer adsorption step could be displaced upward during the subsequent silicate adsorption step to adsorb excess silicate, as depicted in Figure 7.1 and as will be explored in greater detail later in this chapter. Subsequent studies, detailed in Chapter 3, showed that the average amount of each component that adsorbed per cycle could be varied in an apparently continuous manner by changing the concentration of the polymer solution.⁸

To begin the process of elucidating the conditions that would enable preparation of films with the highest possible degree of structural order, we studied the effect of polymer concentration on film growth, structure, composition, and kinetics of adsorption. The natural sheet-silicate mineral montmorillonite was used for these studies rather than Laponite RD. Natural montmorillonite displays a higher degree of crystallinity and has a larger average sheet diameter than its synthetic counterpart; its use was therefore expected to further increase the structural order of the films.

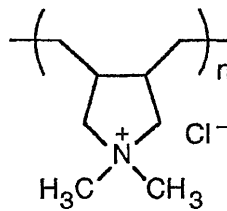
Figure 7.1. Schematic diagram of the formation of a composite film from a solution of PDDA and a suspension of montmorillonite.



7.3 Description of Film Components

The cationic polyelectrolyte used in the preparation of the multilayered films was poly(diallyldimethylammonium chloride), PDDA, depicted in Figure 7.2a.⁹ This linear polymer was obtained from Aldrich as a 20% solution, and had a molecular weight, as reported by the manufacturer, of 200,000–350,000. The sheet-silicate mineral used, montmorillonite, has the ideal unit cell formula $\text{Na}_{0.66}^{0.66+}[\text{Si}_8(\text{OH})_4(\text{Al}_{3.34}\text{Mg}_{0.66})\text{O}_{20}]^{0.66-}$. Its structure consists of a central layer in which aluminum and magnesium are octahedrally coordinated to oxygen, surrounded by two layers in which silicon is tetrahedrally coordinated to oxygen. This structure, depicted schematically in Figure 7.2b, has a thickness of approximately 0.94 nm.¹⁰ A sheet containing four aluminum ions per unit cell and no magnesium ions would bear no charge; the substitution of 0.66 Mg^{2+} ion for 0.66 Al^{3+} ion per unit cell imparts an overall negative charge to the sheet which is balanced by the incorporation of 0.66 Na^+ ion per unit cell in the interlayer space. Unlike the other cations in the structure, the sodium ion can readily be exchanged for other cations. A common impurity in montmorillonite is Fe^{3+} , which also substitutes for Al^{3+} in the octahedral layer. The concentration of this impurity varies depending on the source of the mineral. Although natural montmorillonite, as mined, contains crystallites of stacked sheets, the mineral can be exfoliated under high shear to yield an aqueous suspension containing single anionic sheets. The montmorillonite used in the present work was supplied by Southern Clay, Inc., as a fully exfoliated, Na-ion-exchanged suspension containing 0.36% (w/w) montmorillonite. It was subsequently centrifuged in our laboratories to aid in the removal of any unexfoliated material and to produce a suspension containing the desired size fraction, as described in the Experimental Methods section.

a)



b)

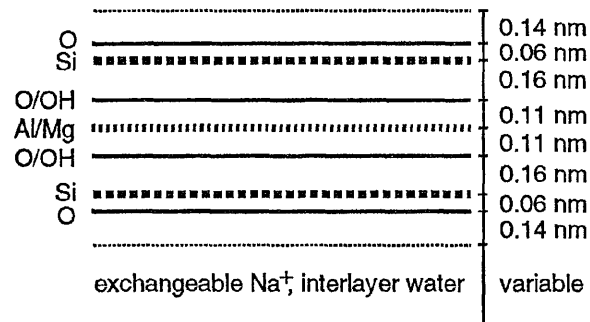


Figure 7.2. Precursors to multilayered composite films: a) PDMA,⁹ b) Montmorillonite.¹⁰ In (b), the heavy solid or dashed lines show the centers of the atomic planes; the light dashed lines show the periphery of the van der Waals radii of the oxygen atoms. The silicon atoms are tetrahedrally coordinated to oxygen, and the aluminum and magnesium atoms are octahedrally coordinated to oxygen.

7.4 Results and Discussion

7.4.1. Film Formation. Multilayered films in the present study were formed by repetition of a two-step process under the following conditions, unless noted otherwise.⁴ In the first step, a substrate was treated with a PDDA solution of chosen concentration, rinsed with water after ~5 s, and blown dry. In the second step, the substrate was treated with a 0.2% (w/w) suspension of exfoliated, Na-ion-exchanged sodium montmorillonite, rinsed after ~5 s, and blown dry. This process is depicted schematically in Figure 7.1.

7.4.2. Ellipsometric Study of the Characteristics of Film Growth. If the overall thickness of a multilayered film is to be precisely controllable, its growth must follow a predictable pattern. The simplest such case is regular growth, meaning growth that is the same in each cycle. As shown in Figure 7.3, PDDA/montmorillonite films display very regular growth, and the overall growth per cycle can be fine-tuned by adjusting the polymer concentration. These results are consistent with those observed for PDDA/Laponite films, which were presented in Chapter 3.⁸ Ranges of growth per cycle that were observed for these 5-s treatments are summarized in Table 7.1.

7.4.3. X-Ray Structural Analysis. For structural analysis by x-ray diffraction, thick samples (~100 nm) were prepared from 0.05%, 1%, or 5% PDDA and 0.2% montmorillonite, using 5-s adsorption treatments. To form these films, 30, 42, and 70 cycles were required, respectively. For comparison, one sample was prepared by the slow evaporation of a 0.33% suspension of montmorillonite alone onto a bare silicon wafer. Details concerning these four samples are summarized in Table 7.2.

The low-angle X-ray diffraction (XRD) patterns of samples **1–3** and **Mont** are presented in Figure 7.4, and the (001) reflections from these samples are highlighted in Figure 7.5. Positions of all peaks, and the corresponding d-spacings,

Figure 7.3. Ellipsometric growth of composite films as a function of polymer concentration (% w/w), using 0.2% montmorillonite and 5-s adsorption treatments for each component. Graph (a) shows growth in thickness on individual samples as a function of the adsorption treatments performed, when polymer solutions of the indicated concentration were used. After each treatment (P = PDDA, M = montmorillonite), measurements were taken at three different sites on the same wafer; these are shown as individual data points in the graph. Graph (b) was derived from the data shown in graph (a). The bars in (b) show ranges in thickness resulting from individual polymer or montmorillonite treatments (bottom and middle traces, respectively) as a function of polymer concentration. Overall ranges in growth per cycle are shown in the top trace. Substrates for the films made using 1% and 5% PDDA were bare silicon wafers; for the film made using 0.05% PDDA, the substrate was a silicon wafer that had been treated with one cycle of 1% PDDA and 0.2% montmorillonite. Lines in (a) connect the averages of the three measured points; the lines in (b) are guides for the eye.

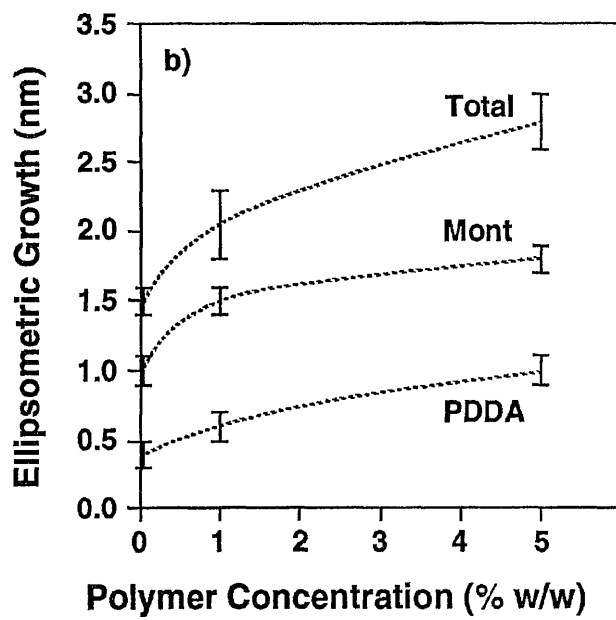
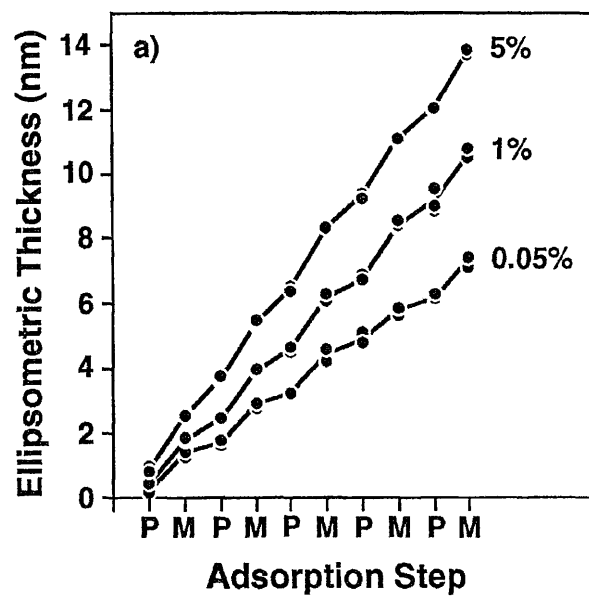


Table 7.1. Growth Characteristics of PDDA/Montmorillonite Films

PDDA Conc. (% w/w)	Growth per Polymer Step	Growth per Montmorillonite Step	Growth per Cycle (average)
5%	0.9 – 1.1 nm	1.7–1.9 nm	2.8 nm
1%	0.5–0.7 nm	1.4–1.6 nm	2.1 nm
0.05%	0.3–0.5 nm	0.9–1.2 nm	1.5 nm

Table 7.2. Samples Prepared for X-Ray Diffraction.

Sample ID	PDDA Conc. (% w/w)	Film Thickness	Overall Ellipsometric Growth per Cycle
1	5%	95 nm (30 cycles)	3.2 nm
2	1%	94 nm (42 cycles)	2.2 nm
3	0.05%	102 nm (70 cycles)	1.5 nm
Mont	---	uneven	---

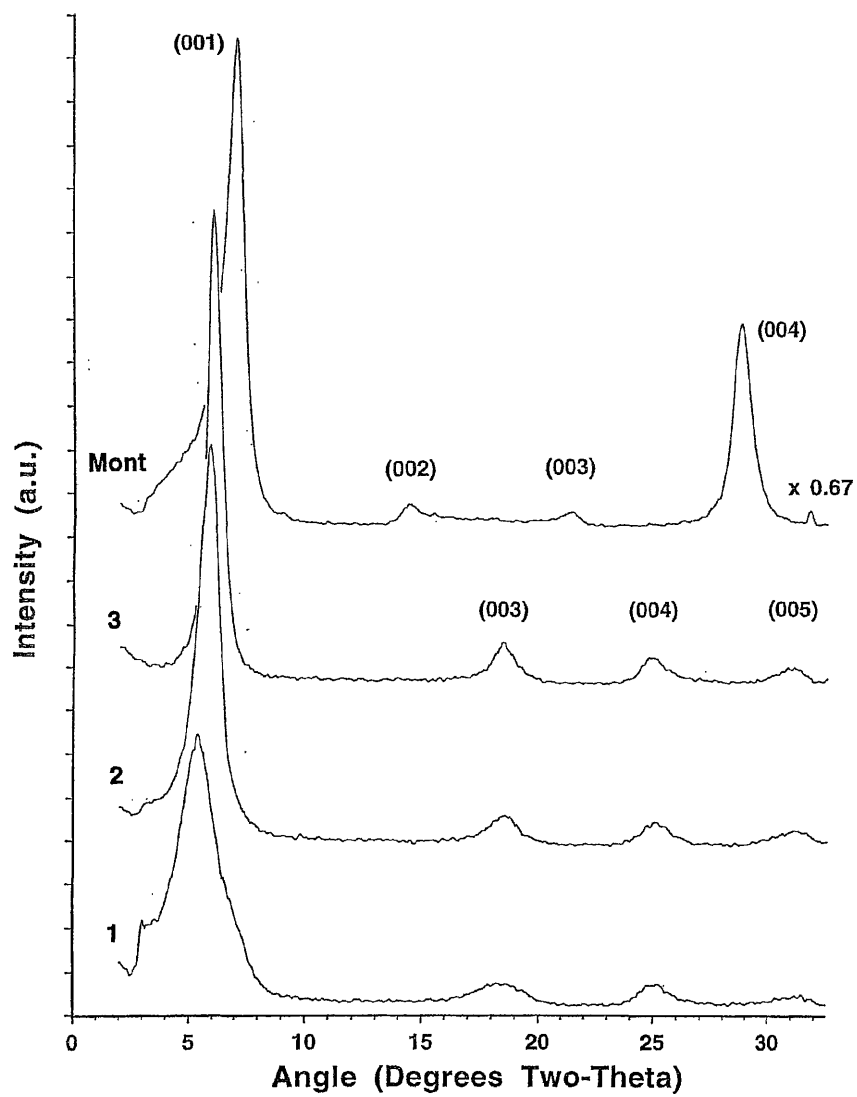


Figure 7.4. X-ray diffraction patterns of samples 1–3 and **Mont**. The basal reflections are labeled; their positions and the calculated d-spacings are given in Table 7.3.

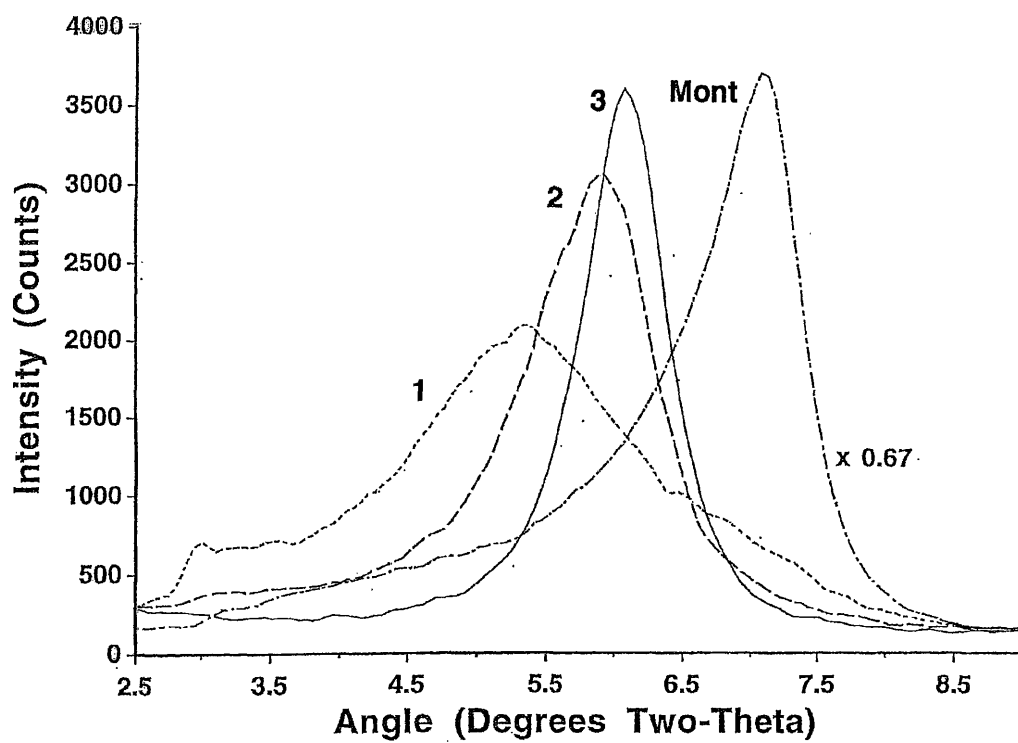


Figure 7.5. Low-angle XRD patterns of samples 1-3 and **Mont** highlighting the (001) reflections of these samples.

are summarized in Table 7.3. The absence of the (002) reflection from the patterns of all the composite films is attributable to destructive interference between x-rays reflected from different scattering planes within the unit cell, as also noted in Chapter 3. The presence of this peak in the pattern for **Mont** indicates that this destructive interference is incomplete (or that the interference is not destructive) when the 0.94-nm-thick sheets are separated by a smaller interlamellar distance (0.30 nm rather than 0.50 nm). One of the most dramatic differences between the patterns of samples 1–3 is that the (001) reflection shifted to higher angle and became sharper as the polymer concentration used in forming the samples was decreased. In contrast, although the higher order (00*l*) reflections became sharper as polymer concentration decreased, their positions did not exhibit a significant shift.¹¹ To a first-order approximation, application of the Bragg equation to the peaks in an XRD pattern allows calculation of the dimensions of crystalline unit cells. In the pattern of sample 1, however, the basal reflections occurred in positions indicating significantly different lattice spacings. This phenomenon, termed “apparent irrationality,”¹² results from the tendency of XRD peaks to shift in the direction of increasing values of the square of the structure factor, an effect which is most noticeable when peaks are significantly broadened.¹² Although all the (00*l*) peaks are shifted as a result of this effect, the (001) peak is affected most strongly, so the true d-spacing is closer to that indicated by the higher-order reflections (~1.44 nm). This lattice spacing is consistent with a structure in which montmorillonite layers, ~0.94 nm in thickness, alternate with PDDA layers ~0.5 nm in thickness to form a composite structure with an ABAB arrangement. The thickness of the polymer layer is approximately equal to a minimum van der Waals diameter of a PDDA chain, determined using a CPK model. Thus the XRD results indicate that not more than one layer of polymer is present in the interlamellar space of the ordered material in the films. Irrationality of peaks in

Table 7.3. Summary of Results from XRD Analysis.

Sample ID	PDDA Conc.	Peak Positions and d-Spacings ^a					FWHM (001), ^b crystallite size ^c
		2 θ (001), d ₍₀₀₁₎	2 θ (002), 2d ₍₀₀₂₎	2 θ (003), 3d ₍₀₀₃₎	2 θ (004), 4d ₍₀₀₄₎	2 θ (005), 5d ₍₀₀₅₎	
1	5%	5.3°, 1.66 nm	(absent)	18.3°, 1.45 nm	25.0°, 1.42 nm	31.2°, 1.43 nm	1.9°, 4.4 nm
2	1%	5.9°, 1.49 nm	(absent)	18.5°, 1.44 nm	25.0°, 1.42 nm	31.1°, 1.44 nm	1.1°, 7.6 nm
3	0.05%	6.1°, 1.45 nm	(absent)	18.4°, 1.44 nm	24.8°, 1.43 nm	31.1°, 1.44 nm	0.7°, 11.9 nm
Mont	---	7.1°, 1.24 nm	14.4°, 1.23 nm	21.4°, 1.24 nm	28.8°, 1.24 nm	N/A ^d	1.0°, 8.3 nm

^a We estimate the uncertainty in all calculated d-spacings to be ± 0.02 nm.

^b Full-width at half-maximum intensity of the (001) reflection.

^c Crystallite size calculated by application of the Scherrer relation, equation 1.

^d The scan did not go to a sufficiently high angle to observe the (005) reflection of Montmorillonite.

the XRD patterns of clays can also arise from random interstratification of materials having different d-spacings, for example, montmorillonite and illite, two silicate minerals that commonly occur together in nature.¹³ In such cases, however, the shifts of all the (00*l*) peaks are typically similar in magnitude, causing them to occur in positions intermediate to those in the patterns of the two pure materials.¹⁴

We applied the Scherrer relation¹⁵ (equation 1) to the (001) reflections of samples 1–3 to assess the relative sizes of the ordered crystallites in the direction normal to the substrate surface. According to this equation, the mean dimension of ordered domains, *L*, is inversely related to the full-widths of the basal reflections at half-maximum intensity:

$$L = \frac{0.94 \lambda}{B(2\theta) \cos(\theta)} \quad (1)$$

in which λ is the x-ray wavelength (0.154 nm for CuK α), *B*(2*θ*) is the full-width at half-height in radians of the peak of interest, and θ is its position (one-half of the 2*θ* value). Thus the full-widths may relate directly to the size of well-ordered crystallites that are separated by blocks of disordered material.¹² Alternatively, they may relate inversely to subtle disorder arising from a distribution in the dimensions of the interlamellar spaces.¹⁶ Values for *L* nearly tripled in size from sample 1 to sample 3, revealing a dramatic improvement in structural order as the polymer concentration was decreased (Table 7.3). Values generated using this equation are useful for making comparisons between similar samples; however, they underestimate the crystallite sizes determined by direct methods such as cross-sectional transmission electron microscopy.^{16a,17}

Strikingly, the domain sizes calculated for Sample 3 were larger than those for the evaporated montmorillonite film (**Mont**); the layer-by-layer adsorption process was

apparently capable of inducing a higher degree of structural order than was afforded “naturally” by evaporation under the conditions that were used. In the pattern of the evaporated montmorillonite film, the (001) reflection occurred at 7.1°, corresponding to a d-spacing of 1.24 nm. This value is consistent with literature reports for sodium montmorillonite with a single interlamellar layer of water.¹⁸ The clear absence of a peak or shoulder in this position in the patterns for samples 2 and 3 indicated that the montmorillonite suspension used in forming the films was indeed fully exfoliated, and thus that the ordered material in the composite films could not merely be unexfoliated crystallites of the precursor mineral. The asymmetry in the (001) reflection may result from broadening due either to the presence of small crystallites or to the presence of a distribution in interlayer spacings associated with material having different amounts of interlamellar water. The low-intensity peak at 31.75° in the pattern of **Mont** is attributed to NaCl.

7.4.4. Study of Crystallite Orientation in Composite Films. The preceding analysis by x-ray diffractometry provided insight into the relative degree of crystallinity in the films. An additional measure of the degree of structural order of a film is the extent to which the silicate sheets lie parallel to the substrate surface. To assess this property, we performed x-ray omega scans of the (003) and (004) reflections of samples 1–3. Omega scans are commonly referred to as rocking curves, although technically the two techniques are not identical.¹⁹ As depicted schematically in Figure 7.6, the source, sample, and detector were positioned such that the Bragg condition was fulfilled for one of the (00*l*) reflections, i.e.,

$$l\lambda = 2d \sin \theta \quad (2)$$

where *l* is the order of the reflection, λ is the x-ray wavelength (0.154 nm), *d* is the lattice spacing (~1.44 nm), and θ is the angle between the sample surface and the

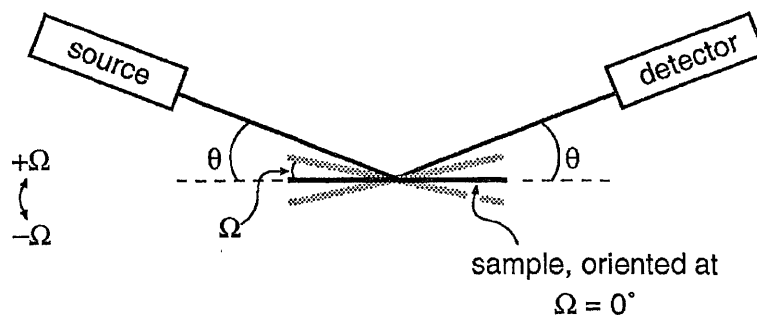


Figure 7.6. Schematic diagram of the experimental setup used to obtain data for omega scans. The heavy black line represents the sample oriented at $\Omega = 0^\circ$, the position in which a typical diffraction pattern can be obtained. The heavy gray lines schematically represent orientations to which the sample was rotated for omega scans. The source and detector were positioned such that the angle θ satisfied the Bragg condition, equation 2, for the (003) or (004) reflection of the film. Diffracted intensity was then measured as the sample was rotated, keeping its surface normal in the plane of incidence of the x-ray radiation (i.e., the plane of this page). Directions of sample rotation corresponding to positive and negative values of Ω are indicated by the double-headed arrow at the left of the diagram.

source and detector (with 90° defined as the surface normal). The sample was then rotated through an angle $\pm\Omega$ about the axis that lies in the plane of the sample but perpendicular to the plane of incidence of the radiation, as depicted in Figure 7.6. This rotation allows slightly mis-oriented crystallites to be brought into the Bragg condition, and a plot of intensity *vs.* Ω allows the orientation of the crystallites in the films to be assessed. A fundamental limitation to the range in which data can be obtained is given by equation (3):

$$\theta - |\Omega| \geq 0^\circ \quad , \quad (3)$$

because rotating the sample beyond this point eclipses the source or detector. The limitations of the particular instrument used further restricted this range to

$$\theta - |\Omega| \geq 2^\circ \quad (4)$$

This limitation eliminated the possibility of obtaining meaningful omega scans on the (001) reflections of the multilayered films, for which $\theta \approx 3^\circ$.

The data were fit using Microcal Origin, version 3.5. Fits of five of the omega scans obtained on the (003) and (004) reflections of samples 1–3 gave similar results; the sixth was qualitatively different and will be discussed later. In the five similar cases, the data could not be fit adequately with a single Gaussian curve; however, a sum of two Gaussian curves (equation 5) fit the data well.

$$y = y' + [A_1(2\sigma_1)^{-1}(\pi/2)^{-1/2}] \exp\{-2(x-x_1)^2(2\sigma_1)^{-2}\} + \\ [A_2(2\sigma_2)^{-1}(\pi/2)^{-1/2}] \exp\{-2(x-x_2)^2(2\sigma_2)^{-2}\} \quad (5)$$

In equation 5, y' is the baseline offset, A_i is the area under the peak, σ_i is the standard deviation, and x_i is the peak center. The standard deviation corresponds to the distribution of crystallite tilts within the films, with ~68% of crystallites oriented with the silicate sheets parallel to the substrate to within $\pm \sigma$. In each of these five omega scans, the narrower Gaussian was centered very close to 0° , whereas the broader one was centered at a positive value of omega. A representative plot,

including the least-squares fit to equation 5, is shown in Figure 7.7.

The presence of two distinct components in the curve-fits suggested that two phenomena were contributing to the observed intensity. One possibility is that the narrow peak corresponds to the tilts of the crystallites, and the broad peak to diffuse scattering, a phenomenon resulting from lateral imperfections within the multilayered films.²⁰ Alternatively, there may exist two independent distributions of crystallites within the films. Further experimentation, including the use of cross-sectional transmission electron microscopy to view the structure of the films directly, should aid in determining the correct interpretation.

In all these curve-fits, the standard deviation of the narrower component (σ_1) was in the range 0.74–1.08 °Ω, and that of the broader component (σ_2) was in the range 4.04–4.44 °Ω. The latter values were most likely resolution limited (*vide infra*). Results for the individual scans are summarized in Table 7.4. If the first interpretation given above is correct, and only the narrower peak relates to the tilt of the crystallites within the film, this analysis indicates that in all samples, ~68% of crystallites were oriented parallel to the substrate to within $\pm 1.1^\circ$ (i.e., $\pm \sigma$ for the narrower Gaussian of each pair). If the second interpretation is correct, and the broader Gaussian relates to a second distribution of crystallites, the orientations of these crystallites would have to be determined by another technique.

No trend was evident in the standard deviations of the broader Gaussians. The standard deviations of the narrower set of Gaussians, however, decreased with decreasing concentration of the polymer solution that had been used in sample preparation. This effect was small, and should be interpreted with caution in view of the high level of scatter in the data. These results indicated that the orientation of the ordered crystallites in samples 1–3 was similar. Furthermore, if the first interpretation given earlier was correct, the propensity of each sample toward

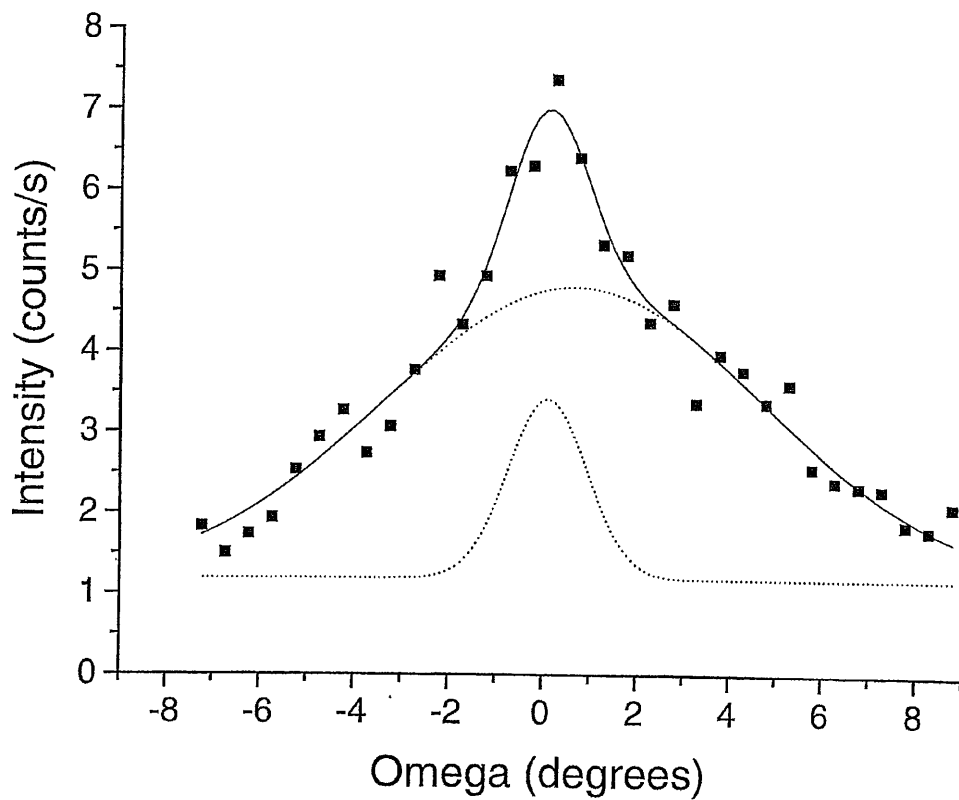


Figure 7.7. Omega scan of the (003) reflection of sample 2. The least-squares curve-fit to equation 5 is shown by the solid line, and the individual Gaussian components are shown by the dotted lines. The other omega scans were similar in appearance to this one, with the exception of the scan shown in Figure 7.8.

Table 7.4. Results of Least-Squares Fits to the Data from the Omega Scans

Sample ID	PDDA Conc. (% w/w)	Reflection	σ_1, A_1, x_1^*	σ_2, A_2, x_2^*
1	5%	(003)	1.1°, 8.8, -0.3°	4.2°, 31, 0.9°
1	5%	(004)	1.0°, 3.5, -0.1°	4.4°, 29, 0.6°
2	1%	(003)	0.8°, 4.7, 0.1°	4.0°, 37, 0.7°
2	1%	(004)	0.9°, 2.8, 0.0°	4.4°, 30, 0.5°
3	0.05%	(003)	2.4°, 31, -0.1°	N/A
3	0.05%	(004)	0.7°, 3.1, 0.2°	4.2°, 30, 0.7°

* The standard deviation (σ_i), area (A_i), and center (x_i) of the Gaussian peaks used to fit the data according to Equation (5). Approximate uncertainties in these parameters are as follows: $\sigma_1, \pm 0.2^\circ$; $A_1, \pm 1$; $x_1, \pm 0.1^\circ$; $\sigma_2, \pm 1$; $A_2, \pm 5$; $x_2, \pm 0.2^\circ$.

diffuse scattering was similar, indicating a similar level of lateral imperfections in the three samples.

The single scan that gave results different in character from the other five was that of the (003) reflection of sample 3. These data could be adequately fit with a single Gaussian curve (i.e., one involving only the first of the two exponential terms in Equation 5) having a standard deviation of 2.37, as shown in Figure 7.8. The discrepancy between this result and the others is most likely an artifact of the large scatter in the data, especially in view of the fact that the omega scan of the (004) reflection from this same sample followed the pattern of the other four scans.

As noted earlier, for the omega scans that were fit using a sum of two Gaussians, the broader component was always centered at a positive value of omega. To determine whether this effect was attributable to a changing instrumental response, several omega scans were obtained of sample 2 and of a bare silicon wafer at angles not satisfying the Bragg condition for any peak (i.e., omega scans of background noise). An omega scan of sample 2 at $29^\circ 2\theta$ could be fit by a single Gaussian peak centered at $2.4^\circ \Omega$ and having $\sigma = 5.06^\circ$. The omega scans at 14° and $22^\circ 2\theta$ on sample 2 gave similar results, as did the omega scans of a bare silicon wafer at 18° and $25^\circ 2\theta$. The asymmetry of the instrumental response is most likely responsible for the displacement of the broader Gaussians in the least-squares fits to the data to positive values of Ω . Although both Gaussians would be affected by such a non-uniform response, the broader peak would be more strongly affected, causing an apparent displacement of its center from that of the narrower peak. Furthermore, the standard deviation of the omega scan of the background noise was similar to (though broader than) that of the broader Gaussian in the least-squares fits to the data, indicating that the instrumental response affected the apparent width of this

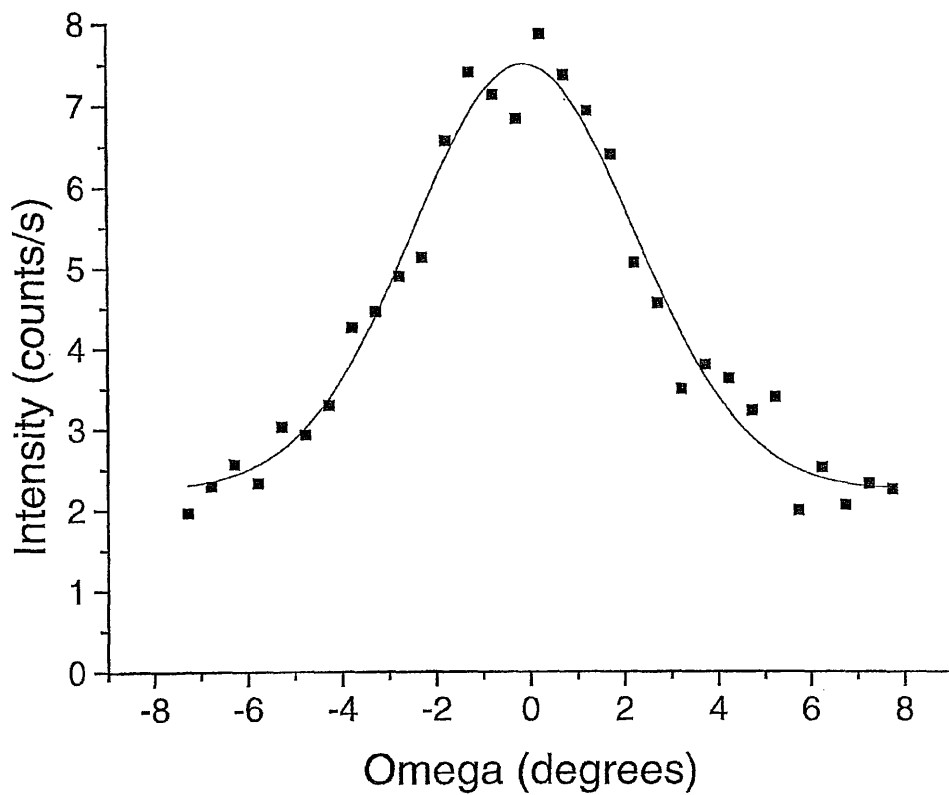


Figure 7.8. Omega scan of the (003) reflection of sample 3. The solid line shows the least-squares curve-fit by a single Gaussian function. These data were distinct from those of the other omega scans, such as the one in Figure 7.7, which required sums of two Gaussian peaks for an adequate fit.

peak, and that σ_2 therefore does not give an accurate measure of the properties of the films.

7.4.5 Evaluation of Sample Composition by X-Ray Photoelectron Spectroscopy (XPS).

The XRD results indicated that the ordered material in the multilayered films was an ABAB arrangement of the polymer and silicate, but that the degree of structural order decreased as the concentration of the polymer solutions used to form the films was increased. As indicated earlier, disorder can occur either in the form of random interruptions to a periodic lattice (Figures 7.9a and 7.9b) or in the form of a distribution in the dimensions of the interlamellar spaces (Figure 7.9c). We used x-ray photoelectron spectroscopy (XPS) to evaluate the relative proportions of polymer and silicate in films made from polymer solutions of different concentration, to gain some insight into the nature of the disorder within the films. Samples 4–6, each 20–21 nm in thickness, were prepared using 0.05%, 1%, or 5% PDDA respectively, and 0.2% montmorillonite. Survey scans were obtained in the binding energy range of 1100 eV to 0 eV, and high-resolution scans were obtained of the Na $1s_{1/2}$, Cl $2p_{1/2,3/2}$, Al $2p_{1/2,3/2}$, and N $1s_{1/2}$ regions. All spectra were taken at a 90° take-off angle (i.e., normal emission), in order to minimize effects due to the different relative positions of the components with respect to distance from the sample surface. Nitrogen was chosen for quantification of the polymer, rather than carbon, as its concentration was less susceptible to artificial enhancement due to adsorption of adventitious contaminants from the air. The survey scans revealed that all samples contained silicon, oxygen, aluminum, iron (trace), and magnesium from the clay, along with nitrogen and carbon from the polymer. Neither sodium nor chloride ions were detected on any sample, nor were any other contaminants. Quantification of the aluminum and nitrogen content of the films from the high-resolution scans is presented in Table 7.5. Ratios of these elements were calculated using both Scofield

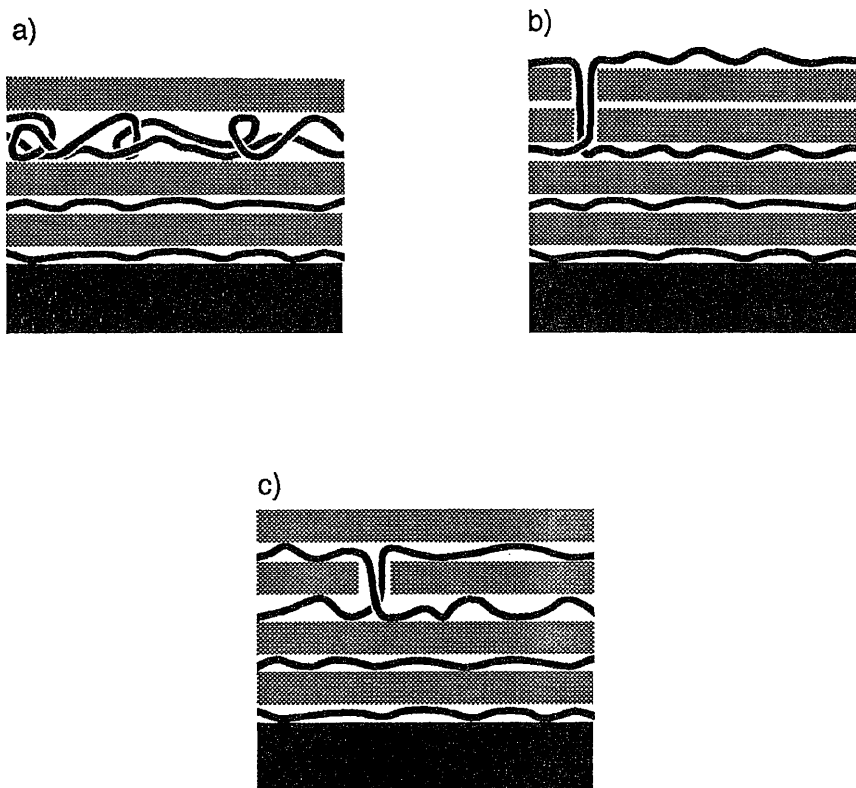


Figure 7.9. Three possibilities for the nature of the disorder within the films. In (a), entangled polymer has been trapped between two silicate sheets in an otherwise periodic structure. In (b), two layers of montmorillonite have been trapped without an intervening layer of polymer in an otherwise periodic structure. In (c), excess polymer has assumed a conformation that results in a distribution in the dimensions of the interlamellar spaces. This effect is exaggerated here for purposes of illustration.

Table 7.5. Quantification of Aluminum and Nitrogen Content of Composite Films by XPS

Sample ID	PDDA Conc.	N : Al (Scofield) ^{a,b}	N : Al ratio (Scienta) ^{a,c}
4	5%	1.0 : 3.8 (4.0)	1.0 : 2.6 (2.8)
5	1%	1.0 : 4.6 (4.9)	1.0 : 3.1 (3.4)
6	0.05%	1.0 : 5.9 (6.2)	1.0 : 4.0 (4.3)

^aThe number in parentheses includes both Al³⁺ and Fe³⁺. Quantification of the iron content using the survey spectra indicated that iron was present in approximately a 1:17 ratio (Scofield) or 1:13 ratio (Scienta) to Al³⁺; the number in parentheses was generated by multiplying the aluminum content from the high-resolution spectra by 1.059 or 1.077, respectively. The sensitivity factor used for the Fe 2p region was 16.42.

^bThese numbers were calculated from the high-resolution spectra using Scofield sensitivity factors:²¹ 0.537 for Al 2p and 1.80 for N 1s.

^cThese numbers were calculated from the high-resolution spectra using sensitivity factors determined for our Scienta ESCA-300 spectrometer:²² 0.705 for Al 2p and 1.62 for N 1s.

sensitivity factors²¹ and sensitivity factors determined specifically for the Scienta ESCA-300 spectrometer.²² Atomic ratios were further corrected for an imbalance between the attenuations experienced by the two film components due to their different average distances from the sample surface;²³ the assumptions used in the calculation of the attenuation correction factor are explained in detail in the Experimental Methods section.

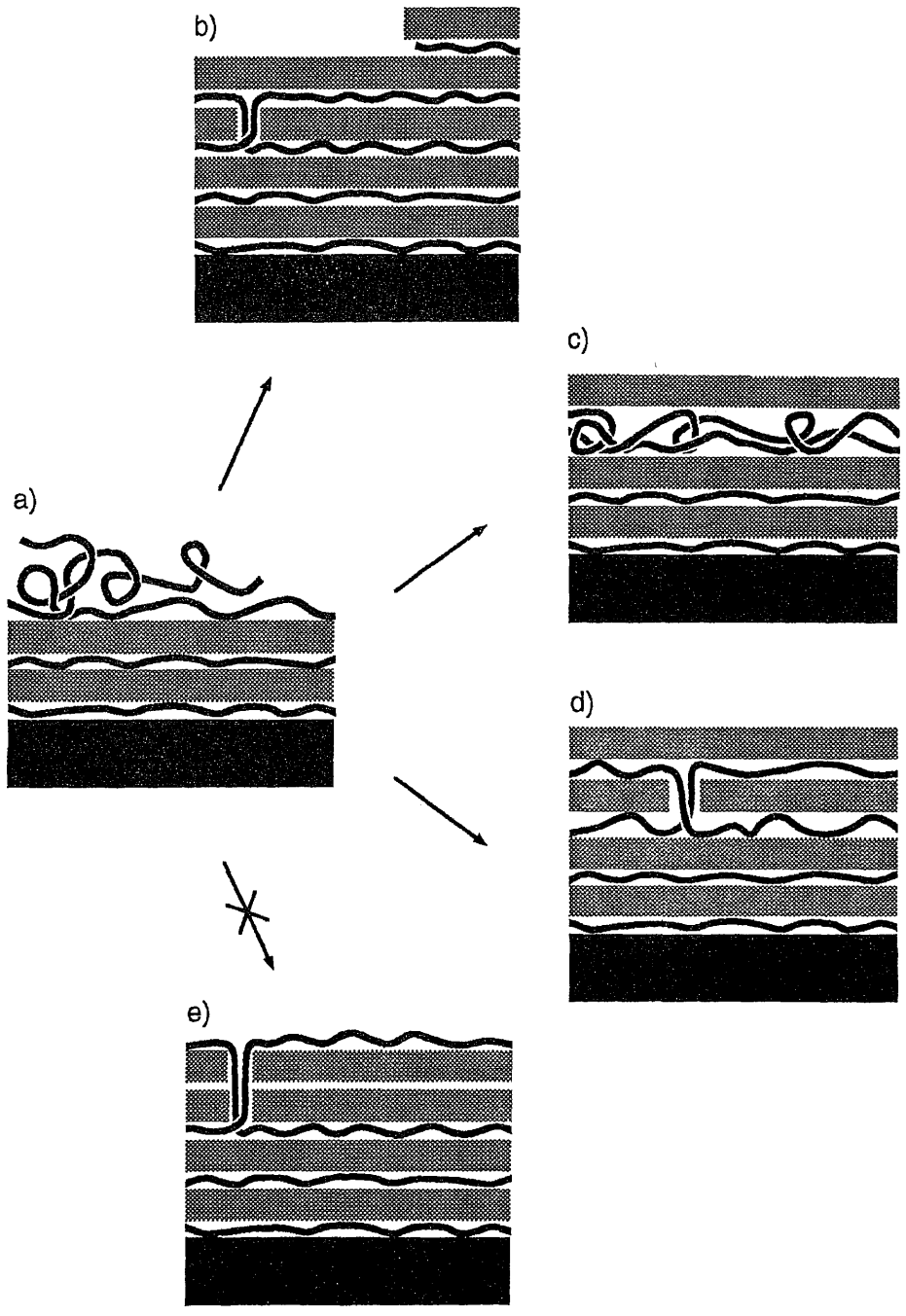
The relative proportions of PDDA and montmorillonite in the films varied as a function of the concentration of the PDDA solution that had been used in film formation. Given that at most one of these films could possess “perfect” charge balance between the positive sites on the polymer backbone and the negative sites on the montmorillonite sheets, the lack of sodium or chloride ions in the films implies either that any charge imbalance between the two immobile components of the film was compensated by protons or hydroxide ions from the aqueous rinses, or that sodium or chloride ions migrated away from the irradiated area during analysis. The migration of any chloride ions may have been induced by our use of an electron flood gun to counteract possible charging effects.

Assuming that the montmorillonite platelets had the ideal composition given earlier, perfect charge balance between the polymer and silicate would result in a 1:5.1 ratio of N : Al. If Scofield sensitivity factors were used, samples 4 and 5 appeared to have N : Al ratios above this value (i.e., an “excess” of polymer), whereas sample 6 appeared to have a ratio below this value (i.e., a “deficiency” of polymer). If the sensitivity factors determined for our instrument were used, all samples appeared to have an excess of polymer. Including trace iron (assumed to be Fe³⁺) with the aluminum in the calculation of the elemental ratios did not affect whether an apparent excess or deficiency of polymer was present for these particular samples.

Several factors introduce uncertainty into the Al:N ratio that would correspond to “perfect” charge balance, however. Foremost among these is the assumption of a perfect film structure that was used in the calculation of the attenuation correction factor. Other possible complications relate to the likelihood that the montmorillonite platelets deviated from the ideal composition stated earlier, including the possibility of iron being present as Fe^{2+} ,⁽²⁴⁾ the possibility of substitution of (OH^-) for (O^{2-}) in the oxygen layers,²⁵ and the possibility of substitution of Al^{3+} for Si^{4+} in the tetrahedral layers.²⁵ Furthermore, even platelets of ideal composition have edges that bear a positive charge.²⁶ Given the high degree of uncertainty that is associated with these various factors, we feel that a deeper analysis of charge balance within the composite films is unwarranted. The data are clear, however, in indicating that the polymer concentration that led to a film with the highest degree of structural order also led to a film with the lowest proportion of PDDA relative to montmorillonite.

The ellipsometric measurements had indicated that when a 5% PDDA solution was used, the amount of polymer that adsorbed during each treatment was equivalent to roughly two full monolayers (~1.0 nm), as reported in Table 7.1 and depicted in Figure 7.10a. We infer that, although some of the excess polymer may typically be displaced in the subsequent montmorillonite treatment to bind a second layer of the silicate (Figure 7.10b), forming an ordered structure, it may sometimes be trapped to form an irregular block that interrupts the ordered structure of the multilayered film (Figure 7.10c). Alternatively, the excess polymer may assume conformations giving rise to a distribution in the dimensions of the interlamellar spaces (Figure 7.10d). Trapping of two layers of montmorillonite with no intervening polymer layer (Figure 7.10e) does not appear to be a dominant mechanism, as it would lead to a lower N:Al ratio, not a higher one, for the films made from higher concentrations of PDDA. It thus appears that minimizing polymer disorder in the

Figure 7.10. Schematic diagram of the adsorption of montmorillonite onto a surface bearing "excess" polymer. Frame (a) shows a site in a growing film in which a preceding treatment with PDDA from a solution of high concentration [e.g., 5% (w/w)] has allowed more than a monolayer of polymer to adsorb locally. In frame (b), the excess polymer has been displaced upward during the subsequent treatment with montmorillonite, allowing more than one unit cell per cycle to adsorb, whereas in frame (c), the excess has been trapped, locally disrupting the order in the film. In frame (d), the excess polymer has assumed a conformation that results in a distribution in the dimensions of the interlamellar spaces. This effect is exaggerated here for purposes of illustration. In frame (e), two layers of montmorillonite have been trapped without an intervening layer of polymer. This last mechanism would lead to a lower proportion of polymer within the films formed from PDDA solutions of higher concentration than in the films formed from PDDA solutions of lower concentration. XPS results showing an opposite trend therefore indicated that this is not a dominant mechanism.



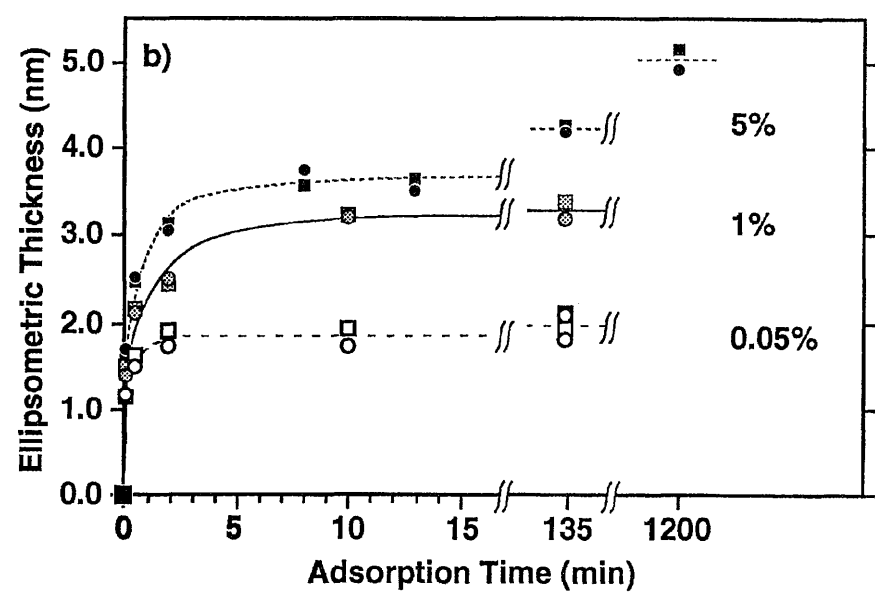
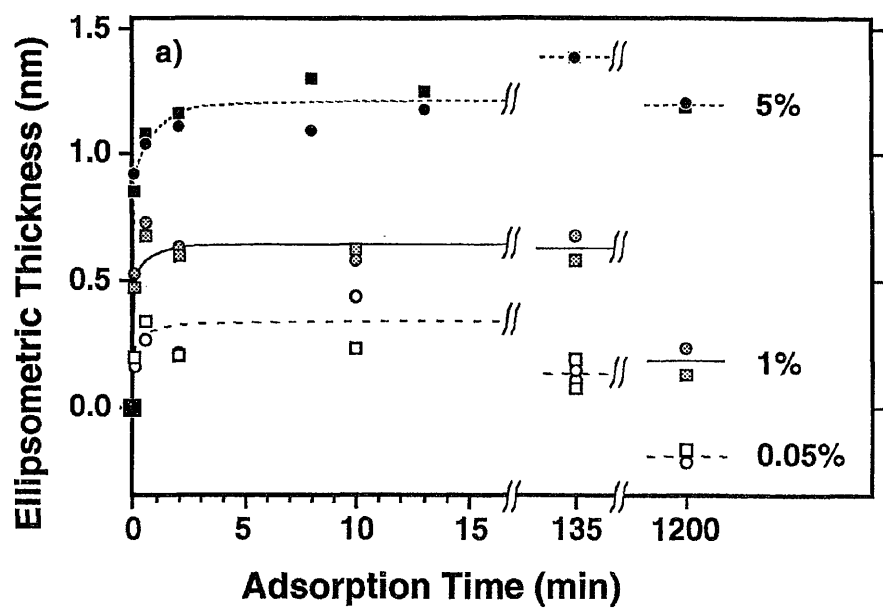
interlayer space is more important for optimizing structure in the composite lattice than “charge-matching” of the polymer and silicate. Although the same conditions (dilute polymer solutions) may favor both, any deficiency or excess of positive charge in the lattice can be compensated by mobile, monomeric ions (Na^+ , H^+Cl^- , or OH^-), which are unlikely to disrupt the periodicity of the lattice.

7.4.6. Kinetics of the Adsorption Processes. Within the brief adsorption periods used to prepare the samples for the preceding studies, the total amount of each component that adsorbed did not reach a limiting value. Others have reported that polymer solutions of higher concentration not only give rise to more rapid initial adsorption,²⁷ but also result in higher apparent limiting values of amount adsorbed.^{28,29} Although such studies were typically conducted at concentrations far lower than those used here, we expected to find qualitative similarities.

The kinetics of adsorption of the PDDA and montmorillonite were studied using 0.05%, 1%, and 5% (w/w) solutions of the polymer, and 0.2% (w/w) solutions of the silicate. To minimize substrate effects in this study, all substrates were initially treated with two cycles of 1% PDDA and 0.2% montmorillonite (5-s treatments) prior to the adsorptions of interest. Each substrate was then exposed to a PDDA solution of chosen concentration for a chosen period of time, rinsed, and dried, and the change in thickness resulting from this treatment was measured. The substrate was subsequently exposed to a 0.2% montmorillonite suspension for the same period of time, rinsed, and dried, and the change in thickness resulting from this treatment was also measured. Only one adsorption cycle was performed per substrate, and each set of conditions was evaluated in duplicate (or more). In Figure 7.11a, the kinetics of adsorption from solutions of 0.05%, 1%, and 5% (w/w) PDDA are compared. As expected, the thickness of the adsorbed layers quickly approached apparent limiting values that increased with increasing polymer solution

Figure 7.11. Adsorption kinetics of the PDDA/montmorillonite system:

a) ellipsometric thickness of PDDA layers adsorbed onto substrates from solutions containing different concentrations of PDDA (% w/w) as a function of time: top trace, 5%; middle trace, 1%; bottom trace, 0.05%; b) ellipsometric thickness of a layer adsorbed onto the samples shown in (a) from a suspension of 0.2% (w/w) montmorillonite for the same period of time that was used to adsorb the polymer layer. The top trace in (b) shows thicknesses for montmorillonite adsorption onto samples that had been previously treated with 5% PDDA, the middle trace, 1% PDDA, and the bottom trace, 0.05% PDDA. Each symbol (square or circle) represents an average of three measurements taken on a single sample under a given set of conditions. A minimum of two samples was used for each adsorption period. Substrates for this study were silicon wafers that had been treated with two cycles of 1% PDDA and 0.2% montmorillonite. The lines are guides for the eye. Each trace in (a) and (b) begins with a point at (0,0).



concentration. The initial adsorption in each case was remarkably rapid, with the ellipsometric thickness closely approaching the apparent limiting value within the first 30 s – 2 min. Treatments lasting 5 s, such as those used to form films for other studies in this chapter, resulted in polymer layers 54%, 83%, and 73% of the thicknesses measured at 10–13 min for adsorptions from 0.05%, 1%, and 5% solutions of PDDA, respectively.

Adsorptions allowed to proceed for much longer than 10 min gave different results depending on the concentration of PDDA used. For 0.05% and 1% solutions, the resulting polymer layers were apparently thinner than those obtained after shorter periods. When the 0.05% polymer was allowed to adsorb for 20 h, for example, an actual decrease in thickness was measured. It is important to bear in mind that ellipsometric measurements of films in this thickness regime cannot distinguish between the outermost polymer layer, the underlying composite film (i.e., the primer layer in these studies), and the native oxide of silicon; the decrease in thickness observed upon the 20-h treatment with 0.05% PDDA therefore only means that the sum of the thicknesses of all these layers decreased. The fates of the individual layers are not known. This sample was, however, subsequently able to adsorb montmorillonite (*vide infra*); this observation suggests that there was indeed a PDDA layer at its surface. Apparently, a decrease in the thickness of the underlying layers was larger than the increase in thickness associated with adsorption of the polymer in this step.

Figure 7.11b shows the kinetics of montmorillonite adsorption onto these surfaces, and Figure 7.12 shows the overall growth per cycle measured under these conditions (i.e., the sums of the thicknesses of the PDDA and montmorillonite layers for each sample). The thickness of the montmorillonite layer adsorbing during any given period increased with the increasing concentration of the polymer solution that

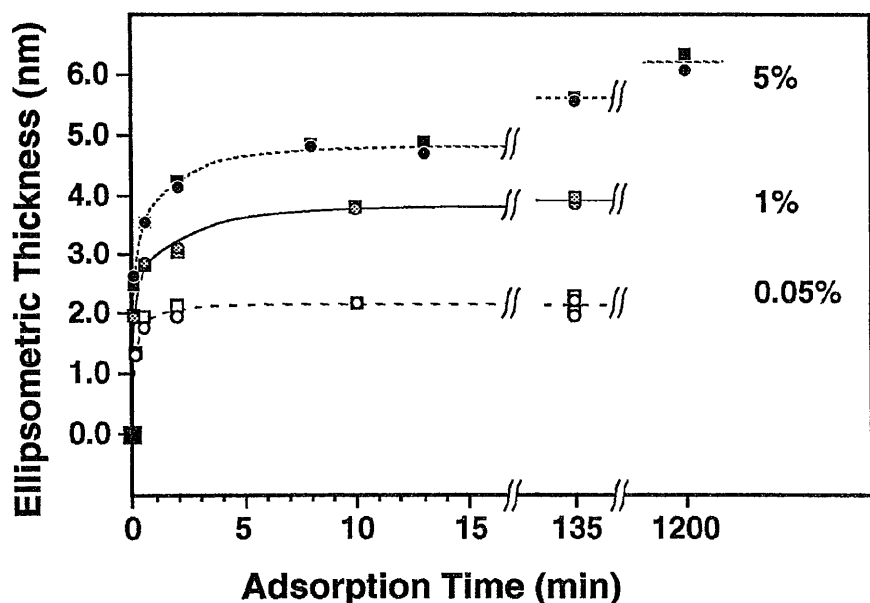


Figure 7.12. Adsorption kinetics of the PDDA/montmorillonite system. Total ellipsometric thicknesses following a complete cycle involving the adsorption of PDDA from solutions of different concentrations (% w/w) followed by the adsorption of montmorillonite from a 0.2% (w/w) suspension, as a function of time: top trace, 5% PDDA and 0.2% montmorillonite; middle trace, 1% PDDA and 0.2% montmorillonite; bottom trace, 0.05% PDDA and 0.2% montmorillonite. Each symbol (square or circle) represents an average of three measurements taken on a single sample under a given set of conditions. A minimum of two samples was used for each adsorption period. Substrates for this study were silicon wafers that had been treated with two cycles of 1% PDDA and 0.2% montmorillonite. The lines are guides for the eye. Each trace begins with a point at (0,0).

had been used during the previous treatment. In contrast to the PDDA adsorptions, which appeared substantially complete after brief treatments, the montmorillonite adsorptions approached apparent limiting thicknesses more slowly. For wafers that had been treated with 0.05%, 1%, and 5% solutions of PDDA in the preceding step, the thicknesses adsorbed in 5-s treatments with 0.2% montmorillonite reached 64%, 45%, and 47%, respectively, of the values attained in 10–13 min. It is important to bear in mind that although the *thicknesses* of the underlying PDDA layers were similar at the longer times when any particular concentration of PDDA had been used, the *structures* of these layers may have been different.³⁰ Differences in polymer-layer structure, in turn, could influence the subsequent adsorption of the silicate. The 20-h treatments with montmorillonite presented a special case: the samples that had previously been treated for 20 h with 0.05% or 1% PDDA emerged from the montmorillonite suspension with a cloudy (and, for the 0.05% samples, a darkened) appearance. The roughness of the surfaces of these samples, evaluated qualitatively by the scatter of a ~30 μ W HeNe laser beam, had increased significantly, and the film thicknesses could not be measured reliably using ellipsometry. Examination of these samples using optical and scanning-electron microscopy indicated that etching had occurred preferentially at the Si/SiO₂ interface, and significant pitting of the silicon substrates was also noted. In contrast, the samples that had been treated previously with 5% PDDA emerged from the montmorillonite suspension with no change in appearance or significant increase in roughness, and the film thicknesses could be measured ellipsometrically. The phenomenology behind these observations is currently under investigation, but the damage to the substrates certainly suggests that extended adsorption treatments should be avoided, at least when silicon substrates are used. This principle would most likely also apply to chemically related substrates such as glass and fused quartz, on which degradation such as that

observed on silicon might be more difficult to detect.

7.5 Conclusions

Multilayered films formed by the alternate adsorption of PDDA and sheet silicates show promise for applications in a variety of fields. For many of these, such as microelectronics and optics, optimizing the structural order of the films is critical. Toward that end, the present work examined how varying the concentration of the polymer solution affected the structural order of the resulting film. As the concentration of the PDDA solution was decreased from 5% to 1% to 0.05%, the proportion of PDDA (relative to montmorillonite) decreased and the degree of structural order dramatically increased. Both of these observations are consistent with poor packing of the excess PDDA present in the films made from polymer solutions of higher concentration. The improvement in structural order realized in films prepared from polymer solutions of lower concentration therefore appears to be attributable to better packing of the polymer in the interlayer space. The kinetics of adsorption of the two film components were also examined, revealing that the 5-s adsorption treatments typically used in film preparation allowed thicknesses of the PDDA and montmorillonite to adsorb that were 54–83% and 45–64%, respectively, of the thicknesses reached during 10- to 13-min treatments. The growth of the films using 5-s treatments was observed to be highly regular and reproducible; however, it is possible that improvements could be realized by increasing the duration of the adsorption treatments, especially in the case of treatment with montmorillonite. Using longer treatments would involve a sacrifice, however, in terms of the convenience with which many-layered samples could be prepared, and may increase the risk of damage to the substrate. Whether or not the use of longer adsorption

treatments would result in films possessing a higher degree of structural order remains to be seen.

7.6 Experimental Methods

7.6.1. Materials. Poly(diallyldimethylammonium chloride), PDDA, was obtained as a 20% (w/w) aqueous solution (Aldrich, MW 200,000–350,000), and was diluted with Millipore Milli-Q water (~16 MΩ-cm) to form solutions of desired concentration. A suspension of montmorillonite, 0.36% (w/w), was supplied by Southern Clay Products, Inc., in the sodium-ion-exchanged, fully exfoliated form. A Sorvall RC-5B Refrigerated Superspeed Centrifuge, equipped with a GSA rotor, was used at ~20°C to obtain a slightly turbid suspension containing the <0.046 μm-diameter fraction. The centrifuging conditions used to obtain this size fraction were calculated using the following equation:³¹

$$D^2 = C \frac{\eta \log_{10}(R/S)}{t (N^2) (\Delta s)} \quad (6)$$

in which D is the maximum particle diameter left in suspension, in μm; C is a constant having the value 6.30×10^{10} (this number is unitless other than conversion factors among various SI units and allows numbers with convenient units to be used in the equation); η is the viscosity of the medium, in Pa s (for water at 20°C, $\eta = 0.001005$ Pa s [equivalent units: $\text{kg m}^{-1} \text{s}^{-1}$]); R is the distance to the sediment from the center of the centrifuge; S is the distance to the meniscus of the suspension from the center of the centrifuge; t is the centrifugation time in minutes; N is the centrifuge speed in revolutions per minute; and Δs is the difference in density between the particles and the medium (1.502 g/mL for montmorillonite in water at 20°C). The suspension was centrifuged at 3050 rpm for 30 min and 8800 rpm for 38 min, with S

= 11.8 cm and $R = 16.5$ cm (using an estimated sediment thickness of 0.3 cm). Following centrifugation, the composition of the suspension was determined by drying three separate aliquots of the suspension, ~10 g each, in 20 mL glass scintillation vials for 24 h at 150°C. The vials were removed from the oven, immediately capped, cooled to room temperature, opened briefly to release the partial vacuum inside, and their mass determined. The suspension composition determined by this analysis [0.33% (w/w)] should be interpreted with caution, as it is strongly dependent upon the temperature used to dry the samples (clays lose mass incrementally up to temperatures in the hundreds of degrees Celsius³²) and to the subsequent treatment of the samples (after 5 h exposure to ambient temperature and humidity, the mass of the clay solids increased 15–18%, a change attributable to the sorption of atmospheric water³³). With the exception of one sample prepared by dripping this 0.33% suspension onto a silicon wafer and allowing the water to evaporate slowly, the montmorillonite suspension was diluted from 0.33% to 0.20% (w/w) with Milli-Q water before use.

7.6.2. Substrate Preparation. Silicon substrates [Wacker Siltronic, (100)-oriented, p-doped] were broken into ~1 x 2.5-cm pieces, swabbed with ethanol to remove silicon dust, and cleaned with a ~1:2 (v/v) solution of 30% H₂O₂ and concentrated H₂SO₄ for a minimum of 30 minutes (Caution: this “piranha solution” reacts violently with organic materials!), and were rinsed thoroughly with Milli-Q water and dried with a jet of nitrogen.

7.6.3. Film Preparation. Multilayered films were formed on silicon substrates by repeating a two-step adsorption cycle using the following conditions, unless stated otherwise. In the first step, the substrate was treated with several drops of an aqueous solution of PDDA of desired concentration, rinsed after approximately 5 s with Milli-Q water, and blown dry with N₂. In the second step, it was treated with

several drops of a 0.2% (w/w) aqueous dispersion of montmorillonite, rinsed after approximately 5 s, and blown dry. Substrates for the formation of films involving 5% or 1% PDDA were bare silicon wafers. For the formation of films involving 0.05% PDDA, however, substrates were silicon wafers that had been treated with one cycle of 1% PDDA and 0.2% montmorillonite to provide a surface more favorable than SiO₂ toward adsorption of the first layer of polymer from the dilute solution. The film of pure montmorillonite was prepared by placing a cleaned silicon wafer onto a glass microscope slide, then dripping several drops of a 0.33% (w/w) suspension of montmorillonite onto the wafer. To reduce the rate of evaporation of the water and also the contamination of the film by dust, a glass Petri dish was inverted over the wafer, with one edge of the glass slide protruding slightly from under the dish to allow some circulation of air.

7.6.4. Ellipsometry. The growth of the multilayered films was monitored under ambient conditions using optical ellipsometry (Rudolph Auto-EL III nulling ellipsometer). Measurements were made with HeNe laser light ($\lambda = 632.8$ nm) at an angle of incidence (ϕ) of 70°. The thickness of the overlayer on the elemental silicon substrates (either the bare native oxide of Si or the thickness of the oxide plus one or two cycles of 1% PDDA and 0.2% montmorillonite), was measured using an assumed refractive index, n , of 1.50 prior to adsorption of the multilayered film. Ellipsometric measurements of refractive index at multiple sites on samples 1–3 at their ultimate thickness all yielded the value 1.50; therefore, this value was used in calculations of multilayer thickness for all samples. The calculations were made with the further assumption that the samples comprised a single smooth film on a silicon substrate.

7.6.5. Adsorption Kinetics. Adsorption kinetics were studied ellipsometrically, by measuring the thickness of each component that had adsorbed during a chosen time period from a solution or suspension of chosen concentration. All adsorptions were

performed under ambient conditions. To minimize substrate effects, the silicon wafers used in this study were treated with two cycles of 1% PDDA and 0.2% montmorillonite, using 5-s treatments, before the adsorptions of interest. The combined thickness of the native oxide of silicon and the two-cycle film was determined ellipsometrically. Each substrate was then exposed to a PDDA solution of chosen concentration for a chosen period of time, and the thickness of the layer was measured. Each substrate was then exposed to a 0.2% montmorillonite suspension for the same period of time, and the thickness of the film was measured. For the treatments lasting 5 s or 30 s, the solution or suspension was *dripped* onto the substrates; for longer treatments, substrates were *immersed* horizontally, face down in the solution/suspensions. To avoid damage to the sample surfaces, these adsorptions were carried out in capped Teflon PFA vials that were laid on their sides, so that only the edges of the sample were in contact with the vial. Each substrate was used for one cycle only, and results were obtained in duplicate (or more) for each set of conditions.

7.6.6. *X-ray Diffractometry.* X-ray diffractometry was performed in $\theta/2\theta$ mode using a Philips APD 3720 powder diffractometer with monochromatized Cu K_{α} radiation ($\lambda = 1.54 \text{ \AA}$) operating at 45 kV and 30 mA. Data were obtained using a 0.05° step and 3 s/step collection time.

7.6.7. *X-Ray Omega Scans.* Omega scans were obtained on the (003) and (004) reflections of samples 1–3 using a modified Scintag X-ray diffractometer equipped with a Seifert goniometer, Bicron thallium-doped NaI scintillation detector and Philips source type PW2273/20 with monochromatized $\text{CuK}_{\alpha 1}$ radiation operating at 45 kV, 1.1 kW, and 25 mA. Data were obtained in 0.5° steps with a 10 s/step or 30 s/step collection time. To evaluate the instrumental response, curves were obtained under similar conditions in regions with no diffraction peaks, i.e., at 7° , 11° , and

14.5° θ on sample 2, and at 9° and 12.5° θ on a bare silicon wafer. All curve-fits were performed using Origin 3.5 (Microcal Software, Inc., Northampton, MA).

7.6.8. *X-ray Photoelectron Spectroscopy (XPS)*. The elemental composition of the films was determined using a Scienta ESCA-300 X-ray photoelectron spectrometer (Uppsala, Sweden) with monochromatized Al K α radiation from a rotating anode source. This technique is surface-sensitive, and as a result, only the material within ~10 nm of the surface was analyzed. The sample chamber was maintained at a pressure below 2×10^{-9} mbar. A single survey scan was taken for each sample in the binding energy range of 1100 eV–0 eV, using a take-off angle of 90°, pass energy of 150 eV, slit width of 0.8 mm, energy step of 0.3 eV, and integration time of 0.3 s. High-resolution spectra were obtained for all samples in the Al 2p $_{1/2,3/2}$, N 1s $_{1/2}$, Na 1s $_{1/2}$ and Cl 2p $_{1/2,3/2}$ regions, using a 0.1 eV step and 0.2 s integration time, with other conditions the same as for the survey scans. To obtain improved signal-to-noise characteristics, two scans were averaged for quantification of Al, and four scans for the other three elements. To compensate for any possible charging effects, the area under study was irradiated with an electron flood gun operated at 0.5 eV. Linear backgrounds were used for the quantifications, and elemental ratios were calculated using both Scofield sensitivity factors²¹ and sensitivity factors determined for this instrument.²² The sensitivity factor for Al was determined using sapphire (Al $_2$ O $_3$), and that for N was determined using several different nitrogen-containing polymers.²² Correction factors for attenuation of the photoelectrons were calculated assuming a perfect PDDA/montmorillonite lattice terminated with a montmorillonite sheet. Thus, the first Al-containing layer was assumed to be centered at a depth of 0.47 nm below the sample surface (one-half the sheet thickness of 0.94 nm); the first N-containing layer was assumed to be centered at a depth of 1.19 nm (one sheet of 0.94 nm and one-half the polymer layer thickness of 0.50 nm), and additional Al-

and N-containing layers were assumed to be centered at increments of 1.44 nm below these respective depths. Attenuation factors (I/I_0) for each Al or N layer were calculated using the formula²³

$$I/I_0 = \exp(-d/\lambda \sin\theta) \quad (7)$$

where d is the depth of an atomic layer below the surface, λ is the inelastic electron mean free path, and θ is the takeoff angle (90° for these scans). A value of 2.5 nm was used for λ , based on literature values for similar materials.³⁴ Summing the attenuation factors for the first eight unit cells gave a result of 1.874 for Al and 1.405 for N; the ratio of these two numbers gave an attenuation correction factor (1.334) by which the raw Al : N ratios were divided in order to obtain corrected Al : N ratios. Extending the calculations to include the first twelve unit cells (rather than the first eight) did not affect the calculated value of the attenuation correction factor.

Acknowledgements. We gratefully acknowledge the extensive technical assistance of T. Siegrist (Bell Laboratories, Lucent Technologies) in obtaining the omega scans. We further acknowledge helpful discussions with Prof. G.W. Simmons, technical assistance from A.C. Miller with the x-ray photoelectron spectroscopy, and support of the Scienta ESCA-300 Laboratory by Lehigh University. Optical and scanning-electron microscopy were performed by B.A. MacNeill. Funding for this work was generously provided by Southern Clay, Inc. E.R.K. acknowledges Ph.D. fellowships from AT&T Bell Laboratories and Lehigh University.

7.7 References and Notes

1. *Applications of Thin-Film Multilayered Structures to Figured X-Ray Optics*; Marshall, G.F., Ed.; SPIE Proceedings 563; SPIE—The International Society for Optical Engineering: Bellingham, WA, 1985. Katz, H.E.; Scheller, G.; Putvinski,

- T.M.; Schilling, M.L.; Wilson, W.L.; Chidsey, C.E.D. *Science*, **1991**, *254*, 1485.
- Li, D.; Ratner, M.A.; Marks, T.J.; Zhang, C.; Yang, J.; Wong, G.K. *J. Am. Chem. Soc.* **1990**, *112*, 7389.
2. Kepley, L.J.; Sackett, D.D.; Bell, C.M.; Mallouk, T.E. *Thin Solid Films* **1992**, *208*, 132. Katz, H.E.; Narvaez, P.; Harley, E.R. *Thin Solid Films* **1994**, *252*, 4. Kaneko, F.; Shibata, M.; Inaba, Y.; Kobayashi, S. *Thin Solid Films* **1989**, *179*, 121.
 3. Ungashe, S.B.; Wilson, W.L.; Katz, H.E.; Scheller, G.R.; Putvinski, T.M. *J. Am. Chem. Soc.* **1992**, *114*, 8717. Keller, S.W.; Johnson, S.A.; Brigham, E.S.; Yonemoto, E.H.; Mallouk, T.E. *J. Am. Chem. Soc.* **1995**, *117*, 12879.
 4. Kleinfeld, E.R.; Ferguson, G.S. *Science* **1994**, *265*, 370. Ferguson, G.S.; Kleinfeld, E.R. *Advanced Mater.* **1995**, *7*, 414.
 5. Schmitt, J.; Grünewald, T.; Decher, G.; Pershan, P.S.; Kjaer, K.; Lösche, M. *Macromolecules* **1993**, *26*, 7058.
 6. Byrd, H.; Whipps, S.; Pike, J.K.; Ma, J.; Nagler, S.E.; Talham, D.R. *J. Am. Chem. Soc.* **1994**, *116*, 295.
 7. Kleinfeld, E.R.; Ferguson, G.S. *Chem. Mater.* **1996**, *8*, 1575.
 8. Kleinfeld, E.R.; Ferguson, G.S. Manuscript in preparation.
 9. For elucidation of the structure of PDDA, see: Masterman, C.; Dando, N.R.; Weaver, D.G.; Seyferth, D. *J. Polymer Sci. B: Polymer Phys.* **1994**, *32*, 2263, and references therein.
 10. MacEwan, D.M.C. *Trans. Faraday Soc.* **1948**, *44*, 349.
 11. The shallow-angle shoulder on the (001) reflections in the patterns of samples **1** and **2** may be attributable to the incorporation of a small amount of very poorly ordered material. Alternatively, it may be due to an instrumental artifact—this feature did not occur in patterns of these or similar samples when

two other diffractometers were used.

12. Reynolds, R.C. *Acta Crystallogr.* **1968**, A24, 319. Trunz, V. *Clays Clay Miner.* **1976**, 24, 84. Ross, M. *Z. Kristallogr.* **1968**, 126, 80.
13. Reynolds, R.C.; Hower, J. *Clays Clay Miner.* **1970**, 18, 25.
14. Grim, R.E. *Clay Mineralogy*; McGraw-Hill: New York, 1968, p 157.
15. Warren, B.E. *X-Ray Diffraction*; Dover: New York, 1990.
16. a) Drits, V.A.; Tchoubar, C. *X-Ray Diffraction by Disordered Lamellar Structures*, Springer-Verlag: New York, 1990, pp 21–22. b) Kodama, H.; Gatinéau, L.; Méring, J. *Clays Clay Miner.* **1971**, 19, 405.
17. Vaia, R.A.; Jandt, K.D.; Kramer, E.J.; Giannelis, E.P. *Chem. Mater.* **1996**, 8, 2628.
18. Ref 14, p 262.
19. For distinctions between the two techniques, see: Blanton, T.N.; Lelental, M.; Barnes, C.L. *Physica C* **1991**, 184, 119.
20. Geer, R.E.; Shashidhar, R.; Thibideaux, A.F.; Duran, R.S. *Phys. Rev. Lett.* **1993**, 71, 1391. Geer, R.E.; Shashidhar, R. *Phys. Rev. E* **1995**, 51, R8.
21. Scofield, J.H. *J. Electron Spectrosc.* **1976**, 8, 129.
22. Miller, A.C., Lehigh University, personal communication.
23. Brunner, J.; Zogg, H. *J. Electron Spectrosc. Rel. Phenom.* **1974**, 5, 911.
24. Deer, W.A.; Howie, R.A.; Zussman, J. *An Introduction to the Rock-Forming Minerals*, 2nd ed.; Wiley: New York, 1992; pp 371–372.
25. Ref. 14, pp 83–84.
26. van Olphen, H. *An Introduction to Clay Colloid Chemistry*, 2nd ed.; Wiley-Interscience: New York, 1977; pp 93–95.
27. See, for example: Parsons, D.; Harrop, R.; Mahers, E.G. *Colloids Surfaces* **1992**, 64, 151.

28. Marra, J.; van der Schee, H.A.; Fleer, G.J.; Lyklema, J. In *Adsorption from Solution*; Ottewill, R.H.; Rochester, C.H.; Smith, A.L., Eds.; Academic: New York, 1983; p 245.
29. Denoyel, R.; Durand, G.; Lafuma, F.; Audebert, R. *J. Colloid Interface Sci.* **1990**, *139*, 281.
30. Evidence has been presented that for adsorption of polycations onto montmorillonite, the conformation of the adsorbed chains is kinetically frozen in upon initial adsorption due to a high enthalpy of displacement of the adsorbed polymer segments.²⁹ Nonetheless, since the identity of the polymer was different in our experiments, and since the polymer solutions we used were significantly more concentrated than those used in the cited work, we must consider the possibility that in our system, subtle but meaningful changes in the character of the adsorbed layer may have occurred during extended contact time with the polymer solutions.
31. Jackson, M.L. *Soil Chemical Analysis—Advanced Course*; Published by the Author, Department of Soil Science, University of Wisconsin, Madison, WI 53706, Ed. 2, pp 127, 129, 144, 146. Note that in the discussion of the angle-head centrifuge on p 144 and in Figure 3-8, p 146, *R* and *S* are interchanged relative to their definitions on pp 127, 129. The author presents on p 144 a discussion of turbidity currents in angle-head centrifuges. If the calculations are modified to include turbidity currents (in this case, $R = 12.1$ cm, $S = 11.8$ cm), the clay fraction left in suspension after centrifugation is calculated as <0.0125 μm . This number seems less credible, if the slight turbidity of the centrifuged suspension is any indication of the particle size.
32. Ref. 14, p 283.

33. Mooney, R.W.; Keenan, A.G.; Wood, L.A. *J. Am. Chem. Soc.* **1952**, *74*, 1367, 1371.
34. Seah, M.P.; Dench, W.A. *Surface Interface Anal.* **1979**, *1*, 2.

Formation of Films from Sheet Silicates and Oxy-Aluminum Species

8.1 Abstract

Multilayered films were formed by the alternate treatment of primed silicon substrates with an aqueous solution of an aluminum polyoxycation, $[\text{Al}_{13}\text{O}_4(\text{OH})_{24}(\text{H}_2\text{O})_{12}]^{7+}$ (Al_{13}), and an aqueous suspension of an exfoliated anionic sheet silicate (Laponite RD or montmorillonite). Regular ellipsometric growth was observed with both silicate minerals. The films that formed, however, were laterally non-uniform in thickness, and growth per cycle appeared to correlate negatively with the concentration of the polyoxycation in the solutions that had been used to form the films. The XRD pattern of a 30-cycle film of Al_{13} and montmorillonite revealed that material with a d-spacing of ~ 2 nm was present, as would be expected for Al_{13} -pillared montmorillonite, but that the level of structural order in the film was not as high as had been observed for films made from an organic polyelectrolyte and sheet silicate. The difficulties in forming uniform and well-ordered films from Al_{13} and sheet silicates are attributed to an insufficient chelate effect in this system.

8.2 Introduction

Chapter 1 briefly describes attempts to form multilayered films from sheet silicates and monomeric cations (Ca^{2+} and Al^{3+}). One additional attempt was made to form films with a monomeric cation, but this time one with a far higher charge: the aluminum polyoxycation $[\text{Al}_{13}\text{O}_4(\text{OH})_{24}(\text{H}_2\text{O})_{12}]^{7+}$. This ion, depicted schematically in Figure 8.1, has a diameter of 0.43 nm,¹ and consists of a central aluminum ion tetrahedrally coordinated to oxygen, surrounded by twelve aluminum ions octahedrally coordinated to oxygen in an edge-sharing arrangement.² Mallouk et al.

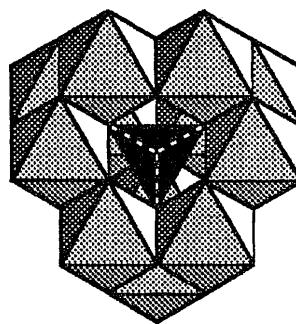


Figure 8.1. Schematic diagram of the structure of the $[Al_{13}O_4(OH)_{24}(H_2O)_{12}]^{7+}$ polyoxycation, which has a radius of 0.43 nm.¹ A central Al^{3+} ion tetrahedrally coordinated to oxygen is surrounded by twelve Al^{3+} ions octahedrally coordinated to oxygen. The octahedra are in an edge-sharing arrangement.

had reported the formation of multilayered films using alternate treatments with this polyoxycation ("Al₁₃") and single exfoliated sheets of α -Zr(HPO₄)₂,³ we hypothesized that the use of this cation in our alternate adsorption scheme would optimize the structural order of a polycation/silicate multilayered film.

8.3 Results and Discussion

8.3.1. Preparation of Starting Materials and Growth of Films. Solutions of Al₁₃ were prepared by dropwise neutralization of a 0.50 M aqueous solution of AlCl₃ (typically 20–50 mL) with an equivolume 0.50–0.52 M aqueous solution of Na₂CO₃, followed by curing the reaction mixture at 50–56°C for a chosen period of time (0 – 60 min). Different extents of neutralization were used, and are reported below by their Na:Al ratios (2.0:1 – 2.4:1). The composition of the solutions was quantified by ²⁷Al nuclear magnetic resonance (NMR) spectrometry. Whereas aluminum ions in highly symmetric environments [Al(H₂O)₆³⁺, Al(OH)₄⁻, and the central, tetrahedrally coordinated Al³⁺ ion in Al₁₃] give rise to sharp peaks in NMR spectra, aluminum ions in environments of lower symmetry ([Al(H₂O)₅OH]²⁺, [Al₂(OH)_x]^{(6-x)+}, amorphous polymeric material,^{4,5} and the outer, octahedrally coordinated Al³⁺ ions in Al₁₃) give rise to peaks broadened to the point of being nearly undetectable.⁶ This effect is associated with the quadrupolar nature of the ²⁷Al nucleus: an exchange of energy between the ellipsoidal nucleus and its surroundings can occur as the nucleus rotates inside of the electric field gradient that results from its asymmetric coordination sphere. This exchange of energy provides an efficient relaxation pathway.⁷ If relaxation is sufficiently rapid (occurring within the period of time between the pulse and the beginning of data acquisition), the signal will not be detected at all. All Al₁₃ solutions we used for film formation contained Al(H₂O)₆³⁺, Al₁₃, and invisible material ("Al_i"). The approximate concentration of the invisible species was

calculated by subtracting the sum of the concentrations of the species that were visible by NMR from the known concentration of Al^{3+} in all forms, 0.25 M.

When aqueous suspensions of Laponite or montmorillonite at a concentration of 0.2% (w/w) were used directly, very poor film growth was observed; film growth became regular only when the pHs of these silicate suspensions were lowered. Laponite suspensions were partially neutralized (from pH 9.1 to pH 8.2 ± 0.2) by the addition of acetic acid to a final concentration of 0.0008 M.⁸ Aqueous montmorillonite suspensions were centrifuged, then dialyzed to reduce their pH (from pH 9.7 to pH 8.6 ± 0.1). Films were formed by alternately treating a substrate for 60 s with an Al_{13} solution and 5 s with one of the partially neutralized silicate suspensions. In between treatments, the films were rinsed with dilute acidic solutions (acetic acid at pH 4 for films made with Laponite,⁸ hydrochloric acid at pH 4 for films made with montmorillonite) and blown dry with N_2 . Substrates for these films were silicon wafers that had been treated with two cycles of 1% poly(diallyldimethylammonium chloride), PDDA, and the silicate of interest.

8.3.2. Characteristics of Silicate/ Al_{13} Systems. In attempting to optimize conditions for the formation of Al_{13} /silicate films, we noted two disturbing trends. First, no film prepared to a sufficient thickness to display interference colors had a uniform appearance, suggesting that irregularities in film formation were occurring. This observation was confirmed by ellipsometric measurements showing lateral non-uniformity in film thickness. Second, an inverse correlation apparently existed between growth per cycle and the concentration of the polyoxycation. For example, in the Al_{13} /Laponite system, an unfiltered solution of Al_{13} (neutralization ratio of 2.1:1), having a concentration of Al_{13} of 0.0094 M, led to growth of 0.9 nm per cycle (from the slope of the linear least-squares fit to the data, Figure 8.2, circles), whereas a solution prepared to a neutralization ratio of 2.0:1, having a concentration of Al_{13}

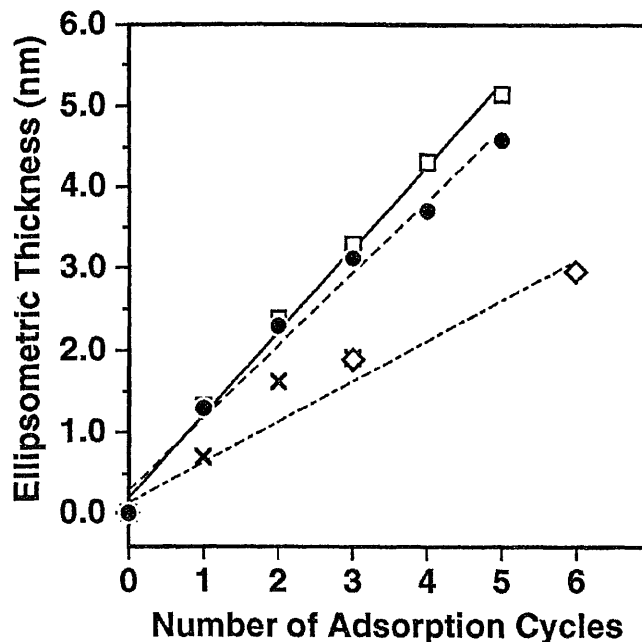


Figure 8.2. Ellipsometric growth of multilayered films formed from partially neutralized Laponite suspensions and Al_{13} solutions. The Al_{13} solutions were prepared under different conditions: circles, slow neutralization to a Na:Al ratio of 2.1:1, with no filtration; squares, rapid neutralization to a ratio of 2.1:1, with no filtration; diamonds, slow neutralization to a ratio of 2.0:1, followed by filtration. The data points represent averages of three measurements taken on each of two samples, except for the diamonds, which represent an average of three measurements taken on a single sample. Data from a duplicate of the latter experiment under identical conditions (simply obtained at different intervals) are represented by crosses. Lines shown in the graph are linear least-squares fits to the data represented by circles, squares, and diamonds.

of 0.0122 M, led to growth of 0.5 nm per cycle under otherwise identical conditions (Figure 8.2, diamonds and crosses). This behavior suggested that growth was positively correlated with a factor other than the concentration of Al_{13} . In the solutions described above, the concentrations of the invisible species were 0.10 M and 0.05 M, respectively, suggesting that the correlation might be to one or more of these species instead.

To test this possibility, while eliminating as a variable the neutralization ratio of the Al_{13} solutions (and therefore their pH), we prepared an Al_{13} solution having the same neutralization ratio as one of the cases above (2.1:1), but having a higher concentration of invisible species. This solution was prepared by increasing the neutralization rate and decreasing the curing time, and its pH (3.7) was the same as that of the solution prepared slowly (3.8), to within experimental error. The rapidly prepared, unfiltered solution, having a concentration of Al_{13} of 0.0037 M and a concentration of Al_i of 0.175 M led to growth of 1.0 nm per cycle (Figure 8.2, squares). Although greater growth per cycle was again (reproducibly) obtained from a solution having a lower concentration of Al_{13} , the difference in the growth observed from the two solutions neutralized to 2.1:1 was not sufficient to allow us to reach an unambiguous conclusion about whether growth correlated with the concentration of Al_i . For example, significant differences in relative humidity on the two days these samples were prepared could most likely have caused an even larger difference in growth patterns than those shown in the two upper traces of Figure 8.2, as detailed in Chapter 5.⁹ The Al_{13} /montmorillonite system also showed an apparent negative correlation between the concentration of Al_{13} and the corresponding film growth per cycle: an Al_{13} solution (neutralization ratio of 2.3:1) having a concentration of Al_{13} of 0.010 M and a concentration of Al_i of 0.10 M gave very regular growth of 2.4 nm/cycle in the first 30 cycles (from the slope of the linear least-squares fit to the

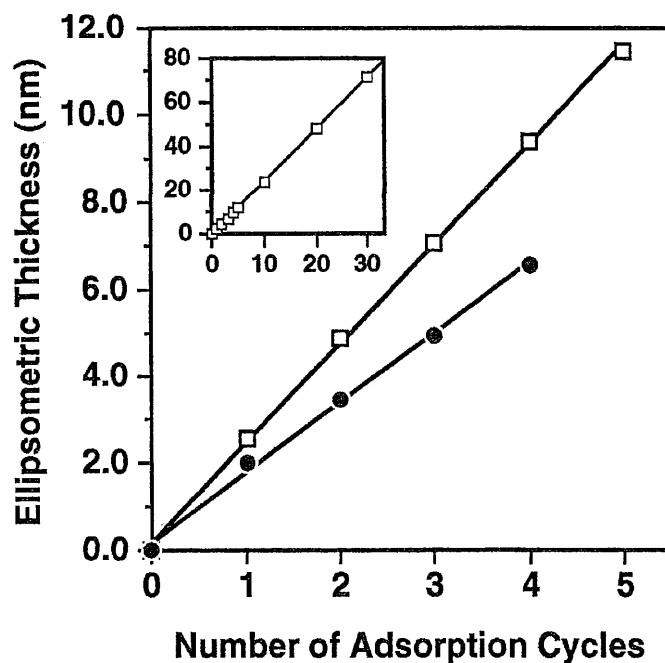


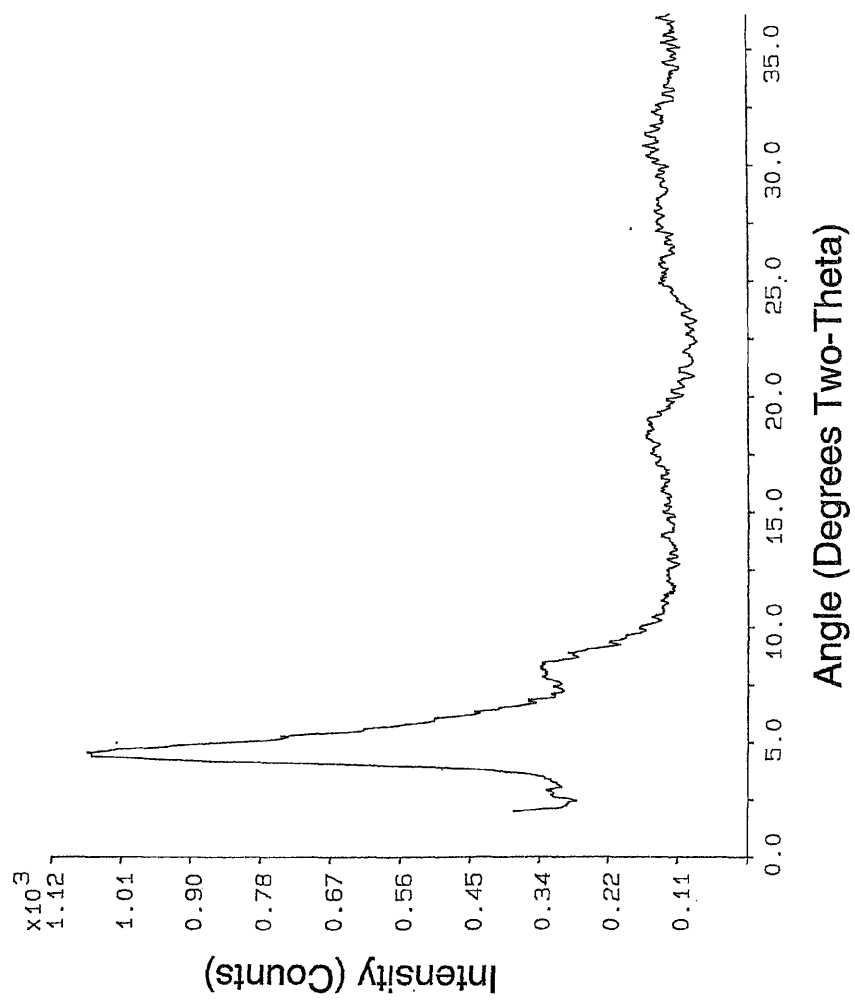
Figure 8.3. Ellipsometric growth of multilayered films formed from dialyzed montmorillonite suspensions and Al_{13} solutions. The Al_{13} solutions were prepared under different conditions: squares, neutralization to a (Na:Al) ratio of 2.3:1; circles, neutralization to a ratio of 2.0:1. Both neutralizations were performed slowly, and both solutions were subsequently filtered. The squares represent averages of three data points taken on each of two samples; the circles represent averages of three data points taken on one sample only. The inset shows growth of a thicker film from the 2.3:1 solution. The squares in the inset correspond to averages of three points obtained on a single sample. Linear least-squares fits to the data are shown.

data; see Figure 8.3, squares), whereas an Al_{13} solution (neutralization ratio of 2.0:1) having a concentration of Al_{13} of 0.013 M and a concentration of Al_1 of 0.040 M gave regular growth of 1.6 nm/cycle in the first four cycles (Figure 8.3, circles).

8.3.3. Structural Characterization of Al_{13} /Silicate Films. The x-ray diffraction pattern of a 30-cycle film formed from Al_{13} (neutralization ratio of 2.3:1) and montmorillonite, 79 nm in thickness, is shown in Figure 8.4. A (001) peak was present having the d-spacing expected for a pillared clay ($2\theta = 4.5^\circ$, $d = 1.96$ nm),¹⁰ and the feature at $\sim 8.3^\circ$ 2θ ($d = 1.1$ nm) may be a (002) reflection, if the apparent position of this peak has been shifted from the expected position (8.8°) due to a partial overlap with the (001) reflection. Features at higher angle appeared to be associated with a lattice having a lower d-spacing, perhaps simply Al-montmorillonite, but are too broad and weak to assign with certainty. The lack of distinct higher-order reflections associated with the pillared-clay lattice, as well as the breadth of the (001) peak itself (1.35° , indicating a domain size of 6.2 nm), suggest that this film was not among our best-ordered (see Chapter 7), a result inconsistent with the concept of the film having been formed under well-defined conditions by the adsorption of discrete Al_{13} ions and silicate sheets.

8.3.4. Analysis of Difficulties with this System. The charge on the Al_{13} cation is extremely sensitive to pH, being fully preserved at [+7] below pH 6 but reduced almost to [0] by pH 7.¹¹ This fact is consistent with our observations that film growth was extremely poor and irreproducible when in the non-optimized systems the silicate suspensions had been used without neutralization, having pHs greater than 9. The pH of the suspensions was later reduced, as explained earlier (Laponite to pH 8.2 ± 0.2 and montmorillonite to 8.6 ± 0.1), but silicate suspensions flocculate below a certain pH, so there was a limit to the extent to which their pHs could be lowered. The pHs of the silicate suspensions used were sufficiently high, in fact, to eliminate

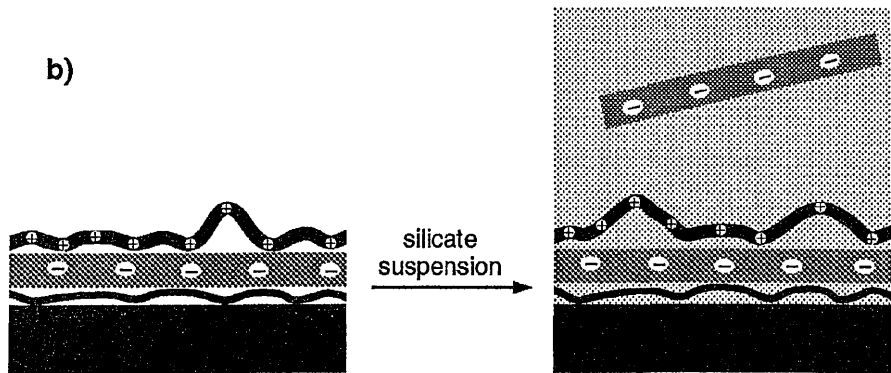
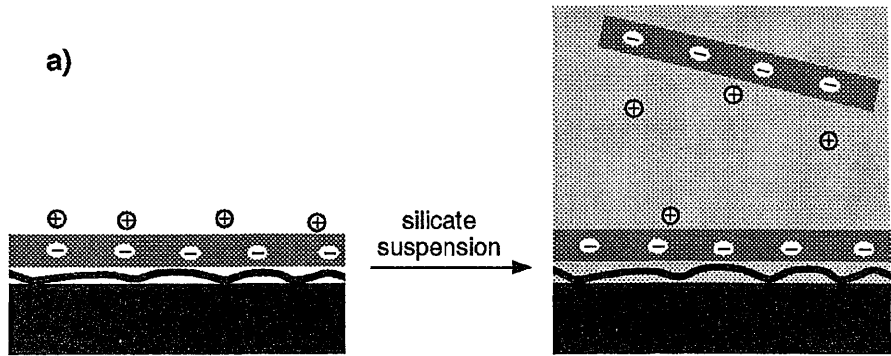
Figure 8.4. The x-ray diffraction pattern of a film prepared by 30 cycles of treatments with an Al_{13} solution (neutralization ratio of 2.3:1) and a dialyzed montmorillonite suspension [0.2% (w/w)]. The prominent peak at $4.5^\circ 2\theta$, presumably a (001) reflection, indicates a lattice spacing of 1.96 nm. The feature at $\sim 8.3^\circ 2\theta$ ($d = 1.1$ nm) may be a (002) reflection whose position has been shifted to shallow angle by its overlap with the broad (001) reflection. The features at $\sim 18^\circ 2\theta$ and $\sim 25^\circ 2\theta$ are too broad and weak to be assigned with certainty, but could be (003) and (004) reflections from a lattice with a d-spacing of ~ 1.45 nm.



almost entirely the positive charge of the Al_{13} species. The aqueous coordination chemistry of aluminum is extremely complex, and is a matter of some controversy;¹² an equilibrium among several species typically exists under any given conditions. Other than the Al_{13} cation, species that may have been present under the conditions we used included monomeric species (e.g., $[Al(H_2O)_6]^{3+}$, $[Al(H_2O)_5OH]^{2+}$) and dimeric species (e.g., $[Al_2(OH)_x]^{(6-x)+}$) as well as amorphous polymeric species.^{4,5}

One final difficulty with this system, relative to the more successful systems described elsewhere in this thesis, may be that it did not take full advantage of the "chelate effect," as described in Chapter 1. Treatment of a silicate-terminated sample with an " Al_{13} " solution allows any or all of the cationic species that are present in solution to adsorb to the anionic silicate surface. Small species may, in addition, intercalate into the lattice below the surface. The smaller species would be associated with one, or at most, two anionic sites on the clay sheet, whereas polymeric aluminum oxycations have the ability to span several anionic sites.^{4,5} Upon rinsing this surface or treating it with a silicate suspension, therefore, the smaller species may be displaced by protons from the contacting water, while the polymeric species would be more difficult to displace from the surface due to a "surface-chelate" effect, as depicted schematically in Figure 8.5. Under appropriate conditions, adsorption of the polymeric, amorphous material should invert the surface charge, allowing more silicate to adsorb in a subsequent step, and providing for the regular growth that was observed. Upon these subsequent treatments with the highly basic silicate suspensions, however, it is conceivable that the now-intercalated amorphous polymeric material may decompose into smaller species (monomers, dimers, tridecamers), giving rise to a multilayered film with unit cells having dimensions characteristic of pillared silicate or Al-silicate. While Mallouk and coworkers reported regular growth of multilayers containing the Al_{13} cation, they did

Figure 8.5. Schematic illustration of the proposed "surface chelate effect." In (a), each adsorbed Al_{13} ion (\oplus) is, due to its limited size, most likely associated with only one or two negative sites on the silicate sheet. These ions are therefore readily lost to a silicate suspension to which the sample is exposed in a subsequent step. For entropic reasons, few of the ions that leave the surface are likely to re-adsorb. In contrast, in (b), an amorphous polymeric aluminum oxyanion is bound to the silicate sheet through multiple points of attachment. Although the conformation of this adsorbed molecule may change, with individual sites adsorbing or desorbing from the silicate sheet, the large number of polymer segments that would have to desorb simultaneously in order for the entire chain to be lost makes such an event unlikely. In both (a) and (b), monovalent cations or anions needed for charge neutrality (e.g., Na^+ , Cl^-) have been omitted for clarity.



not report structural characterization of the films.³ In addition, the “Al₁₃” solution used in the formation of their Al₁₃/α-Zr(HPO₄)₂ films had been neutralized to a pH of 7 with tetra-*n*-butylammonium hydroxide, which should have been sufficient to deprotonate any Al₁₃ present¹¹ but which may have allowed formation of the polymeric material that could lead to growth in their and our systems.

8.4 Experimental Methods

8.4.1. Materials. All water used in this work was Milli-Pore Milli-Q water, with a resistivity of at least 15 MΩ-cm. Chemicals used in the synthesis of the Al₁₃ polyoxycation, AlCl₃•6H₂O (Aldrich, 99%) and Na₂CO₃ (Thorn Smith, Anhydrous, Primary Standard, or Aldrich, anhydrous, 99.5+%), were used as received. Laponite RD was provided as a free-flowing powder and montmorillonite as a sodium-ion-exchanged suspension (0.36% w/w), both by Southern Clay, Inc. Stock solutions of Laponite RD [0.5% (w/w)] were prepared as described in Chapter 1. To form partially neutralized 0.2% (w/w) Laponite suspensions, the following components were mixed (in order): 4.0 mL H₂O, 4.0 mL 0.5% (w/w) Laponite RD suspension, and 1.0 mL 0.0040 M acetic acid. After several hours, a second 1-mL aliquot of 0.0040 M acetic acid was added,¹³ and the suspension was allowed to equilibrate unstirred overnight. The pH of these suspensions was 8.2 ± 0.2, compared to non-neutralized Laponite RD solutions [0.2% (w/w)], which have a pH of 9.1. The montmorillonite suspension was prepared by centrifugation of the montmorillonite, by the method described in Chapter 1, followed by dialysis to reduce its pH (~24 h, cellulose membrane) to a pH of 8.6 ± 0.1. The solids content of the suspension following dialysis was 0.2%.

8.4.2. Synthesis of the Al₁₃ Polyoxycation.^{4,14} The Al₁₃ polyoxycation was synthesized by the neutralization, with stirring, of 20 – 50 mL of an aqueous solution

of 0.500 M AlCl_3 by dropwise addition of an aqueous solution of Na_2CO_3 of the same volume, and of the concentration (0.50 – 0.52 M) necessary to effect the desired degree of neutralization (expressed as the Na:Al ratio of the final solution). Upon completion of the addition, the reaction solutions either were used as is, or were “cured” at 50–56°C for 7 – 60 min to aid in formation of the desired cation. Some solutions were then filtered through a 4 – 8 μm filter to remove large particulate matter. Quantification of solution composition was conducted following all these treatments.

8.4.3. NMR Spectrometry. The concentrations of $\text{Al}(\text{H}_2\text{O})_6^{3+}$ and Al_{13} in the reaction solutions were measured by ^{27}Al nuclear magnetic resonance spectrometry. A capillary containing the $\text{Al}(\text{OH})_4^-$ ion was used as an internal standard. Because this aluminum species is present only in solutions of elevated pH,¹² it was not found in our reaction solutions (pH 3.5–4.1). The reference $\text{Al}(\text{OH})_4^-$ solution was prepared by mixing 0.5 mL of 0.5 M AlCl_3 (aq) and 2.5 mL of 1 M NaOH (aq). The exact concentrations and ratio of these two solutions were not critical. A glass capillary tube was filled by syringe to a height of 3 – 4 cm with this solution, and was then sealed by melting the glass with a Bunsen burner flame 2–3 cm above the liquid level. The capillary was placed in a 5-mm NMR tube filled with a 0.0500 M solution of AlCl_3 , a spectrum was obtained, and, following baseline correction, the peaks due to $\text{Al}(\text{H}_2\text{O})_6^{3+}$ ($\delta = 0$ ppm) and $\text{Al}(\text{OH})_4^-$ ($\delta = 79.8 - 79.9$ ppm) were integrated. The same capillary was then rinsed, dried, and placed in an NMR tube containing the reaction solution to be analyzed. A sample NMR spectrum of a reaction solution containing a capillary is shown in Figure 8.6. Baseline correction and integration of the peaks in the spectra that were due to $\text{Al}(\text{H}_2\text{O})_6^{3+}$, $\text{Al}(\text{OH})_4^-$, and the central, tetrahedrally coordinated Al^{3+} ion in Al_{13} ($\delta = 62.7 - 62.8$ ppm) thus allowed quantification of the concentrations of the various Al species in the reaction

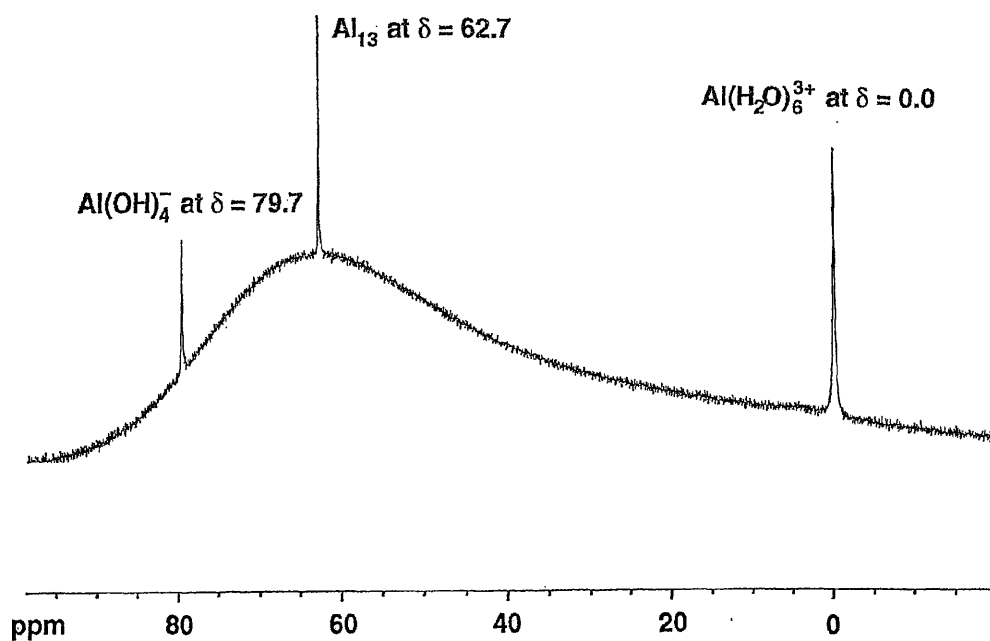


Figure 8.6. The ^{27}Al NMR spectrum of an Al_{13} polyoxycation solution containing an external aqueous $\text{Al}(\text{OH})_4^-$ reference. Resonances corresponding to the various species are labelled. The broad feature centered at $\delta \approx 65$ ppm is attributed to aluminum species present in the spectrometer itself, as it was also present in the spectrum of a tube of pure water.

solution. Because the overall concentration of aluminum ions in all species was nominally known to be 0.25 M (“nominally” because of potential losses in volume or solids associated with curing and/or filtration), the concentrations of aluminum ions in the monomeric and tridecameric ions could be subtracted from this value to obtain an estimate of the concentration of ions present in an invisible form,^{4,5} denoted $[Al_i]$. The NMR spectra were obtained using a Bruker AMX 360 spectrometer. On this 8.4-T instrument, spectra were obtained at 93.84 MHz using a sweep width of 17.9 kHz, and collecting 8192 points per scan. The average of 128 scans was typically taken, with an acquisition time per scan of 0.23 s and delay of 0.01 s, for a total time between pulses of 0.24 s. An experiment in which the delay was lengthened demonstrated that saturation of the ^{27}Al nuclei was not occurring under these conditions.

8.4.4. Film Formation from Al_{13} Polyoxylation Solutions and Silicate Suspensions.

The substrates used in this chapter were prepared by treating a clean silicon wafer with two cycles (5-s treatments) of 1% (w/w) PDDA and the partially neutralized silicate suspension that was to be used in formation of the film. A two-step cycle was then repeated to form a multilayered film. In the first step, the sample was treated for 60 s with the Al_{13} solution, and in the second step it was treated for 5 s with the silicate suspension. Following each step, the sample was thoroughly rinsed with an acidic aqueous solution (dilute acetic acid, pH 4, for the Laponite-based films;⁸ dilute HCl, pH 4, for the montmorillonite-based films), and was blown dry with a jet of nitrogen.

Acknowledgements. We thank Prof. J.E. Roberts and D.J. Wang for helpful discussions of the ^{27}Al NMR spectrometry. We gratefully acknowledge financial support and donations of Laponite RD and montmorillonite from Southern Clay, Inc.

E.R.K. acknowledges fellowships from AT&T Bell Laboratories and Lehigh University.

8.5 References and Notes

1. Rausch, W.V.; Bale, H.D. *J. Chem. Phys.* **1964**, *40*, 3391.
2. Johansson, G.; Lundgren, G.; Sillén, L.G.; Söderquist, R. *Acta Chem. Scand.* **1960**, *14*, 769. Johansson, G. *Acta Chem. Scand.* **1960**, *14*, 771.
3. Keller, S.W.; Kim, H.-N.; Mallouk, T.E. *J. Am. Chem. Soc.* **1994**, *116*, 8817. For an additional, but brief, account of the use of various aluminous species to invert the surface charge of glass, see: Iler, R.K. *J. Colloid Interface Sci.* **1966**, *21*, 569.
4. Bottero, J.Y.; Cases, J.M.; Fiessinger, F.; Poirier, J.E. *J. Phys. Chem.* **1980**, *84*, 2933.
5. Axelos, M.A.V.; Tchoubar, D.; Jullien, R. *J. Physique* **1986**, *47*, 1843.
6. Akitt, J.W.; Elders, J.M. *J. Chem. Soc. Dalton Trans.* **1988**, 1347.
7. Akitt, J.W. *NMR and Chemistry: An Introduction to the Fourier Transform–Multinuclear Era*, 2nd ed.; Chapman and Hall: New York, 1983; pp 68–71.
8. Dilute, aqueous acetic acid was used for partial neutralization of the Laponite suspensions, rather than hydrochloric acid, because we had determined that the pH could be lowered further, while avoiding flocculation, when acetic acid was used. For consistency, a dilute aqueous solution of this same acid was used for the rinses in the preparation of films involving Laponite.
9. Kleinfeld, E.R.; Ferguson, G.S. *Chem. Mater.* **1995**, *7*, 2327.
10. Bottero, J.Y.; Bruant, M.; Cases, J.M. *Clay Minerals* **1988**, *23*, 213.
11. Furrer, G.; Ludwig, C.; Schindler, P.W. *J. Colloid Interface Sci.* **1992**, *149*, 56.
12. Orvig, C. In *Coordination Chemistry of Aluminum*; Robinson, G.H., Ed.; VCH:

New York, 1993.

13. In preliminary experiments to determine the extent to which the Laponite suspension could be neutralized while avoiding flocculation, we found that, under otherwise identical conditions, addition of 2.0 mL of 0.0040 M acetic acid in one aliquot resulted in flocculation of the suspension, but addition of the same volume of acid in two aliquots separated by several hours preserved the quality of the suspension. This difference is attributed to slow exchange of protons at the clay surface.
14. Akitt, J.W.; Farthing, A. *J. Chem. Soc. Dalton* **1981**, 1617.

Conclusions

9.1 Concluding Remarks

Synthetic chemists have traditionally focused on the preparation of small molecules, often exploiting kinetic control for the formation of desired products. In contrast, solid-state chemists have focused on the preparation of new phases of interest under thermodynamic conditions. The challenge of bridging these two fields, of assembling molecules into two-dimensional and three-dimensional structures while preserving the functional and often metastable nature of the components, has defined the interests of materials chemists.

In a pioneering work in 1966, Iler introduced the concept of forming multilayered films via electrostatic interactions, i.e., by treating a surface alternately with polyvalent precursors having opposite charge.¹ The film precursors he chose were anionic colloidal silica (spheres ~ 100 nm in diameter) and cationic alumina fibrils (cylinders ~5–6 nm in diameter and of extended but unspecified length). This work was extended in the early 1990s to the formation of films from linear organic polyelectrolytes by Decher and co-workers.² Films formed by both of these methods grow regularly, but the degree of structural order they exhibit is limited by interpenetration of the two components. We introduced the use of an anionic sheet silicate mineral, or clay, in the formation of multilayered films by electrostatic interactions.³ The sheets possess a large aspect ratio, being over 25 nm in diameter but only 0.93 nm in thickness. Films formed by alternately adsorbing such sheets and a linear cationic polyelectrolyte onto various surfaces possessed a degree of structural order unprecedented among films formed by adsorption from solution onto flat substrates, as a result of the ability of the sheets not only to limit interpenetration by the polyelectrolyte, but also to patch over the defects that are a natural part of film formation by this technique. Preparative methods and the general properties of

the resulting films were discussed in chapters 2 and 3, while chapter 4 delved into the ability of the films to heal defects. Chapter 7 detailed a study we performed to begin to elucidate the factors that result in an optimal degree of structural order in the films. Chapter 8 presented evidence in support of the hypothesis that the assembly of films involving sheet silicates relies upon a surface chelate effect.

The development of an adsorption scheme involving cationic polyelectrolytes and anionic sheet minerals created the possibility of the preparation of films for a myriad of applications, due to its flexibility with respect to the incorporation of a variety of cationically and anionically charged precursors. Studies we performed investigated the films' potential usefulness as humidity sensors (Chapter 5) and as anti-reflective coatings (Chapter 6), whereas Mallouk and co-workers have addressed the use of the films in microelectronic and photosynthetic applications.⁴ The potential usefulness of similar films toward a variety of possible applications seems to be limited only by the imaginations of the researchers who pursue them.

9.2 References and Notes

1. Iler, R.K. *J. Colloid Interface Sci.* **1966**, *21*, 569.
2. Decher, G.; Eßler, F.; Hong, J.-D.; Lowack, K.; Schmitt, J.; Lvov, Y. *Polym. Prepr.* **1993**, *34(1)*, 745. Lvov, Y.; Haas, H.; Decher, G.; Möhwald, H.; Kalachev, A. *J. Phys. Chem.* **1993**, *97*, 12835.
3. Kleinfeld, E.R.; Ferguson, G.S. *Science* **1994**, *265*, 370.
4. Feldheim, D.L.; Grabar, K.C.; Natan, M.J.; Mallouk, T.E. *J. Am. Chem. Soc.* **1996**, *118*, 7640. Keller, S.W.; Johnson, S.A.; Brigham, E.S.; Yonemoto, E.H.; Mallouk, T.E. *J. Am. Chem. Soc.* **1995**, *117*, 12879.

Biography of Elaine Robbins Kleinfeld

Born August 28, 1967 in Concord, New Hampshire, to Dian Peterson Robbins and Edward Lowell Robbins.

Education **Bradley University**, Peoria, Illinois.
B.S. in Chemistry (Summa Cum Laude), May 1989.

Miami University, Oxford, Ohio.
Master of Technical and Scientific Communication, May 1992.

Lehigh University, Bethlehem, Pennsylvania.
Ph.D. in Physical Chemistry, June 1997.

Honors and Awards AT&T Bell Laboratories Ph.D. Foundation Fellowship, 1992–1996.
Dean's Fellowship, Lehigh University, 1996–1997.
Materials Research Society Graduate Student Award, 1994,
"For Outstanding Performance in the Conduct of Research."
ΣΞ Honor Society, 1995.
P.E.O. Scholar Award, 1995.
Academic Hall of Fame, Bradley University, 1989.
American Chemical Society Collegiate Scholastic Award, 1989.
Dean's List, Bradley University, Fall and Spring Semesters 1985–1989.
ΦΚΦ Honor Society, 1988.

Publications E.R. Kleinfeld and G.S. Ferguson, "Stepwise Formation of Multilayered Nanostructural Films from Macromolecular Precursors," *Science* **1994**, *265*, 370.

E.R. Kleinfeld and G.S. Ferguson, "Healing of Defects in the Stepwise Formation of Polymer/Silicate Multilayer Films," *Chemistry of Materials*, **1996**, *8*, 1575.

E.R. Kleinfeld and G.S. Ferguson, "Rapid, Reversible Sorption of Water from the Vapor by a Multilayered Composite Film: A Nanostructured Humidity Sensor," *Chemistry of Materials* **1995**, *7*, 2327.

G.S. Ferguson and E.R. Kleinfeld, "Mosaic Tiling in Molecular Dimensions," *Advanced Materials* **1995**, *7*, 414. (*Invited Paper*.)

E.R. Kleinfeld and G.S. Ferguson, "Nanostructured Organic/Inorganic Films from Poly(D-lysine hydrobromide) or poly(*N*-methyl-4-vinylpyridinium bromide) and Hectorite," in *Solid State Ionics*; G.-A. Nazri, J.-M. Tarascon, M. Schreiber, Eds.; Materials Research Society Symposium Proceedings Volume 369; MRS: Pittsburgh, 1995, p. 697.

E.R. Kleinfeld and G.S. Ferguson, "A Molecular Approach to Ultrathin Multilayered Films of Titanium Dioxide," in *Molecularly Designed Ultrafine/Nanostructured Materials*; K.E. Gonsalves, G.-M. Chow, T.D. Xiao, R.C. Cammarata, Eds.; Materials Research Society Symposium Proceedings Volume 351; MRS: Pittsburgh, 1994, p. 419.

ProQuest Number: 31510241

INFORMATION TO ALL USERS

The quality and completeness of this reproduction is dependent on the quality and completeness of the copy made available to ProQuest.



Distributed by ProQuest LLC (2024).

Copyright of the Dissertation is held by the Author unless otherwise noted.

This work may be used in accordance with the terms of the Creative Commons license or other rights statement, as indicated in the copyright statement or in the metadata associated with this work. Unless otherwise specified in the copyright statement or the metadata, all rights are reserved by the copyright holder.

This work is protected against unauthorized copying under Title 17, United States Code and other applicable copyright laws.

Microform Edition where available © ProQuest LLC. No reproduction or digitization of the Microform Edition is authorized without permission of ProQuest LLC.

ProQuest LLC
789 East Eisenhower Parkway
P.O. Box 1346
Ann Arbor, MI 48106 - 1346 USA